Preparation and Characterization of Photo-, Thermo-, and Solvatochromic Materials containing Benzospiropyran

Robert J. Byrne B.Sc.

Thesis submitted for the Degree of Doctor of Philosophy

Supervisor: Professor Dermot Diamond

Dublin City University   December 2007

Declaration

I hereby certify that this material, which I now submit for assessment on the programme of study leading to the award of Doctor of Philosophy is entirely my own work, that I have exercised reasonable care to ensure that the work is original, and does not to the best of my knowledge breach any law of copyright, and has not been taken from the work of others save and to the extent that such work has been cited and acknowledged within the text of my work.

Signed: _____

Robert Byrne

ID No.: 50403733

Date: 25/1/2008

Dedication

I hereby dedicate this work to my heroes, me "Ma and Da".

Le grá,

Robert.

Acknowledgements

I would like to thank Professor Dermot Diamond for the support, guidance and confidence to pursue my research, oh and not to forget the many free pints in the Porterhouse North. Thanks to all the members of the Adaptive Sensors Group and the technical staff within the School of Chemical Sciences and National Centre of Sensor Research.

Thanks to my fellow researchers at DCU, in particular to Ben, Shannon, Connor, Alek and Martina for their help and guidance. Thanks to my good buddy Brian Moran for being a real friend, we've come along way from the schooners at 'west' and will we ever get a September Sunday in Croke Park. Thanks to the Thursday night poker lads for their financial support, hahaha......Thanks to Professor Doug MacFarlane and his group at the Monash University in Melbourne, in particular Kevin and Katya.

I would like to thank my mother Gillian and father Bertie, without your support I would not have made it this far. Thanks for being great friends as well as parents. Thanks to my brother Keith for being ...... a brother. Thanks to my dogs Daisy and Holly for listening when no one else will.

Last but not least, thanks to my best friend and beautiful girlfriend Teresa, thanks for supporting me through the good and bad times. I love ya darling.

Publications

- Robert Byrne, Dermot Diamond **Chemo/bio-sensor networks.** Nature Materials (2006), 5(6), 421-424.

- Robert Byrne, Shannon Stitzel, Dermot Diamond. **Photoregenerable surface with potential for optical sensing.** Journal of Materials Chemistry (2006), 16(14), 1332-1337.

- Shannon Stitzel, Robert Byrne, Dermot Diamond. **LED switching of spiropyran-doped polymer films.** Journal of Materials Science (2006), 41(18), 5841-5844.

- Aleksandar Radu, Silvia Scarmagnani, Robert Byrne, Conor Slater, King Tong Lau, Dermot Diamond. **Photonic modulation of surface properties: A novel concept in chemical sensing** *J. Phys. D: Appl. Phys.* **40** (23) 7238-7244

Patents

- Diamond, Dermot; Byrne, Robert; Stitzel, Shannon. **Photo-switchable surfaces with controllable physico-chemical properties.** PCT Int. Appl. (2007), 23pp.

Conference contributions

- Robert Byrne, Kevin J Fraser, Ekaterina Izgorodina, Douglas R. MacFarlane, Dermot Diamond. **Photochromism of Spiropyran in Ionic Liquids.** COIL-2. Yokohama, Japan. August 2007.

- Robert Byrne, Dermot Diamond. **Ligands with Photo-switchable Activity - An Added Dimension for Analytical Measurements.** 59th Irish Universities Chemistry Research Colloquium. Dublin City University. June 2007.

- Radu, Aleksandar; Byrne, Robert; Alhashimy, Nameer; Diamond, Dermot. **Spiropyran-based smart surfaces: Development and characterization.** Abstracts of Papers, 231st ACS National Meeting, Atlanta, GA, United States, March 26-30, 2006.

- Robert Byrne, Aleksander Radu, Nameer Alhashimy and Dermot Diamond. **Adaptive materials based on the molecular switch spiropyran.** MED 06- International Conference on Materials Energy and Design, March 14th-17th 2006, Dublin Institute of Technology.

- Robert Byrne, Shannon.E.Stitzel,Dermot Diamond. **Development of a Renewable Chemical Sensing System: Harnessing the Power of Photochromic Molecules on Thin Films for Environmental Monitoring.** 2nd World Congress on Synthetic Receptors.7 Sept. -9 Sept 2005 Salzburg, Austria.

- Robert Byrne, Shannon.E.Stitzel,Dermot Diamond.**Photoreversible metal complexation with spirobenzopyran in polymer films for use in environmental sensor systems.** I3S 2005, International Symposium on Sensor Science.18 July - 21 July 2005 Juelich, Germany.

- Robert Byrne, Aleksander Radu, Nameer Alhashimy, Conor Slater, William S. Yerazunis, Dermot Diamond. **Photoswitchable Surfaces for Sensing Applications**. European Coatings Conference, Berlin, Germany. June 2006.

Abstract

The photo-, thermo- and solvatochromic behavior of spiropyran derivatives in various media were investigated by spectroscopic methods in this thesis. It was found that the molecular environment controlled the BSP-MC equilibrium, solvatochromic shift and specific interactions with itself (aggregation) and with guest ions (metal ions).

A benzospiropyran derivative was immobilized via a diamino linker to a polymer support for chemical sensing applications. This is the first demonstration of the cycling of covalently immobilised spiropyran on a solid support to merocyanine for repeat detection of metal ions. These results demonstrate a polymer-modified surface that can adapt its functionality through reversible molecular rearrangements triggered by external stimuli (photons).

The photo- thermo and solvatochromic behavior of spiropyran was studied in a selection of ionic liquids. Our results clearly show that the kinetics and thermodynamics of the process are sensitive to the nature of the ionic liquids cation. It was found that the polarity of ILs ranged from polar aprotic to polar protic solvents. It was also observed that the imidazolium and phosphonium cations formed complexes with the MC isomer; this is due to strong interactions with these cations. Relatively diffuse cations like imidazolium can form a through space orbital interaction rather than just electrostatic interactions, thus inhibiting the MC conversion back to the aplanar isomer. One of the important practical outcomes of this work is that the phosphonium based system selectively exhibits photochromism only (i.e. no thermal relaxation), thus producing a potentially permanent effect or certainly a sufficiently long term effect for many applications. The control of this solute-solvent interaction by photons was coupled with an increase in viscosity and decreases in ionic conductivity. The demonstration of this reversible photo-viscosity effect has quite important practical outcomes as the rheological properties of the IL can be altered by photons. This "photo-rheological" material has the possibility to transduce photonic energy into mechanical energy.

List of abbreviations

BSP	Benzospiropyran
MC	Merocyanine
UV	Ultraviolet
MO	Molecular orbital
HOMO	Highest occupied molecular orbital
LUMO	Lowest unoccupied molecular orbital
Vis	Visible
Perp	Perpendicular
SPMA	Spiropyran methacrylate
FHMA	Perfluorooctylhydroxy methacrylate
NIPAAm	N-isopropyl acrylamide
LCST	Lower critical solution temperature
THF	Tetrahydrofuran
SPAA	Spiropyran acrylate
EPD	Electron pair donor
NMR	Nuclear magnetic resonance
DMSO	Dimethyl sulfoxide
CT	Charge transfer
DMF	Dimethylformamide
COSY	Correlation spectroscopy
FT	Fourier transform
IR	Infrared
DCC	Dicyclohexylcarbodiimide
ATR	Attenuated total reflection
PVC	Poly (vinyl) chloride
PMMA	Poly (methylmethacrylate)
PMAA	Poly (methacrylic acid)
PS	Poly (styrene)
LED	Light-emitting diodes

EDC	1-ethyl-3-(3-dimethylaminopropyl) carbodiimide hydrochloride
SPCOOH	1'-(3-carboxypropyl)-3',3'-dimethyl-6-nitrospiro[2H-1]-benzopyran-2,2'-indoline
PARISS	Prism and Reflector Imaging Spectroscopic System
VOC	Volatile organic compound
IL	Ionic liquid
LPDE	Lithium perchlorate in diethyl ether
NARTLIS	Non-aqueous, at room temperature liquid, (fully) ionic solvents
HBA	Hydrogen-bond acceptor
HBD	Hydrogen-bond donor
EPA	Electron pair acceptor
DFT	Density functional theory
ER	Electrorheological
PER	Photo-electrorheological
TGA	Thermogravimetric analysis
DSC	Differential scanning calorimetry
HPLC	High performance liquid chromatography
NIR	Near infrared

2

1.0 Introduction

Photochromism was first reported by Fritsche in 1867 who observed that tetracene in the presence of air and light produced a colourless material which regenerated tetracene on heating[1]. Shortly after, in 1876, ter Meer described the same phenomenon with potassium salt of nitroethane[2]. Phipson observed that a gate post painted with a zinc pigment (probably some kind of a lithophone) was black when exposed to sun but white during the night[3]. Marckwald, when investigating in 1899 the behaviour of benzo-1-naphthyridine and tetra-chloro-1,2-keto-naphthalenone in light, recognized that the resulting colour changes are in fact due to a new phenomenon. He coined the term 'phototropy'[4] for this experimental fact. However, today phototropy is understood as the light-induced interactions occurring in biological systems, including the effects of light on the nutritional systems of plants or microorganisms, whereas phototropism is the tendency of plants to turn towards the source of light[5].

$$A \underset{h\nu_1, \Delta}{\overset{h\nu}{\rightleftharpoons}} B \qquad \textbf{Equation 1.1.}$$

Reversible rearrangements of a chemical species between two forms, **A** and **B**, induced in one or both directions by absorption of electromagnetic radiation and resulting in changes in the absorption spectra (and other physical properties as well), form the basis of the extensively studied phenomenon of photochromism. The term 'photochromism' was first suggested by Hirshberg in 1950[6] in the following way; *'Photochromism is a reversible transformation of a single chemical species being induced in one or both directions by*

3

electromagnetic radiations between two states having different distinguishable absorption spectra'. The radiation changes may be induced by ultra-violet, visible and infra-red radiation. Reversibility is the important criterion. All irreversible reactions are classified as normal photochemistry.

The term photochromism, derived from the Greek words *phos* (light) and *chroma* (colour) means the generation of colour under the influence of predominantly UV-light, (A → B). When restricted to the molecular world, this term implies the reversible photoinduced colouration of an ensemble of molecules in an amorphous, crystalline or solution state. The photogenerated and coloured form must be able to revert back to the original and colourless state.

The back reaction (B → A) can occur thermally and/or photochemically, as is the case with spiropyran, spirooxazines and chromenes. A photoinduced decoloration, however, requires the irradiation wavelength to be sufficiently different from that causing colouration, but the thermal reaction normally predominates. For other systems, the photochemically induced forms (B) are thermally stable. For such systems, (e.g. fulgides or arylethenes) the back reactions (B → A) are predominantly photochemical.

The photochromic transformation and the observed spectral changes or changes in physical or chemical behaviour are related to the modifications of the geometry of the system and its electronic distribution. Also, the importance of the medium in which the photochromic compound is incorporated can strongly influence or control the kinetics of

4

the thermal back reaction when it occurs, the colour of the species formed in the forward photochemical reaction, and other properties of the photochromic process.

Early observations of the reversible photocoloration of organic compounds were reported in the literature more than a century ago. Only much later with the advent of modern spectroscopic techniques have studies on photochromic compounds evolved into a mature field of research. Over the course of the past four decades, numerous families of organic molecules with photochromic properties have been identified and studied in detail. Most of them rely on unimolecular reactions for their coloration and decoloration, which generally involve $2\pi + 2\pi + 2\pi$ pericyclic reactions (ring closing and opening steps) or cis→trans and trans→cis isomerizations. Biomolecular processes, based on photoinduced cycloadditions or electron transfer, have also been employed to design and implement photochromic systems, although they are certainly less common than their unimolecular counterparts.
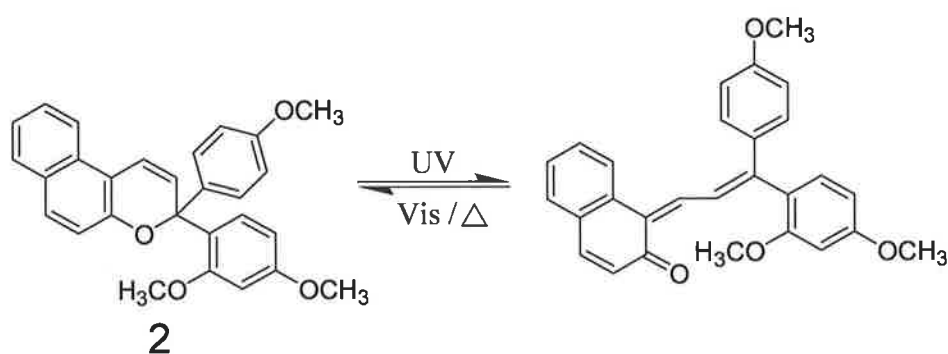
1.1 Photochromic compounds

The discovery of the photochromic behavior of spiropyran[7] and recognition of the potential of their bistability for a "photochemical erasable memory"[8] spurred active research on the general phenomenon of photochromism. Until recently, spiropyran **1** (**Scheme 1.1**) (X = CH, CR') comprised the most closely studied family of photochromic compounds, and only during the past decade have these given way to their more practicable congeners, spirooxazines **1** (X = N)[9]. These close relatives of spiropyran have been receiving increased interest, because of their excellent photochromic properties and

their resistance to photodegradiation or fatigue. In general, the resistance to fatigue of the spirooxazine is much better than that of the spiropyran. Their stability under conditions involving continuous irradiation has led to their use in various applications, including ophthalmic lenses[10].
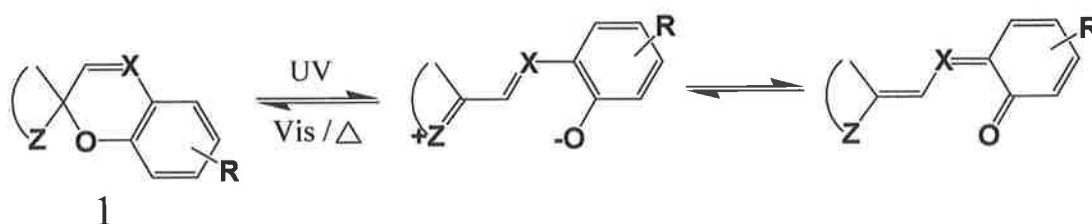

Scheme 1.1. Photochromic-isomers of spiropyran (X = CH, CR') and spirooxazines (X = N).

Benzo and naphthopyrans or chromenes are another important type of thermoreversible photochromic compounds that have found application in the variable optical transmission materials field, specifically ophthalmic lenses. Their development into commercially useful materials has been fairly recent, within the last ten years. The broad absorption bands exhibited by the open forms of the naphthopyrans **2** (**Scheme 1.2**) and the heteroannallated naphthopyrans are somewhat complementary to the absorption bands of the naphthoxazines, leading to colour neutralization when they are used together. Their resistance to photooxidation is also good relative to most other families of photochromic compounds. In this respect they are comparable to the spirooxazines, which again adds to the complementary character of the two families. The colour of the opened forms can be tuned over a large range of the visible spectrum, by substituents on the naphthyl moiety or on the aromatic groups present on the sp^3 carbon atom of the pyran ring.

**Scheme 1.2.** Photoisomerization of naphthopyran.

The fulgides are a class of photochromic compounds for which the thermal reversal or decoloration of the coloured species is disallowed. Therefore, the reversion is largely driven photochemically as is illustrated with compound **3** (**Scheme 1.3**). Because of the stability of the coloured species toward thermal reversion, the fulgides have potential application in the field of optical storage and security printing. Another use, in actinometry, is well known.
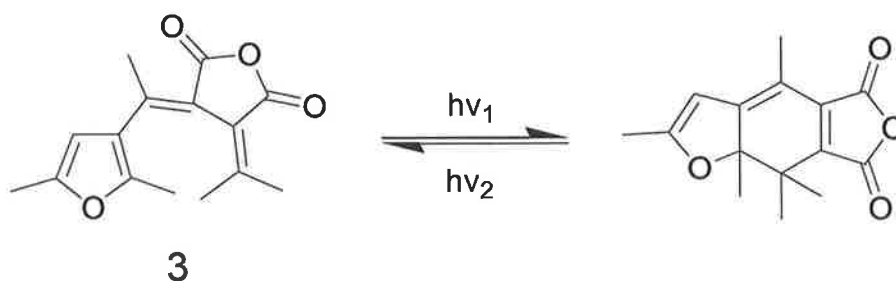
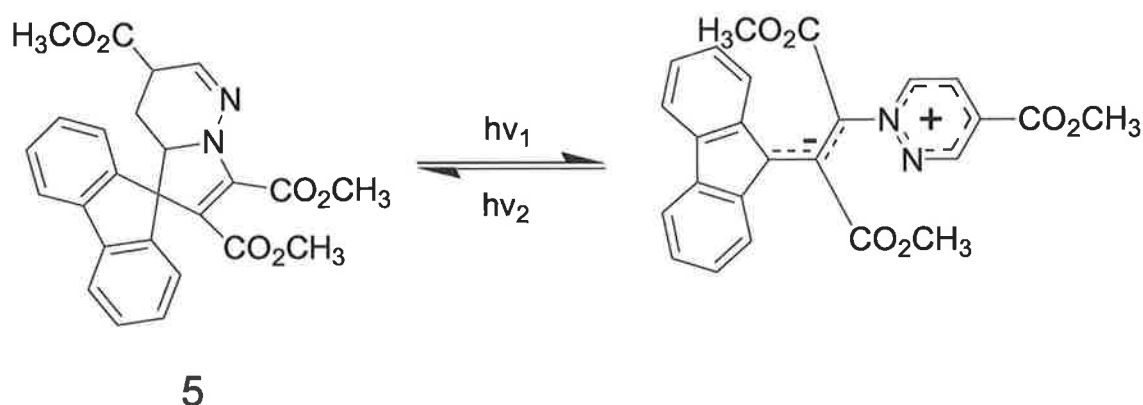**Scheme 1.3.** Photoisomerization of fulgides.

The diarylethenes with heteroaryl groups, for example the bis-heteroaryl ethenes **4**, **Scheme 1.4**, are photochromic compounds similar to the fulgides in that the coloured or cyclized forms are thermally stable. Decoloration is again driven photochemically.

Increasing the thermal stability of the coloured has been a major goal of the research on this family as their targeted use is information storage.
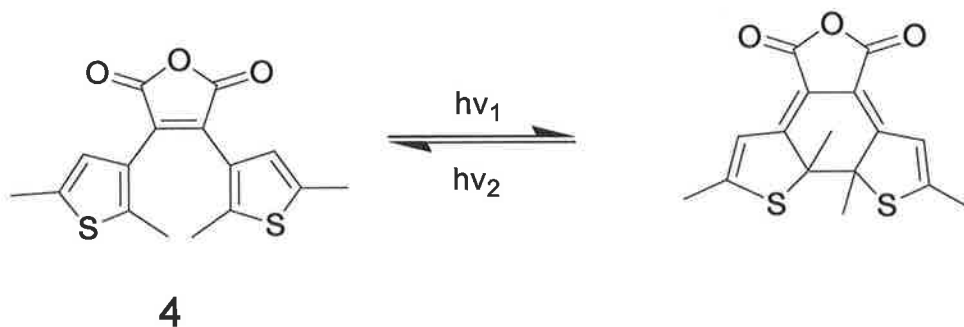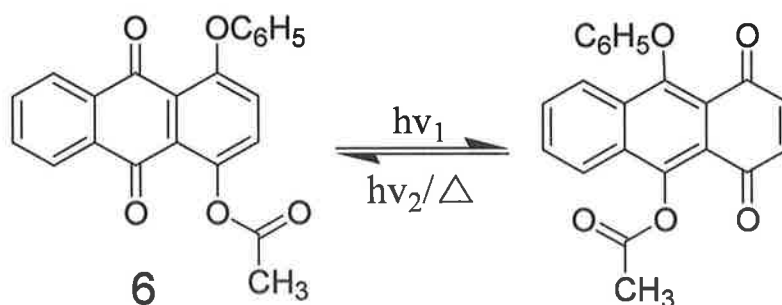

Scheme 1.4. Photoisomerization of diarylethene.

The dihydro-, tetrahydro-, and hexahydroindolizine compounds involving one, two or three nitrogen atoms makes up another family of compounds that exhibits a generally thermoreversible photochromic system based on spiropyran and spirooxazines, the photochemical and thermal rearrangements of **5** are driven by a 6π-electron pericyclic reaction (**Scheme 1.5**), with the difference that one pair of π-electrons in their electronic system is located on a nitrogen or a carbanionic center. This leads to a 1,5-, instead of a 1,6-, electrocyclic route. Photobleaching is sometimes superimposed on the thermal back reaction. They can be associated in supramolecular systems through interaction with inorganic salts or inorganic guests, in liquid crystalline phases or in polymer matrices (dissolved, absorbed or bound to a suitable polymer) or as bichromophoric units.

5

Scheme 1.5. 1, 5-electrocyclic photoisomerization of dihydroindolizine.

The mechanism for the photochromic quinones involves proton or group transfer (**Scheme 1.6**). Special emphasis has been placed on the synthesis of representative polycyclic quinones and their photochromic behaviour, including the spectral, kinetic, and fatigue characteristics of such systems. Potential applications are focused on recording and multiplications of images, optical memories, and gradation masking.

Scheme 1.6. Photoisomerization of quinones involves proton or group transfer.

The photo-, thermo-, and electrochromic behaviour of the next group of spiroheterocyclic compounds, derivatives of 2,3-dihydro-2-spiro-4'-(cyclohexadien-2',5'-one)perimidine **7** (**Scheme 1.7**) is determined by a combination of two principal reaction mechanisms

9

involving cleavage of a C-N bond occurring in the first singlet excited state and the
intramolecular proton transfer (**Scheme 1.6**).
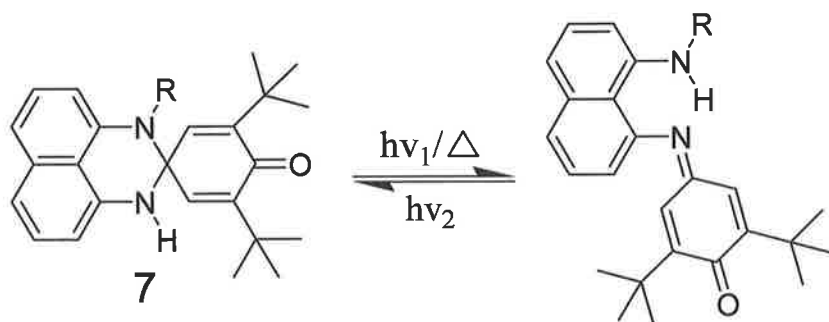
Scheme 1.7. Photo-, thermo-, and electroisomerization of 2,3-dihydro-2-spiro-4'-
(cyclohexadien-2',5'-one)perimidine.

The photochromic viologens **8** behave in a manner similar to the inorganic photochromic
systems, in that they switch between isomeric forms via electron transfer (**Scheme 1.8**),
unlike the organic photochromic compounds which operate by isomerizations, heterolytic
(or homolytic) cleavage or pericyclic reactions. The formation of coloured radical cations
(and accompanying radical anion's) and the possibility of oxidation (or reduction) by an
electrochemical process indicates the possibility of erasable photo-electrochromic
devices.
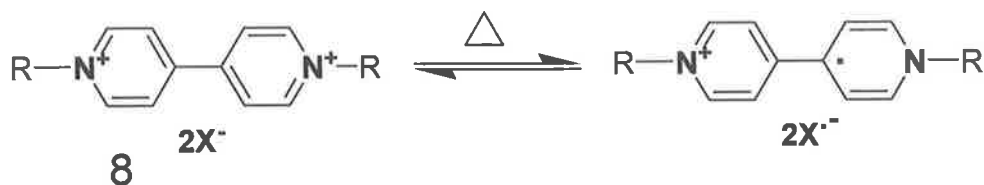
Scheme 1.8. Photoisomerization of viologen via electron transfer.

1.2 Conjugation in Spiroheterocyclic Compounds

In compounds **1** and **5-7**, the through-space interaction of two orthogonal π-networks connected by a tetrahedral carbon center, i.e., spiroconjugation, may lead to nonadditivity of the photoelectron, electronic absorption spectra, and some other properties of the compounds[11, 12]. Contrary to expectations, no such effect had been revealed in studies of the absorption spectra of various spiropyran and spirooxazines **1** (X = CR, N), which were found to consist of localized transitions belonging to the two orthogonal halves of their molecules[9, 13]. This result can be explained in terms of the qualitative molecular orbital (MO) analysis of the factors determining the effects of spiroconjugation. The nonzero overlap between MOs of the two π-subsystems leading to the formation of MOs spanning the entire system and, thus, to delocalization of the electronic density over this system is achieved, provided that the interacting MOs have the same symmetry. For the spiroconjugated π-subsystems, this requirement must be supplemented with the condition that the MOs of the mutually perpendicular fragments are antisymmetric with respect to the two perpendicular bisecting planes,[11] as shown by the relative phases of the atomic orbitals at the centers adjacent to the spiro atom in **Scheme 1.9**.
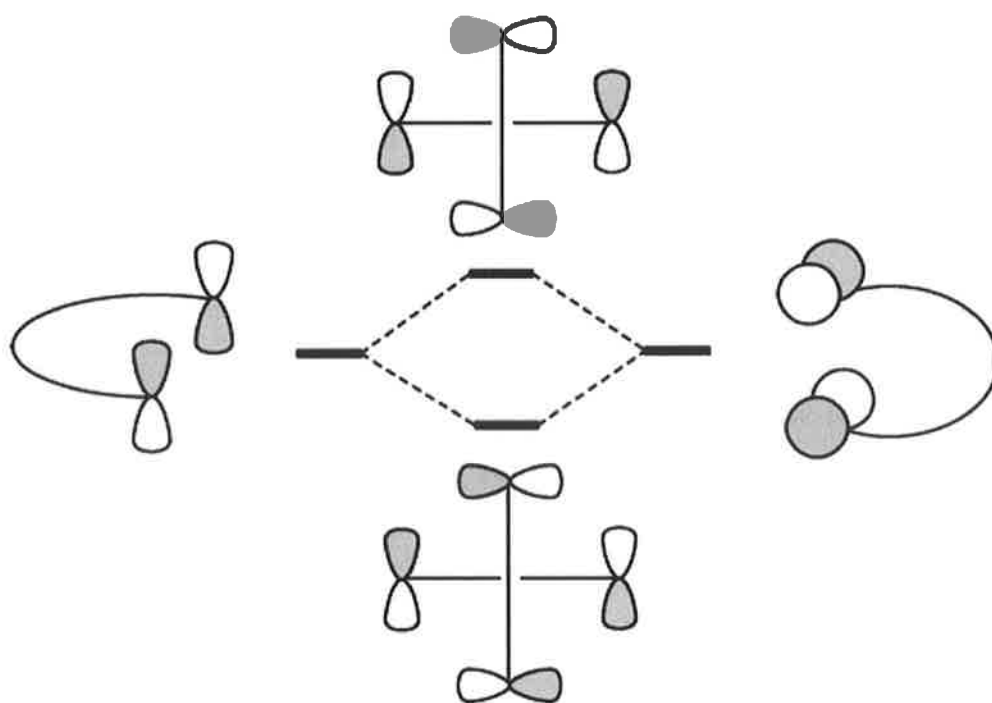
Scheme 1.9. Illustration of the required assymetric atomic orbital phases at the spiro atom needed for spiroconjugation[14].

On the basis of this concept, and restricting themselves to consideration of only frontier orbitals of fragments of the spiroconjugated systems, Maslak and coauthors[15] designed a number of spiroheterocyclic dyes (**Figure 1.1**) with useful optical properties, in which interaction of the antisymmetric LUMO of the acceptor part (1,3-indandione) with the HOMO of the donor part (aromatic diamines) results in the appearance of new absorption bands in the visible region due to the intramolecular charge transfer between the spiroconjugated fragments. For **9a,b,** the intensity of these charge-transfer bands is low because 1,2-phenylene derivatives possess symmetrical HOMOs, the symmetry of which is mismatched with that of the acceptor's LUMO. In contrast, 1,8-naphthylene derivatives **9c,d** have antisymmetric HOMOs overlapping with the acceptor's LUMO, which

12

provides for spiroconjugation and rather intense charge-transfer bands in the absorption spectra of these compounds and some of their close analogues[15].
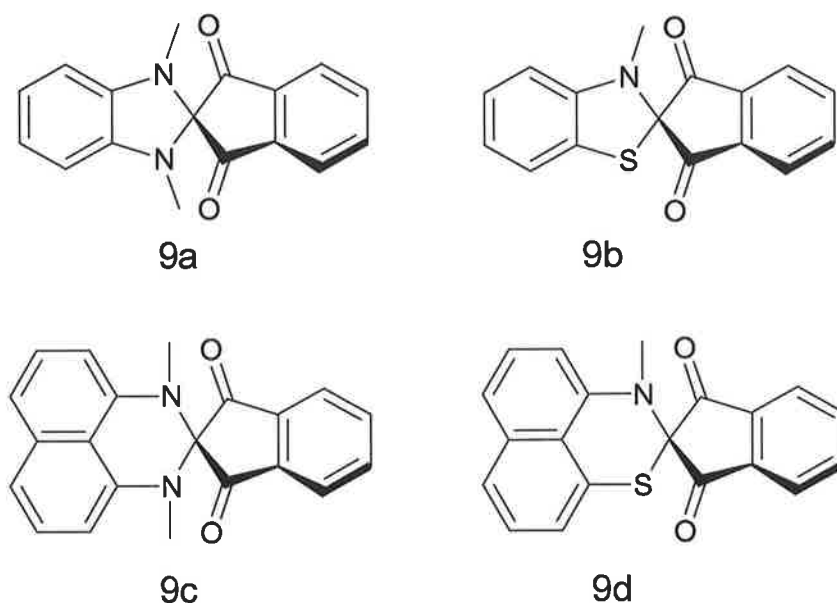

Figure 1.1. Spiroheterocyclic dyes prepared by Maslak demonstrating the importance of symmetry for charge transfer between the aromatic diamine section (left hand side) and the 1,3-indandione section (right hand side).

In spiropyran and spirooxazines **1**, LUMOs of the 2*H*-chromene and 2*H*-4-azachromene fragments are conceptually (no strict symmetry) antisymmetric[16], whereas HOMOs of 1,2-phenylenediamine, 1,2-phenylenedithiol, and other 1,2-phenylene moieties of various five-membered heterocycles constituting the "left" part of **1** are symmetric. Such a combination does not fit the requirements of spiroconjugation. On the other hand, in the spiroheterocyclic compounds **5-7**, both conjugated fragments linked by a spiro carbon atom possess antisymmetric frontier orbitals, and their spectra contain additional red-shifted absorption bands that originate from charge transfer between the orthogonal fragments.

13

While the compatibility in the HOMO-LUMO symmetry properties depicted by **Scheme 1.9** seems to be an essential factor accounting for the occurrence of the electronic transitions unobserved in the separated conjugated moieties of certain spiroheterocyclic compounds, it should not be considered as the dominant factor defining other consequences of spiroconjugation. Another important stereoelectronic effect operating in molecules of spiropyran and spirooxazines **1,** that affects the structural parameters of their spiro sites and their proneness to the isomerizations shown in **Scheme 1.1**, is caused by a specific orbital interaction that results in partial donation of a lone electron pair at the heteroatom Z to a vacant antibonding σ^*-orbital of the C_{spiro}-O bond. Such orbital interactions (negative hyperconjugation) have been recognized as the main factor determining anomeric effects[17], strong attractive closed-shell interactions[18], and even the nature of hydrogen bonds. The $n_Z \rightarrow \sigma^*_{CO}$ interaction shown in **Figure 1.2(a)** manifests itself in lengthening the C_{spiro}-O bonds in indolinospiropyran (X = CH), spiroindolinonaphthoxazines (X = N, R' = C_6H_4), and many other spiropyran and spirooxazines **1.**
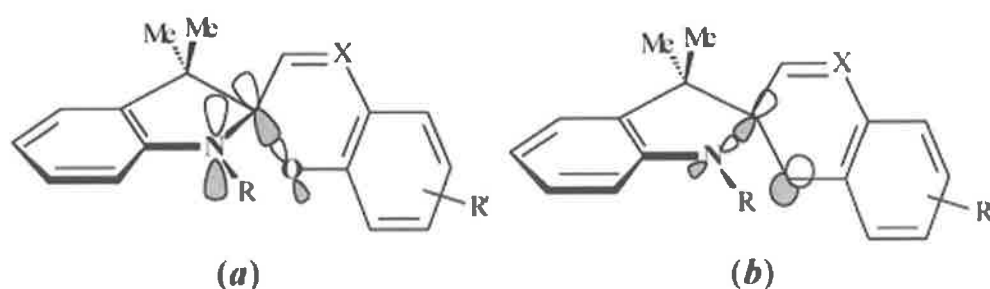

(*a*)   (*b*)

Figure 1.2. The $n_O \rightarrow \sigma^*_{CN}$ orbital interactions in the C_{spiro}-O bond[14].

The structural consequences of this effect are only partly compensated by the $n_O \rightarrow \sigma^*_{CN}$ orbital interaction, **Figure 1.2(b)**, which is substantially weaker than that shown in **Figure 1.2(a)** because of the poorer donating properties of the more electronegative oxygen center and, therefore, the larger energy gap between the interacting orbitals. As shown by X-ray structural determinations of a broad variety of indolinospiropyran and spirooxazines, the C_{spiro}-O bond lengths in these compounds fall into the range of 1.452-1.501 Å and 1.45-1.478 Å, respectively, which is considerably longer than normal C_{sp3}-O bonds (1.41-1.43 Å).

As was shown by quantum chemical modeling of reaction paths for the valence isomerization of spiropyran[16], the reaction coordinate at the early stage of the reaction in both ground and first singlet excited states corresponds well to stretching a C_{spiro}-O bond. It is not, therefore, surprising that the proneness of compounds **1** to the thermal and photoinitiated rearrangements shown in **Scheme 1.1** correlates with degree of initial stretching of this bond in the ground state, determined by the efficacy of the $n_Z \rightarrow \sigma^*_{CO}$ orbital interaction.

In 2-oxaindano spiropyran **14a**, this interaction is relatively weak compared with that shown in **Figure 1.3**, which is due to the lower energy level of the lone electron pair orbital located at the oxygen in the five-membered ring. This is also true for spiropyran **14b,c** because of the involvement of the n_N orbital at the nitrogen centers in π-conjugation with the adjacent carbonyl group. Both of these effects operate in spiropyran

of the 2-oxaindan-3-one series **14d**, in which case the lengths of the C_{spiro}-O bonds reach the minimal values currently known for spiropyran.
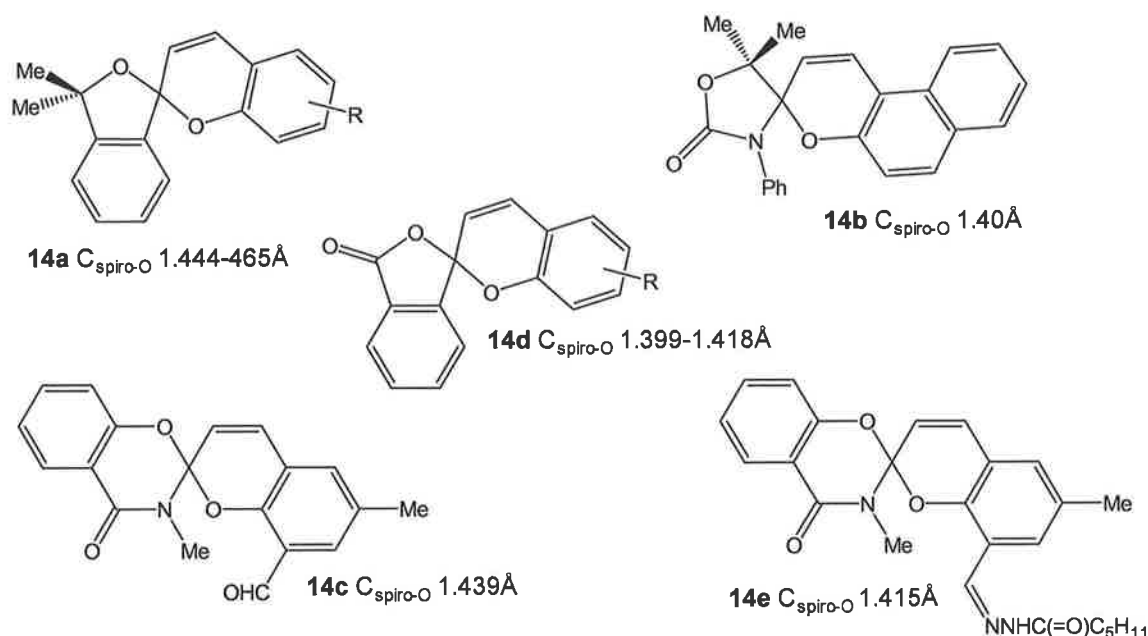

Figure 1.3. Various C_{spiro}-O bond lengths in spiropyran of the 2-oxaindano series, **14a-e**. [R-group = H, CHO, and NO$_2$].

Under continuous irradiation of their liquid or glassy solutions, all spiropyran with C_{spiro}-O bonds longer than 1.42 Å can undergo the thermal and photochemical transformations described by **Scheme 1.1**. However, spiropyran **14d**, with shorter C_{spiro}-O bonds, exhibit neither thermochromic nor photochromic properties.

After consideration of the photochromic materials reported above, it was decided to concentrate efforts on one particular family of photochromes, this being spiropyran. This decision was made on the basis that their synthesis, spectral and photochemical properties

are very extensively documented[9, 19-21] and a great deal of work is still on going[22-25]. This literature survey is focused on studies aimed at gaining insight into the mechanisms governing photo- and thermally driven rearrangements (**Equation 1.1**) and structure-property relationships important for optimization of thermodynamic, kinetic, spectral, and other important parameters of the photochromic systems.
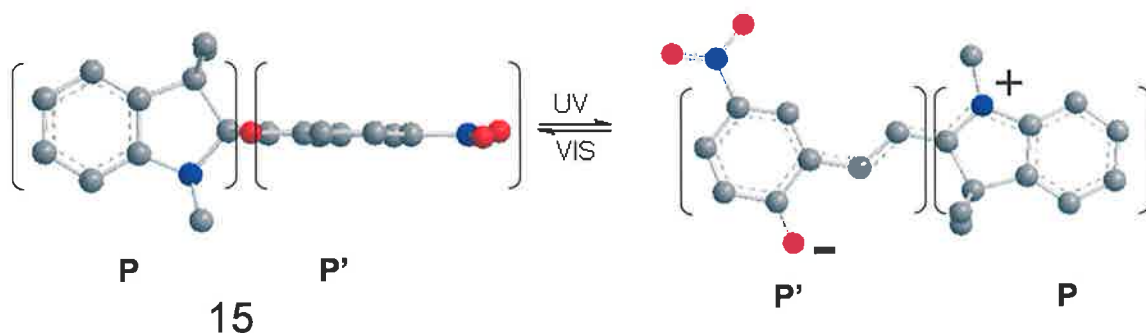
1.3 Benzospiropyran

During the past few decades, interest has been rapidly growing in gaining insight into the properties and transformations of the so-called bistable compounds and molecular systems, i.e. the chemical species may exist in two thermodynamically stable states and are capable of interconversion under the action of various external stimuli. This interest is motivated by the fact that the bistable molecules and molecular systems represent, in effect, two-bit logic elements of sub-nanoscopic size and have diverse potential applications in the areas of molecular electronics[26], photonics[27], sensors[28], and computing[29]. In addition, they have demonstrated interesting behaviour in the transport of biochemical information and signal transmission across biological membranes and photochemically switched enzymatic systems[30]. The most efficient and technological adaptable way to address bistable molecules and systems from the macroscopic level is the use of light.

1.3.1 Molecular Structure

The photochromic properties of spiropyran were discovered by Fischer and Hirshberg back in 1952[7]. For the next two decades, research on photochromism concentrated mainly

on these compounds, or in particular the 2,3-dihydro-1',3',3'-trimethyl-6-nitrospiro[1-benzopyran-2,2'-1*H*-indole], **15**. Spiropyran consists of two heterocyclic parts linked together by a common tetrahedral sp^3 carbon atom. The two halves of the molecule are in two orthogonal planes (P and P'), **Scheme 1.10**. The benzopyran or 2H-chromene part (P') is the common structure to all spiropyran compounds. The (P) heterocyclic part is variable and often is built upon mono or bi-heteroatomic azaheterocycles either saturated or benzofused.

P   **P'**

15

P'   **P**

Scheme 1.10. The 2,3-dihydro-1',3',3'-trimethyl-6-nitrospiro[1-benzopyran-2,2'-1H-indole], aplanar (left) and merocyanine isomer, planar (right), 15.

In solution, typically spiropyran presents an absorption spectrum in the UV range 200-400 nm with an actinic band mostly situated near 320-380 nm. Absorption in this range leads to an isomerization wherein the C-O spiro bond in **16**, is cleaved heterolytically, which results in the highly polar and coloured merocyanine dye that absorbs strongly in the visible region, **Figure 1.4**, (λ_{max} in acetonitrile, 554 nm) **17a, 17b**.
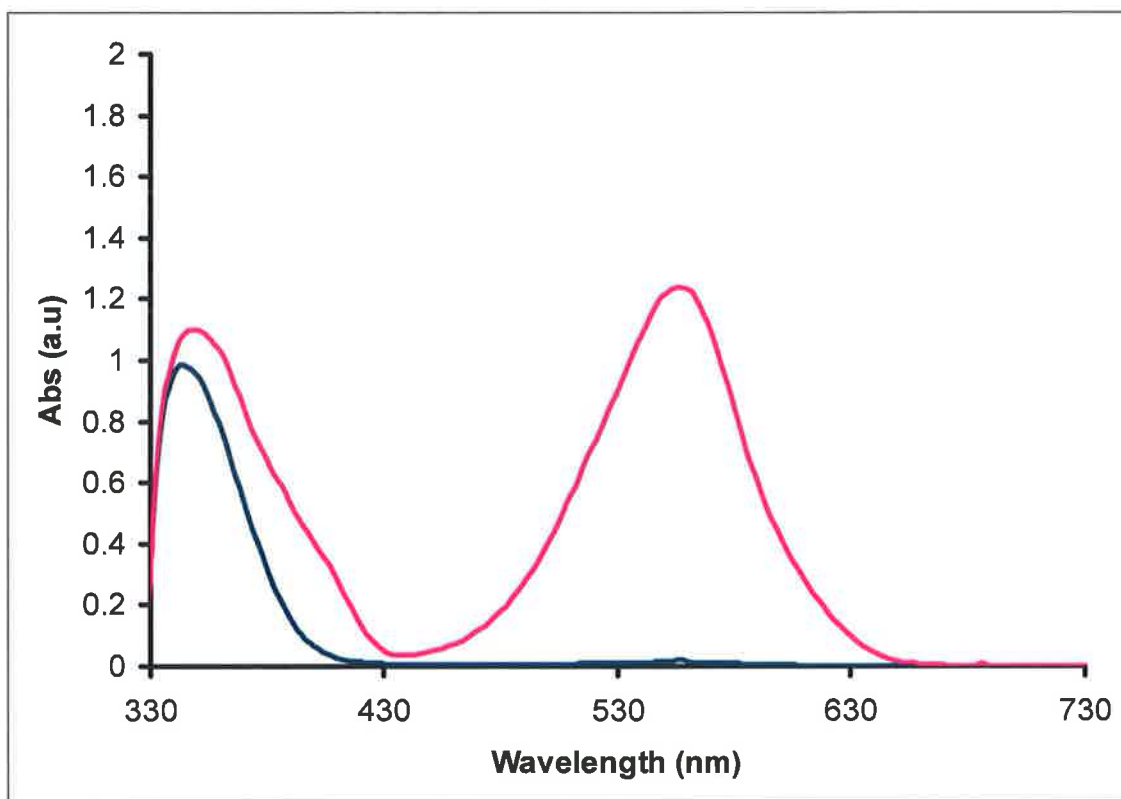
Figure 1.4. UV-vis spectra of 2,3-dihydro-1',3',3'-trimethyl-6-nitrospiro[1-benzopyran-2,2'-1H-indole], (blue) and merocyanine isomer(pink).

As shown in **Scheme 1.11**, the structure of this merocyanine 'open' form is a resonance hybrid between a zwitterion **17a**, and a neutral quinonoid **17b**. The zwitterionic form contributes significantly to the structure of the open form because the aromaticity of the oxygen-bearing ring is lost in the neutral form[31]. The 'open' isomer so-called because of its transoid structure is generally the most stable one, and is structurally quite similar to the merocyanine dyes. Spiropyran may be defined as a potential dye generated by a photochemical induction.
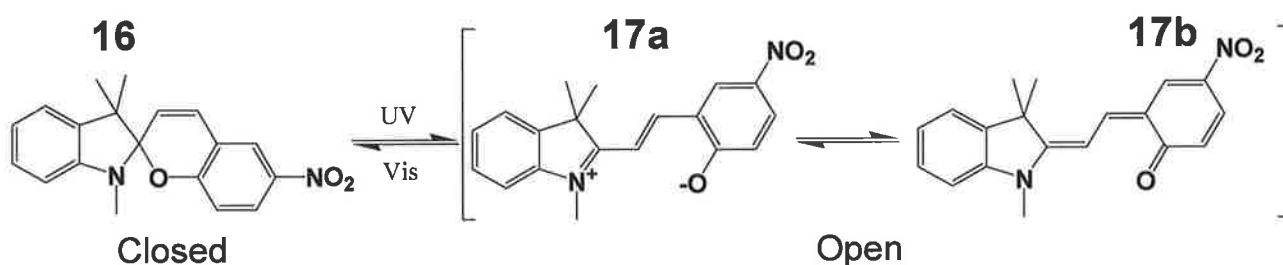
Scheme 1.11. Molecular structure of spiropyran 16 in the closed and open forms. In the "open form" zwitterionic 17a, and neutral resonance 17b, forms contribute to the merocyanine structure.

1.4 Ring-Opening/ Ring-Closing in Spiropyran

The ring-opening/ ring-closing behaviour of depends on a number of factors including;

- the structure of the compounds (length of the C_{spiro}-O bond, nature of the heteroatom and substituents in different positions of the molecule and some positions are fundamental and characteristic for the results)

- the medium (solvent, viscosity…)

- the temperature, the photolysis energy and the range of absorption of the open form.

The appearance of ring-opening for an observer depends also on the colouration intensity, optical density of the coloured form which is a function of concentration. These parameters are quantitatively observable by spectrophotometric methods. The quantitative determination of spectro-kinetic or photo-chemical parameters is generally achieved in solution but many applications require use of plastic or other solid supports

20

such as paper, films, semi-conductors or polymeric materials, so immobilization strategies are important to consider.

For a complete understanding of the photochromic equilibrium, it is necessary to take into account the electronic structures of the open forms (depending on the molecular structure and the medium) as well as their geometries. For example different stereoisomers of cisoid configuration are formed just after the breaking of the C-O bond, while isomers of transoid configuration are formed after isomerization. The trans configuration appears to be the more stable because it minimizes the non-bonding interactions. The electronic distribution in transoid merocyanines is often symbolized by a delocalized repartition of π electrons with an excess of negative charge on the phenolic oxygen and an excess of positive charge on the heteroatoms. This representation, which corresponds to the experimental situation, seems the most satisfactory for the formation of a dipolar zwitterionic with localized charges form and apolar quinonic form. This will be discussed in greater detail below. Actually, the heterolytic cleavage leading to colour formation is more complex than shown in **Scheme 1.11**, and will be discussed in further detail.

1.4.1 Thermochromism

In solutions of non-polar solvents, most spiropyran exist as ring-closed isomers, but upon dissolving in polar solvents they can undergo thermal ring opening to the corresponding merocyanine forms. The position of the established complex equilibrium depends on many factors, primarily solvent polarity, the nature of the substituents, and the concentrations of the solution. Thermal equilibrium established in solutions of spiropyran

21

is depicted in **Scheme 1.12**, with indolinospirobenzopyran by way of example. The ring-opening reaction starts with cleavage of the C-O bonds in the stereoisomers to give rise to sterically strained chiral intermediates, which rapidly convert to nearly planar merocyanine isomers, labelled according to the configurations of the molecular fragments relative to the two double bonds (cis, trans: **C** and **T**) and a partially double bond, neutral quinonoid or the zwitterionic oxygen (*s-cis, s-trans*: **C, T**). Because *s-cis* conformers are significantly higher in energy than their *s-trans* isomers, **Scheme 1.12** is restricted to the interconversions of the latter. The presence of more than one merocyanine isomer in solutions of spiropyran has been shown in several studies using transient spectroscopy, ^{1}H, ^{13}C and time-resolved resonance Raman spectroscopy experiments[32]. The structure of the most stable isomers was determined as TTC and CTC conformers. This finding is in accord with the conclusions made on the basis of theoretical modelling of the equilibria[33].

The dependence of the relative stability of the ring-closed and ring-opened forms of spiropyran on the structure of their indoline section and the type of annulation of the 2H-pyran moiety with benzene ring(s) was studied in much detail. Electron-withdrawing substituents in 2*H*-chromene moieties of spirobenzopyrans favour the stabilisation of the ring-opened forms. The maximal effect is attained when strong electron-accepting groups, such as nitro or arylazo groups, are placed in the *p*- or/and *o*-position relative to the phenolate oxygen of the merocyanine acquiring the zwitterionic character. Solutions of these compounds in polar solvents at room temperature contain measurable amounts of the ring-opened forms.

As shown in **Scheme 1.12**, the polar merocyanine forms of spiropyran tend to associate into stack-like aggregates[19]. This tendency is very strong, and rather stable associates are formed in very dilute solutions and even in polymeric films. Absorption spectra of *J*-aggregates, which have a head-to-tail arrangement of the molecular dipoles, are shifted to longer wavelengths relative to the spectra of the isolated merocyanine molecules. For *H*-aggregates having a head-to-head arrangement of the molecular dipoles, the spectra are shifted to shorter wavelengths. An important property of the *J*-aggregates produced by irradiation of solutions in non-polar solvents is that their spectra consist of very narrow absorption bands (absorption peak widths are a few tens of nanometers), which is a necessary condition for design of wavelength-multiplexed memory systems. It has also been shown that the formation of the spiropyran aggregates causes very large changes in the refractive indices and, thus, provides a new approach towards the synthesis of tunable photonic gap materials[19].
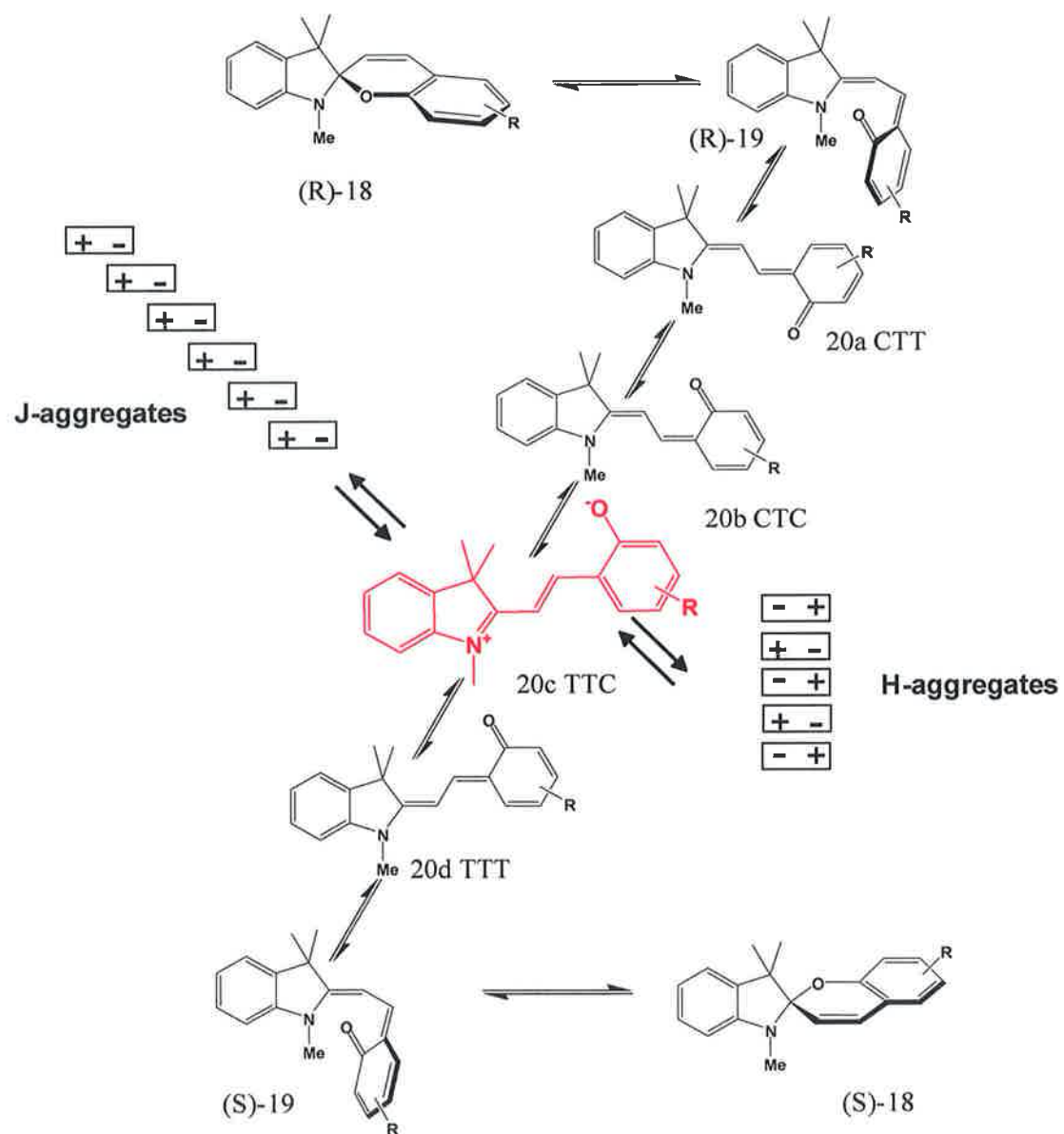
Scheme 1.12. Ring opening mechanism of spiropyran via the various merocyanine isomers.

1.4.2 Solvatochromism

Another known characteristic of the spiropyran system that cannot be neglected is solvatochromism. The solvatochromic behaviour of spiropyran, which is exhibited as pronounced changes in the position and intensity of their UV-Vis absorption bands induced by variation in the polarity of a medium, may be governed by two different mechanisms. The first one is related to the shift of the equilibrium when passing from one solvent to another. The manifestation of this mechanism is the redistribution of the intensities of absorption bands in the spectrum of a solution containing an equilibrium mixture of the isomers or even the appearance of new bands if only one of the isomers was present in a solution of a certain solvent. The second mechanism is related to differences in solute-solvent interactions in solvents of different polarity. Since solvent effects on the absorption spectra are usually studied by measuring the longest-wavelength absorption band shifts, and since these bands in solutions of spiropyran belong to the ring-opened forms, determining the origin of these interactions requires an understanding of the structure and polarity of the merocyanine.

Experimental data on dipole moments of spiropyran and their merocyanine isomers are very scarce. For two 6-nitro- and two 6,8-dinitro- substituted spiropyran ($R=CH_3$, CH_2CH_2COOH; $R_1=6-NO_2$ and $6,8-(NO_2)_2$), the most accurate electrooptical absorption measurements gave the values 3.0-4.5 D (10-15 C.m) and 15-18 D (50-60 C.m) for the ground-state dipole moments of the spiro and the merocyanine forms, respectively. Although these high values are in large measure determined by the presence in the molecules of polar nitro groups, they indicate convincingly that the merocyanine isomers

25

are much more polarized than the ring-closed forms. This conclusion is corroborated by quantum mechanical calculations at various levels of approximation. This explains the significant stabilisation of the merocyanine isomers in polar media which is predicted by calculations and observed experimentally. This effect is generally explained in terms of the balance between the quinoidal 17b and zwitterionic resonance 17a forms, which is manifested through trends in solvents of varying polarity.
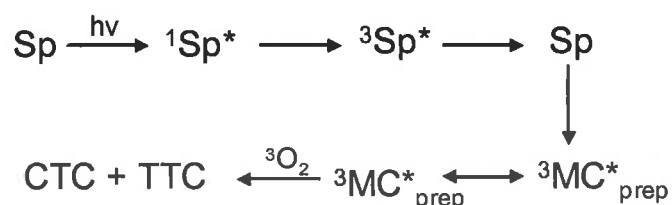
Positive solvatochromism (i.e., bathochromic shift of the longest wavelength of the UV-vis spectrum with increase in the polarity of a solvent) observed for a limited set of spiropyran derivatives was widely accepted to arise from a predominantly quinoidal structure of merocyanines[34]. It has been shown, however, that the electronic structure of the merocyanine-derivatives of **20**-is extremely sensitive to the influence of substituents in the indoline ring of these compounds. By varying the acceptor or donor properties and the position of the substituents, it is possible to polarize the π-system of the ring opened form sufficiently to reach a zwitterionic-like structure and observe negative solvatochromism in the *push-pull* type compounds containing electron-releasing groups in the indoline ring. Negative solvatochromism was also observed for the open forms of indolinospiropyran with a 6-nitro group in the 2*H*-chromene ring[31], **17a**. These results imply that the ground-state merocyanine structures of the considered spiropyran are better solvated than their first electron excited states and the ground-state dipole moments are larger than those of the excited states. The latter conclusion has been confirmed by the electro-optical absorption measurements of the dipole moments of the merocyanine

26

forms of spiropyran **1**, (R = H) in the first singlet excited state. It was found that, with the excitation, the dipole moments of the merocyanines decrease by about 3.3-6.6 D.

Thermochromism and solvatochromism in spiropyran systems also need to be taken into account when designing a spiro-system. The dynamic behaviour of photochromism in spiropyran is the very property that makes these compounds so interesting. Controlled manipulation of a molecular switching opens the door to many exciting opportunites on fundamental and applied materials science.

1.4.3 Photochromism

The primary step of the photochromic reaction of spiropyran is the dissociation of a C-O bond in an electronic excited state. The nature of the active excited state depends on substitution in the benzopyran ring of the spiropyran. The studies of the reaction dynamics with the use of time-resolved resonance Raman spectroscopy, laser flash photolysis and quenching experiments have shown that, for spiropyran with a nitro group, a triplet state plays a crucial role in the photochemical ring-opening reaction[35, 36].

$$Sp \xrightarrow{h\nu} {}^{1}Sp^{*} \longrightarrow {}^{3}Sp^{*} \longrightarrow Sp$$

$$CTC + TTC \xleftarrow{{}^{3}O_{2}} {}^{3}MC^{*}_{prep} \longleftrightarrow {}^{3}MC^{*}_{prep}$$
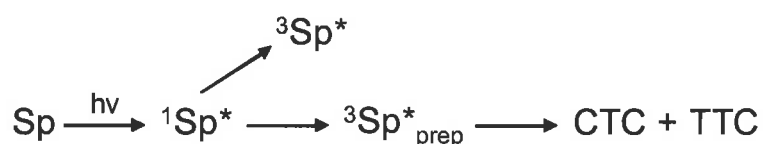
Scheme 1.13. Photochemical ring-opening reaction of nitro containing spiropyrans and the intermediates involved in the mechanism.

The mechanism in **Scheme 1.13** suggested for description of the photochemical behaviour of a series of indolinobenzopyrans 16 with a nitro group in position 6 and with or without substituents in position 8 involves intersystem crossing to the short lived triplet state of the ring closed isomer ^{3}**Sp***. It serves as the precursor to the triplet so called 'perpendicular' merocyanine form ^{3}**MC***$_{perp}$ that may be correlated with structure **19** in **Scheme 1.12**. The ^{3}**MC***$_{perp}$ conformation is in equilibrium with the triplet of the trans isomer, observed as a short lived transient with absorption maxima at 420-440 and 560-590nm and a lifetime <10ms. The reaction ends with quenching the triplet with oxygen and establishing a thermal equilibrium between the most stable merocyanine isomers, presumably **CTC** and **TTC** (**Scheme 1.12**). This mechanism is evidenced by the extreme sensitivity of the dynamics to the presence of oxygen in solution and the identity of the quantum yields of population of the merocyanine triplet state and the overall process of a spiropyran-to-merocyanine photoconversion[36, 37].

A nitro group in spiropyran has a dual effect on their photochromic capacity. On the one hand, it strongly enhances the quantum yield of the photocolouration (up to 0.7-0.9 in solvents of low polarity), and on the other hand, it also enhances the quantum yield of the intersystem crossing, which facilitates formation of singlet molecular oxygen from the triplet excited state and ^{3}**MC***, thus, photodegradation of spiropyran via oxidation by singlet oxygen. The adverse influence of the inclusion of highly reactive triplet states (both ^{3}**Sp*** and ^{3}**MC***) of spiropyran into the mechanism of the ring opening on their fatigue resistance properties has been recognised by many authors. It was found that the quantum yields of irreversible photodegradation of various spiropyran are virtually

independent of the nature of their 'left-half' heterocyclic moiety and are directly correlated with the lifetime of the triplet-state intermediate formed upon excitation. For spiropyran without nitro groups in the benzopyran rings, the quantum yields of the photocolouration are essentially independent of solvent polarity and are substantially lower than those for spiropyran with nitro groups. In contrast to the latter, spiropyran without nitro groups display photochromism only in the excited singlet manifold.

$$\text{Sp} \xrightarrow{h\nu} {}^1\text{Sp}^* \longrightarrow {}^3\text{Sp}^*_{\text{prep}} \longrightarrow \text{CTC} + \text{TTC}$$

with ${}^3\text{Sp}^*$ branching from ${}^1\text{Sp}^*$.

Scheme 1.14. Photochemical ring-opening reaction of spiropyran not containing nitro group and the intermediates involved in the mechanism.

The mechanism of the photochemical process is represented relatively simply in **Scheme 1.14**, where the structure of the singlet excited-state intermediate ${}^1\text{Sp}^*_{\text{perp}}$ corresponds to that formed upon immediate cleavage of the C_{spiro}-O bond and is, therefore, close to **19** in **Scheme 1.12**. According to the CASSCF[*] modelling of this process, the structure similar to ${}^1\text{Sp}^*_{\text{perp}}$ in **Scheme 1.12** does not conform to a real intermediate but rather a crossing point, i.e., a conical intersection between the lowest singlet excited-state and ground-state energy surfaces. At this point, two reaction valleys are generated, one of which leads to ring closing to the initial spirocyclic form and the other one to the formation of the *cis-cisoid* (**CCC**) ring-opened form, to be compared with **19**. The existence of this intermediate, usually called the X-form, was first proposed on the basis of the studies of the photochemistry of spiropyran in low-temperature matrices[38].

[*] Complete Active Space-Self Consistent Field

29

The solution dynamics of a series of indolinospiropyran were studied with picosecond and femtosecond transient electronic absorption spectroscopy. The first work in this series, preformed at picosecond time resolution, demonstrated that the coloured ring-opened photoisomers of spiropyran arose as soon as 15 ps after an exciting pulse. Of three characteristic times revealed in the kinetics of absorption formation and disappearance for indolinospiropyran, **18**, under excitation at 370 nm (150 fs), those in the ranges 50-100 ps and 1.3-1.7 ns were assigned to the relaxation of the cis-cisoid isomers to various possible merocyanine forms[39, 40]. The initial step of this reaction, associated with fission of the C_{spiro}-O bond, is even faster. For the 6-hydroxy derivative of indolinospirobenzopyran, **18**, [41], it takes less than 100 fs after excitation at 300 nm to form a metastable species **X,** for which an acoplanar cis-cisoid structure, corresponding to **19** [R = 6-OH] in **Scheme 1.12**, was assigned in accordance with the assumptions based on nano- and picosecond spectroscopic data. A minor fraction of **X** re-establishes the broken bond on the time scale of 200 fs, whereas the rest of the formed metastable species vibrationally relaxes in a few picoseconds and after this vibrational cooling converts to a mixture of merocyanine conformers with a decay time constant of about 100 ps. **Scheme 1.15** illustrates the principal scheme of the photochemical reaction described above.
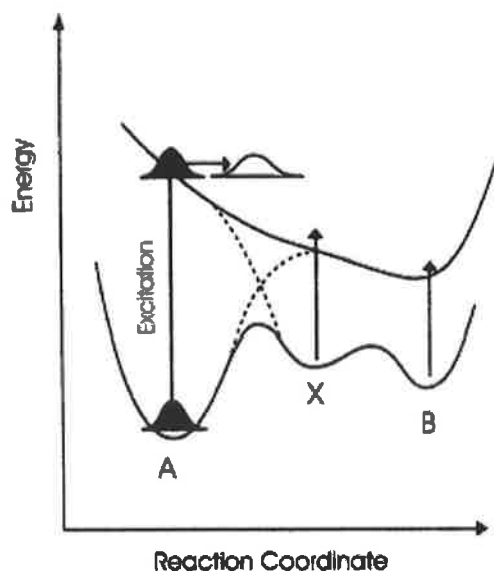
Scheme 1.15. Illustration of the photochemical reaction (**Scheme 1.1**) of a spiropyran in a wave packet picture. The adiabatic surfaces are represented by the solid curves, and the dashed lines indicate the diabatic surfaces. A and B correspond to ring closed and ring-opened (trans-merocyanine) isomeric forms, and **X** refers to the initial (presumably cis-cisoid) product formed after the C-O bond is broken. The reaction coordinate is considered as a combination of C-O stretching and rotation around a C-C bond of the molecule[42].

1.5 Mechanistic studies of spiropyran-derived merocyanine complexes with metal ions

Spiropyran forms complexes with certain d- and f-elements in solution. While the colour of a spiropyran in polar solvents originates from absorption of its merocyanine-type trans isomer, a marked blue shift is caused by complexation with the phenolate oxygen atom of the trans isomer. The type of metal ion only slightly influences the spectral properties of the complexes, in contrast to the relaxation time which can differ by one order of magnitude. For complexes with Co^{2+}, Ni^{2+} and Cu^{2+}, one may also expect an increase in fatigue resistance for spiro compounds from efficient excited state quenching due to intramolecular energy transfer to the lower positioned energy levels of the metal ions. Thus, complexation provides a possibility to influence the photochromic properties of spiro compounds. Gorner published a complete mechanism study into the complexation of metal ions in solution with derivatives of 6-NO_2-SP[43] (**Table 1.1**).
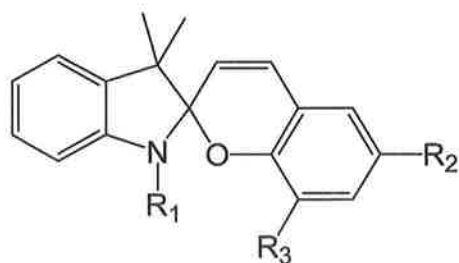
	R1	R2	R3
20	CH_3	NO_2	H
21	CH_3	NO_2	$CH_2CH=CH_2$
22	CH_3	NO_2	OCH_3
23	C_2H_4OH	NO_2	OCH_3
24	C_6H_5	NO_2	OCH_3
25	CH_3	H	OCH_3
26	CH_3	OCH_3	H

Table 1.1. Spiropyran derivatives analysed in metal ion study[43].

The properties of 6-NO$_2$-SP derivatives in solution are determined by the ground state equilibrium **Scheme 1.16** between the Sp form and the trans-merocyanine. The rate constants for **Scheme 1.16** are k$_1$ and k$_{-1}$ and the equilibrium constant is K$_1$ = k$_1$/k$_{-1}$. The absorption spectrum has two bands, e.g. that of 22 in acetonitrile has maxima at λ_{SP}356 nm and λ_{MC} 580 nm, referring to the spiropyran and trans-merocyanine form, respectively, see **Figure 1.5a**.
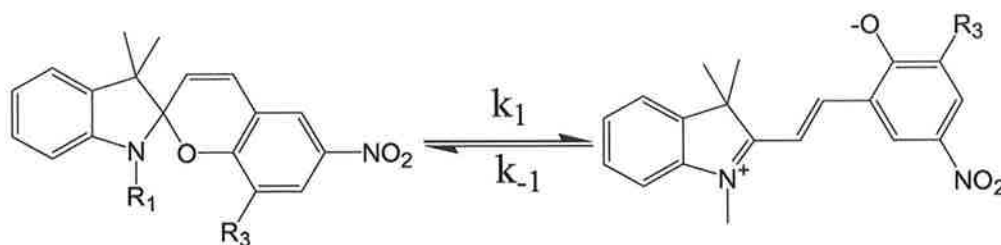
Scheme 1.16. Ground state equilibrium of spiropyran.

The molar absorption coefficients of the 6-NO$_2$-SPs at λ_{SP}=335–355 nm and λ_{MC} are ε_{SP}= (0.8–1.0)×10^4 M^{-1} cm^{-1} and ε_{MC} ≈ 4×10^4 M^{-1} cm^{-1}, respectively. K$_1$ is estimated using A$_t$/A$_{Sp}$, the ratio of absorbances at λ_{MC} and λ_{SP} and the ratio of the absorption coefficients ε_{SP}/ ε_{MC} = 0.25. For all cases examined, A$_t$/A$_{Sp}$ is relatively small (**Table 1.2Error! Reference source not found.**).
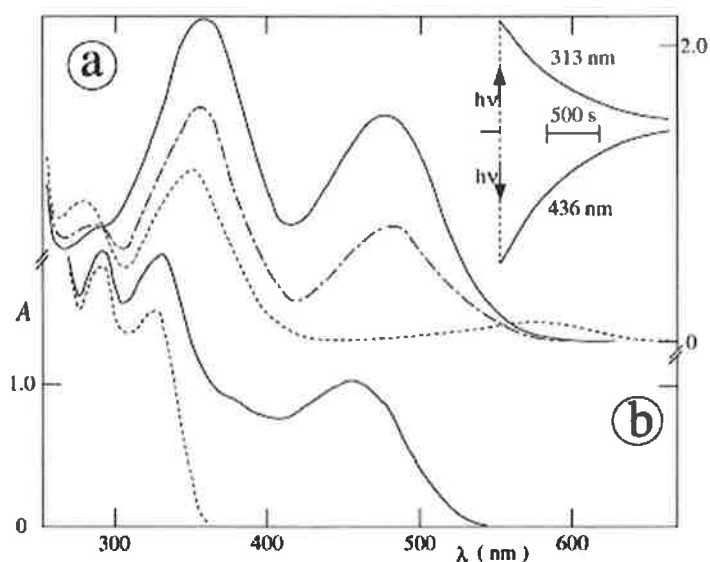
Figure 1.5. Absorption spectra in acetonitrile for (a) 22 in the absence of additives (- - -) and in the presence of 30 μM (—–) and 70 μM (——) Nd3$^+$ and (b) 26 for [Nd^{3+}] = 0.1 mM; inset: absorption changes at 480nm upon and after irradiation at 313nm (upper) and 436nm (lower)[44].

Compound	Solvent	λ_{MC} (nm)	A_{MC}/A_{SP}	$1/k_{-1}(s)$	$1/k_1(s)$
20	Acetone	565	0.03	80	1×10^4
	Acetonitrile	562	0.01	160	6×10^4
21	Acetone	598	0.12	60	2000
	Butyronitrile	595	0.12		
	Acetonitrile	595	0.26	50	770
22	Dioxane	600	0.02	30	6000
	Acetone	580	0.06	25	1700
	Butyronitrile	578	0.07	35	1750
	Acetonitrile	580	0.12	35	1200
23	Acetone	594	0.06	15	1000
	Acetonitrile	583	0.15	20	500
24	Acetone	605	0.01	12	4800
	Acetonitrile	595	0.02	15	3000
25	Acetonitrile	-	<0.01		
26	Acetonitrile	-	<0.01		

Table 1.2. Absorption λ_{max}, ratio of MC/SP absorbances, and ring opening (k_1) and ring closing (k_{-1}) kinetics.

Complex formation by irradiation of 6-NO$_2$-SPs involves the merocyanine cis and trans isomers. The photocolouration occurs via the trans triplet state (^{3}trans*), which is in equilibrium with the perpendicular triplet configuration (^{3}perp*). The proposed sequence after population of the excited singlet state is intersystem crossing at the Sp geometry, reaction (7), ring opening in the triplet manifold (8), establishment of equilibrium (9) between the trans and the perpendicular triplet configurations, intersystem crossing at the perpendicular configuration and internal rotation in the ground state to the cis and trans isomers, sequence (10). Thermal isomerization (12) yields the trans isomer, **Scheme 1.17**. The lifetime of the cis isomer of **20-24** in solution at room temperature is in the micro- to millisecond range. Colour formation is delayed due to the intermediacy of the observed triplet having a lifetime of 3–10 µs and accelerated in the presence of oxygen due to quenching reaction (11). The fraction of the ^{3}perp* state decaying into the cis isomer under these conditions (α′) only slightly differs from that (α) in the absence of oxygen.

$$\text{cis} + \text{M}^{n+} \longrightarrow \text{trans- M}^{n+} \qquad (2')$$
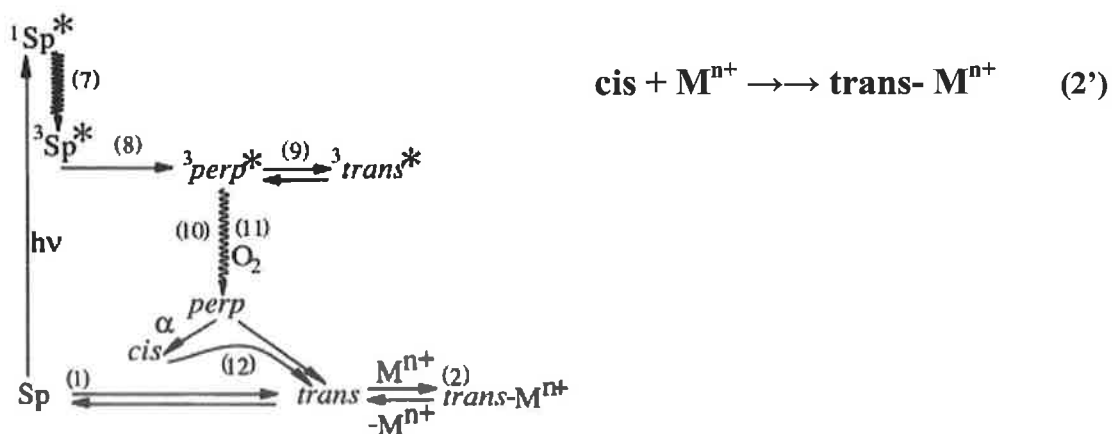
Scheme 1.17. Mechanistic scheme of metal-complex formation by irradiation of 6-NO$_2$-SP.[44]

Upon excitation of 20-24/M^{n+} (0.1/0.1 mM) in the absence of oxygen, the spectra after the end of the 308 nm pulse and within a few microseconds remain the same as without additive. After 10–100 μs this band at λ_{MC}= 560–600 nm is converted into a new band centered at 480 nm, as shown in **Figure 1.5a** for 22/Nd^{3+}.

The formation of complexes of 6-NO_2-SPs with metal nitrates in solvents of medium or higher polarity accompanies a major broad absorption band in the visible range (maximum: λ_{com}). A typical case is shown in **Figure 1.5a** for **22** in acetonitrile in the presence of Nd^{3+}, λ_{com} = 485 nm. The λ_{com} values are slightly specific for a given metal nitrate and rather independent of the choice of the 6-NO_2-SPs (**Table 1.3**) and, to a certain extent, of solvent (not shown). Only for Cu^{2+} in acetonitrile, but not in acetone, is λ_{com} further blue-shifted. For **25** and **26**, where almost no colouration occurs in the absence of metal ions, complexation also occurs in the presence of Nd^{3+}. The observed complex (trans-M^{n+}) is suggested to be due to coupled **Scheme 1.18** and **Scheme 1.19**, where $K_2 = k_2/k_{-2}$. Here, S is the organic solvent and m the number of molecules coordinated on the metal ion.

Scheme 1.18.

36
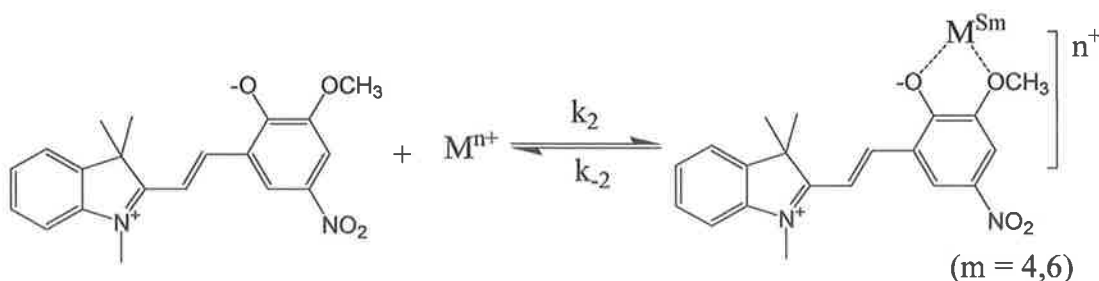
Compound	M^{n+}	λ_{com} (nm)	A_{com}/A_{Sp}
20	Nd^{3+}	485	0.03
21	Nd^{3+}	492	0.9
22	Mg^{2+}	490	0.2
	Mn^{2+}	492	0.4
	Co^{2+}	485	0.5
	Ni^{2+}	490	0.06
	Cu^{2+}	360	--[b]
	Zn^{2+}	468	0.8
	Cd^{2+}	495	0.3
	Pb^{2+}	478	0.7
	Y^{3+}	470	0.7
	Pr^{3+}	478	1.6
	Nd^{3+}	485	1.6
	Eu^{3+}	474	1.5
	Tb^{3+}	470	1.45
	La^{3+}	475	1.0
23	Mg^{2+}	490	0.3
	Ni^{2+}	475	0.3
	Zn^{2+}	468	0.9
	Pb^{2+}	478	0.7
	Nd^{3+}	485	1.64
24	Nd^{3+}	520	<0.03
25	Nd^{3+}	520	0.3
26	Nd^{3+}	460	0.6

[a] In air-saturated acetonitrile; [Sp] = 0.08-0.12mM and $[M^{n+}]$ = 0.10mM.
[b] Different complex than in the other cases.

Table 1.3. Absorption maximum, ratio of absorbances in the VIS versus UV and slow relaxation time of the complex.

When water is added to the **22**/Nd^{3+}/acetonitrile mixture, the absorption band at 480 nm decreases and a new band appears at 540 nm (**Figure 1.6a**), which originates from the non-complexed trans isomer.
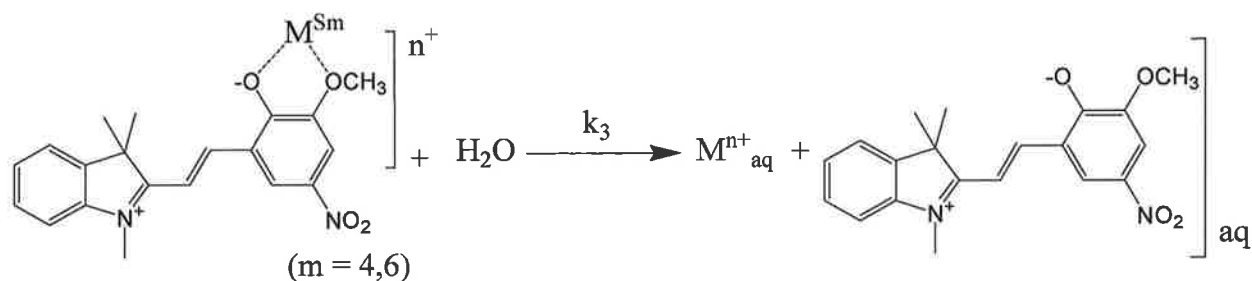
Scheme 1.19.
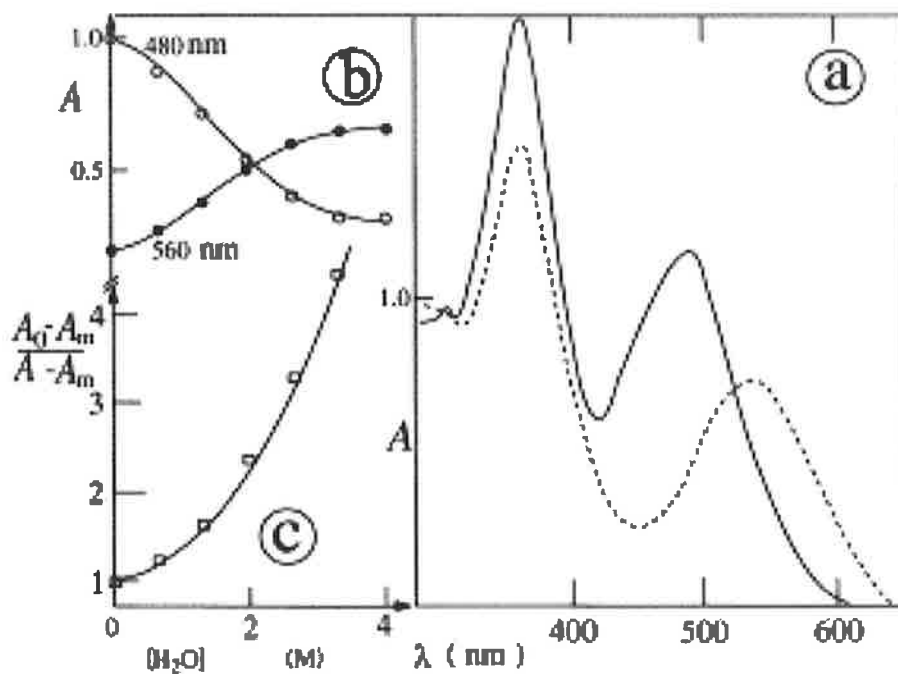
Figure 1.6. (a) Absorption spectra of 22 in acetonitrile in the presence of Nd^{3+} (0.10 mM) with $[H_2O] = 0.1$ M (——) and 4 M (---); (b) absorption changes at 480 ($\circ$) and 560 ($\bullet$) nm; and (c) $(A_o-A_m)/A-A_m$ as a function of water concentration.[44]

On the other hand, addition of water to **22** in acetonitrile (not shown) causes a blue-shift of λ_{MC} from 580 to 540 nm for 10% water and a ca. 10-fold increase in absorbance at λ_{MC}. Protonation is not the cause of these spectral changes since the zwitterionic form, when protonated at the phenolic oxygen, absorbs only below 450 nm.

38

The conclusion from this set of data is that complexation of spiropyran with metal ions in solution arises from two coupled reactions: (i) formation of merocyanine-type ligand and (ii) substitution of the solvent (coordinated at the metal ion) by the ligand. The overall rate of thermal complexation is limited by the rate of thermally activated ring opening, whereas the rate of light-induced complexation is determined by the rate of thermal substitution. For the trans isomer of 6-NO_2-8-OMe-SP as bidentate ligand the rate of complexation is limited by that of replacement of a solvent molecule. The decrease of the equilibrating complex concentration on addition of water is due to both ligand replacement in metal-complexed ion and non-complexed metal ions by water. This problem was dealt with in subsequent work, and will be discussed later.

For many applications related to the phenomenon of photochromism, it is important to have compounds that show photochromic properties in the solid state or in crystals, which helps to increase the lifetime of the photogenerated merocyanine isomeric form by retarding the dark back reaction and hindering the photodegradation pathways. Another way to enhance the stability of the coloured merocyanine isomers involves the inclusion of spiropyran into host polymer matrices[45], sol-gels[46], clays, zeolites, complexes with cyclodextrins[47], and self-assembled monolayers[25, 48]. Significant increases in the lifetimes of the merocyanines may also be achieved through complexation reactions of photo- or thermally induced polar merocyanine with metal cations. The complexation reactions of photochromic spiropyran have been successfully employed in the development of a new family of photodynamic chemosensors for metals ions[22, 28, 49]. There are many potential diverse applications for spiropyran and these will be discussed below.

1.6   Applications

Two general types of applications can be defined:

1. *Applications directly dependent upon the colour change caused by the molecular and electronic structures of the two species (A, B) and their corresponding absorption or emission spectra.*

Examples would be:

- Variable-transmission optical materials such as the photochromic ophthalmic lenses or camera filters;

- Fluid flow visualization;

- Optical information storage;

- Novelty items (toys, T-shirts, etc.);

- Authentication systems (security printing inks);

- Cosmetics

2. *Applications dependent upon changes in the physical or chemical properties that occur along with the more easily observed colour change during the photochromic reaction.*

Examples of such properties are conductivity, refractive index, electrical moment, dielectric constant, chelate formation, ion dissociation, phase transitions, solubility, and viscosity.

Examples include:

- Optoelectronic systems (semi-conductors modulated by photochromic pigments);

- Reversible holographic systems;

40

- Optical switches;

- Optical information storage;

- Photochemically switchable enzymatic systems;

- Nonlinear optical devices;

- Molecular actuation of swelling and contraction.

Due to the nature of this project, we focused on the applications that are dependent upon the changes in the physical and chemical properties of the spiropyran. The ability to control a binding event by photons was of particular interest to us and recent work that has emerged in this field will be discussed below. Spiropyran was reported as a photochromic chelating agent back in 1965[50]. Since then there have been major advances in terms of selectivity and sensitivity of metal ion binding. The following section is an introduction to spiropyran as a transducer in a chemosensor system for metal ion sensing.

1.6.1 Photoreversible metal complexation in aqueous solution

Winkler and Evans reported the first demonstration of rapid and reversible photoinduced switching of a quinolinospiropyranindoline-metal complex in aqueous solution[49, 51]. The ability to eject the metal ion photoreversibly in water is critical to the eventual application of these materials to sensor transducers operated in aqueous systems for environmental monitoring. The stabilization of the merocyanine isomer in aqueous media prevents the photoinduced ejection of the trapped metal ion. This work describes the molecular design issues critical to promoting photoreversible metal complexation for spirobenzopyrans in polar solvents, and the first demonstration of rapid and reversible, photoinduced

switching of metal complexation from a quinlinospiropranindoline-metal complex in aqueous media.

Two 8-hydroxylquinoline-derived spiropyranindolines **27a** (R = H) and **27b** (R = NO$_2$), which differ only by the addition of a nitro group *para* to the pyran oxygen, are shown in **Scheme 1.20**. While the denticity of 8-hydroxyquinoline for metal ions is well precedented, initial expectation was that the stability of the metal/merocyanine complex **29a** would prevent photoisomerization to **27a** with concomitant release of metal ion. Spirobenzopyran **27b** was, therefore, prepared to promote photoreversibility of metal complexation by withdrawing electron density away from the phenolate oxygen and decreasing the denticity of **28b**. Spirobenzopyran **27b** does indeed exhibit significant, photoreversible metal complexation in organic solvents with low polarity, such as tetrahydrofuran. Unfortunately, there is little to no observable reversibility in solvents of higher polarity, such as acetonitrile. The inability to achieve the conversion of **29b** to **27b** *via* irradiation can be explained by the enhanced stabilization of the zwitterionic merocyanine form, **28b**, by the nitro group, which serves to delocalize the phenoxide anion in **28b**. This stabilizing effect of the nitro group in **28b** is underscored by the rapid conversion of **27b** in the dark to the colored, merocyanine form **28b** in solvents with dielectric constants higher than that of tetrahydrofuran. Ultimately, the lifetime of any free zinc ions ejected into solution is significantly attenuated due to the rapid recomplexation event, **28b**→**29b**. The thermodynamic stability of the closed quinolinospiropyranindoline, **27**, must be enhanced to promote photoreversibility of metal complexation of **29** in polar solvents.
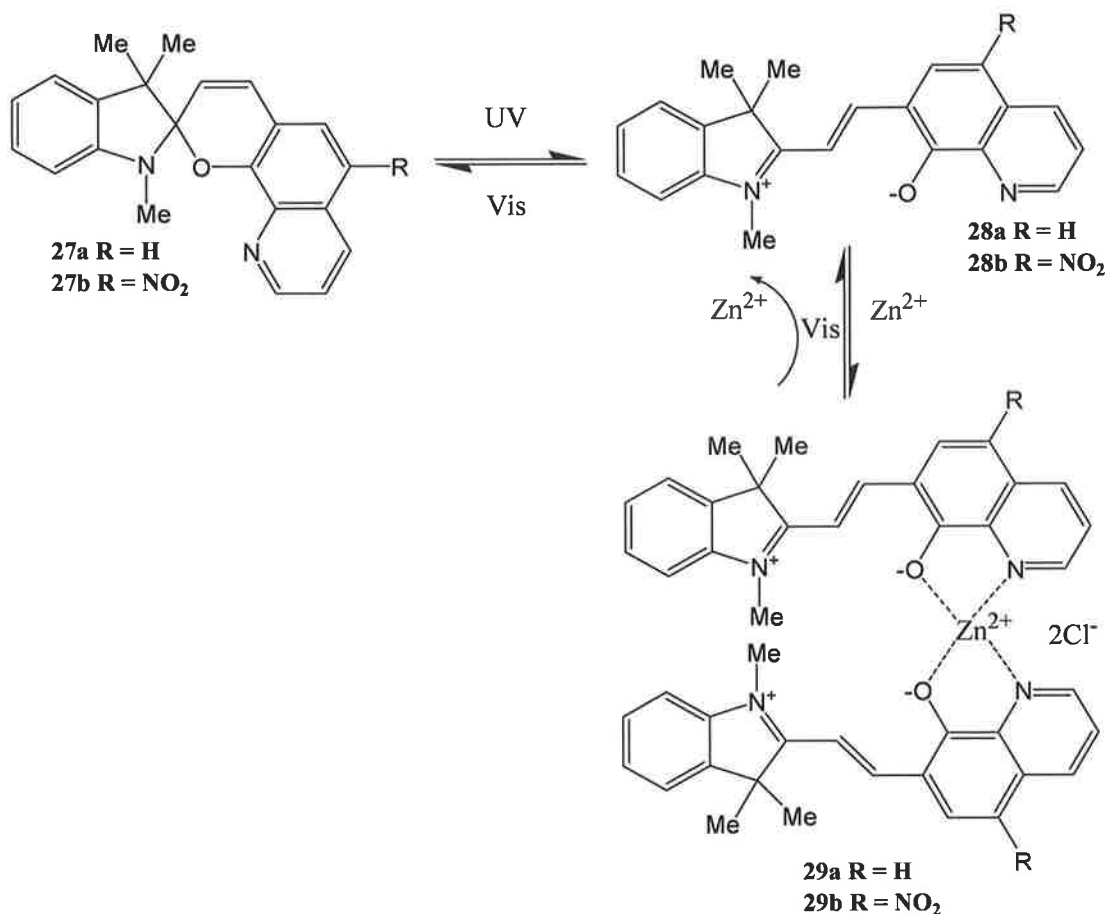
Scheme 1.20. Photoreversible equilibria of quinolinospiropyranindoline (27a, R = H) and nitroquinolinospiropyranindoline (27b, R = NO₂).

The simplest way of doing this is to remove the nitro group *para* to the phenoxide anion, as in **27a**. Evidence for the improved stability of **27a** relative to **27b** is apparent from the colourless solution, indicative of the closed spiropyran, obtained for **27a** in acetonitrile (2.4 x 10⁻⁵M; **Figure 1.7a**). The dark addition of 0.5 equivalents of Zn^{2+} to this solution of **27a** in acetonitrile (**Figure 1.7b**) results in the formation of a bright red complex **29a**, with Zn^{2+} in a 2 : 1 ligand : metal ratio, based upon stoichiometric determinations using the molar ratio absorbance method. Exposure of a solution of **29a** in acetonitrile to visible

light (150 W tungsten flood lamp) causes the temporary ejection of the complexed metal ion, and a transition to the colourless, closed form of the quinolinospiropyranindoline (29a→27a). Evidence for this shift is shown in **Figure 1.7**, which shows the effect of exposure of a solution of **29a** to visible light as a function of time.
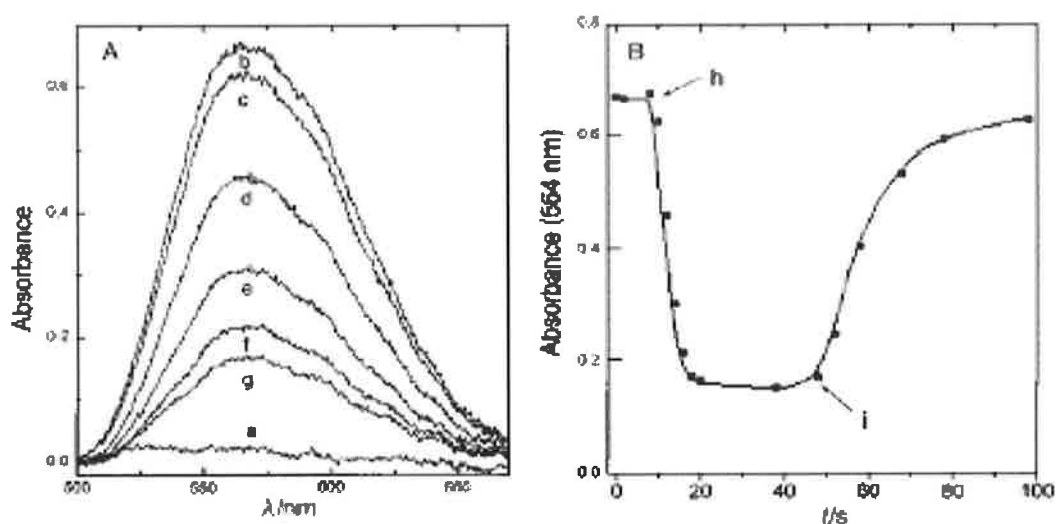
Figure 1.7. (**A**) UV–VIS spectra of 2.4×10^{-5}M 27a in acetonitrile with (a) no Zn^{2+} added; (b) 1.2×10^{-5}M Zn^{2+} added; and solution (b) after exposure to visible light for (c) 2, (d) 12, (e) 14, (f) 16, (g) 20 s. (**B**) Switching behaviour observed in the absorbance intensity at 564 nm with visible light on at 8 s (h) and off at 48 s (i).[52]

The photochemically mediated ejection of the metal ion from **29a** is fast, with an 8 s response time following the onset of visible light irradiation (**Figure 1.7B**). Immediately following the cessation of light, the free metal ion is quickly re-complexed (50s time response) as the equilibrium shifts back to its original state (27a→29a). In contrast, ejection of Zn^{2+} ion from a solution of **29b** in acetonitrile upon irradiation with visible light is minimal (14%), a result which can be ascribed to the enhanced stability of **28b** in

44

polar solvents, as described above. This rapid switching behavior in the metal complexation properties of spiropyranindoline **27a** is an important step toward the development of molecular devices and sensors. In conclusion, a rapid, switching type mechanism for photoreversible metal complexation by quinolinospiropyranindoline **27a** in aqueous solution has been demonstrated.

1.6.2 Reversible fluorescent metal ion sensors

The spectroscopic study of spiropyrandinolines that function as sensors for metal ions in the parts per billion range was reported by Winkler[28]. These systems operate by either photochemically or chemically induced reversible formation of merocyanine metal ion complexes. Previously, merocyanine metal ion complexes were detected by molecular absorbance, but in this paper the metal complex was observed by fluorescence.

Minimal fluorescence at 610 nm is observed with a 10^{-5} M ethanolic solution of quinolinespiropyranindoline (SP) **27a** upon excitation at 550 nm, the absorbance maximum of the merocyanine (MC) **28a**, a result that is consistent with the predominance of **27a** in the absence of exogenous metal ion or UV light (**Scheme 1.20Error! Reference source not found.**). Addition of 1 equiv of $ZnCl_2$ to the solution of **27a** and excitation at 572 nm (the absorbance λ_{max} of chelate **29a** in ethanol where $M^+ = Zn^{2+}$) led to a 14-fold increase in emission intensity at 610 nm, **Figure 1.8**. Similar effects have been observed with other divalent and trivalent cations, and results are summarized in **Figure 1.9**.

45
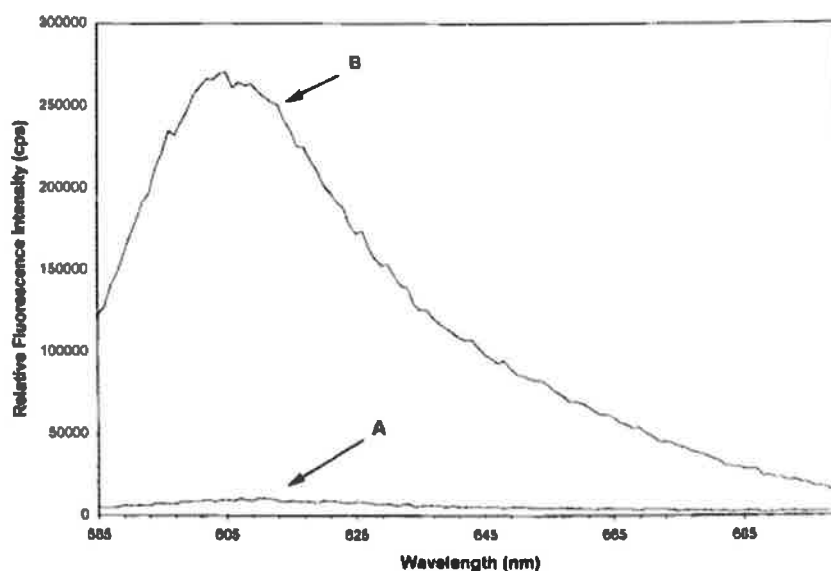
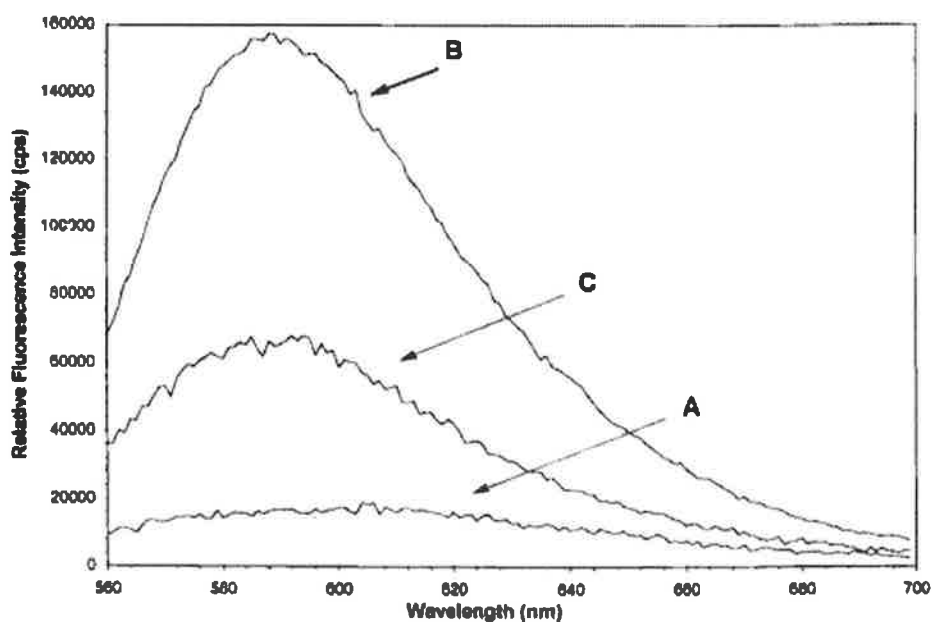**Figure 1.8.** Fluorescence emission spectra of spiropyran **27a** (10^{-5}M ethanol, room temperature): (A) emission of 'metal free' solution; (B) emission after addition of 1 equiv of $ZnCl_2$.[28]
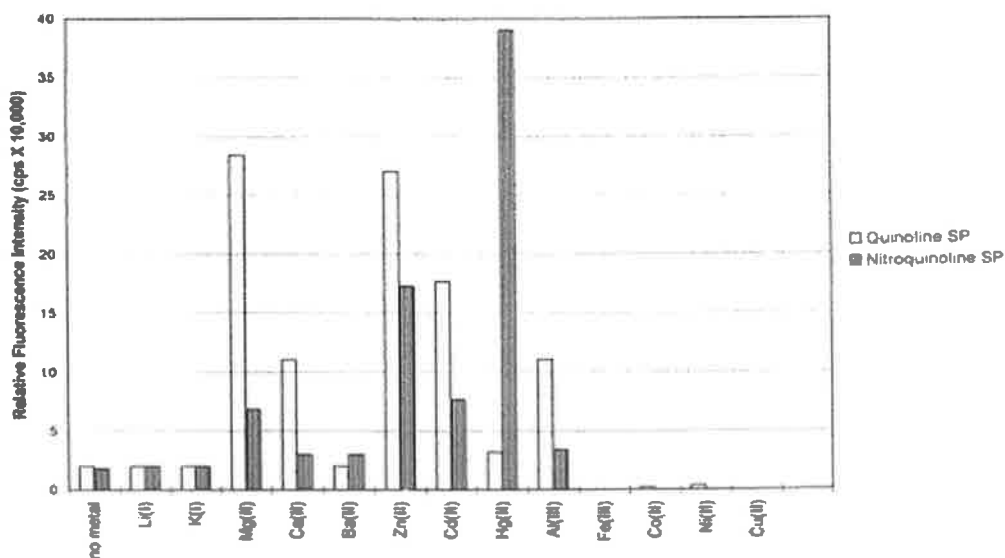
Figure 1.9. Relative fluorescence emission intensities of **27a** (10^{-5} M in benzene) at room temperature for 'metal-free' solutions and these spiropyran in the presence of several metal chlorides[28].

46

This dramatic increase in fluorescence intensity is due not only to an increase in the concentration of **29a** but also to the coordination of metal ion by the fluorophore. While the changes in the absorbance maxima of an ethanolic solution of **28a** at 550 nm upon addition of 1 equivalent of $ZnCl_2$ to form **29a** at 572 nm are small, the changes in the fluorescence emission intensities are dramatic. These results are consistent with data reported for metal-bound and metal-free 8-hydroxyquinoline and have been recently attributed to the role of the metal cation in inhibiting photoinduced tautomerization of the 8-hydroxyquinoline moiety which leads to nonradiative deexcitation[53]. Emission in **29a** (metal-bound) is enhanced relative to **28a** (metal-free) when the pathways for radiationless relaxation of the excited state available to **28a** are no longer available in the Zn^{2+}-chelated species **29a**.

The magnitude of the fluorescence enhancement of **27a** in the presence of Cd^{2+}, another group IIb metal ion, is smaller than that observed with Zn^{2+}, which could be attributed to the larger size of Cd^{2+} relative to Zn^{2+}. The formation of chelates of **29a** with other transition metals (Cu^{2+}, Ni^{2+}, Co^{2+}, and Fe^{3+}) can be monitored by an increase in the long-wavelength absorbance maxima. For example, addition of 1 equiv of $CuCl_2$ to an ethanolic solution of **27a** results in a blue shift of the absorbance maximum and an increase in the absorbance value at 548 nm. In the Cu^{2+} chelate of **29a**, the proximity of the paramagnetic metal ion to the unpaired electrons of the ligand leads to spin-orbit coupling and intersystem crossing, resulting in complete quenching of fluorescence emission from the **29a** chelate. Similar effects were observed with Ni^{2+}, Co^{2+}, and Fe^{3+}.

While irradiation of metal chelate **29a** ($M^+ = Zn^{2+}$) did not liberate metal ion with regeneration of **27a**, the liberation of the metal ion could be achieved chemically, i.e. by addition of 1 equiv of nitrilotriacetic acid, $N(CH_2CO_2H)_3$, which sequesters the metal ion, liberating the closed spiropyran **27a**. The chemically regenerated **27a** can then be recycled for another metal ion binding event. While this result demonstrates that the metal binding is chemically reversible, it does not establish the facile photochemical reversibility that was characteristic of earlier studies with the piperidinomethyl spiropyran **27b** ↔ **29b** (**Scheme 1.20**).

It was proposed the phenolate in **29a** (**Scheme 1.20**) was a better ligand for the metal ion than *p*-nitrophenolate **29b** (**Scheme 1.20**). The *p*-nitro group withdraws electron density from the phenolate oxygen, decreasing the denticity of **29b** and thereby facilitating reversible binding. In contrast to the modest absorbance bands (554 and 592 nm) that were observed with ethanolic solution of **27a**, strong absorbance at 560 nm was observed with an ethanolic solution of the nitro-quinolinespiropyran **27b**. The introduction of the nitro substituent shifts the spiropyran ↔ merocyanine equilibrium in polar solvents such as ethanol to favour the open form **28b**. In less polar solvents, i.e. benzene or ethyl acetate, the predominant form is **27b**. Like spiropyranquinoline **27a**, the fluorescence emission of **27b** is also sensitive to group IIb and several other transition metals but inert to alkali metal chlorides (**Figure 1.9**). However, unlike **27a**, **27b** is also relatively inert to alkaline earth cations.

Addition of 1 equivalent of $ZnCl_2$ to a benzene solution of **27b** resulted in a 9-fold enhancement of fluorescence emission (**Figure 1.10**). The magnitude of this increase in relative intensity is less than that observed with **27a**. Likewise, only a 3-4 fold increase in emission intensity of **29b** was observed upon addition of 1 equivalent of $MgCl_2$ or $CdCl_2$. These differences may be due simply to the reduced chelating ability of the nitrated hydroxyquinoline chromophore. The metal ion binding constants of 5-nitro-8-hydroxyquinoline are typically lower than those of 8-hydroxyquinoline. It is interesting to note that $HgCl_2$ does not follow the trend exhibited by other group IIb metals.

Figure 1.10. Fluorescence emission spectra of spiropyran **27b** (10-5M benzene, room temperature): (A) emission of 'metal free' solution; (B) emission after addition of 1 equiv of $ZnCl_2$; (C) emission after 30s of irradiation with visible light. [28]

A nearly 20-fold increase of emission intensity of **29b** was observed upon addition of 1 equiv of $HgCl_2$. The ejection of metal ion from **29b** occurs upon brief irradiation of the Zn^{2+} chelate with visible light. Rapid dissociation of approximately 60% of the

fluorescent Zn^{2+} chelate **29b** accompanied by regeneration of **27b** occurs with expulsion of the metal ion (**Figure 1.10**). The regenerated spiropyran is fully functional and has been run through 10 cycles of metal binding-release without detectable fatigue.

It was mentioned at the end of this article that these materials were currently being covalently immobilised to fibre optic surfaces which could lead to a practically useful metal-ion sensing device. As no publications have been reported since regarding this comment, it must be concluded that this application failed to materialise.

1.6.3 Metal complexation in polymer matrices containing spiropyran

When developing devices based on photochromism of spiropyran one of the crucial issues is to choose a solid host that allows the photochromic reactions to occur at the same rate and efficiency as those found in solution. Generally, the fast response to light exposure is no longer achievable when spiropyran are adsorbed on solid matrices or supports. The response time varies depending on the type of materials used. An ideal support should be inert, not alter the course of the photochromic reaction and permit the remarkable conformational changes induced during the photochromic reaction. In addition, the adsorption of the photochromic molecule should not compromise the mechanical properties of the material support. Glasses, sol–gel derived materials and polymers have been the preferred solids to study the photochromism of spiropyran. There have been many publications reporting the properties of spiropyran within these materials.

Suzuki and co-workers[54] reported the first metal complexation with an insoluble photochromic spiropyran co-polymer. They describe the photoreversible Pb^{2+}-complexation for a synthetic spiropyran methacrylate (SPMA) in polar solvents (mixtures of methanol and water). Furthermore, they illustrate the first demonstration of reversible photo-induced Pb^{2+}-complexation of an insoluble copolymer consisting of SPMA and perfluorooctylhydroxy methacrylate (FHMA), P(SPMA-FHMA) **Figure 1.11**, in aqueous solutions.
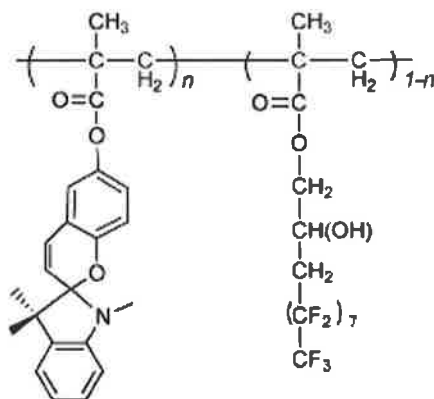
Figure 1.11. Molecular structure of P(SPMA-FHMA).

As shown in **Figure 1.12(A)**, the absorption spectrum of a solution of SPMA in CH_3OH–H_2O (9: 1 v/v) in the dark exhibited a purplish-blue band ($\lambda_{max} = 560$ nm) that is attributable to the open form of SPMA. Solutions of SPMA in toluene or THF did not exhibit any absorption bands in the visible regions. Results indicate that the open form of SPMA was stabilized in polar environments. Addition of a tenfold molar excess of $Pb(ClO_4)_2$ into the solution resulted in the appearance of a yellow band ($\lambda max = 435$ nm) in the dark, as shown in **Figure 1.12(B)**, along with the disappearance of the 560 nm band. These changes in the absorption spectra suggest the generation of a different open

form of SPMA, which could be the Pb^{2+}-complex. Subsequently, as shown in **Figure 1.12**(C), the yellow band disappeared upon irradiation with visible light (> 420 nm). The 435 nm band appeared again in the dark, and attained the same absorbance as spectrum (B) in the equilibrium. Stabilization of the open form of SPMA in polar solvents did not prevent the photo-induced ejection of the complexed Pb^{2+} ions.
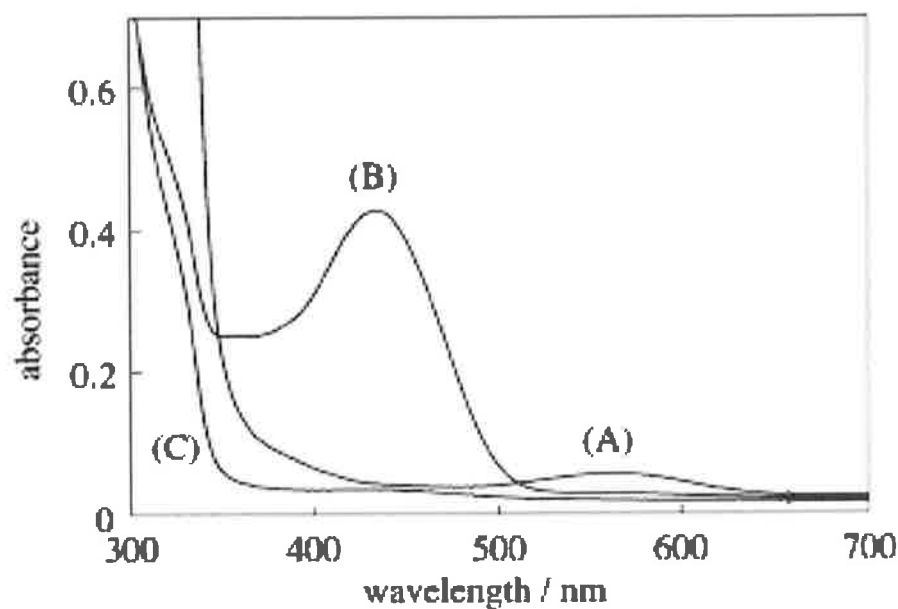
Figure 1.12. Absorption spectra of a CH$_3$OH-H$_2$O (9:1v/v) solution of SPMA. (A): [SPMA] = 0.5M, (B): [SPMA] = 0.1M, [Pb(ClO$_4$)$_2$] = 1.0mM, (C): same solution as (B), measured under visible irradiation. [54]

Although P(SPMA) was insoluble in methanol and water, the polymer became soluble after addition of Pb(ClO$_4$)$_2$. The resulting solution showed an absorption band (λmax = 435 nm), which was identical to spectrum (B) in **Figure 1.12**. In contrast, P(SPMA-FHMA) was completely insoluble in methanol and water, even after complexation with Pb^{2+} ions. The color of the solid P(SPMA-FHMA) in H$_2$O–CH$_3$OH (8 : 2v/v) changed as follows:

1) It existed as purplish-blue in the dark, as shown in **Figure 1.13**(A);

2) Upon addition of Pb^{2+} ions, started turning yellow, initially at the surfaces of the solid, as shown in **Figure 1.13**(B);

3) After diffusion of the Pb^{2+} ions into the solid, turned completely yellow, as shown in **Figure 1.13**(C);

4) Upon irradiation of visible light, although the interior was still yellow, the surface of the solid turned white, as shown in **Figure 1.13**(D).

The white color of the solid is attributable to the closed form of the SPMA portion (15 mol%) and the FHMA portion (85 mol%) of P(SPMA-FHMA). Moreover, the solid turned yellow again in the dark. Removal of the ejected Pb^{2+} in the solution upon irradiation with visible light resulted in the purplish-blue solid of P(SPMA-FHMA) in the dark as observed in **Figure 1.13**(A).
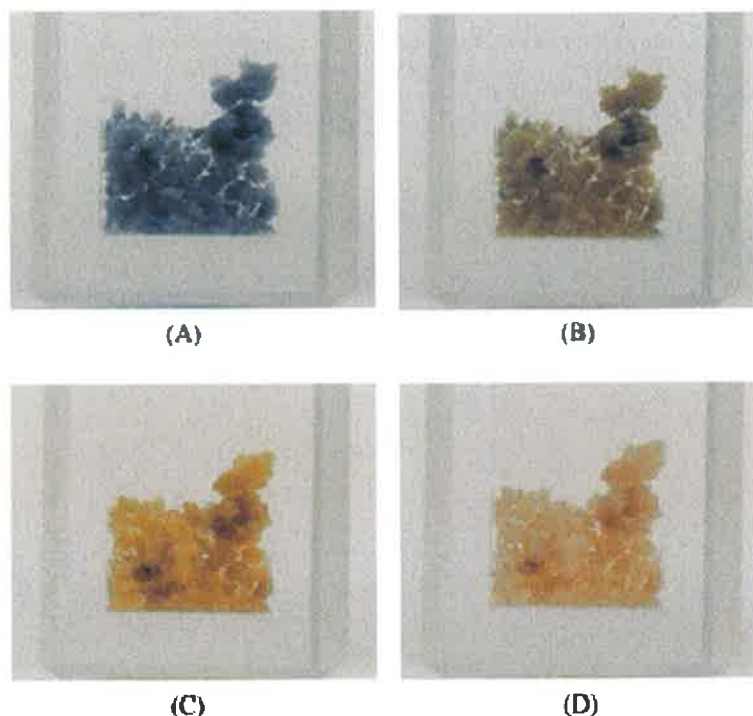
Figure 1.13. Colour changes of solid P(SPMA-FHMA) in H_2O-CH_3OH (8:2 v/v): (A) in the dark, (B) 15s after addition of Pb(ClO$_4$)$_2$, (C) a minute after addition of Pb(ClO$_4$)$_2$, (D) for a minute under visible light irradiation.[54]

Suzuki recognized the problem of removing the metal ion once the measurement was taken was essential for realization as a sensing device. As complete removal of the metal ion was not observed for the P(SPMA-FHMA), it was evident a new polymer system was required. In 2004, Suzuki[55] published the photo-reversible Pb^{2+}-complexation of a thermosensitive copolymer consisting of N-isopropyl acrylamide (NIPAAm) and a synthetic spiropyran acrylate (SPAA), **38 (Figure 1.14)**, in water. Poly(N-isopropyl acrylamide), P(NIPAAm), is thermosensitive in water showing a lower critical solution temperature (LCST). Above the LCST, the aqueous solution generates a solid polymer and separates into two phases. A thermosensitive copolymer that displays such phase

transition behavior at the LCST is attractive for use as a metal-ion adsorbent. Above the LCST, the solid phase, containing bound metal-ions, can be easily separated from solution. However, because the solid phase forms a transparent solution below the LCST, it is easy to subsequently recover these metal-ions from the copolymer by irradiation with visible light.
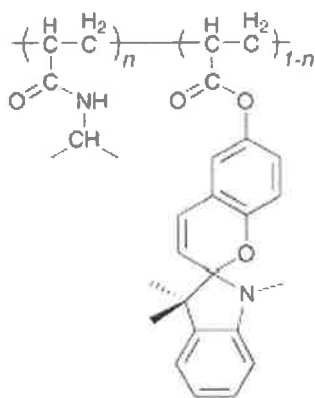
Figure 1.14. Copolymer of N-isopropyl acrylamide (NIPAAm) and a spiropyran acrylate (SPAA) **38**.

An aqueous solution of **38** was prepared by adding **38** to water (pH ~ 7.0) at 5 °C, below the LCST (29 °C). The absorption spectrum of the purplish-red solution shows a strong band at 533 nm, **Figure 1.15**(A), attributed to the open form of the SPAA unit. This band is photobleached by irradiating with visible light (>420 nm), but reappears on standing in the dark. Solutions of **38** in non-polar THF or polar acetonitrile, kept in the dark, do not exhibit absorption bands in the visible. Clearly, the open form of the SPAA unit is stabilized in the more polar water environment. Absorption measurements after addition in the dark of a tenfold molar excess (relative to the SPAA unit) of $Pb(ClO_4)_2$ revealed a band at 433 nm **Figure 1.15**(B) along with the almost complete disappearance of the 533

nm band. These changes suggest the generation of a different open form of the SPAA unit, which is thought to be the Pb^{2+}-complex. **Figure 1.15**(C) shows the complete disappearance of the 433 nm band upon subsequent irradiation with visible light. This band reappeared after standing in the dark, attaining the same absorbance as spectrum (B) under equilibrium conditions.
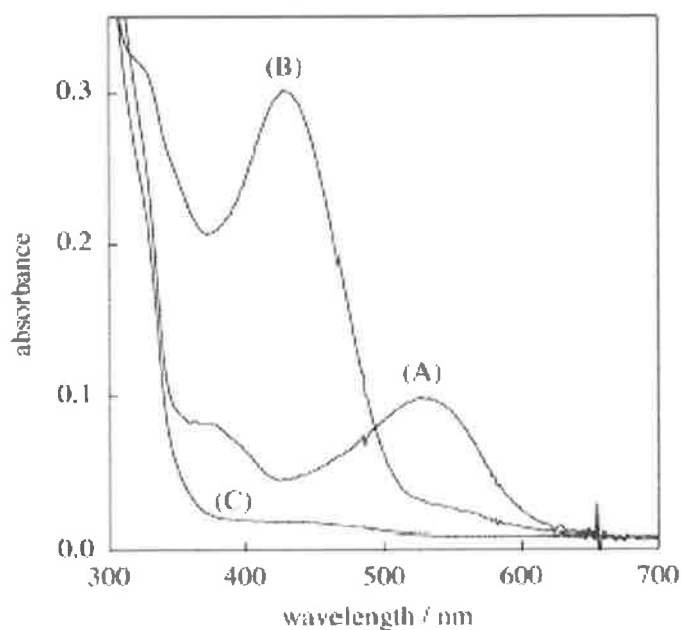
Figure 1.15. Absorption spectra of aqueous solution of 38 at 5°C. (A) 0.04wt% of 38 ([SPAA unit] = 0.1mM). (B) Solution after addition of $Pb(ClO_4)_2$ (1.0 mM) to solution (A). (C) The same solution as used in (B) measured under visible light irradiation. [55]

Thus, stabilization of the Pb^{2+}-complexed open form in an extremely polar solvent such as water did not prevent isomerization to the closed form under visible light. The complexed Pb^{2+} ions were subsequently liberated by shifting the equilibrium of the SPAA unit. The transmittance of an aqueous solution of **38** suddenly decreased as temperature increased due to the thermosensitive NIPAAm units, which exhibited an

LCST at 29 °C, as shown in **Figure 1.16**. The increase in hydrophobicity of **38** would result in a lower LCST than that of the P(NIPAAm) homopolymer (32 °C). Pb(ClO$_4$)$_2$ at a concentration of 1mM did not influence the LCST of the solution.
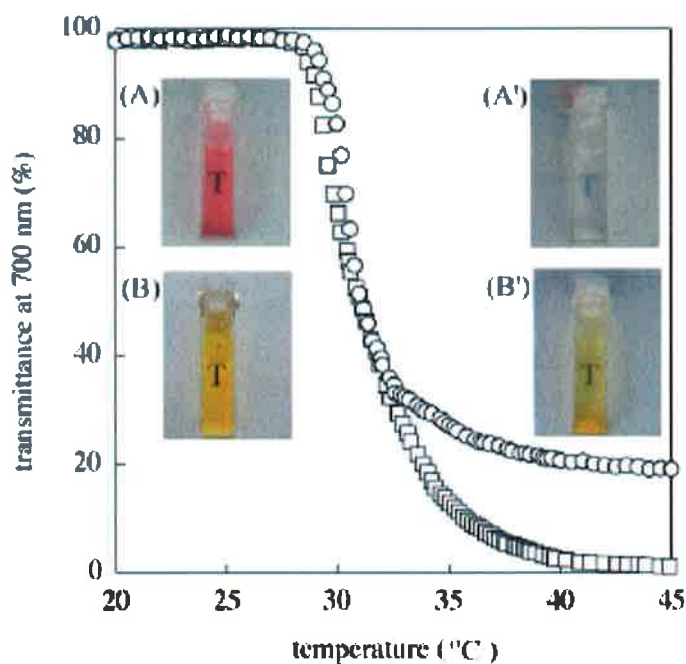
Figure 1.16. Temperature dependence of optical transmittance of aqueous solution of 38, measured in the dark at a rate of about +1 °C min^{-1}. (O) 0.04 wt% of 38 in water, (□) addition of Pb(ClO$_4$)$_2$ (1.0 mM, [Pb^{2+}]:[SPAA unit] = 10:1) to the solution of 38 (0.04 wt%). *Inset: color changes of 38 in water. 0.23 wt% of 38 at 10 °C (A) and at 40 °C (A').* *0.23 wt% of 38 and Pb(ClO$_4$)$_2$ (5.0 mM) at 10°C (B) and at 40 °C (B').The letter 'T' was placed behind the cuvette (thickness 1cm) in order to confirm the transparency of the solution.*[55]

At temperatures above the LCST, **38** precipitated in water, as shown in **Figure 1.16**(A') and (B'). The dehydration of the copolymer chain of **38** above the LCST may result in

closing of the open form of the SPAA unit, followed by the appearance of a white precipitate of (A'). This supports the suggestion that water thermodynamically stabilizes the open form of the SPAA units. In contrast, for the Pb^{2+} solution a yellow precipitate of **38** was obtained above the LCST, **Figure 1.16** (B').

The major step from solution to solid phase detection of metal ions was significant and Suzuki's work has shown a possible approach for the eventual integration of spiropyran derived polymers as transducers in a chemosensing platform. But some work needs to be done before this can be realized. Specifically; (1) the need for a solid state sensing platform, polymer is immobilized to platform, (2) the ability for the polymer to expel all metal ions through irradiation with visible light, and (3) the need for a low-cost optical device to achieve efficient photo-switching between both isomers, unlike the lasers and powerful light sources that are used in the work presented above.

2.0 Spectroscopic study of BSP-MC equilibrium

2.1 Introduction

Interest in the photo- and thermo-chromic effects in benzospiropyran (BSP), **Scheme 2.1**, has gained much renewed attention over the last decade due to its attractive properties and transformations[14]. BSP can exist in two thermodynamically stable states and is capable of interconversion between the two states under various external stimuli. This ability to reversibly switch the molecular form has led to great interest for applications such as light-sensitive eyewear[10], information recording and processing[13], optical memory[39], molecular devices[30, 56], and optical sensing [57-59].
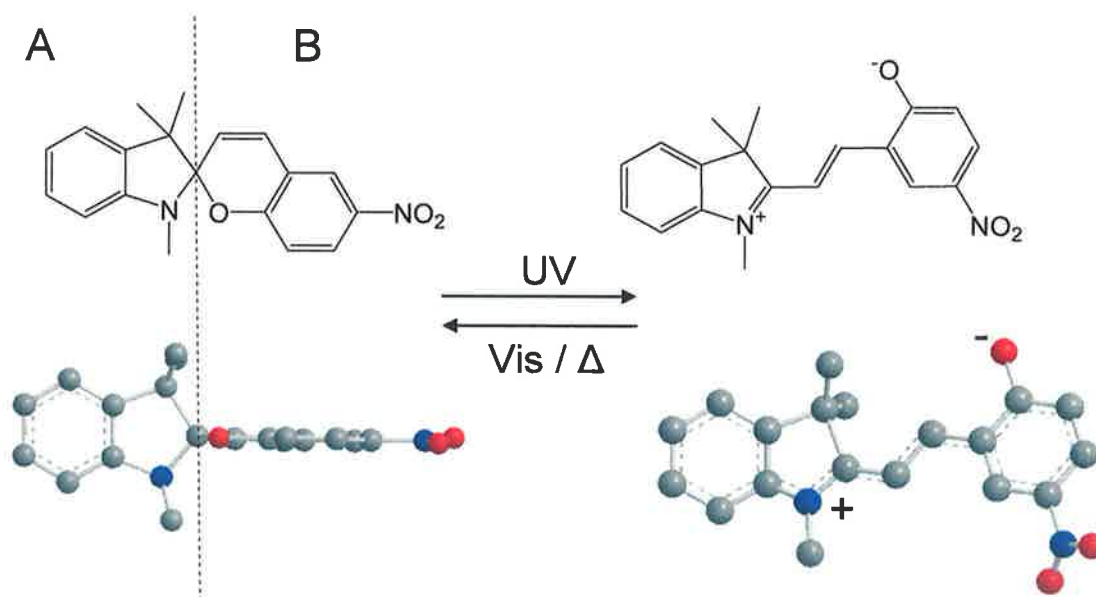
Scheme 2.1. Structure of benzospiropyran in 2D (above) and 3D (below) format, BSP (left) and MC (right) isomers.

BSP consists of two heterocyclic moieties linked together by a common tetrahedral sp^3 carbon atom. The two halves of the molecule are in two orthogonal planes (A and B),

Scheme 2.1. The benzopyran part (B) is the common structure to all spiropyran compounds, and the heterocyclic part (A) is built upon a benzofused azaheterocycle. BSP undergoes a heterocyclic ring cleavage at the C-O spiro bond that results in the formation of a planar, zwitterionic and highly conjugated chromophore that absorbs strongly in the visible region, this being the merocyanine isomer (MC).

Scientifically this simple reaction presents a rather complex puzzle. Not only is there the issue of whether singlet and triplet states both are involved,[36, 60] but also the product can appear as eight different cis–trans isomers[61]. On top of that the merocyanine product can aggregate[62, 63]. The merocyanine thermally reverts back to the BSP isomer following first order kinetics[60]. The BSP↔MC isomerization can reveal a significant amount of information about its surrounding molecular environment (i) at equilibrium an estimate of polarity can be calculated from the value K_e, the population of non-polar BSP versus the highly polar MC, (ii) the MC isomer exhibits a large negative solvatochromic shift with increasing polarity, (iii) the MC isomer possesses a large polarizable π-electron system, suitable for the registration of dispersion interaction, (iv) the phenolate oxygen on the MC exhibits a highly basic EPD (electron pair donor) centre, suitable for interaction with hydrogen bond donors and Lewis acids, an example is the coordination with the metal ion Co^{2+}, also (v) the thermal isomerization of MC to BSP is dependent on all of the above, an example is the interaction of amino acids at the complimentary binding sites on the MC retarding the thermal back reaction.

Before the photochromic moiety can be incorporated into an application, this dynamic equilibrium must be studied. This chapter describes a solution phase study of the solvato-

, thermo- and photochromic reactions of BSP in various molecular solvents using spectroscopic techniques such as UV-vis, fluorescence, and NMR. Two case studies are discussed at the end of this chapter, detailing an aggregation study of a BSP derivative and an unexpected result observed upon thermal irradiation of BSP in the molecular solvent DMSO.

2.2 Results and Discussion

2.2.1 UV-vis spectroscopy

Like other merocyanines, the MC, or BSP 'open form', is a negative solvatochromic dye[14], i.e. with increasing solvent polarity; the absorption band undergoes a hypsochromic (or blue) shift. The effect of the solvent on the electronic spectra has been investigated previously and it has been shown that, when the absorption maxima of MC (expressed in wavenumbers) or the transition energies are plotted against solvent polarity parameters such as ET(30) values[64], Kosower's Z values[65], Brooker's Xb values[66] and Brownstein's values,[67] reasonably linear plots are obtained. In addition to the solvatochromic effect, it has also been shown that changes in the absorption maxima, the intramolecular Lewis acid-base equilibrium between BSP and MC, and the thermal relaxation rates of MC back to BSP are intrinsically solvent dependent.[68]

The physical properties of BSP in solution are determined by the ground state equilibrium, between the BSP and MC form. In determining the equilibrium constants K_e, **Equation 2.1**, it was required that the samples were kept in the dark at 20 °C for 15 hours to reach equilibrium.

At equilibrium, from Beer's law, we have

$$K_e = \frac{[MC]}{[BSP]} = \frac{A}{3.5x10^4 \; x \; C - A}$$

Equation 2.1.

where K_e is the equilibrium constant between BSP and MC, A is the equilibrium absorbance at the absorption maximum, C is the total concentration of BSP initially dissolved and $\varepsilon_{MC} = 3.5 \times 10^4 \; M^{-1}cm^{-1}$ for the MC form of BSP according to Flannery.[69] K_e indicates the type of environment in which the BSP molecule resides, as this thermal equilibrium between the BSP and MC is affected by the change in solvent polarity; polar solvents promote the formation of the coloured (MC) form and non-polar solvents promote the formation of the colourless (BSP) form. **Table 2.1** consists of ground state equilibrium and the photo-physical properties of MC in various molecular solvents. The large solvatochromic shift of the λ_{max} of MC isomer stems from the differential solvation of its highly dipolar electronic ground state ($\mu_G = 15\text{-}18$ D) and its considerably less dipolar first excited state ($\mu_E = 8.4\text{-}11.7$ D), as illustrated in **Figure 2.2.2**. With increasing solvent polarity, the dipolar ground state is more stabilized by solvation than the less dipolar Frank-Condon excited state. As a result, the long-wavelength solvatochromic, intramolecular CT absorption band is hypsochromically shift from $\lambda_{max} = 605$ nm in hexane to $\lambda_{max} = 518$ nm in a binary solution of ethanol: deionised water. Since the solvatochromic absorption band of MC lies within the visible region of the spectrum, a visual estimate of solvent polarity can often be made, for example the MC isomer in methanol is red and in toluene is blue, see **Figure 2.1**.
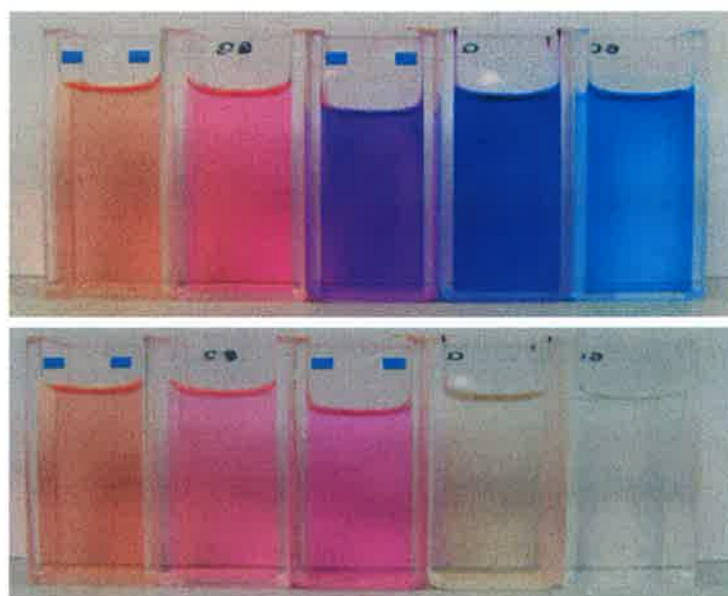
Figure 2.1. Photograph of MC (top) and BSP(below) in various solvents. From left to right; ethanol-10% H_2O, methanol, chloroform, THF and toluene.
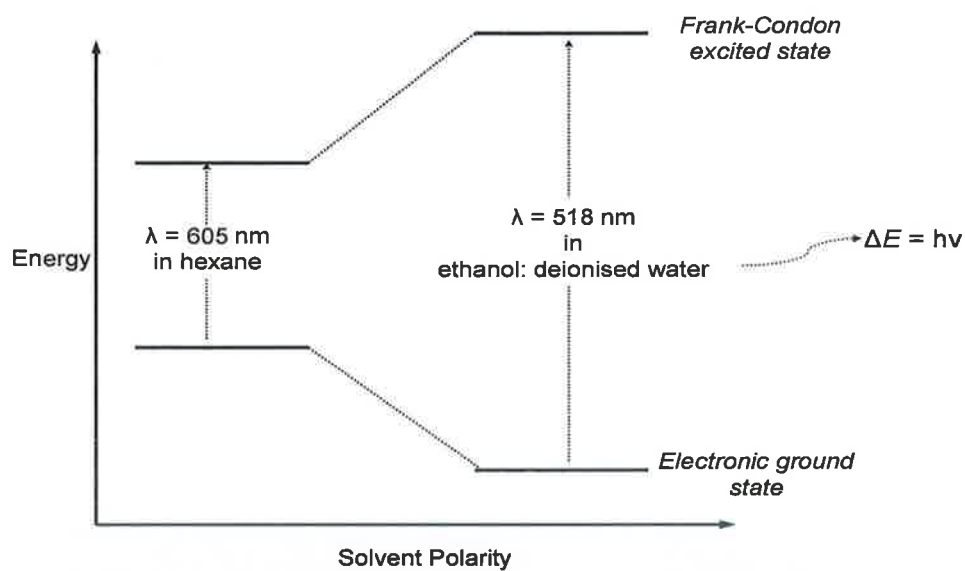
Figure 2.2. Qualitative illustration of the solvent influence on the intramolecular charge-transfer of the merocyanine isomer.

The largest hypsochromic shift was observed in the binary solution of ethanol and deionised water, we would also expect to observe the highest K_e value, it was calculated to be 0.1283, considering the corresponding K_e value of MC in hexane was over three orders of magnitude lower, calculated to be 8 x 10^{-4}. This data correlates well with the general hypothesis that the population of MC is greater in polar solvents than in non-polar solvents.

Solvent	Dielectric constant (ε_r)	λ_{max} MC (nm)	$A_e^{\,a}$	$K_e \times 10^{-2\,b}$	$k\,(s^{-1})\,\lambda_{max}^{\,c}$
Acetone	20.7	560	0.095	2.79	0.247
Acetonitrile	37.5	554	0.13	3.85	0.088
1-Butanol	17.8	539	0.144	4.29	0.045
2-Butanol	15.8	542	0.131	3.88	0.051
2-Butanone	18.5	554	0.12	3.55	0.149
Carbon tetrachloride	2.24	602	0.009	0.25	1.242
Chloroform	4.81	578	0.025	0.71	0.661
Cyclohexanone	-	572	0.030	0.86	0.32
Dichloromethane	9.08	578	0.018	0.51	0.70
Diethyl ether	4.34	596	0.008	0.22	1.88
DMF	36.7	563	0.049	1.41	0.06
DMSO	47	557	0.078	2.27	0.08^d
1,4 Dioxane	2.21	587	0.007	0.20	2.14
Ethanol	24.6	539	0.153	4.57	0.021
Ethanol-10% H_2O	-	536	0.196	5.93	0.018
Ethanol(50%)-H_2O(50%)	-	518	0.398	12.83	0.007^d
Ethyl Acetate	6	578	0.007	0.20	1.37
Ethylene Glycol	37.7	542	0.129	3.82	0.019
Hexane	1.89	605	0.003	0.08	2.73^e
Hexyl alcohol		545	0.127	3.76	0.053
Methanol	32.6	527	0.278	8.62	0.018
Methyl ethyl ketone		566	0.039	1.12	0.218
2-Methoxy ethanol		539	0.147	4.38	0.022
Pentanol		545	0.128	3.70	0.032
Propanol	20.1	542	0.144	4.29	0.022
2-Propanol	18.3	545	0.128	3.79	0.042
THF	7.6	584	0.019	0.54	1.47
Toluene	2.38	605	0.004	0.11	2.84

[a] Absorbance measured at λ max of MC after 15hrs in dark.
[b] Calculated from Equation 2.1.
[c] Calculated from Equation 2.2.
[d] Exhibited negative photochromism.
[e] After irradiation with 365 nm, material precipitated out of hexane solution, data relates to population of dissolved MC.

Table 2.1. Ground state equilibrium and photo-physical properties of MC in various molecular solvents. BSP concentration in solvent = 1.0×10^{-4} mol L^{-1}.

Figure 2.3 illustrates the spectral shifts of the photo-generated MC isomer in several solvents. A clear difference is seen in the spectral features of MC in ethanol and toluene, this feature being the shoulder present at approximately 560 nm. It is known that in non-polar solvents, the MC isomer can form different types of aggregates, with the absorption spectrum of the particular aggregate self-indicating as to which type of ordered structure is present. Absorption spectra of *J*-aggregates, which have a parallel (head-to-head) arrangement of the molecular dipoles, are shifted to longer wavelengths relative to the spectra of the isolated merocyanine molecules. For H-aggregates having a head-to-tail arrangement of the molecular dipoles, the spectra are shifted to shorter wavelengths. An important property of the *J*-aggregates produced by irradiation of solutions in non-polar solvents is that their spectra consist of very narrow absorption bands. This would indicate that for MC in toluene, the $\lambda_{max} = 605$ nm is due to *J*-aggregates present and the shoulder band arises from the isolated MC molecule. This phenomenon is seen in most non-polar solvents and in the instance of UV-irradiation of BSP in hexane, the aggregates produce peculiar colloidal-sized beads with submicrometer *J*-aggregate cores and an amphorous exterior.[70] A UV-vis absorption spectrum for BSP at a concentration of 1.0×10^{-4}M in hexane was not possible due to the precipitation of these colloidal sized beads and coating of the quartz glass surface after irradiation at 365 nm.
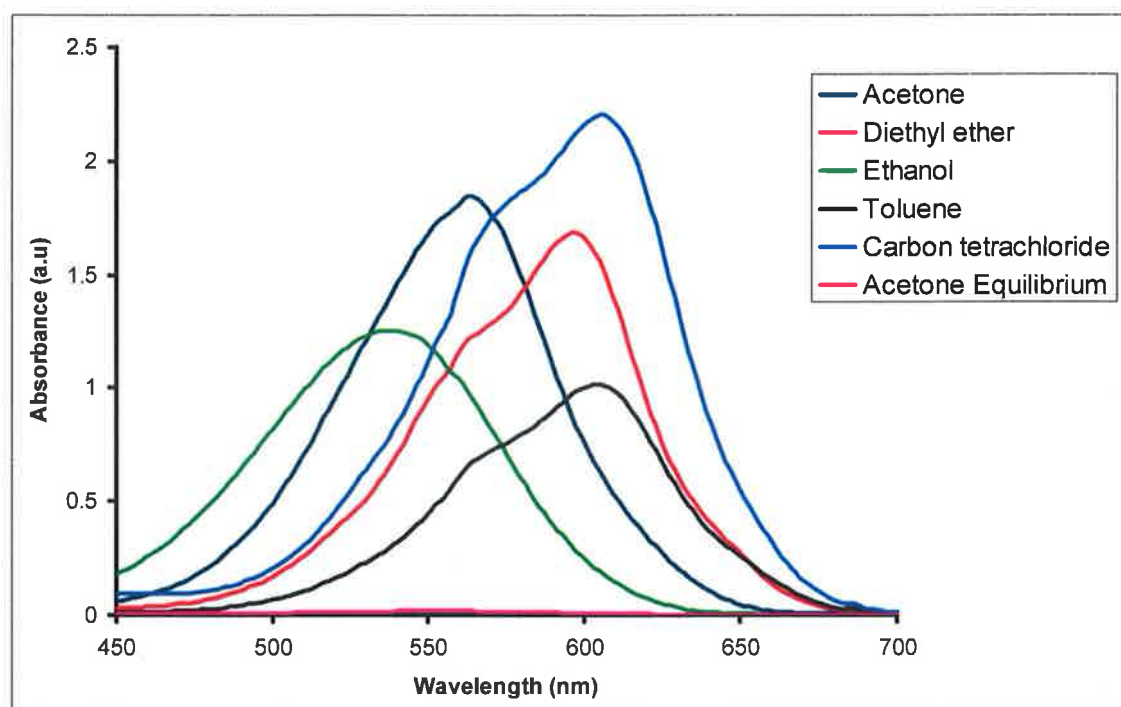
Figure 2.3. UV-vis spectrum of solvatochromic shift of MC in various solvents after 1min UV irradiation (365 nm), spectrum 'Acetone Equilibrium' represents MC absorbance after 15 hours in dark conditions.

The equilibrium between BSP and MC is strongly displaced upon irradiation with visible ($\geq$450 nm) light towards the BSP isomer and when irradiated with UV light (365 nm) towards the MC isomer. **Figure 2.3** displays the resulting spectra of all solvents containing 10^{-4}M BSP after 1 minute of UV irradiation. The spectrum 'Acetone Equilibrium' represents MC absorbance after 15 hours in dark conditions, to show the significant intensity difference between the MC band after UV irradiation and MC at equilibrium. It is well known that, after removal of UV light, the predominant MC form generated will thermally isomerize back to its equilibrium state (A_e), this decay in absorbance should follow first order kinetics[41]. The rate at which the thermal

isomerization follows is strongly solvent dependent. First-order rate constants for the thermal isomerization back to equilibrium were determined using Microsoft Excel Solver, by fitting the absorbance data to the following equation

$$y = a\,e^{-kt} + b$$

Equation 2.2.

Where y is the absorbance value at the λ_{max}, a is the absorbance at t = 0, k is the rate constant, t is time and b is asymptotic value[71]. The rate constants are tabulated in **Table 2.1**. It can be seen that the thermal isomerization of MC to BSP in ethanol takes place at the rate of 2.1×10^{-2} s^{-1} and in acetone at a rate of 0.247 s^{-1} (ten times faster), whereas the same isomerization in toluene is over one hundred fifty times faster than in ethanol at a rate of 2.84 s^{-1}, see **Figure 2.4**.
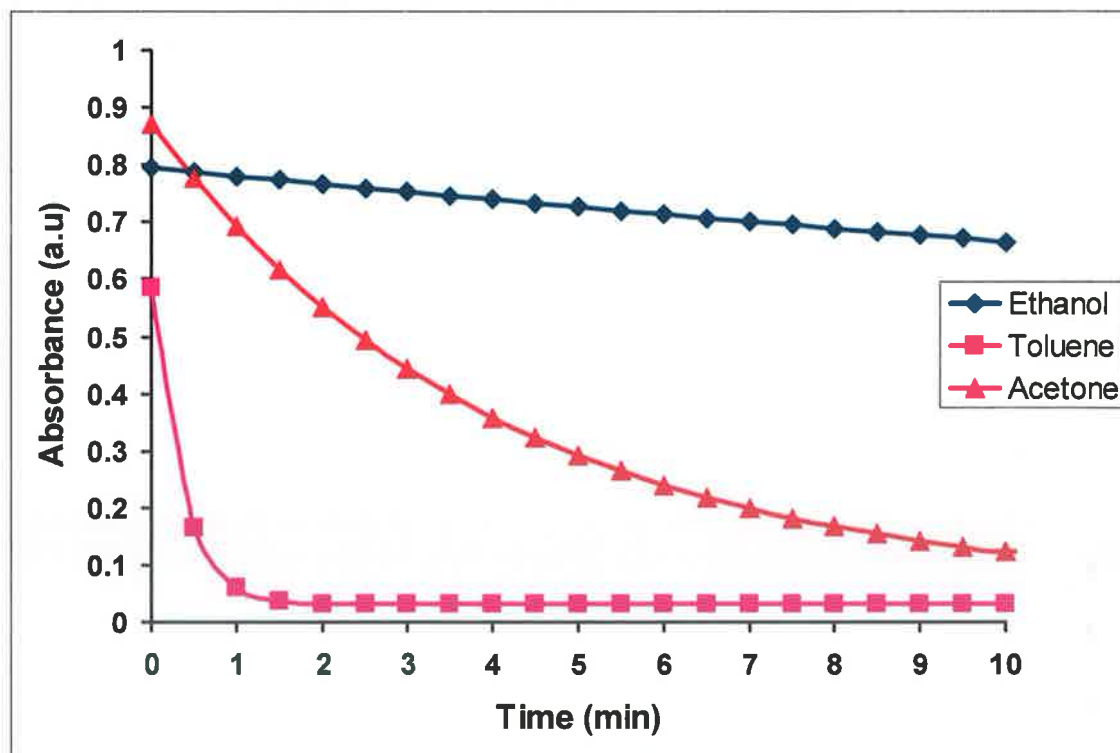
Figure 2.4. Absorbance decay of MC after 1min 365 nm irradiation in ethanol, toluene and acetone at their respective λ_{max}.

When the thermodynamically less stable state is the more deeply coloured form, the system is called a "positive" photochromic system. But, when we observe the opposite, the thermodynamically less stable state is the colourless form; the system is called a "negative" photochromic system. Most spiropyrans show positive photochromism as in the case of the systems studied in **Figure 2.4**. Although, for two of the solvent systems studied, negative photochromism was observed. At equilibrium, we observe the MC band in the binary solvent system of ethanol: deionised water at 518 nm with a K_e value of 0.1283, we would expect this value to increase upon 365 nm irradiation, but surprisingly the opposite was observed. In fact, the absorbance value decreased by 71% at 518 nm after irradiation with 365 nm, **Figure 2.5**, indicating the thermodynamically stable state is the coloured MC form. From **Figure 2.5** (inset), this hypothesis is further reinforced, by studying its thermal relaxation after 1 minute irradiation at 365 nm; its return to equilibrium was calculated at a rate of $0.007s^{-1}$. Similar behaviour was observed in the case of DMSO.
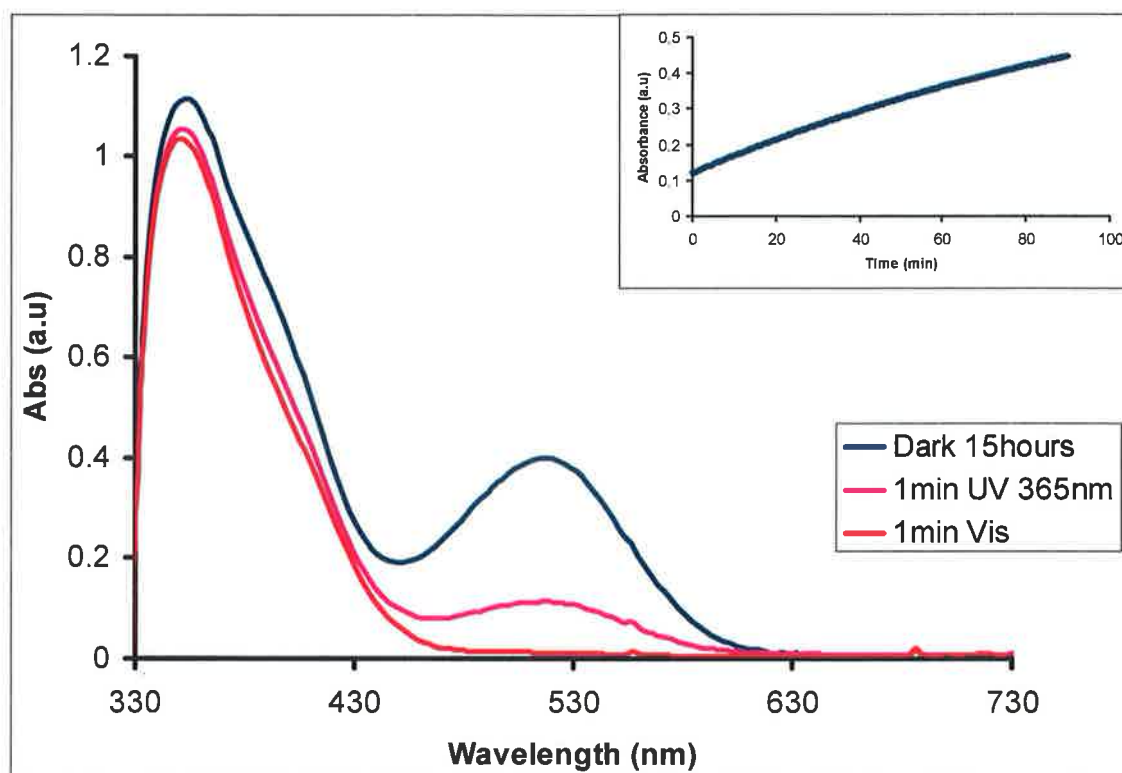
Figure 2.5. Negative-photochromism of BSP in binary solvent system of ethanol (1): (1) deionised water. Inset, thermal relaxation of BSP to MC isomer after 1min UV irradiation, in this case we have an increase of absorbance at λ_{max} compared to other solvent systems in which there is a decrease, such as ethanol, seen in Figure 2.4.

At equilibrium, we observe the MC band in DMSO at 557 nm with a K_e value of 2.27 $\times 10^{-2}$, we would expect this value to increase upon 365 nm irradiation, but as in the case with the binary solvent (ethanol: deionised water), the opposite was observed, **Figure 2.6**. The absorbance value decreased by over 90% at the MC band, 557 nm. An uncharacteristic band at approximately 430 nm was also observed, an increase of absorbance in this particular region is very similar to the acidichromic effects reported by

Song[68] but protonation as a reason for the spectral changes seen here can be excluded, since

(i) DMSO does not contain any labile protons,

(ii) reversible process is observed with irradiation of light. Removal of the proton can only be achieved by a chemical means, usually treatment with an appropriate base[72],

(iii) it has also been reported by McCoy[63] that H-aggregates of a similar BSP derivative in dichloromethane are found in this region, but detection of H-aggregates is unlikely due to the high polarity of DMSO.

Although, we cannot rule out the presence of trace amounts of liable protons (ppm) or maybe even heavy metals (ppb), which cause a blue shift, it is highly unlikely we are seeing this band due to trace quantities of these impurities. Therefore the new band must be due to a solute-solvent interaction. This will be discussed in further detail later.

With regards to negative-photochromism, a strange question must be asked as to why it happens? For example, in the case of the binary solvent (ethanol: deionised water), this would be regarded as a dipolar, hydrogen bonding donor 'protic' solvent, similar to methanol. But, why do they behave so differently? Furthermore DMSO is classed as a dipolar, non-hydrogen bonding donor solvent, similar to acetone, yet MC exhibits strikingly different behaviour in these solvents. And finally, the two solvents that do exhibit negative photochromism do not even lie within the same class as each other. It

71

would seem that a classification dependent on solvent types would be too simplistic to apply to the complex equilibrium of BSP-MC.
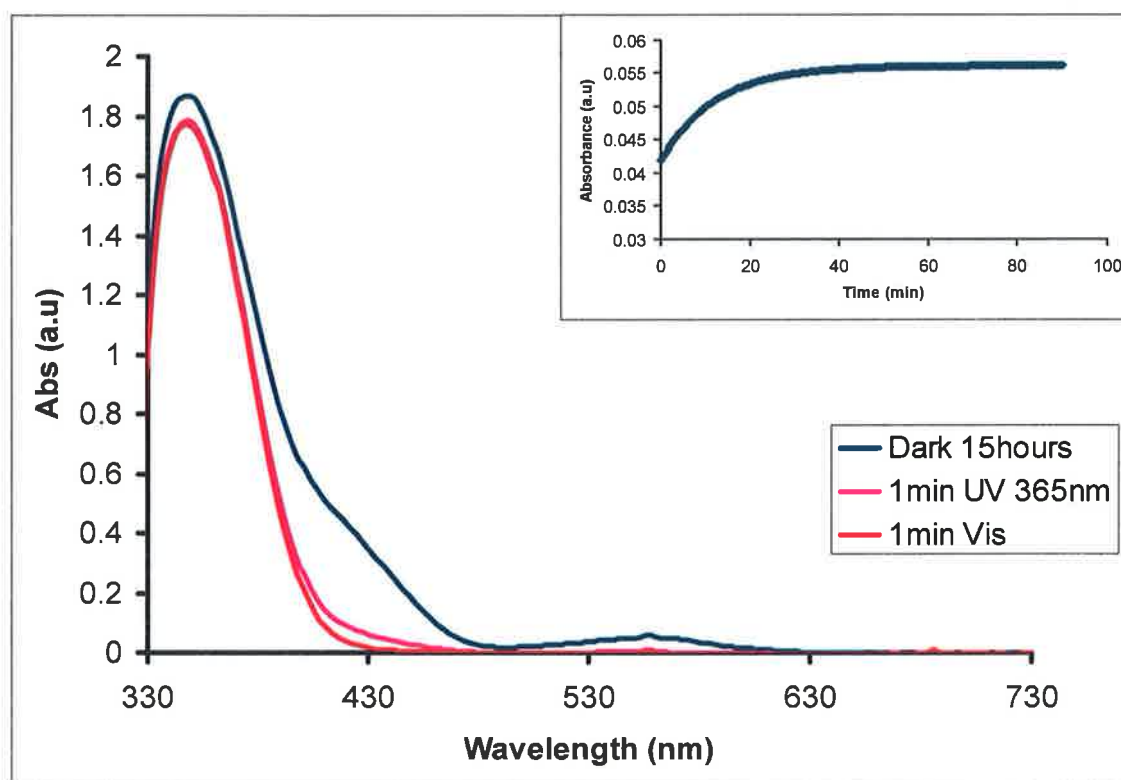
Figure 2.6. Negative-photochromism of BSP in DMSO. Inset, thermal relaxation of BSP to MC isomer after 1min UV irradiation.

BSP forms complexes with certain d- and f-elements in solution. While the colour of BSP in polar solvents originates from absorption of the MC isomer, a marked blue shift is caused by complexation with the phenolate oxygen atom of the MC isomer. In solution phase experiments, it was found that the MC form to be sensitive to a number of guest ions, and in particular Co^{2+}, although the effect is relatively unselective. **Figure 2.7** shows the effect of Co^{2+} on the MC spectroscopy and also the ability to dissociate the

complex with visible light; and reform the MC- Co^{2+} complex upon exposure to UV light. This photonic control of the binding event in solution is an exciting feature of the molecule and holds much promise for the ability of BSP to act as a 'smart' or 'switchable' chemical sensor.
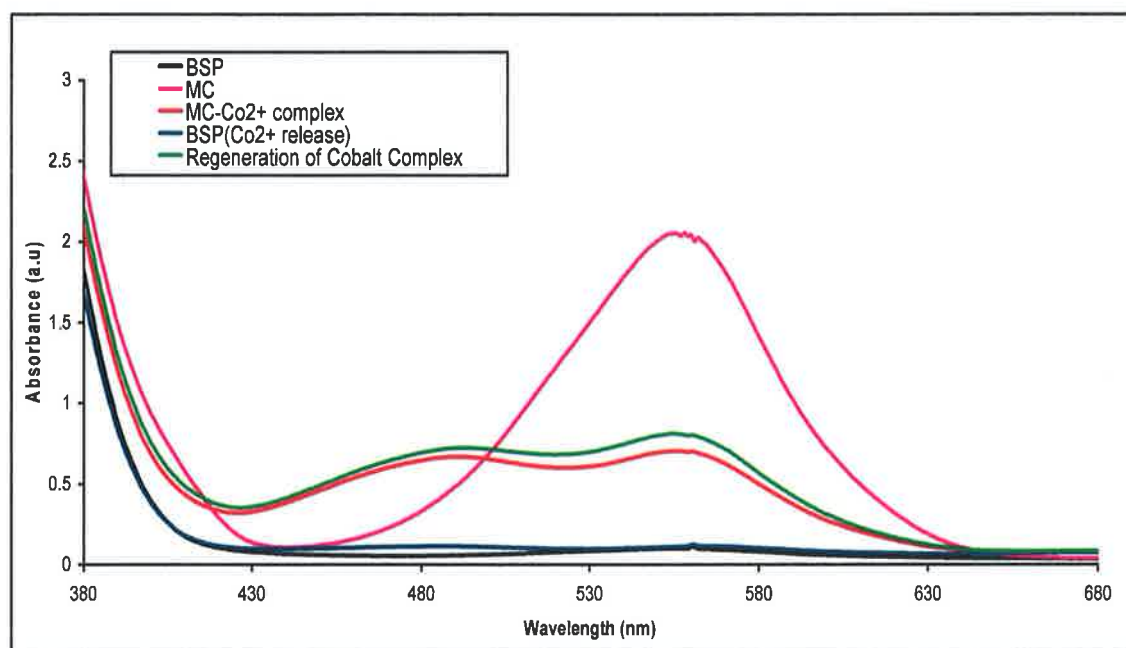
Figure 2.7. Regeneration of BSP and MC-Co^{2+} complex in acetonitrile.

2.2.2 Fluorescence spectroscopy

Fluorescence spectroscopy compliments the data observed in UV-vis absorption spectroscopy, although it is a significantly more sensitive technique for analysis of interactions within a host-guest system as discussed in Chapter 1. Similar to UV-vis absorption spectroscopy, where we can generate a strong visible band upon UV light irradiation of BSP, this situation also applies to fluorescence spectroscopy. It is possible to switch on and off fluorescence with UV and visible light as seen in **Figure 2.8,**

emission λ_{max} = 616 nm. It can be seen in **Figure 2.8**, that excitation of the BSP isomer at 408, 488, 525, and 590 nm results in minimal fluorescence whereas when the BSP isomer is irradiated with 365 nm light for 1 minute and immediately excited at 408, 488, 525 and 590 nm fluorescence at 616 nm is observed. This strong emission is due to the extension of π-conjugation within the MC isomer and the rigid planar geometry brought about by the photo-isomerization. The excitation wavelength that results in the maximum emission intensity is that of 525 nm, this emission intensity decreases as we excite to the right and left of 525 nm in accordance with the *Frank-Condon principle*.
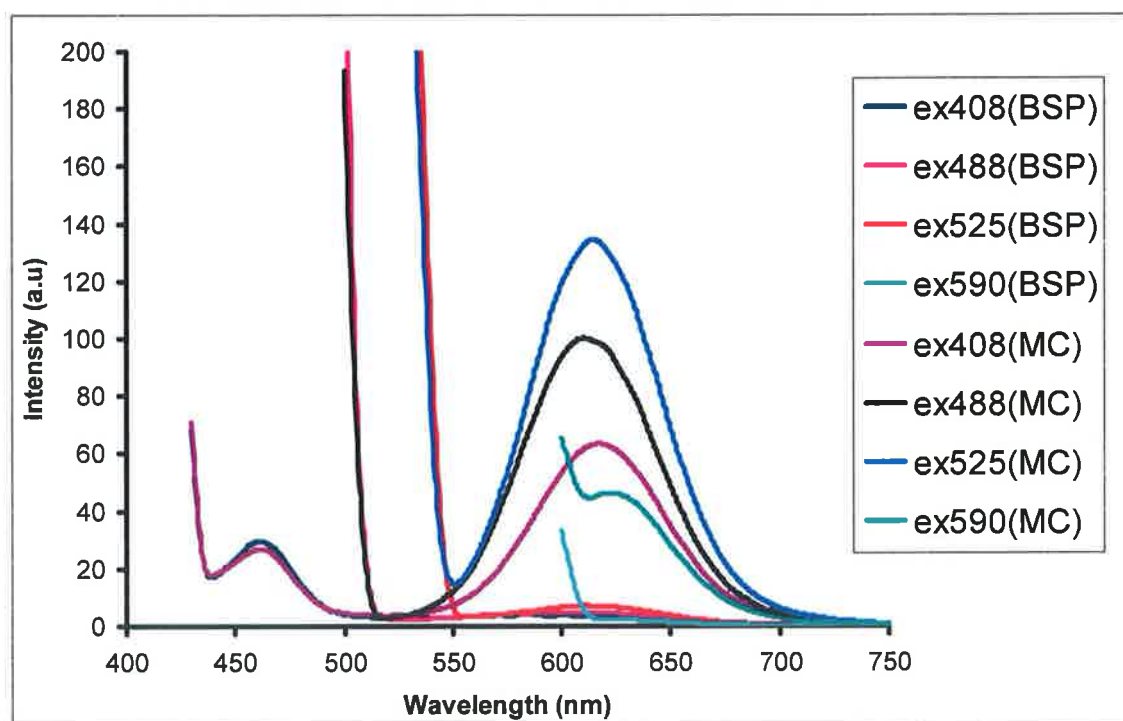
Figure 2.8. Emission spectra of BSP (1 min visible 450 nm) and MC (1 min UV 365 nm) at several excitations in acetonitrile.

74

2.2.3 Nuclear Magnetic Resonance

Nuclear magnetic resonance (NMR) is used to study many molecular structure, usually via hydrogen and carbon resonance spectra. NMR gives information about the number of magnetically distinct atoms of the type being studied. When hydrogen nuclei are studied, for instance, one can determine the number of each distinct type of hydrogen nuclei as well as obtaining information regarding the nature of the immediate environment of each type, and their relative spatial location.

This spectroscopic technique is extremely important to gain an understanding of the interactions of a molecule with its immediate environment. A ^{1}H-NMR solvatochromic study was carried out using the following deuterated solvents; acetone, acetonitrile, chloroform, DMSO, methanol and toluene. A series of NMR experiments were carried out in dark conditions to establish if there is correlation between the UV-vis data presented previously in **Table 2.1** with the ^{1}H-NMR data obtained in **Table 2.2**. Experimental conditions in accordance with UV-vis experiments so as to correlate results between the two instruments. It was found that ^{1}H-NMR data obtained was for the BSP isomer in all cases. Assignment was assisted by ^{13}C- and COSY NMR experiments.
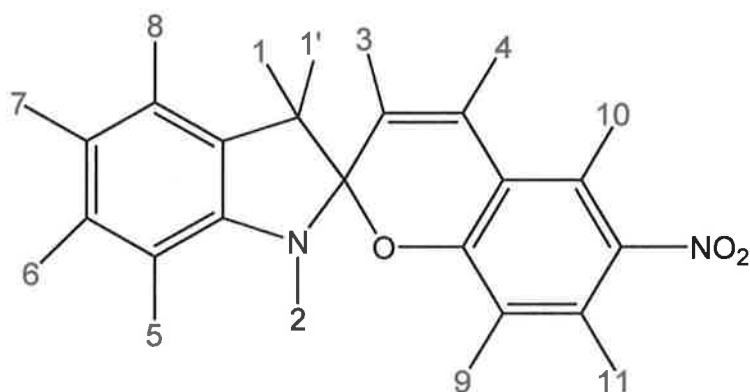
Proton	Acetonitrile	Acetone	Chloroform	DMSO	Methanol	Toluene
1	1.289	1.311	1.321	1.217	1.185	1.191
1'	1.177	1.2	1.214	1.116	1.079	0.996
2	2.746	2.775	2.768	2.678	2.635	2.484
3	5.986	6.05	5.898	6.009	5.885	5.354
4	7.076	7.219	6.937	7.217	6.967	6.143
5	6.631	6.646	6.598	6.629	6.479	6.39
6	7.196	7.162	7.231	7.137	7.039	7.135
7	6.874	6.857	6.915	6.812	6.726	6.869
8	7.176	7.175	7.109	7.119	6.978	6.936
9	6.77	6.88	6.805	6.903	6.708	6.078
10	8.106	8.164	8.047	8.217	7.998	7.632
11	8.018	8.056	8.027	8.02	7.92	7.619
$J (H_3\text{-}H_4)$	10.358	-	-	-	-	-
$J (H_{10}\text{-}H_{11})$	2.779	-	-	-	-	-

Table 2.2. ^{1}H-NMR chemical shifts (ppm) and coupling constants (Hz) for BSP isomer in various solvents.

Unfortunately, a comparison study of the ^{1}H-NMR of BSP and MC was not possible due to instrumental limitations, but Zhou has reported on the ^{1}H-NMR study of a similar derivative of BSP in the MC isomer state.[73] In theory it would be possible to monitor the zwitterionic character of the sample being analyzed by monitoring the chemical shift of the protons positioned at **2** in **Table 2.2**, adjacent to the indolinium nitrogen. The chemical shifts of these protons in the MC state reported by Zhou corresponds to $\delta = 4.60$

(in d-acetone), indicating that the MC isomer is a more polar species than BSP $\delta = 2.77$ (in d-acetone). The large downfield shift is due to the increased positive charge density on the nitrogen, corresponding to the MC zwitterionic character as represented in **Scheme 2.1**. If this hypothesis is true, we should expect varying degrees of downfield shifts with relation to solvent polarity. In the case of the non-polar d-toluene we observe a value of $\delta = 2.48$ for proton **2**, which is an upfield shift of 0.29 ppm compared to the dipolar solvent d-acetone. In the case of d-methanol, a value of $\delta = 2.63$ is observed, an upfield shift of 0.14 ppm. This is surprising, as methanol would be regarded from our UV-vis study as a more polar solvent and should enhance the MC zwitterionic character compared to acetone. This could possibly arise from the nature of hydrogen bonding within the solvent system of methanol and MC. If the phenolate anion experiences hydrogen bonding this could cause a loss in zwitterionic character and hence a reduced increase in positive charge density on the indolinium nitrogen than expected. From the coupling constant of the vinylic protons located at positions **3** and **4** (10.35 Hz) the conclusion that the BSP isomer is present is re-enforced. This coupling constant value represents that of a *cis* conformation. The coupling constant of the J_4 couple for protons **10** and **11** results in a value of 2.77 Hz, which is similar to other J_4 couples. These coupling constants were found to be independent of the solvent system analyzed, as expected. NMR experiments are used for the characterization of many systems within this project, it was important to choose a solvent in which proton signals could be resolved without overlapping, and even more importantly, which do not interact with the zwitterionic character of the MC. As **Figure 2.9** illustrates, it seems the most resolved

signals within the area of most interest (5.5-10 ppm) are exhibited by the solvent system d-acetonitrile.
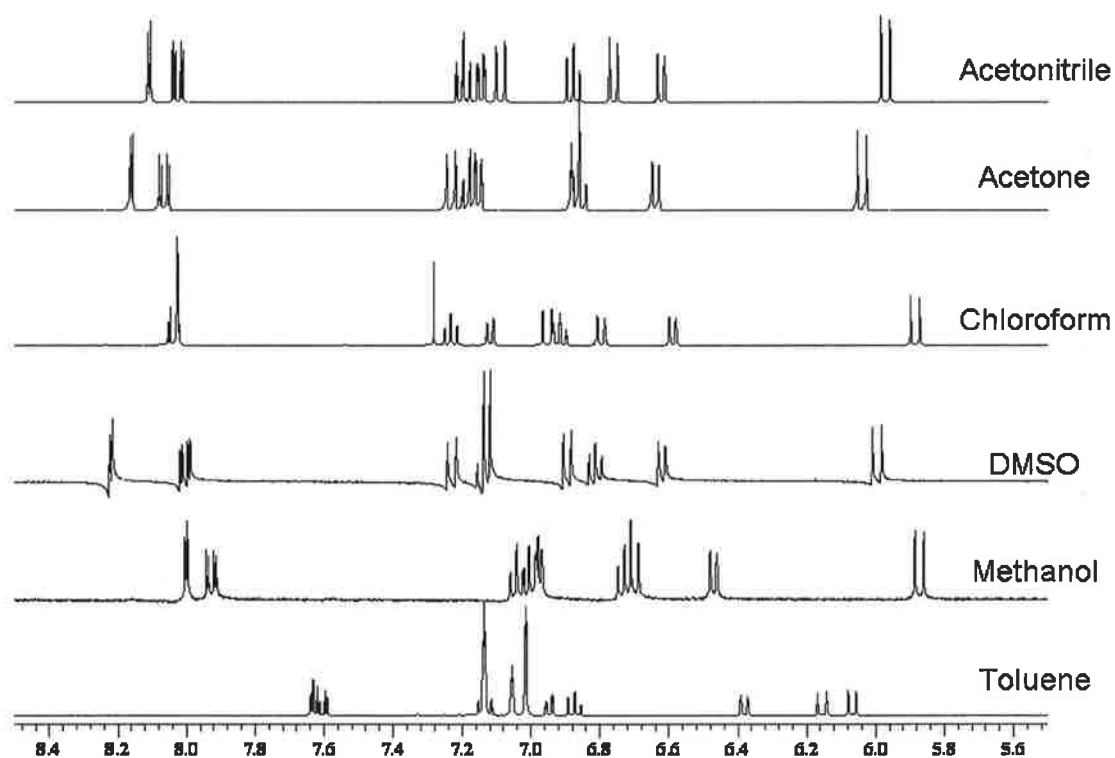
Figure 2.9. ^{1}H-NMR spectral shifts of BSP in several deuterated solvents.

2.2.4 Case study 1: UV-vis analysis of BSP-C$_{14}$ aggregates in molecular solvents

Discovery of the photochromic reactions of spiropyrans by Fischer and Hirshberg in 1952 and Hirshberg's idea of using the phenomenon for a "photochemical erasable memory" initiated active research on photochromism. Potential applications such as molecular switches and memory storage originate from the ability of the spiropyran to form

organized structures such as aggregates and mesophases whose optical properties, including nonlinear ones, can be affected by electric fields.

The MC isomer of BSP has a very strong tendency to associate into aggregates with a stack-like arrangement of the MC molecules. As discussed earlier in the chapter, when the molecular dipoles are arranged in a parallel structure (head-to-head) they form J-aggregates shifting the absorption spectra to the red compared to the isolated MC isomer. In the case of anti-parallel (head-to-tail) dipole arrangement they form H-aggregates shifting the absorption spectra to the blue. When a spiropyran solution is irradiated in a non-polar solvent, the aggregates produce colloidal-sized beads with beads with submicrometer J-aggregate cores. Under an external electrostatic field the beads form threads along the electric lines of force[74]. The tendency for merocyanine aggregation is so strong that aggregation occurs in polymer substrates[75].

With such a rearrangement of molecules in solution, from a disperse solute (BSP) to a highly organized system of J- and H- aggregates of MC upon irradiation with UV light, it is conceivable that there would be a significant change in the macroscopic physical constants of the solvent systems, such as conductivity and viscosity. It has been reported that spiropyrans with long hydrocarbon tails covalently connected to the basic spiropyran structure can form stable J-aggregates. This hypothesis was studied, firstly by synthesizing a C_{14} alkyl chain connected to the indolinium nitrogen of the spiropyran structure and studying their ground state and photo-physical properties in various molecular solvents.

Table 2.3 contains the ground state and photo-physical properties data obtained for the MC- C_{14} isomer in various solvents. Ethanol has the largest K_e value of 4.63 x 10^{-2} with λ_{max} = 539 nm, diethyl ether has the lowest K_e value of 1.51 x 10^{-2} with a λ_{max} = 596 nm. The thermal ring closing rate constant for the slowest solvent system is 0.03 s^{-1}, this being ethanol as anticipated. However, one would expect diethyl ether to have the fastest ring closing rate constant from the ground state data, but instead it is hexane, 1.52 s^{-1}. It can also be seen, that in the case of DMSO system, we observe negative photochromism as was the case for the BSP system.

Solvent	λ_{max} MC (nm)	$A_e{}^a$	K_e x $10^{-2\ b}$	k (s^{-1}) $\lambda_{max}{}^c$
Acetonitrile	562	0.127	3.74	0.11
Chloroform	578	0.077	2.24	0.35
Diethyl ether	596	0.052	1.51	1.40
DMSO	551	0.096	2.6	0.027^d
1,4 Dioxane	593	0.053	1.53	1.15
Ethanol	539	0.155	4.63	0.03
Ethyl Acetate	581	0.078	2.27	1.06
Ethylene Glycol	542	0.102	3.0	0.03
Hexane	611	0.059	1.71	1.52
THF	584	0.057	1.65	1.21

[a] Absorbance measured at λ max of MC after 15hrs in dark.
[b] Calculated from equation (1).
[c] Calculated from equation (2).
[d] Exhibited negative photochromism.

Table 2.3. Ground state equilibrium and photo-physical properties of MC-C_{14} in various molecular solvents. BSP- C_{14} concentration in solvent = 1.0 x 10^{-4} mol L^{-1}.

A direct comparison can be made between the data collected for the BSP- C_{14} in **Table 2.3** and the data for BSP in **Table 2.1**, as experimental procedures were kept constant. With respect to the solvatochromic shifts of the MC band in the visible region, a very interesting observation is made, for the solvents acetonitrile, 1, 4-dioxane, ethyl acetate,

and hexane a red shift of between 3 and 18 nm is seen for the MC-C_{14} with respect to MC. But, in the case of the solvents chloroform, diethyl ether, ethanol, ethylene glycol and THF, the MC-C_{14} λ_{max} is exactly the same as the MC λ_{max}. Even more interesting is the fact that the MC-C_{14} in DMSO is blue shifted by 6 nm compared to the MC isomer in DMSO.

Figure 2.10 illustrates the spectral features of MC-C_{14} in various solvents in the visible region. The spectra of MC-C_{14} in all solvents studied are very similar compared to the MC spectra in **Figure 2.3**, except for hexane, in which it can clearly be seen that there are two separate bands present in the spectra, the first located at 578 nm and the second more intense at 611 nm. This spectral feature, as discussed above, is indicative of *J*-aggregate formation, and a similar result has been reported with another MC-alkyl chain derivative absorbed onto a surface [62]. As discussed earlier, a precipitate formed upon UV irradiation of the BSP in hexane, this was not observed in the BSP- C_{14} case. A possible explanation of this behaviour is that the aggregates formed in BSP-C_{14} are not the same colloidal-type aggregates formed in BSP, as the long chain alkyl groups in BSP- C_{14} help to solubilize the newly formed species in hexane. Studying the thermal relaxation rate constants in **Table 2.3** provides some insight into the mechanistic process happening after UV irradiation. For chloroform, diethyl ether, 1, 4-dioxane, ethyl acetate, THF and hexane the MC-C_{14} rate constants are between 17-48% slower than the rate constants calculated for the MC isomer in the same solvents.
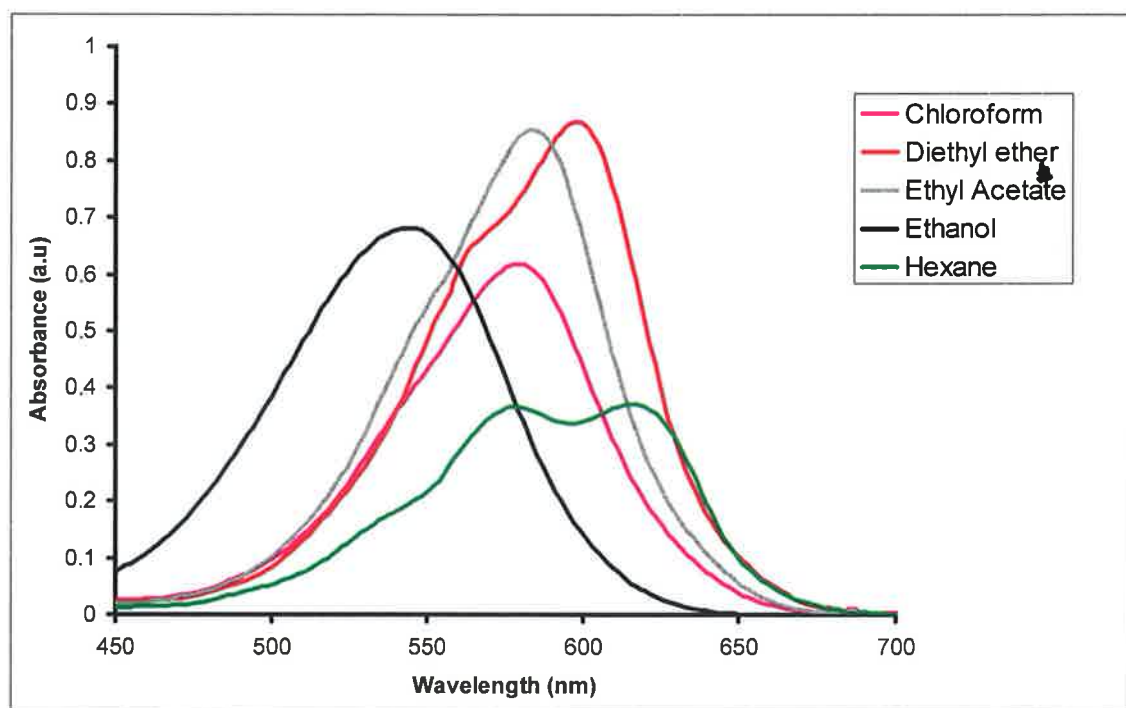
Figure 2.10. UV-vis spectrum of solvatochromic shift of MC-C_{14} in various solvents after 1min UV irradiation (365 nm).

This clearly supports the argument that the aggregate formed in BSP-C_{14} is a more stable species than that found in the BSP aggregate, but does not indicate if the species is different. Also, even though the thermal relaxation rate constants have decreased the process is still relatively fast as seen in **Figure 2.11**. It seems irradiating BSP derivatives with UV light while evaporating the solvent makes it is possible to cast these aggregates as stable materials that do not thermally revert to the 'closed' isomer[62]. Hashida has reported multilayered *J*-aggregated, thin films on glass surfaces. The aggregates had well-separated, sharp absorption maxima, and it was also claimed that the they could be erased separately by irradiation with a pulsed dye laser beam of different frequencies[76].
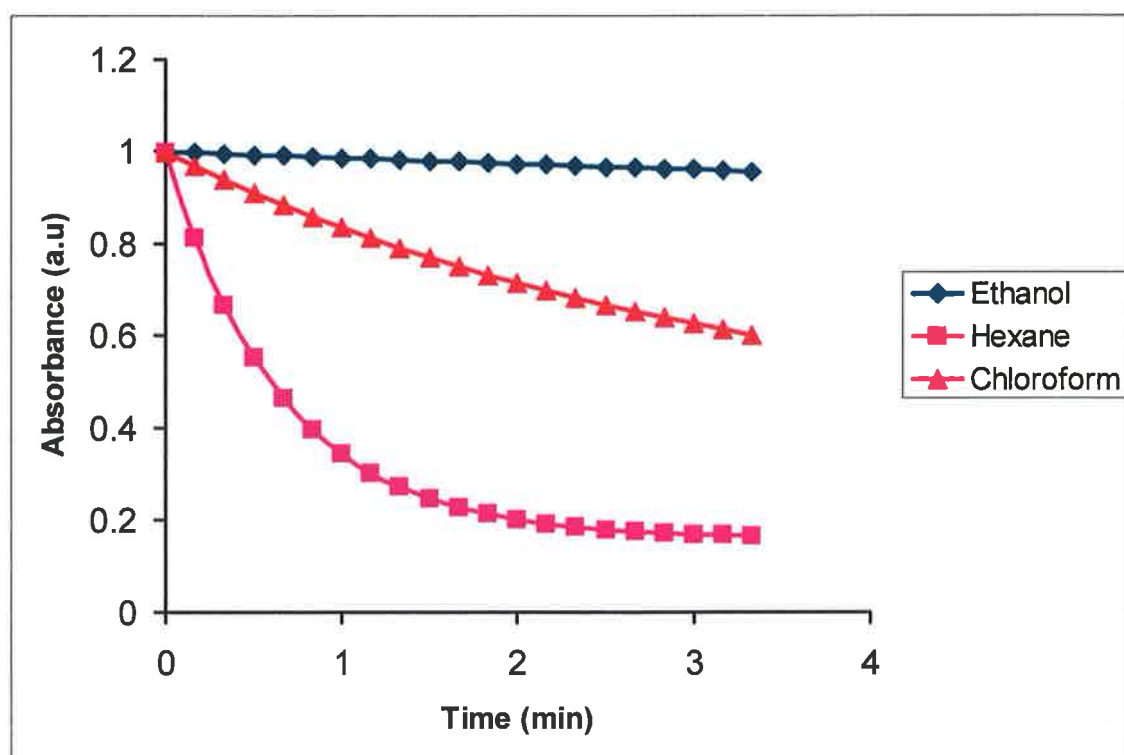
Figure 2.11. Thermal relaxation rates of MC-C_{14} after 1min 365 nm irradiation in ethanol (539 nm), hexane (611 nm) and chloroform (578 nm) at their respective λ_{max}.

FT-IR analysis has previously been shown to distinguish between single BSP molecules and J-aggregates[70]. The FT-IR vibrational differences in BSP-C_{14} solid and BSP-C_{14} aggregate are seen in **Figure 2.12**. Based on our results and published IR data for BSP derivatives we can make the following band assignments for the standard sample of 'BSP-C_{14}' in the region of interest 1600-1100 cm^{-1}: $v_{as}(NO_2)$ asymmetric and $v_s(NO_2)$ symmetric stretching modes at 1507 and 1332 cm^{-1} respectively, N-CH$_2$ stretching at 1303 cm^{-1}, phenyl-N stretching near 1268 cm^{-1}. The 'BSP-C_{14} aggregate' is prepared from the evaporation of a solution of hexane containing BSP-C_{14} while under continuous irradiation with UV light at 365 nm. Many spectral changes are observed compared to the

'BSP-C_{14}', a decrease in intensity of some peaks are due to the transformation of the BSP to MC form, decrease in intensity is due to the out-of-plane Φ-H bending indicating significant average increase in a tilt angle of both indolenine and benzene part of the molecule. The frequencies of the nitro group in the open MC form can be affected through an inductive effect, a resonance effect and formation of aci-nitro structures. Indeed, the loss of intensity of the $v_{as}(NO_2)$ asymmetric stretch at 1507 cm^{-1} and the hypsochromic shift of the symmetric vibration to 1342 cm^{-1} are observed. The band at 1296 cm^{-1} can be attributed to the phenyl-N stretch, and the N-CH$_2$ stretch band now appears as a shoulder to the phenyl-N stretch at 1315cm^{-1}. The band located at 1153 cm^{-1} can be assigned to the $C_{aryl} = N^+$ bond vibration. This only appears in the 'BSP-C_{14} aggregate' sample and can be attributed to the zwitterionic structure of the MC isomer, as this causes an increase in positive charge on the indoline nitrogen. This data correlates well with previous results, but it also gives an indication the nitro group character is changing slightly, as it is evident that the nitro is still there but the asymmetric vibration has been lost and we can see the emergence of a vibrational band at 1398 cm^{-1} corresponding to N^+-O^- bond in the nitro group. It has been reported that when positions and intensities of the nitro group are effected in the way observed in our sample, it corresponds to the NO_2 group weakly coupling with other vibrational modes in the molecule, which alters the chemical nature of the group. This effect has been related to the formation of aggregates and would explain the increase in molecular ordering that gives rise to the shoulder band in the UV-vis absorption spectra, **Figure 2.10**.
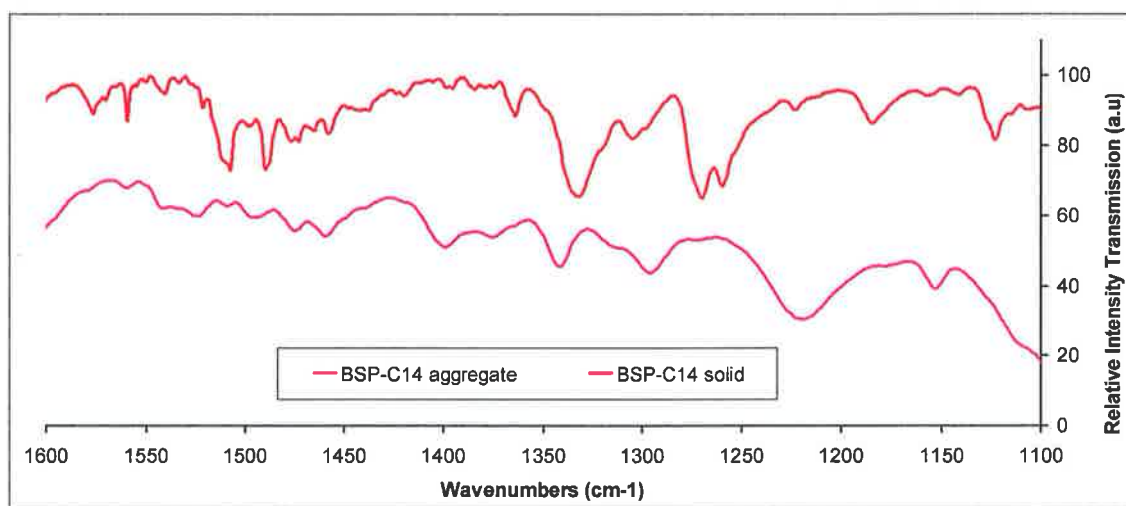
Figure 2.12. FT-IR spectra of BSP-C_{14} solid and BSP-C_{14} aggregate. Spectra are offset to clarify difference between samples.

2.2.5 Case study 2: Thermal study of BSP in DMSO.

Dimethyl sulfoxide (DMSO) is a colourless polar aprotic solvent that dissolves both polar and nonpolar compounds, and is miscible in a wide range of organic solvents as well as water. Because of its excellent solvating power, DMSO is frequently used as solvent for chemical reactions involving salts. Its polarity accelerates reactions with charged transition states, such as S_N2 alkylations of indoles and phenols. Because DMSO is only weakly acidic, it tolerates relatively strong bases. The center in DMSO is nucleophilic toward soft electrophiles and the oxygen is nucleophilic toward hard electrophiles. The methyl groups of DMSO are weakly acidic in character (pK_a=35) due to the stabilization of the resultant carbanion by the S(O)R group. Sulfoxides have a fixed pyramidal shape (the non-bonding electron pair occupies one corner of a tetrahedron), **Scheme 2.2.**
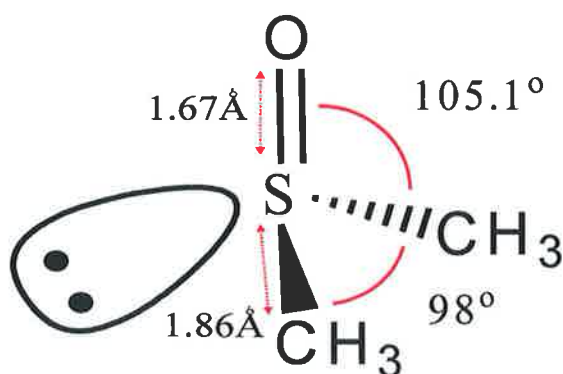
Scheme 2.2. 2-D representation of DMSO molecule containing bond lengths and dihedral angles.

Although, acetone is a similar molecule in terms of being a polar aprotic solvent, the nucleophilicity of sulfur is much greater than that of oxygen, leading to a number of interesting and useful electrophilic substitutions of sulfur that are not normally observed for oxygen. In organic synthesis, DMSO is used as an oxidant, for example, the Pfitzner-Moffatt oxidation and the Swern oxidation. The Pfitzner-Moffatt oxidation, is a chemical reaction which involves the oxidation of primary and secondary alcohols by DMSO activated with a carbodiimide, such as dicyclohexylcarbodiimide (DCC). The resulting alkoxysulfonium ylide rearranges to generate aldehydes and ketones.

Scheme 2.3. DMSO molecule at equilibrium with the partial negative formal charge on oxygen and partial positive charge on sulfur.

In solutions of non-polar solvents, most BSP derivatives exist as ring-closed isomers, but upon dissolving in polar solvents they can undergo thermal ring opening to the corresponding merocyanine forms. The position of the established complex equilibrium depends on many factors, primarily solvent polarity, nature of the substituents, the concentration of the solution, and the temperature at which the system exists. It has been discussed earlier that BSP in DMSO exhibits negative photochromism as shown in **Figure 2.6**, as when BSP at equilibrium is exposed to 365 nm irradiation, the MC band in the visible region decreases. But when BSP at equilibrium, is thermally irradiated the MC band increases in intensity, an observation which is indicative of the ring opening process. Thermally induced ring opening is also observed in 'positive' photochromic BSP systems, such as acetonitrile and toluene. **Figure 2.13** illustrates the thermally induced formation of the MC isomer at 10 °C intervals from equilibrium at 20 °C to 100 °C. We can see an immediate increase in MC absorbance of 34.8% after only 10 minutes at 30 °C; this absorbance is further increased by 36% when the temperature is elevated to 40 °C. Percentage is calculated by the difference in absorbance of the MC absorbance at 20 °C and 100 °C.
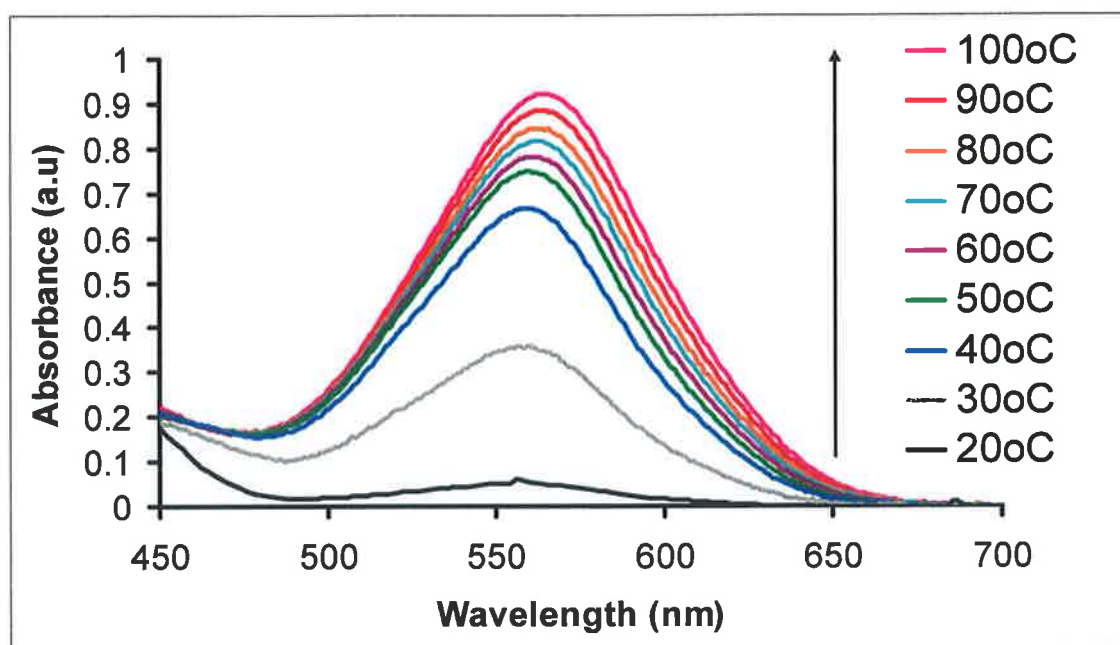
Figure 2.13. Overlaid UV-vis absorbance spectra of BSP following thermal irradiation. Arrow indicates trend in spectral change with temperature, spectrum recorded 10 minutes after selected temperature was reached.

This thermally induced ring opening process was analyzed using ^{1}H-NMR spectroscopy; using the exact same conditions as in the experimental set-up for the UV-vis absorption study. **Figure 2.14** shows overlaid ^{1}H-NMR spectra of BSP at 20 °C and 100 °C, there are no dramatic shifts, proton **10** shifts upfield from 8.24 to 8.15 ppm. Protons **1, 1'** and **2** shift downfield by approximately 0.4 ppm. It is also noted that all the proton signals have broadened due to molecular vibrations from the temperature increase; therefore coupling constants could not accurately be calculated.
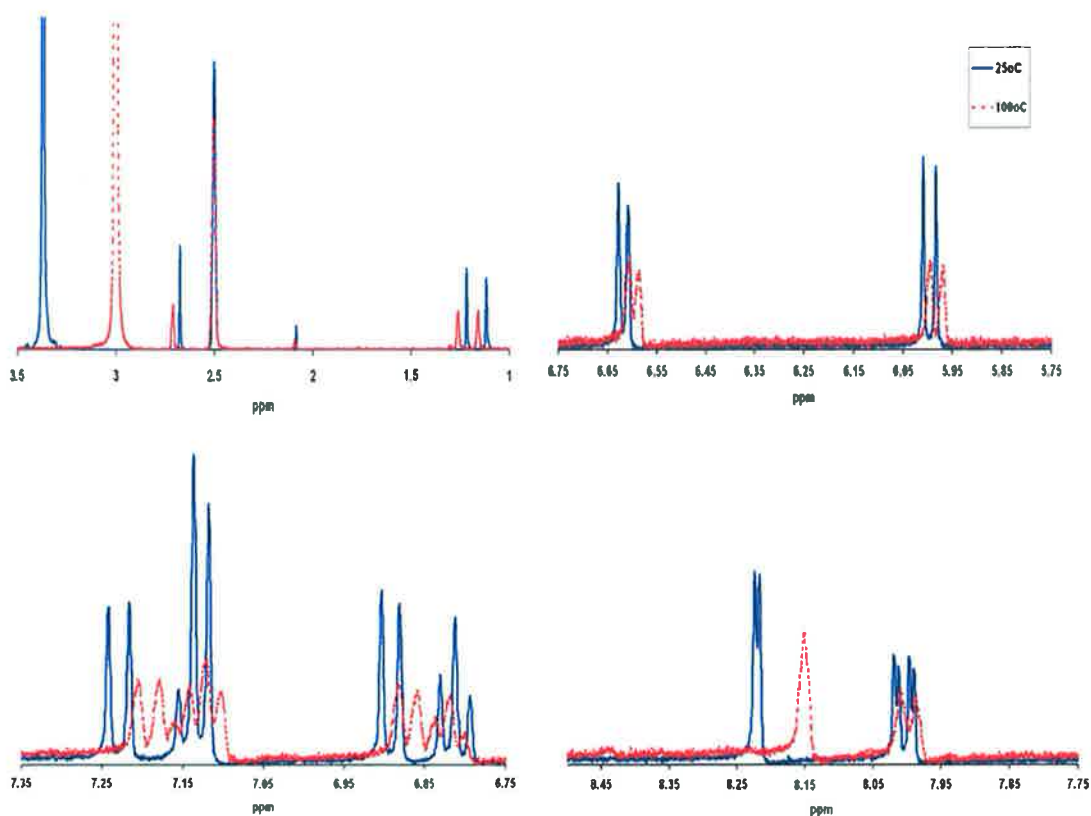
Figure 2.14. Overlaid ^{1}H-NMR spectra of BSP at 20 $^\circ$C and 100 $^\circ$C, spectra recorded 10 minutes after selected temperature was reached.

This NMR experiment was not as informative as hoped but an unusual observation was made after NMR experiment. A UV-vis absorbance measurement was recorded for the NMR sample after 15 hours in the dark, the MC absorbance band never returned to its original equilibrium absorbance value recorded before the NMR experiment. This observation raised many questions and a more detailed UV-vis-NMR study was carried out.

BSP was dissolved in d-DMSO and allowed to reach equilibrium in the dark. This sample was analyzed by ^{1}H-NMR (**Figure 2.15a**) and then a 10^{-4}M sample was analyzed by UV-

vis absorbance (**Figure 2.16**), this data was discussed in sections 2.2.1 UV-vis spectroscopy and 2.2.3 Nuclear Magnetic Resonance and for the section will be discussed as a reference. The d-DMSO sample was placed in a pressure tube, sealed under a nitrogen environment and placed in an oil bath at 100 °C. This sample was removed after 5 hours and analyzed by ^{1}H-NMR (**Figure 2.15b**), spectrum B contains all the peaks that are present within spectrum A but also contains additional peaks, and these are contained in **Table 2.4**. It appears as if a proportion of the sample is in the MC form and we therefore have a mixture, as the peak shifts are very similar to the reported MC form[73], although one peak at 10.3 ppm does not conform to the reported data. This peak could be assigned to a phenol proton but as the UV-vis absorbance (**Figure 2.16**) spectrum indicates this is not the case, as protonation of the phenolate results in a yellow coloured solution with a λ_{max} = 410 nm. A 10^{-4}M sample was analyzed by UV-vis absorbance (**Figure 2.16**), this spectrum is very interesting as a shoulder has formed at 510 nm with the λ_{max} = 542 nm, the λ_{max} has blue shifted by 15 nm from 557 nm after thermal treatment. This shoulder at 510 nm could possibly be a vibronic transition as the difference between the two peaks is only 32 nm; this is a very interesting observation as vibration transitions are usually broadened beyond recognition in polar solvents, such as DMSO. The shoulder band has been ruled out as a separate molecular entity formed upon thermal treatment because this band does not increase in intensity relative to a decrease in the band at 542 nm, which you would expect if a reaction product was forming.

It can also be seen that the MC band at equilibrium has significantly increased in absorbance; these results can only mean that at higher temperatures the MC is stabilized

by some intermolecular process (aggregation) or species (possible interaction with DMSO), even when cooled and diluted to 10^{-4}M this MC band and shoulder are still present, this would lead us to believe that the MC isomer has had an increase in structural order.

The possibility of degradation of BSP is ruled out at this stage as upon exposure to visible light in acetonitrile 10^{-4}M, the MC bands decrease in intensity which correlates to the ring closing process to the BSP isomer. It has also been reported that the MC isomer is stable up to 177 °C, where it isomerizes back to the BSP isomer[77].
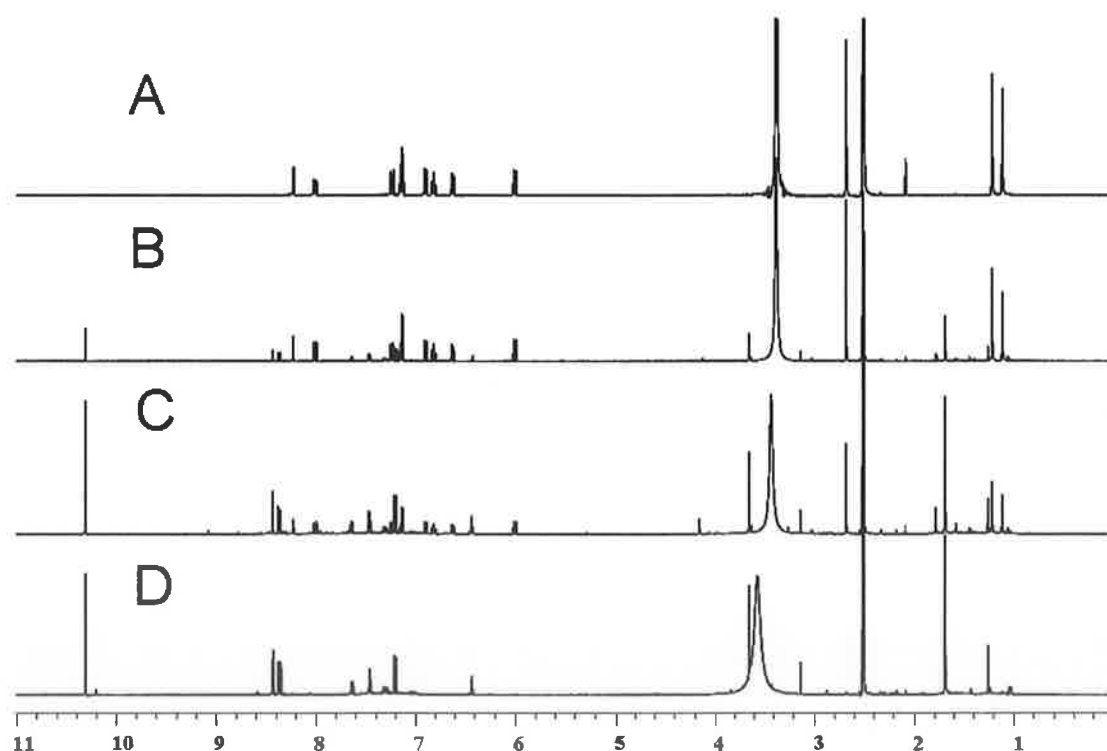
Figure 2.15. Overlaid ^{1}H-NMR spectra of BSP at certain conditions; (A) equilibrium, (B) sample thermally irradiated for 5 hours, (C) 10 hours and (D) 15 hours to 100 °C. Samples allowed to cool and spectra recorded at 25°C.

91

The sample analyzed in spectrum B was placed in a pressure tube under a nitrogen environment and placed in oil bath at 100 °C for a further 5 hours. This sample was allowed to cool to room temperature and analyzed by UV-vis and ^{1}H-NMR spectroscopy. The new peaks observed in spectrum B in **Figure 2.15**, have increased in intensity in spectrum C with relation to a decrease in intensity of the peaks in spectrum A. This process can be attributed to the thermal generation of a new species in the presence of DMSO. Although, major changes have occurred in the overall spectral features of spectrum C, two significant peak signals are of interest. The decrease in intensity of the diastereospecific methyls **1** and **1'** at 1.21 and 1.11 ppm respectively, and increase of signal at 1.68 ppm. This occurrence is similar to the formation of the planar MC isomer, in which case the two methyls experience the same magnetic field and coalesce from two separate signals into one signal. Also the peak signal located at 10.3 ppm, has increased significantly in intensity compared to spectrum C. This signal would be expected from a proton located on a hydroxyl oxygen, in this case the phenolate oxygen. This protonation of the phenolate would cause a distinct colour change of the sample, from the purple colour associated with the MC isomer to a bright yellow attributed to the protonated phenolate (MC-H$^+$)[73]. For our system this colour change is not observed, and from the UV-vis spectrum in **Figure 2.16** we can confirm that the species MC-H$^+$ is not present. The 10^{-4}M sample investigated shows an increase in molecular absorption at 510 and 542 nm compared to the 5 hour 100 °C sample.

The sample shown in the NMR spectrum C was placed in a pressure tube under a nitrogen environment and placed in oil bath at 100 °C for a further 5 hours. This sample,

after an overall exposure to 100 °C for a 15 hour period, was allowed to cool to room temperature and analyzed by UV-vis, ^{1}H- and COSY-NMR, and FT-IR spectroscopy and compared to previous analysis.
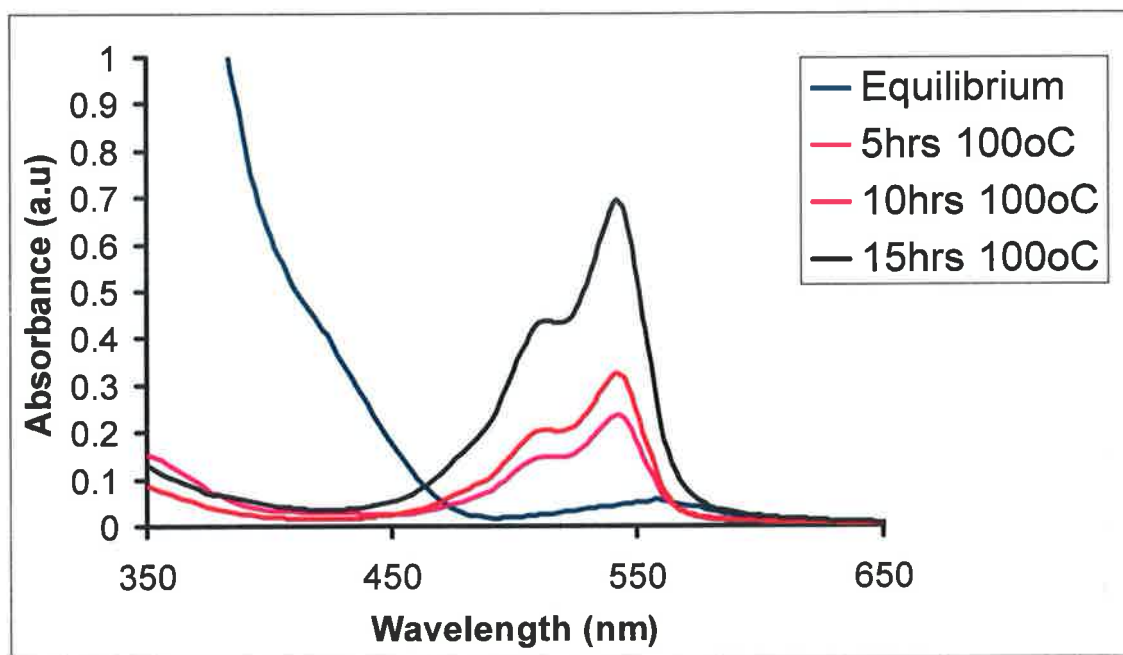
Figure 2.16. UV-vis absorbance spectra of BSP 10^{-4}M in DMSO at equilibrium, 5, 10, and 15 hours irradiation of 100 °C heat. All spectra recorded after 15 hours in the dark at 25°C.

The ^{1}H-NMR comparison of spectrum A and D in **Figure 2.15** shows drastic changes have happened, such as the disappearance of all peak signals in spectrum A and emergence of new peaks in spectrum B and C. This will be discussed in more detail shortly. The UV-vis spectroscopy seen in **Figure 2.16** shows a marked increase in molecular absorbance at 510 and 542 nm compared to the 10 hour 100 °C sample. It was also observed that the MC band in acetonitrile 10^{-4}M did not decrease in intensity after 10

minutes visible light irradiation (not shown); this would lead to the conclusion that the MC band has become locked in its coloured isomeric configuration.

If the new band observed at 510 nm was associated with a DMSO interaction then diluting in acetonitrile should encourage dissociation to the free MC isomer. This was not possible, as the spectrum seen in **Figure 2.16** is markedly like that seen in acetonitrile in **Figure 2.17** . As the photophysical properties have been altered by thermal irradiation in DMSO, it was important to characterize the chemical properties of the new coloured species, if as we believed the coloured species was in fact the MC zwitterion 'locked' in configuration then the phenolate should interact with cobalt (II) chloride forming a complex as seen in **Figure 2.7**. This complex was not seen for our thermally treated BSP; a 10^{-3}M solution of the thermally treated BSP was dissolved in acetonitrile and treated to a 10^{-2}M solution of cobalt (II) chloride in acetonitrile as seen in **Figure 2.17**. This leads us to believe that some type of chemical reaction or interaction has occurred that inhibits access at the phenolate position. It was also observed that the BSP thermally treated material was no longer soluble in non-polar solvents, such as toluene and hexane.
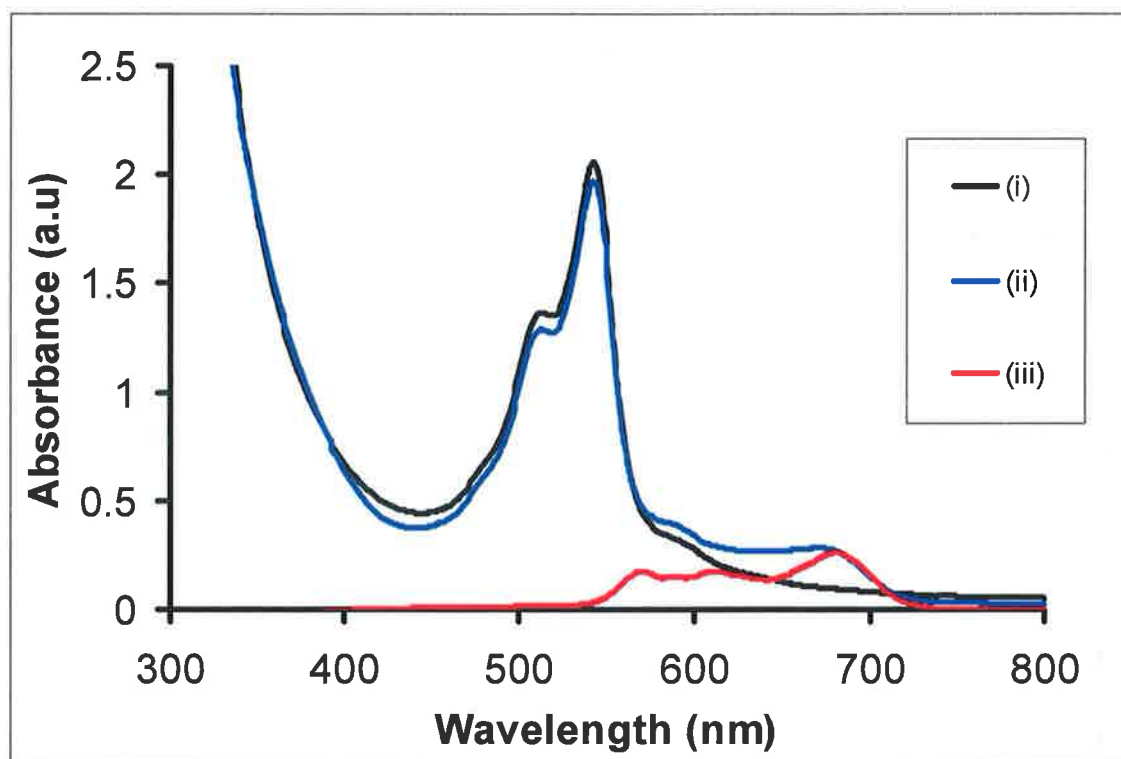
Figure 2.17. UV-vis spectra of (i) 10^{-3}M BSP thermally treated for 15hrs in DMSO then dissolved in acetonitrile at equilibrium, (ii) addition of 10^{-2}M CoCl$_2$ to previous sample and (iii) 10^{-2}M CoCl$_2$ in acetonitrile.

More detailed information regarding the chemical shifts observed in the above experiments can be seen in **Table 2.4** and **Figure 2.18**. The chemical shifts of 1 and 1'in the 15hrs 100 °C and MC-H$^+$ samples exhibit a type of coalescence between the two diastereotopic methyls as their integration has become unequivalent. This behaviour could only arise if the methyl groups began to experience the same magnetic environment. This could happen if the aco-planar BSP reorganizes its geometry to the planar MC isomer. The chemical shift of the protons adjacent to the indoline nitrogen has been shifted downfield in the case of the 15 hrs 100 °C sample. The chemical shift of this

signal in MC and MC-H$^+$ has also been shifted downfield compared to the BSP 'Equilibrium' chemical shift. Which implies that the proton signal of **2** (N-CH$_3$) shifts to lower fields when the positive charge density is increased in the presence of the zwitterion, as it is in the case of MC and MC-H$^+$. The same can be said for the chemical shifts of **9, 10** and **11** in which formation of the MC isomer, results in shifts to lower fields for benzopyran section of the BSP structure. It seems the thermally treated sample (15 hrs 100 ^{o}C) exhibits the same chemical shifts as the MC and MC-H$^+$ for the selected protons in **Table 2.4**, apart from the proton located at 10.3 ppm.

Proton	1	1'	2	9	10	11
Equilibrium	1.21	1.11	2.67	6.9	8.21	8.02
15hrs 100 ^{o}C	1.6*	1.25*	3.64	7.2	8.42	8.37
MC^a	--	--	4.6	--	8.59	9.65
MC-H$^+$ ^{b}	1.8*	1.68*	4.09	7.45	8.83	8.29

Table 2.4. ^{1}H-NMR chemical shifts (ppm) for BSP (equilibrium), after thermal treatment in DMSO (15hrs 100 ^{o}C), MC isomer and the prontonated MC isomer. Assignments are in correlation with **Table 2.2**.

^{a} From Ref.[73]
b BSP + 10 µl of 0.1M HCl.
* Unequal integration of these peaks, proton H-1 integrates to 4, while H-2 integrates to 2.
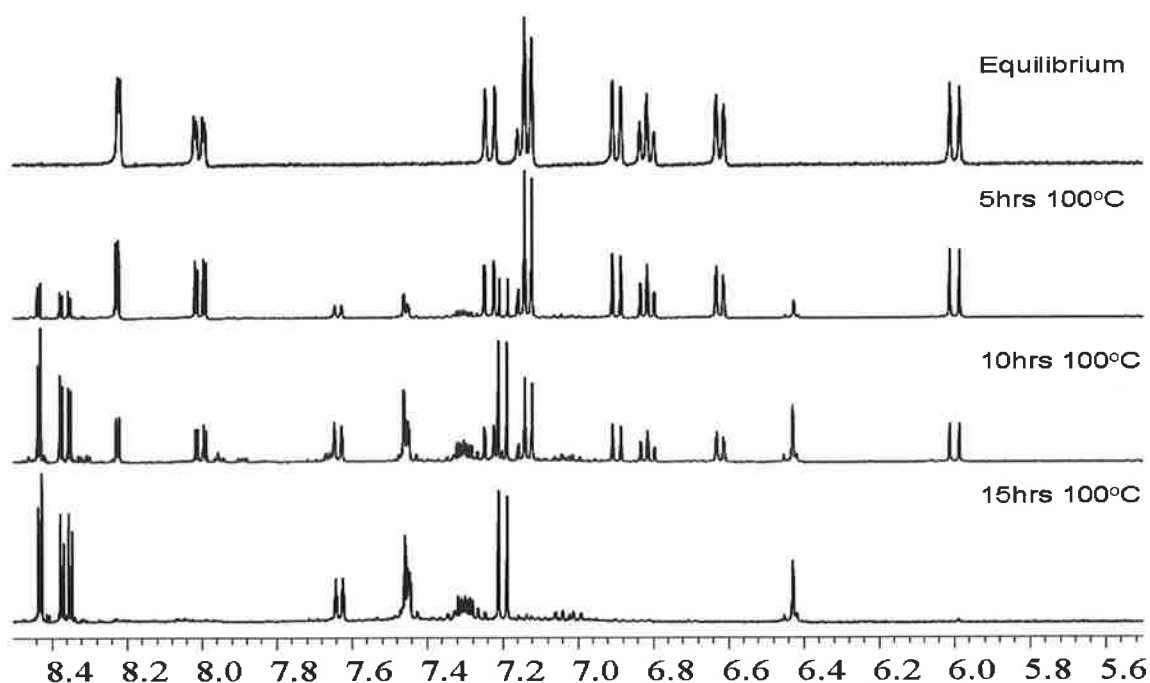
Figure 2.18. Overlaid ¹H-NMR spectra of BSP in the region of 5.5 -8.5 ppm after varying thermal exposure times.

The COSY NMR experiment confirms our earlier thoughts that the BSP molecule has undergone a chemical change. The vinylic protons 3 and 4, located at 6.0 and 7.21 ppm respectively in the equilibrium ¹H-spectrum, no longer couple with each other in the '15hrs 100 °C' sample. From the ¹H-NMR in **Figure 2.18** we observe the decrease in intensity of the doublet at 6.0 ppm and corresponding increase of a singlet at 6.42 ppm with increase exposure to heat. This would indicate that the BSP molecule has broken apart at the methylene bridge, separating the indoline and benzopyran moieties. This hypothesis was highlighted as the UV-vis spectrum of the starting materials of BSP; 2-methylene-1, 3, 3-trimethylindoline and 2-hydroxy-5-nitrobenzaldehyde seen in **Figure 2.19** appear to be very similar to our spectra of thermally treated BSP. This hypothesis

contradicts the literature as BSP is reported to be stable up to 177 °C as discussed earlier, although from the literature this thermal stability analysis was of BSP in the crystalline state. ^{1}H-NMR spectra of our starting materials indeed look very similar to our "15hr 100 °C" and the proton located at 10.3 ppm would appear to be the aldehyde proton of 2-hydroxy-5-nitrobenzaldehyde.
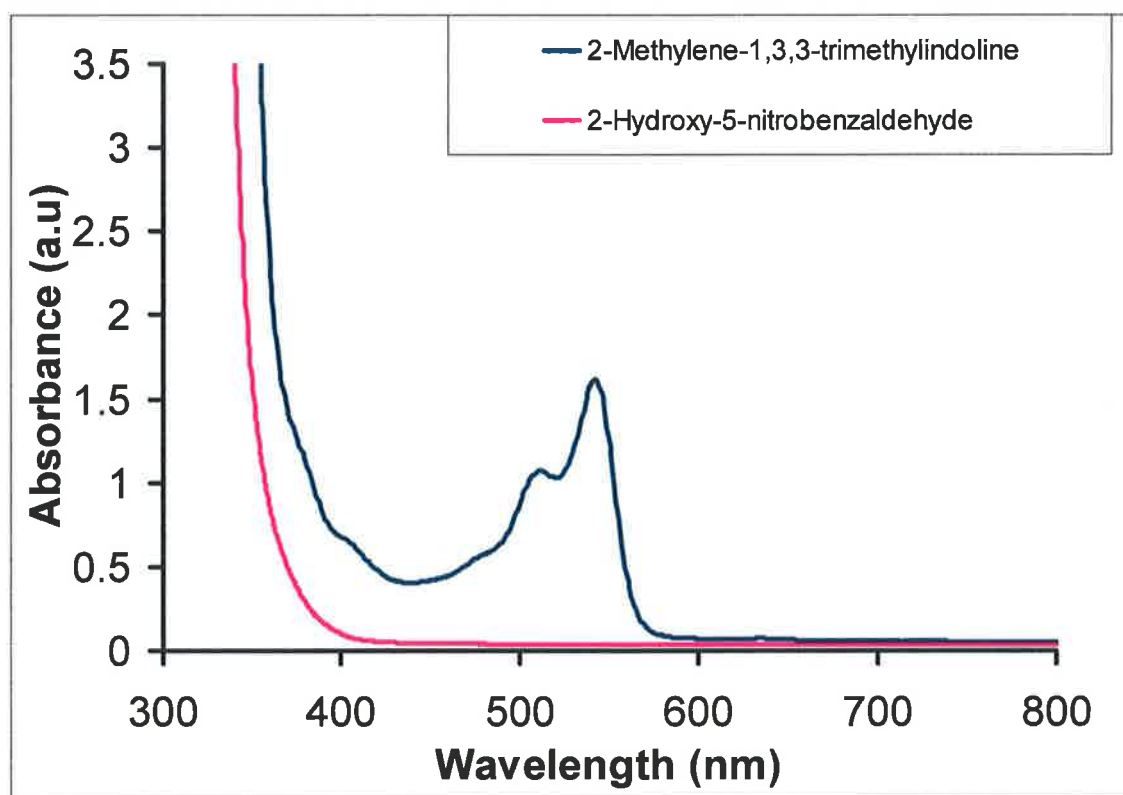
Figure 2.19. UV-vis spectrum of 10^{-3}M solutions of 2-methylene-1, 3, 3-trimethylindoline and 2-hydroxy-5-nitrobenzaldehyde in acetonitrile.

Fluorescence spectroscopy was carried out on the thermally treated sample (15 hrs) in DMSO and acetonitrile at concentrations of 10^{-4}M. **Figure 2.20** shows the emission spectrum of BSP before (A) and after 15hrs thermal irradiation to 100 °C (B) in DMSO. From spectrum A, at equilibrium we can see two emission bands (530 and 640 nm) after

excitation at 442 nm, after excitation at 520 nm we observe one emission band at 567 nm with a long absorption tail up to 680 nm. Upon exposure to visible light, the fluorescence spectroscopy changed, excitation at 442 nm yielded only one weak emission band at approximately 500 nm, the emission band at 640 nm seen at equilibrium has disappeared. After exposure to visible light, the emission intensity at 567 nm increased in comparison to the emission intensity at equilibrium, the shoulder also diminished back to 650 nm. This data could indicate that the fluorescent species seen at 640 nm after excitation at 442 nm at equilibrium is destroyed upon exposure to visible light; this in turn increases the intensity of the fluorescent species at 567 nm. Exposure to UV light has the same effect as visible light in this case. From spectrum B, at equilibrium we see an emission bands at 460 and 580 nm after excitation at 410 and 520 nm respectively. Upon exposure to visible or UV light there is no change observed. This leads us to believe that the photochemistry observed in spectrum A is not possible when the sample is thermally irradiated in DMSO. Similar emission bands were seen with samples in acetonitrile.
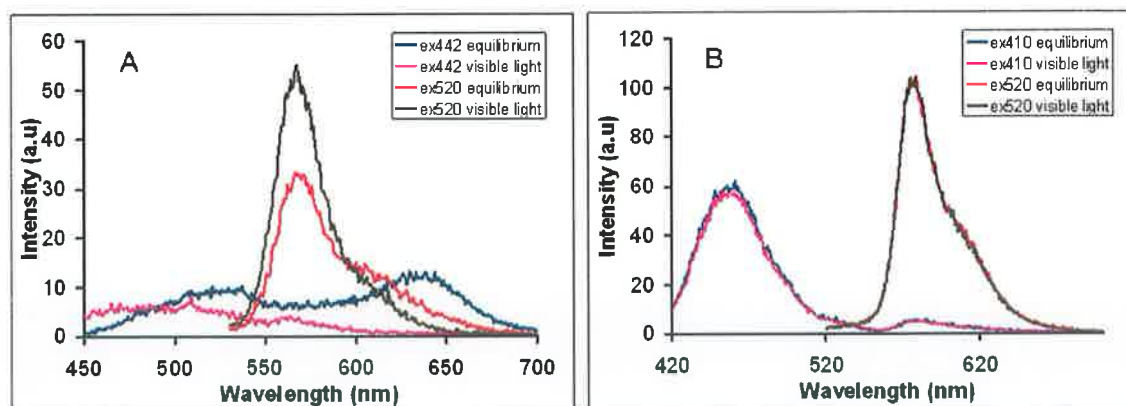
Figure 2.20. Emission spectra of BSP in DMSO (A) equilibrium 0hrs thermal treatment and (B) after 15 hrs thermal irradiation to 100 °C. All samples in DMSO and recorded at 25°C.

If the BSP molecule has broken apart into its starting materials, as it looks from the UV-vis and NMR data, FT-IR spectroscopy should show the molecular changes observed in UV-vis and NMR, specifically the aldehyde and hydroxyl vibrations. The vibrational stretching differences in BSP-DMSO "thermally treated for 15 hrs at 100 °C" and BSP are shown in

Figure 2.21 and it can be seen that the changes seen in UV-vis and NMR are reflected in the IR region of 3900-1100 cm^{-1} of the spectrum.
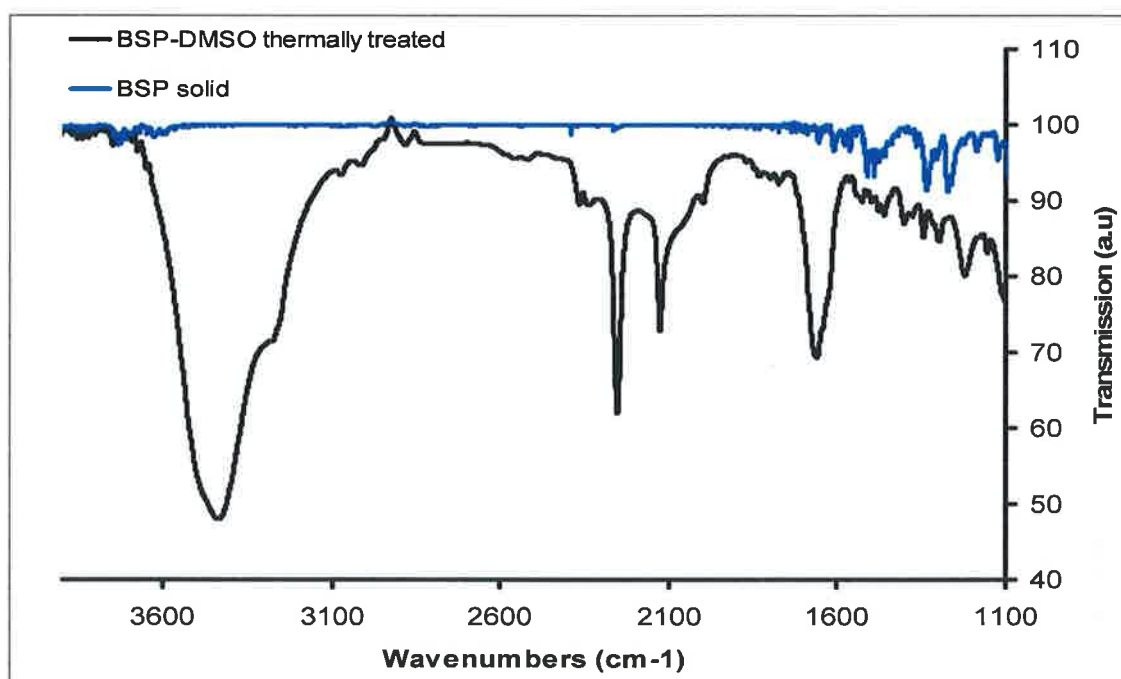
Figure 2.21. Overlaid FT-IR spectra of BSP-DMSO thermally treated for 15 hrs at 100 °C and BSP. Spectra are offset to clarify difference between samples.

The broad hydroxyl vibration located at 3430 cm^{-1} and the carbonyl stretch at 1651 cm^{-1} present in the thermally treated sample spectrum is indicative of the dissociation of the BSP molecule into its starting materials as the BSP spectrum does not contain any of

these vibrations. The hydroxyl and carbonyl stretches correspond to the stretching within the 2-hydroxy-5-nitrobenzaldehyde molecule.

The exact same experimental procedure was carried out substituting DMSO with DMF to see if the DMSO was the cause for the observed chemical rearrangement; the outcome from thermal irradiation in DMF was very similar.

2.3 Conclusions

In this chapter we analyzed the photo-, thermo-, and solvatochromic compound BSP using UV-vis, fluorescence, FT-IR, and NMR spectroscopy. It is evident from our experiments that the ground state physical properties of BSP are quite sensitive to its molecular, micro and macro environment. This can be seen in our solvatochromic study as the MC isomer is stabilized in polar solvents whereas the BSP is the predominant isomer in non-polar solvents. This sensitivity is increased when the BSP is converted to its zwitterionic isomer MC using UV light. The self-indicating nature of the BSP↔MC system provides us with facile access to important molecular and environmental information which could lead to important applications for this system as a molecular probe. The thermal relaxation of the MC to the BSP isomer is also seen to be very sensitive to the solvent system, with faster relaxation rates in non-polar solvents compared to polar solvents. In some cases the difference is over two orders of magnitude. In some solvents, such as DMSO, the BSP exhibited negative photochromism, in which the MC state appears to be the thermodynamically favoured state, in contrast to positive photochromism, in which the BSP is typically the thermodynamically favoured.

It was also observed, that BSP could switch and transduce between a passive (BSP) isomer and an active (MC) isomer which can bind ions forming a complex (MC-M^{n+}). Furthermore, the complexation and decomplexation processes could be controlled photonically using light at 360 nm and >450 nm, respectively.

The formation of *J*-aggregates in non-polar solvents when BSP is irradiated was also observed by UV-vis analysis. A BSP derivative containing a C$_{14}$ alkyl chain anchored to the indoline nitrogen was synthesized to promote aggregation formation. This derivative BSP-C$_{14}$ did not promote aggregation although from preliminary kinetic experiments it would appear the *J*-aggregates were more stable than the aggregates formed from BSP, due to their enhanced solubility in non-polar solvents.

After a standard NMR thermal experiment, an unusual UV-vis spectrum was recorded. This spectrum appeared to contain a distinct shoulder at 510 nm on the 542 nm band, similar to that seen previously with metal ion complexes. A more detailed investigation using UV-vis, NMR, fluorescence and FT-IR was completed and found that the BSP molecule was degrading upon exposure to thermal conditions above 100 °C in DMSO and DMF. This contradicts Onai *et al* as they reported BSP in the crystalline state to be thermally stable up to 177 °C, although this was in the solid state. The chemically reactive nature of DMSO and DMF seem to aid in the degradation of the BSP molecule.

In conclusion, the BSP↔MC system, its molecular interactions, such as metal ion binding, and the formation of aggregates can be controlled by light. These molecular interactions which can be formed upon exposure to UV light holds promise for the

possibility of altering a systems macro-environment. The ability to switch between two unique photo-physical states that have two distinct chemical and physical properties such as conductivity and viscosity would be truly ground breaking. Although, from the results reported herein, more research must be carried out on the BSP↔MC system and its specific molecular interactions, as it would appear that deeper interactions are present within this system that account for unexpected behaviour we have seen. Classification of this system by solvation interactions and thermal ring closing kinetics would seem to simplistic for this unique molecule.

2.4 Experimental

UV-vis measurements were recorded on UV-Vis-NIR Perkin-Elmer Lambda 900 spectrometer. Fluorescence spectra were recorded on a Perkin Elmer luminescence spectrometer model LS50B. The Ultraviolet irradiation source was a BONDwand UV-365 nm obtained from Electrolite Corporation. Samples were irradiated at a distance of 5 cm. The white light source was a Lumina obtained from Chiu Technical Corporation. In this case, samples irradiated at a distance of 7 cm. To determine the equilibrium constant K_e between BSP and MC, standard solutions of BSP were made up to 10^{-4}M in the various solvents. UV-excitation and thermal relaxation experiments were conducted as follows; sample at equilibrium was exposed to 1 minute UV light while stirring with magnet and immediately placed in spectrometer for experiment. For renewable binding studies, stock solutions of BSP (10^{-3}M) and cobalt (II) chloride (10^{-3}M) in acetonitrile were prepared, and stored in dark at room temperature. The absorbance spectrum of the

BSP solution was taken (before illumination with UV light) after allowing a measuring solution to stand overnight under dark conditions at room temperature. The solution was illuminated for 1 minute using the UV light source and the absorbance spectrum was taken immediately after illumination. The solution was then spiked with an equimolar amount of cobalt (II) chloride, the mixture was allowed to rest for 3 minutes without stirring, and the spectrum was then taken. The solution was irradiated with white light for 1 minute and the spectrum taken. The solution (still containing Co^{2+} ions) was illuminated with UV light for 1 minute and the spectrum taken. In all cases, 1 cm quartz cuvettes were used and experiments carried out in dark. NMR spectroscopy was carried out using a Bruker UXNMR-XWIN-NMR 400 MHz model equipped with a temperature controller. Thermal NMR experiment carried out as follows; sample at equilibrium held at 20 °C for ten minutes before spectrum recorded, sample then exposed to a 10 °C increment and a wait of ten minutes before spectrum recorded, this process was continued up to 100 °C.

BSP-C_{14}, **Scheme 2.4**, was synthesized according to a similar procedure reported by McCoy et al[63]. ^{1}H-NMR (400MHz, $CDCl_3$) proton assignment as in **Table 2.1** except for when mentioned otherwise, δ = 0.83 (t, 3H, $(CH_2)_{13}$-CH_3), 1.12 (s, 3H, Proton 1'), 1.29 (m, 24H, $(CH_2)_{12}$), 1.49 (s, 3H, Proton 1), 3.08 (m, 2H, N-CH_2), 5.80 (d, 1H, Proton 3), 6.51 (d, 1H, Proton 5), 6.68 (d, 1H, Proton 9), 6.79 (t, 1H, Proton 7), 6.81 (d, 1H, Proton 8), 7.02 (d, 1H, Proton 4), 7.31 (t, 1H, Proton 6), 7.93 (m, 1H, Proton 11), 7.96 (d, 1H, Proton 10). ESI-MS m/z = 505.6. BSP-C_{14} spectroscopic analysis as for BSP sample.
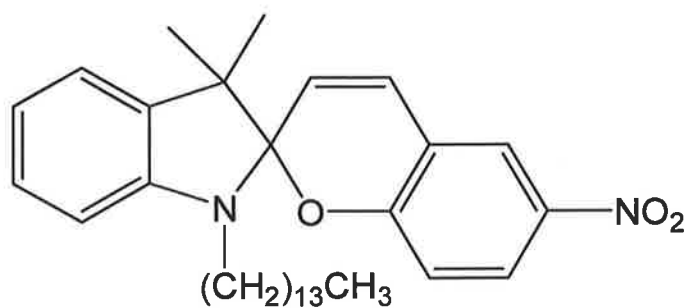
Scheme 2.4. Molecular structure of BSP-C_{14}.

BSP-C_{14} ground state and excited state properties were calculated as for BSP. FT-IR analysis was carried out on a ATR cell set-up. BSP-C_{14} aggregates were formed, from a 10^{-3}M solution of BSP-C_{14} in hexane, through an evaporation process aided by 360 nm UV light.

BSP thermal experiment in DMSO was carried out in deuterated solvent, 32 mg of BSP was dissolved in 3 ml of d-DMSO, this was placed in a sonicator for 20 minutes to aid solvation of BSP. Sample was the placed in the dark overnight at ambient conditions before analysis. Thermal treatment was carried out in pressure tube under a nitrogen environment and placed in an oil bath at 100 °C for 5 hour periods. After thermal treatment, samples allowed to cool back to room temperature in the dark overnight, before analysis. After each 5 hour thermal treatment, 0.1 ml of the sample is removed and dissolved by a factor of 100 in DMSO and acetonitrile for UV-vis analysis. 10^{-5}M BSP samples were analysed by fluorescence spectroscopy. FT-IR analysis was measured on a Perkin-Elmer Spectrum GX FT-IR system using a ATR sample holder.

3.0 Benzospiropyran as an Optical Sensor

3.1 Introduction

Since the introduction of PVC membrane electrodes over 30 years ago, developments in chemical sensing have essentially been incremental, with little in the way of fundamental rethinking of the 'chemical sensing' process. And while there have been some major advances in the theory of membrane based sensors (e.g. to demonstrate very low limits of detection through the control of ion fluxes through membranes[78]), the actual measurement process has remained unchanged.

Essentially, chemical sensor measurements involve the following processes;

- Molecular recognition – the sensor typically contains immobilised chemo-recognition agents (e.g. ligand) that selectively bind with a particular target species in the sample, and ideally does not bind with other 'interfering' species that may be present in the sample matrix. Ideally, the binding behaviour of the ligand at the sample membrane interface should remain constant and predictable over time.

- Transduction – the molecular binding event is transduced into an electronic or optical signal that can be monitored externally. The sensor may therefore have specific molecular transducers (e.g. chromophores, fluorophores or redox agents) co-immobilised with the recognition agent (or built into the molecular structure of the recognition agent), or the binding event inherently generates a signal (e.g. in

potentiometry, perm-selective binding of ions leads to the generation of an interfacial potential).

Typically, the molecular recognition and transduction agents are immobilised within a membrane or on an active surface, and this is exposed to the sample. Accurate measurements require calibration, due to the fact that sensor surfaces/membranes are 'active' i.e., they must interact chemically with the sample to generate a signal and must therefore be in intimate contact with the sample to generate the signal. This is in contrast to physical transducers such as thermistors, that can be completely encapsulated in a protective coating (e.g. epoxy) which nonetheless does not interfere with their ability to function.

Hence, chemical sensors must be regularly recalibrated for accurate measurements as the surface and bulk characteristics change with time due to various interactions with the sample. For example, active components may leach out into the sample, chromophores may become photo-bleached, or surfaces may become fouled. The need for calibration means that the sensing surface must be regularly removed from the sample and exposed to usually two or more reagents that ideally mimic closely the matrix of the sample and contain differing concentrations of the target species. Calibration thus enables the response slope and intercept to be re-estimated (for non-linear responses, more that two calibrants are required), and experimental signals to be more accurately related to the unknown concentrations.

This is the procedure that is used almost uniformly for chemical sensor measurements. It implies, however, that autonomous field deployable sensors must incorporate a calibration regime, and the instruments are therefore relatively expensive and complex, as they must incorporate the necessary reagents, pump, valves, power, electronics and self-diagnostics required to ensure that the device is functioning properly. Consequently, chemical sensors (and similarly, biosensors) in their current manifestation described above, are too complex and expensive to be function autonomously in large numbers. Hence these devices are almost completely ignored in the emerging area of 'sensor-nets' (i.e., deployments of wireless networks of sensing devices) and it is difficult to imagine how the current technology can be scaled up to the numbers involved in wide-area distributed monitoring.

This project describes a new concept for chemical sensing based on the following principles;

- The sensor surface should be populated with inactive species when a measurement is not being conducted

- The surface is converted into an active form under an external stimulus (optical in this case)

- The active form binds with the target and generates a signal that enables the analytical measurement to be made

- After the measurement is completed, the guest species is expelled by an external stimulus (optical) and the surface returns to its inactive form.

Using this approach, it may be possible to maintain sensing surfaces in an inactive form that would remain relatively unchanged over time, potentially extending the sensor's useful lifetime by minimizing poisoning effects, and simplifying calibration as a new sensing surface is generated 'on demand' each time a measurement is made. Utilizing photo-switchable molecules such as spiropyrans[9], which can be switched between active or passive forms, may enable such behaviour to be realised.

As described in Chapter 1 and 2, upon exposure to UV light BSP undergoes a heterocyclic ring cleavage that results in the open MC form, **Figure 3.1**. While the spiropyran or closed form of the dye is colourless, the open merocyanine structure has a strong absorption in the visible region. When the spiropyran is converted to the merocyanine form, this structure has an active binding site for cations, in contrast to the spiropyran form, which does not bind cations. The merocyanine forms complexes with certain d- and f-elements in solution[43]. The merocyanine structure has a strong absorption in the visible region and a marked blue shift is caused by complexation with the phenolate oxygen atom of the merocyanine. By shining white light on the coloured complex, the dye is reverted to the closed, inactive spiropyran form, and the cation is released. This reversible binding of cations in solution is well documented[28, 49, 51, 52], but we are interested in developing a solid-state version of this chemistry.
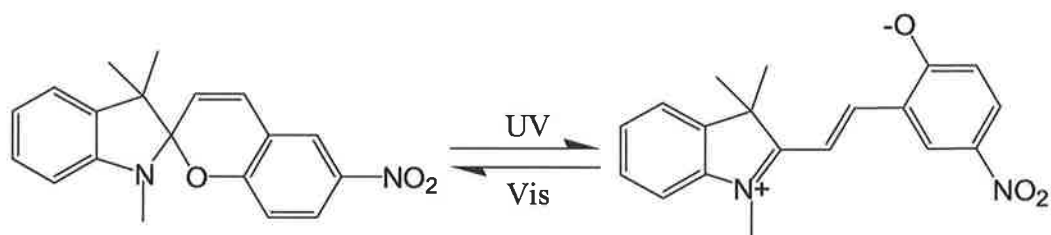
Figure 3.1. Structure of benzospiropyran in closed (spiropyran) and open (merocyanine) form.

In principle, this would provide a novel opportunity to produce a sensor with unique capabilities for metal ion sensing. For example, it would be attractive if the spiropyran molecule could be entrapped or immobilised to a particular material (e.g. polymeric membrane). The sensing material could be maintained in an inactive state between measurements, and switched to an active state under an external stimulus (optical in this case) when a measurement is required. Once in the active form, binding with the metal ion happens and the analytical signal is generated. After the measurement is completed, the metal ion is expelled by an external stimulus (optical once again) and the material returns to its inactive form.

It seems that the material with which the spiropyran is entrapped/ immobilised is key to the realization of a physical device. There has been a lot of work completed on the inclusion of spiropyrans into host polymer matrices[45], sol-gels[79], complexes with cyclodextrins[47], and self-assembled monolayers[25, 48] for applications such as photochromic ophthalmic lenses[10] or camera filters, optical information storage[19], optoelectronic systems (semi-conductors modulated by photochromic pigments)[80] and computing[29]. As it has been stated before, spiropyrans have been extensively investigated

110

in solution for various applications and none more so than metal-ion recognition, but a solid-state version of photoreversible metal binding incorporating spiropyran has had limited success[54, 55].

For the application of metal ion sensing it requires the spiropyran molecule to be attached to a surface such as glass or gold or entrapped within polymeric matrices. This is significant because the polarity of the microenvironment of the spiropyran dramatically affects its photochromism. It is known that in polar environments the open, merocyanine form is stabilized[52]. Thus, the polarity of the spiropyran microenvironment is an important factor to be taken into account during the design of any command surfaces using spiropyrans[81]. Both the absorption and the emission wavelengths of the open form of the spiropyran may be used to indicate polarity of the microenvironment of the solvatochromic species.

Photo-reversible metal ion complexation with spiropyran in solution is well understood, the real challenge is to develop a material that can capture and realize metal ions optically. The inclusion of spiropyran in numerous polymer matrices and various spiropyran immobilization techniques to polymer supports was investigated. This work also details the realization of a potentially low cost solid-sate sensing system for photoreversible metal binding. Typically spiropyrans are switched between the BSP and MC states using mercury arc lamps or lasers. However, in order to easily incorporate spiropyrans and other photochromic materials into optical sensor platforms, they should ideally be actuated with an inexpensive, low-power light source such as a light-emitting

diode (LED). While LEDs have been used to switch diarylethenes[82] in solution, to our knowledge, their use with spiropyrans has not yet been reported. Their potential use as optical actuators for use in photochromic materials was investigated.

3.2 Results and Discussion

3.2.1 LED switching of spiropyran doped polymer matrices

In order to develop devices that combine LEDs with BSP doped polymer films, the effectiveness of using LED light sources to actuate the colouring and bleaching process in these films needed to be determined. To this end, three different polymer films were spun onto PMMA substrates to create photochromic surfaces. PMMA was chosen for its optical transparency in the visible spectrum so as not to interfere in the characterization of the spiropyran film. Depending on the polarity of the polymer film, the MC had a different absorption maximum as seen in **Figure 3.2**. This shift in the absorbance spectrum is due to the solvatochromic nature of the dye, as has previously been reported[41, 81]. The dye exhibited a red shift as the polymer matrix became more non-polar, with the polymethacrylic acid (PMAA) film having an absorbance maximum at 530 nm, while the more non-polar polystyrene (PS) film had an absorbance maximum at 566 nm. This demonstrates that the absorbance of the merocyanine dye can be tuned by controlling the polarity of polymer matrix.
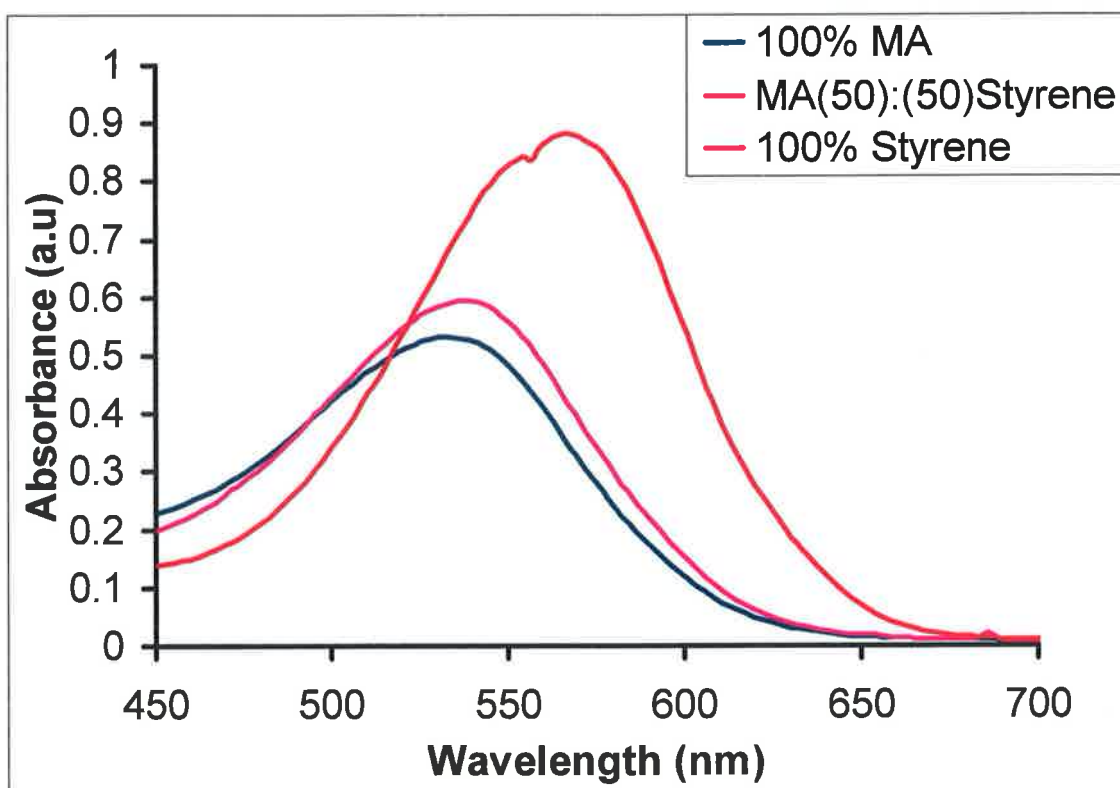
Figure 3.2. UV-vis spectra of MC isomer entrapped in a thin films consisting of 100% poly(methacrylic acid), 50/50 poly(methacrylic acid)/ polystyrene and 100% polystyrene.

The three different photochromic films were also characterized in terms of their thermal relaxation kinetics for switching between the MC and BSP forms of the films under LED irradiation. It has been previously reported that the thermal relaxation rates can be different in different polymer matrixes[83, 84], to determine if there was a significant difference based on the compositions of our films first-order rate constants for the colouring and bleaching of the dye-doped polymers were determined using the non-linear optimization add-on 'Solver' (Microsoft Excel), by fitting the absorbance data to a standard first order model [71].

The photochromic rate constant k is subscripted UV and VIS to denote the forward and reverse processes, respectively, as shown in **Figure 3.1**. **Figure 3.3** shows an example of the k_{UV} data obtained from a 50:50 PMAA/PS BSP-doped polymer film. As seen in **Figure 3.3a**, the absorbance value increases as soon as the UV LED is illuminated, indicating the opening of the BSP into the MS isomer. The photostationary state was reached after only three minutes of UV irradiation compared to 10-30 minutes reported by others[83, 85]. Upon exposure to a green LED, the MC closed again to the BSP state as seen in **Figure 3.3b**, returning to the baseline absorbance value within five minutes. The models obtained fit the data well as demonstrated by having less then 2% error for most data points (insets **Figure 3.3a** and **b**).
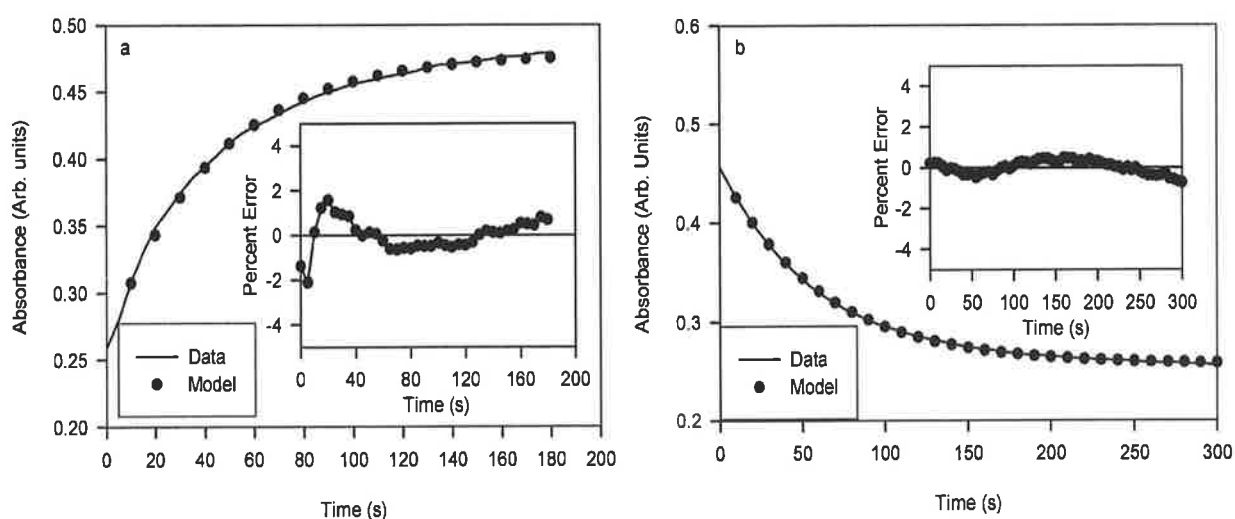
Figure 3.3. Kinetics (absorbance vs. time) plots of a 50/50 polymethacrylic acid/ polystyrene film at 540 nm and 20 °C for; (a) ring opening using a UV [380 nm] LED (left) and, (b) Ring closing using a green [525 nm] LED (right). In both cases, the fit to a single exponential (first order) model is shown, with a residuals plot of percent error for the single exponential model as an inset.

The k_{UV} and k_{VIS} rates for the different polymer matrixes are reported in **Table 3.1**. The rate constants obtained in these polymer films (2 x 10^{-2} s^{-1}) are larger than those previously reported (2 x 10^{-3} s^{-1}) by Tork *et. al.*[83], but are probably due to differences in the film composition and the photon source used. Interestingly, although the different ratios of methacrylic acid and styrene in the polymer films led to changes in the absorbance maximum of the MC (**Figure 3.2**), the switching kinetics of the films seemed to be unaffected by this polarity change as seen by the similarity in the rate constants reported in **Table 3.1**.

Polymer Formulation	k_{UV} (s^{-1})	k_{VIS} (s^{-1})
PMAA	(2.6 ± 0.1) x 10^{-2}	(1.2 ± 0.1) x 10^{-2}
PMAA / PS	(2.5 ± 0.2) x 10^{-2}	(1.7 ± 0.1) x 10^{-2}
PS	(2.2 ± 0.3) x 10^{-2}	(1.4 ± 0.1) x 10^{-2}

Table 3.1. Spiropyran opening and closing kinetics in different polymer films.

While most papers report using 50-100 W white-light power sources equipped with bandpass filters to provide an irradiance in the mW /cm^2 range[81, 83, 86], in this work we used a low-power UV LED, which still provides an irradiance of approximately 1 mW /cm^2. Despite the drastic difference in current and voltage requirements of LEDs relative to arc lamps, the LEDs are still able to switch the BSP-doped polymer films with remarkable effectiveness. Using the LED set-up shown in **Scheme 3.2**, the PMAA/PS film was switched between the coloured and uncoloured forms of the dye 100 times using

10 second exposures of UV light (**Figure 3.4**), generating approximately 25% of the steady-state absorbance. Photo-fatigue of the film was observed, culminating in an 11% loss in the maximum absorbance value at 540 nm after 100 cycles. Despite this loss in absorbance, the effectiveness of using LEDs as photoactuators for BSP is clearly demonstrated.
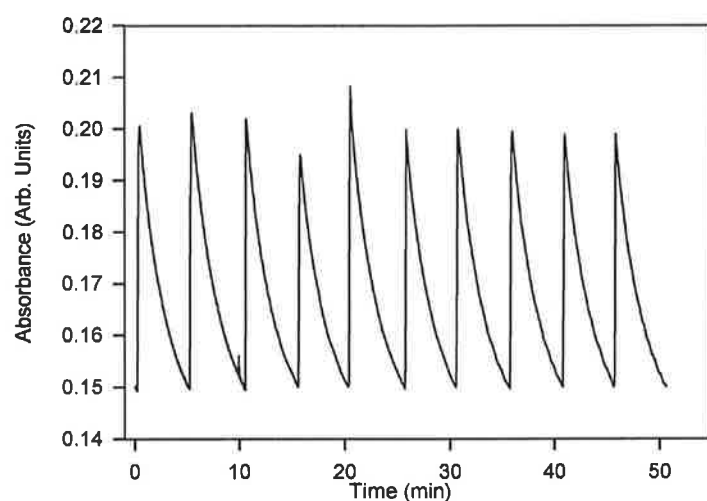
Figure 3.4. LED switching of photochromic PMAA/ PS polymer film; first 10 switches between coloured and uncoloured forms of the dye.

3.2.2 Immobilisation of spiropyran derivatives to polymer surfaces

For the realisation of an optical sensing device a solid substrate must be needed to conduct the experimental measurement. PVC is currently the most commonly used polymer for membrane-based ion-selective electrodes because of its strength, compatibility with ionophores, and chemical inertness[78, 87]. However, it has some limitations in applications such as optical sensors because of its poor adhesion to solid supports. Upon long exposure to aqueous environments, PVC membranes can peel off the substrate. Further, the preparation of PVC membranes often involves the use of solvents, such as tetrahydrofuran, that are incompatible with some of the plastics used in microfluidic devices. Methacrylic-acrylic materials generated by chemical or optical methods of polymerization have been used in ion sensing in the form of films[88] and are better suited for integration into microfluidic devices. The methacrylate group also allows for covalent attachment to a pretreated substrate during photopolymerization. Additionally, use of a structurally similar solid substrate, such as poly(methyl methacrylate) (PMMA) enhances adherence of the photopolymerized material through non-covalent interactions. Therefore, PMMA was chosen for its optical transparency in the visible spectrum so as not to interfere in the characterization and actuation of the BSP film.

Incorporating the BSP into various PMAA/Styrene matrices allowed us to switch between the BSP and MC form using low powered LED light sources, this shows that there must be some flexibility within the polymer matrix for the molecule to switch back

117

and forth. Will there be enough flexibility for the merocyanine to form the preferred complex with the cation as in solution? Job's plots in acetonitrile indicated that the cation complex was due to a 2 :1 MC–cation complex (**Figure 3.5**), suggesting that the Co^{2+} ion is sandwiched between two merocyanine molecules. This is an important finding, as it has implications for effective Co^{2+} complexation *via* surface bound merocyanine ligands in terms of their ability to rearrange sufficiently to generate the appropriate conformation. Solution phase chemistry can differ greatly from solid phase chemistry[89], particularly if the stoichiometry requires convergence of multiple ligands around a single guest species.
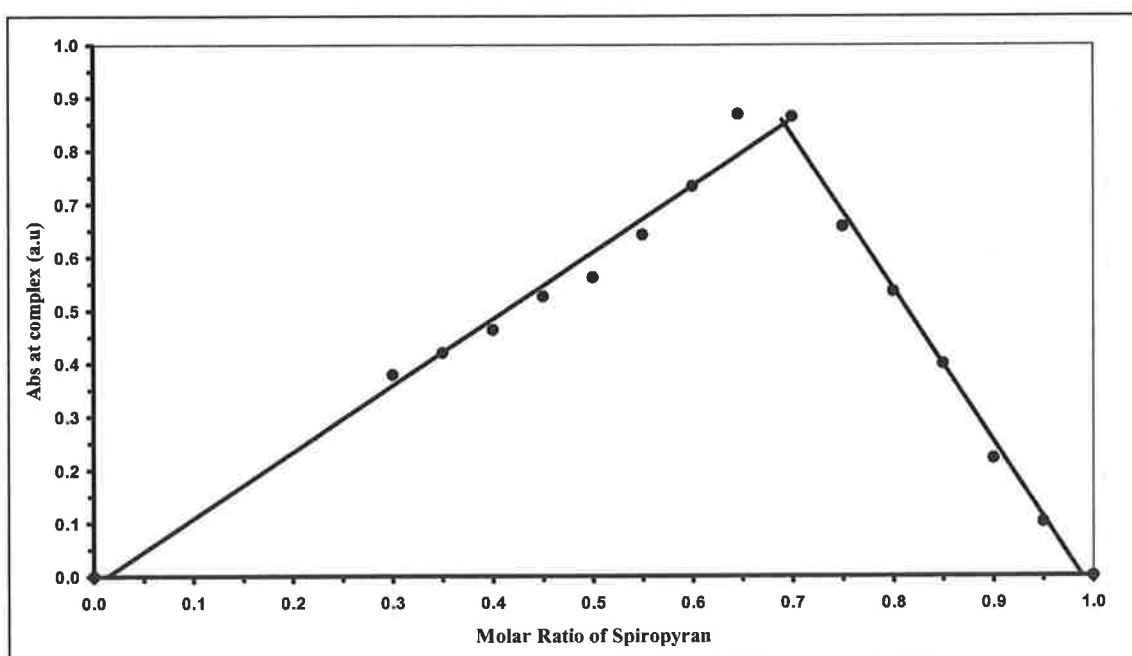
Figure 3.5. Job's Plot of MC-Co^{2+} complex formation in acetonitrile.

No metal ion complexation was observed for BSP entrapped within the PMAA/Styrene matrices. After several experiments were preformed on these materials, we believed that the preferred MC-cobalt complex could not form due to several reasons; steric hindrance of the PMAA/Styrene polymer backbone inhibiting the merocyanine from interacting

with the cation and forming the coloured complex, the 1 mol% dispersion of BSP was too dilute throughout the polymer matrix (especially when the complex requires two merocyanine molecules to conform around one cobalt atom), and when experiments were carried out in PMAA/Styrene matrices containing various plasticizers it was found these plasticizers inhibited the merocyanine form from interacting with the metal ion due to their polarity and zwitterionic characteristics.

Given that the solution phase studies indicated that a 2:1 complexing ratio of MC to metal ion was needed, we were concerned that covalent immobilization of the BSP molecules to a polymer backbone might inhibit or completely eliminate the ability of the complex to form as in the BSP entrapped polymer matrices. The immobilization strategy therefore needed to allow enough flexibility for the BSP molecules not only to photoisomerize between the active and passive forms, but also to come together in a sandwich metal complex with neighbouring MSP molecules. We therefore used a series of diamino alkyl linkers, ranging in length from two to eight carbons, as a method to covalently attach BSP-CO_2H derivative version of the BSP to PMMA (**Scheme 3.1**).
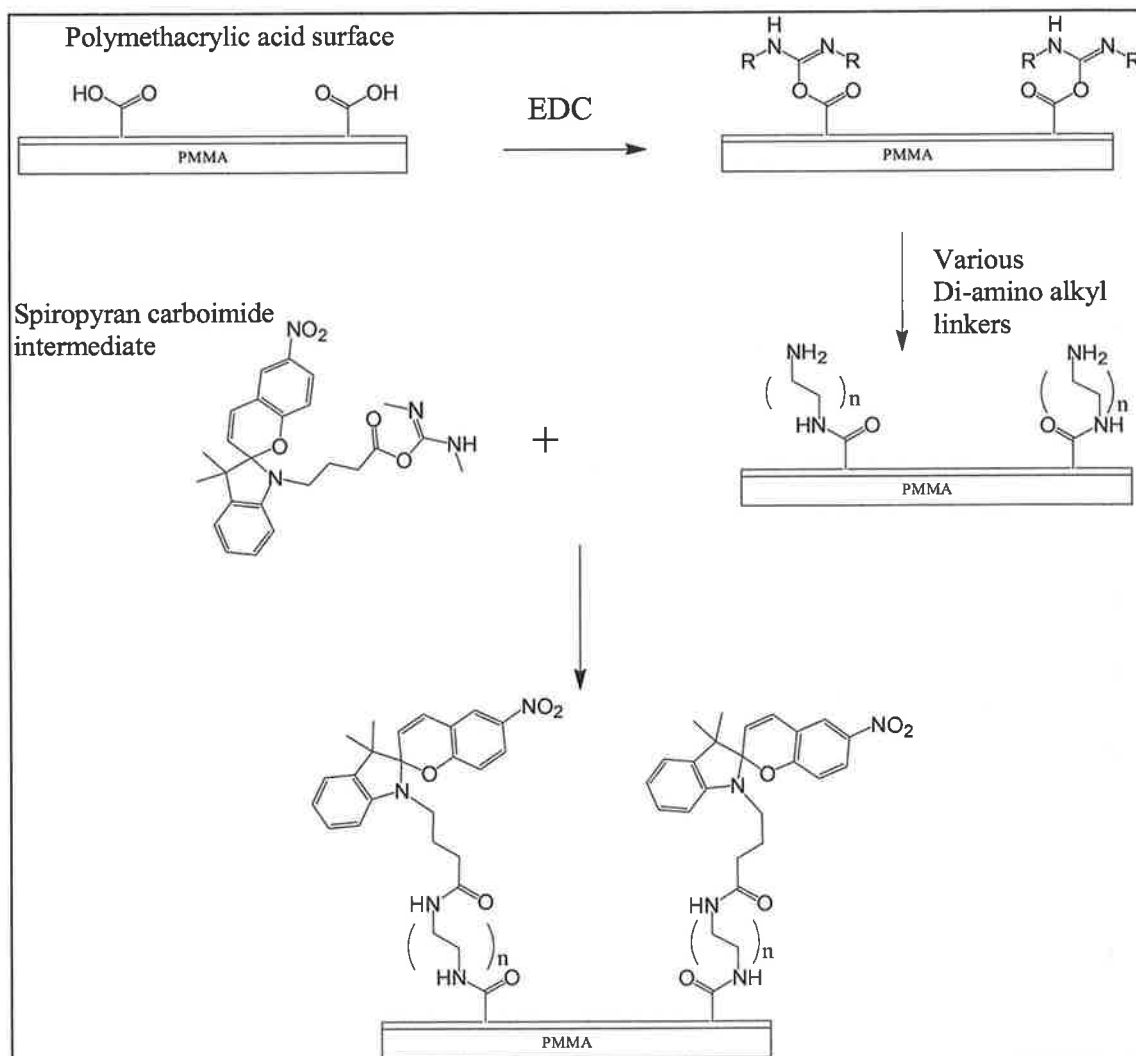
Scheme 3.1. Immobilization of BSP-CO$_2$H to PMAA polymer via di-amino alkyl linkers.

3.2.3 Characterization of spiropyran immobilized films

The BSP-modified polymer substrates were treated to a series of experiments to determine whether the tether length influenced the efficiency of photo-switching, ion complexation and de-complexation, and regeneration of surface-bound spiropyran for further measurements. It was expected that formation of the 2 : 1 complex would be affected by molecular flexibility, and therefore tether length would be important.

120
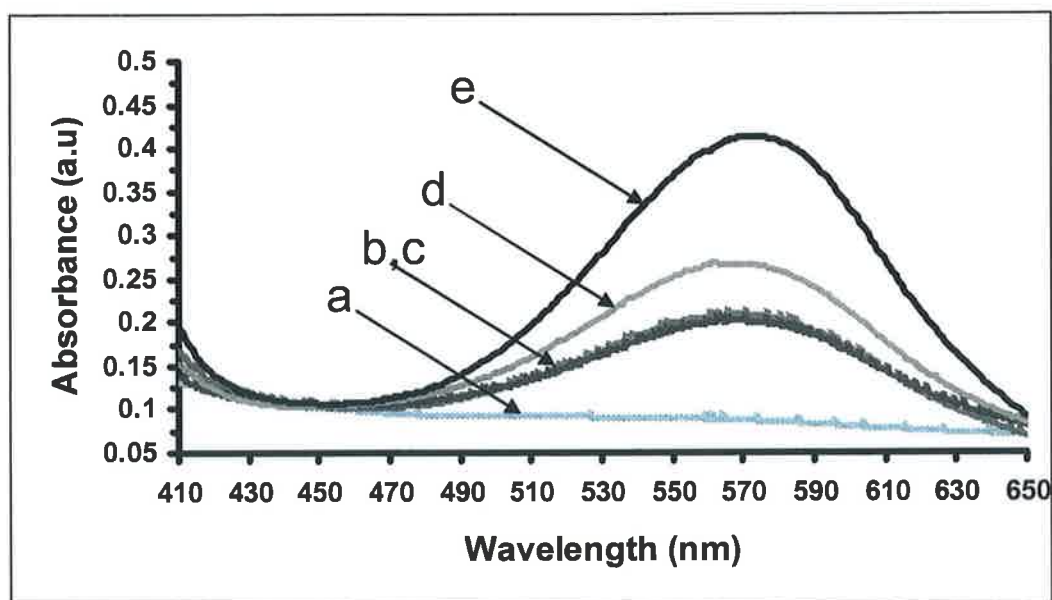
Figure 3.6. UV-Vis spectra of (a) average of BSP-2, BSP-4, BSP-6 and BSP-8 control spectra prior to UV-illumination and merocyanine form (b, c) of BSP-2, BSP-4, (d) BSP-6 and (e) BSP-8 after 60 seconds UV-illumination. Data normalised at 450 nm.

Figure 3.6 shows the effect of tether length on the switching efficiency between the BSP and MC isomers. Clearly, the ability of BSP to photoisomerize dramatically improves with increasing tether length, as evidenced by the increasing absorbance at 570 nm, the absorbance maximum for the covalently bound MC. There is little change in the absorbance for the BSP-2 and BSP-4 films, however, the BSP-6 and BSP-8 films show increasing absorbances at 570 nm. These data suggest that a certain minimum distance from the polymer backbone is required to facilitate efficient switching to the merocyanine form, which involves rearrangement of the molecular structure into a planar, extensively conjugated zwitterion. The λ_{max} of the MC isomer also indicates that the molecule exists within an environment similar to cyclohexanone, due to its solvatochromic nature. The

121

solvatochromic environment of the molecule is just as important as the steric issue discussed previously, as ion binding does not occur favorably in polar solvents such as ethanol.

Given that isomerization to the active merocyanine form was evident with all four tether lengths, the BSP-modified films were then exposed to Co^{2+} to determine firstly, if ion binding occurs and secondly, whether the tethers length enhanced metal complexation. **Figure 3.7** shows the change in UV-Vis spectra of the merocyanine forms of BSP-2, BSP-4, BSP-6 and BSP-8 when exposed to 1×10^{-2} M cobalt (II) chloride solution. In the case of BSP-2 and BSP-4, there is little change in the spectra (a, b), indicating that complexation is greatly inhibited. With the BSP-6 coating (c), some change is observed, but this is still not significant. However, in the case of the BSP-8 coating (d), in the presence of the metal salt there is a large decrease in absorbance at 570 nm (free merocyanine), and a correspondingly large increase at 430 nm (Co^{2+}-complex). Clearly, complexation is happening much more effectively in the case of BSP-8 tethered films. While the BSP-2, BSP-4 and particularly the BSP-6 films have enough flexibility to switch to some degree between the two isomers (BSP↔MC), formation of the metal complex is greatly inhibited. In the case of the BSP-8 film, these results strongly suggest that the 8-carbon spacer provides enough flexibility to enable the Co^{2+}–MC complex to form.
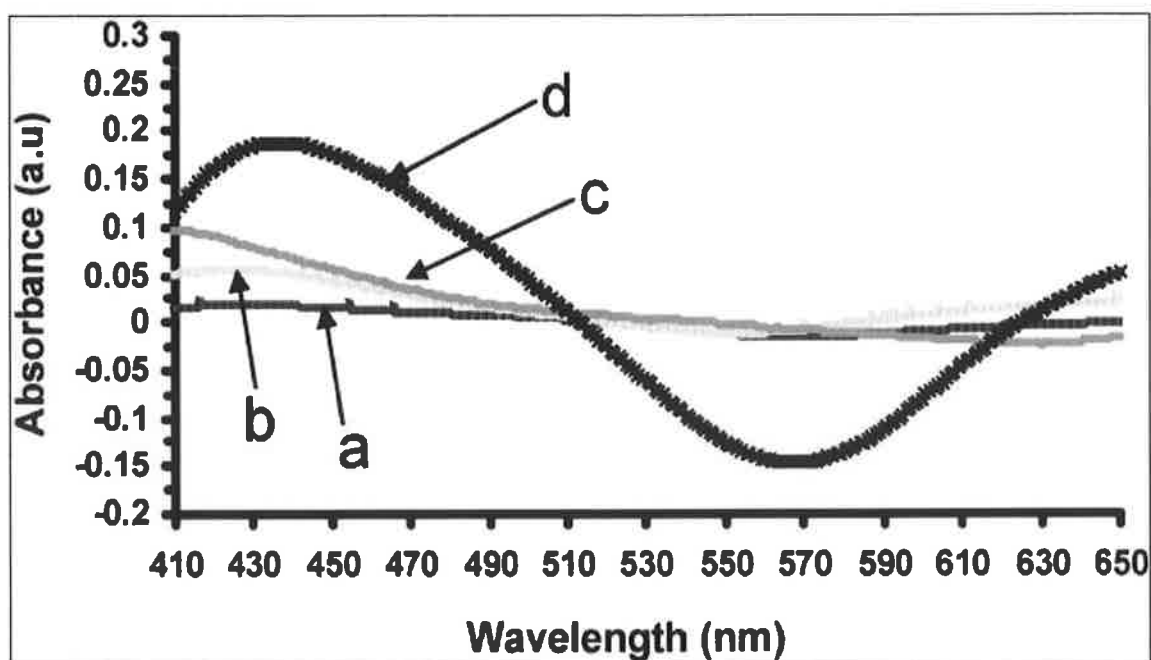
Figure 3.7. UV-Vis spectra recorded for the merocyanine form of (a) SP-2, (b) SP-4, (c) SP-6 and (d) SP-8, in the presence of 1×10^{-2} mol cobalt (II) chloride solution.

Figure 3.8 gives some indication of the kinetics of the complexation reaction obtained with the BSP-8 films. Addition of Co^{2+} ions leads to a decrease in absorbance at 570 nm and a corresponding increase at 430 nm as expected, with the steady state being reached after about 1 minute (no stirring). Note that the gradual decrease in the absorbance at 570 nm obtained with the control sample (no metal ions) is expected, due to the tendency of the merocyanine form to revert naturally to the spiropyran form. This result is important as it demonstrates the sensor has a relatively fast response, compared to many optical sensors. This is probably due to the open structure of the PMAA film, which allows rapid establishment of a pseudo steady-state upon contact with the sample solution.
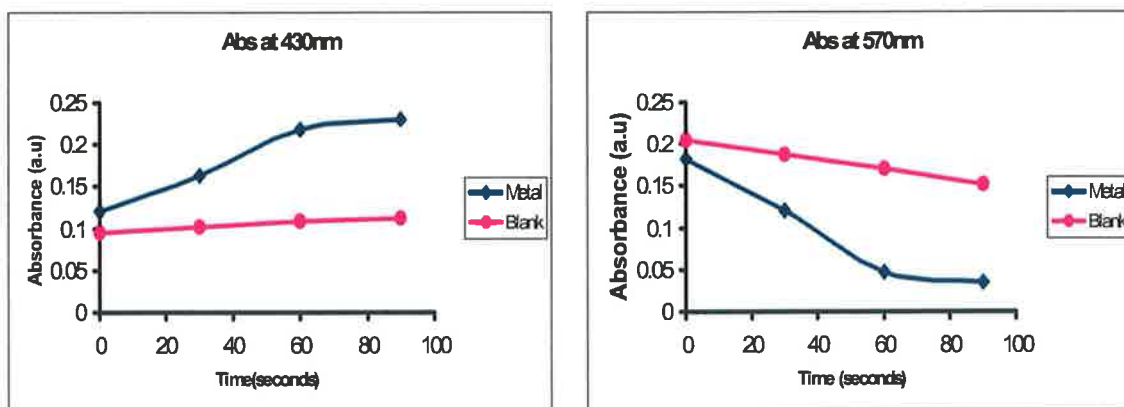
Figure 3.8. Absorbance of 8-carbon tether system when exposed to control (blank) and cobalt chloride solution at 430nm (right) and 570nm (left).

Having demonstrated that it is possible to switch between the BSP–MC forms and that the Co^{2+} complex could form, the next step was to regenerate the original passive BSP film, and repeat the binding cycle, as had been demonstrated previously in solution phase experiments. **Figure 3.9** shows the average of absorbance spectra measurements carried out on a single BSP-8 coated substrate cycled through exposure to 1×10^{-3} M cobalt(II) chloride three times. Each cycle involved the generation of the passive spiropyran surface using white light; switching to the active merocyanine surface using UV light; formation of the Co^{2+} complex; and expulsion of the Co^{2+} ions and regeneration of passive BSP surface using white light. The absorbance spectra show that the binding process can be repeated at least three times on a given BSP-8 film.
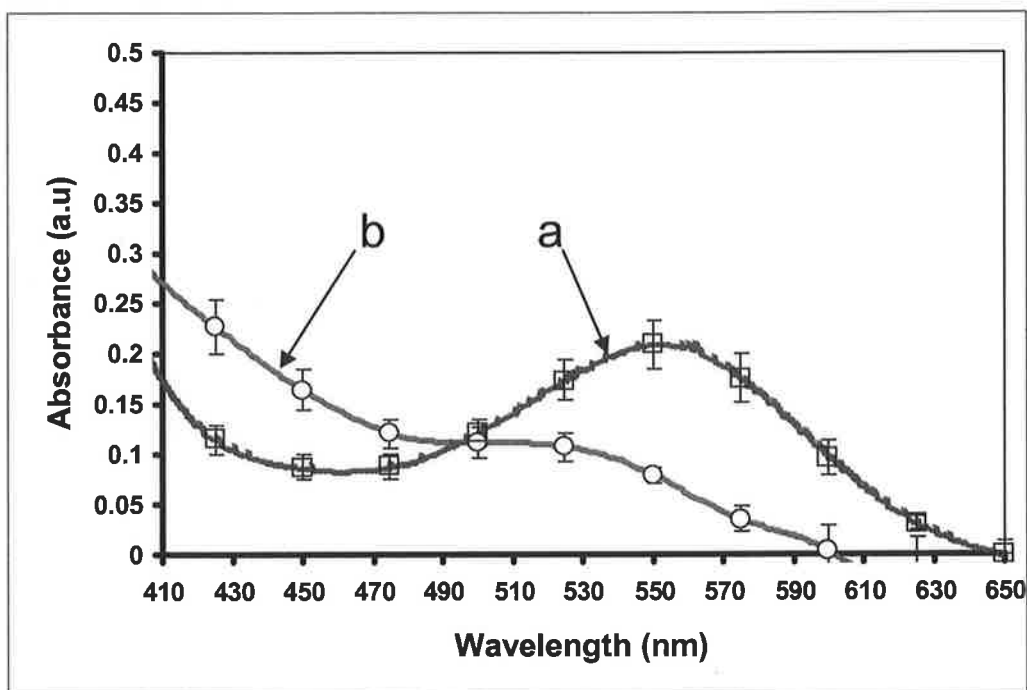
Figure 3.9. Spectra obtained after cycling through conversion of BSP-8 film to merocyanine form, generation of Co-complex, and regeneration of BSP-8 film 3 times. (a) Average of 3 spectra obtained for the merocyanine form, and (b) average of 3 spectra obtained for the Co-complex.

Figure 3.10 shows two photographs, the picture on the left corresponds to the merocyanine form of the BSP-8 film and the picture on the right corresponds to one of the MC films exposed to 1×10^{-3} M cobalt(II) chloride in ethanol (pink colour) and the other merocyanine film exposed to just ethanol (purple colour). **Figure 3.11** is a schematic representation of two BSP-8 tethered MC molecules arranging themselves around the cobalt ion forming the coloured complex.
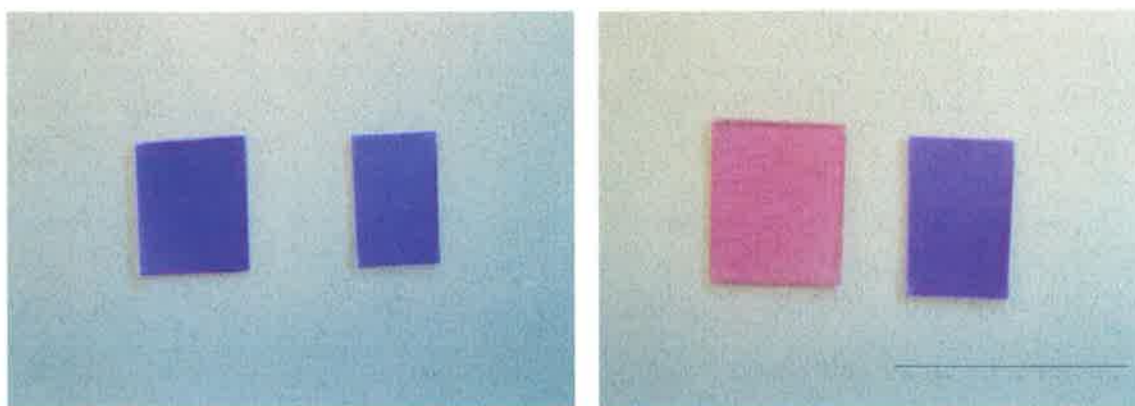
Figure 3.10. Left picture-photograph of two BSP-8 films irradiated with 1 minute UV light BondWAND (360nm); Right picture-photograph of previous BSP-8 films one immersed in ethanolic solution of 1×10^{-3} M cobalt(II) chloride for 1 minute (pink film) and the other BSP-8 film immersed in just ethanolic solution for 1 minute (purple).
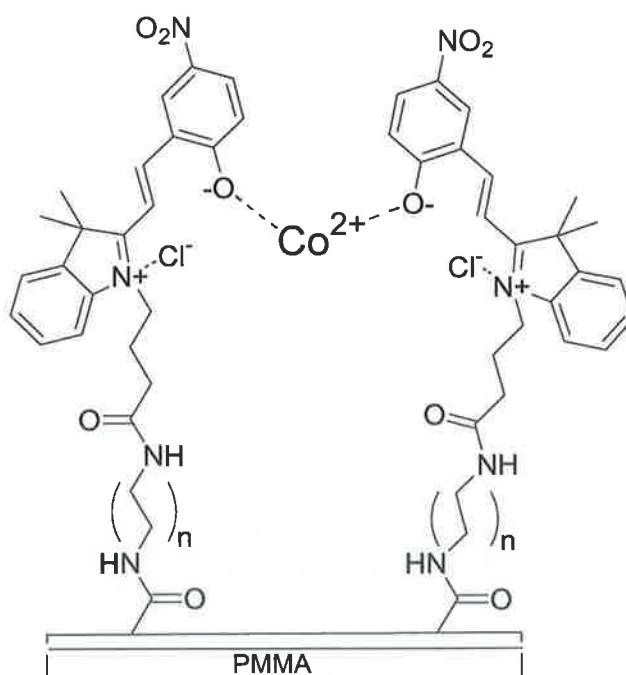
Figure 3.11. Schematic representation of two BSP-8 tethered merocyanine molecules arranging themselves around the cobalt ion forming the coloured complex.

The BSP-8 polymer substrate was further characterized by various techniques to calculate the molar absorptivity of the photochromic polymer. PMMA is well known to have a porous polymer structure, **Figure 3.12**, and it is expected that the BSP-immobilised polymer will adsorb into the existing PMMA polymer structure.
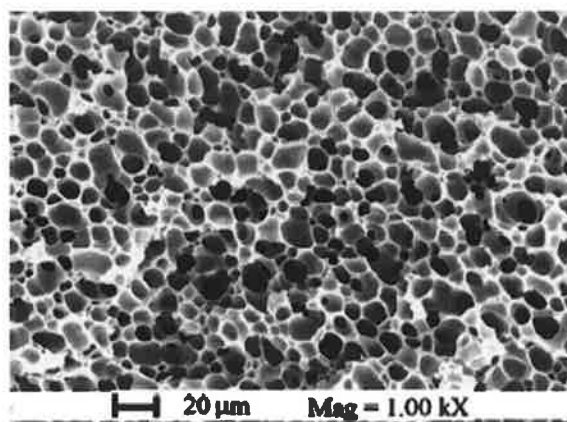
Figure 3.12. Structure morphology of PMMA obtained by SEM[90]

Under imaging microscopy, the BSP-immobilised polymer was found to be approximately 130 µm thick (130 ± 15 µm, $n = 10$). **Figure 3.13** shows the adsorption of the BSP-immobilised polymer into the porous PMMA substrate. The polymer-spiropyran loading was calculated to be 8.026 x 10^{-4}M and from this the extinction coefficient for the merocyanine form of the SP-8 film was calculated to be 3.98 x 10^4 $M^{-1}cm^{-1}$.
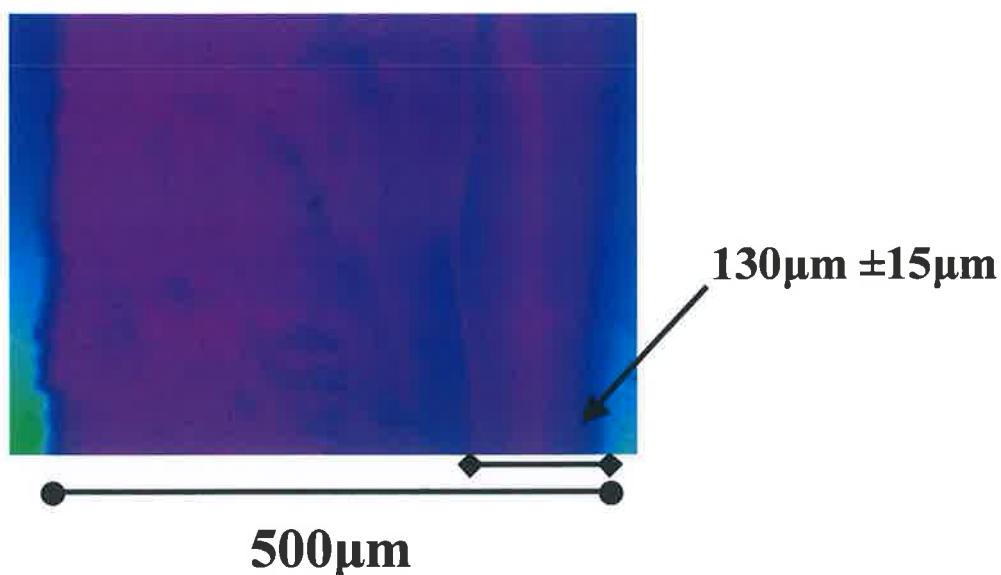
Figure 3.13. Image (looking down) of a cross section of SP-8 polymer film adsorbed into PMMA polymer.

Recently there has been much interest in the general field of microfluidics for a number of emerging applications in analytical chemistry[91-93]. This miniaturization of fluid processing poses many unique challenges requiring new methods and materials. Tasks essential to the operation of all microfluidic devices are the ability to move small volumes of fluid through microchannels and to control fluid flow. With decreasing scale, pumps and valves with moving parts become less attractive from an economic perspective and create daunting manufacturing challenges. For applications needing only occasional use or when sterility is required, single-use microfluidic devices face even greater economic pressure. These concerns have stimulated research into the control of fluid flow in microchannels using systems with no moving parts that can be scaled down to very small volumetric flows.

Manipulation of microchannel or capillary surface properties using a readily controlled external stimulus holds promise as a means for developing new modes of liquid transport for very small volumes. At these small characteristic dimensions, intermolecular and interfacial forces dominate over the force of gravity. Researchers have proposed the use of a variety of means of changing the interfacial properties of materials to induce or control surface wetting by liquids, including electrical potentials and fields[94], temperature[95], and optically[96].

The use of light offers unique opportunities. Advances in the integration of LED sources into systems hold promise for the production of low-cost miniaturized systems. Also, light fluxes are easily controlled temporally, and the action of light can be independent of the liquid properties. But perhaps most importantly for biological solutions, conditions for photoactuation may be relatively mild. For biological applications, extremes in temperature, the use of nonaqueous solutions, and the use of aqueous conditions differing radically from physiological norms must be avoided.

Contact angle measurements were carried out for the BSP (off) form of the polymer and the MC (on) form of the polymer. The BSP polymer should be hydrophobic to water since it's in the non-polar form and should repel the water droplet from the surface. On the other hand, the merocyanine polymer should be hydrophilic to water since it's in the polar zwitterionic form and should attract the water droplet to the surface. From the data obtained in **Figure 3.14**, our expectations were realised. The BSP polymer gave a surface to water droplet contact angle to be $76.42° \pm 1.2°$, where as the MC polymer gave a

surface to water droplet contact angle to be $63.23° \pm 1.6°$ after 1 minute UV irradiation. That's a $13.19°$ degree change from the BSP (off) to the MC (on) state, where n = 3.

The concept of moving water on a surface could be realized using the BSP-8 films and experiments prove that contact angle changes are similar to that reported by Rosario[96] but the BSP-8 films show much more promise with regards to potential, Rosario work reports $11°$-$14°$ changes on a glass surface after 30 minutes irradiation with UV light, we have a $13.19°$ after only 1 minute UV irradiation.
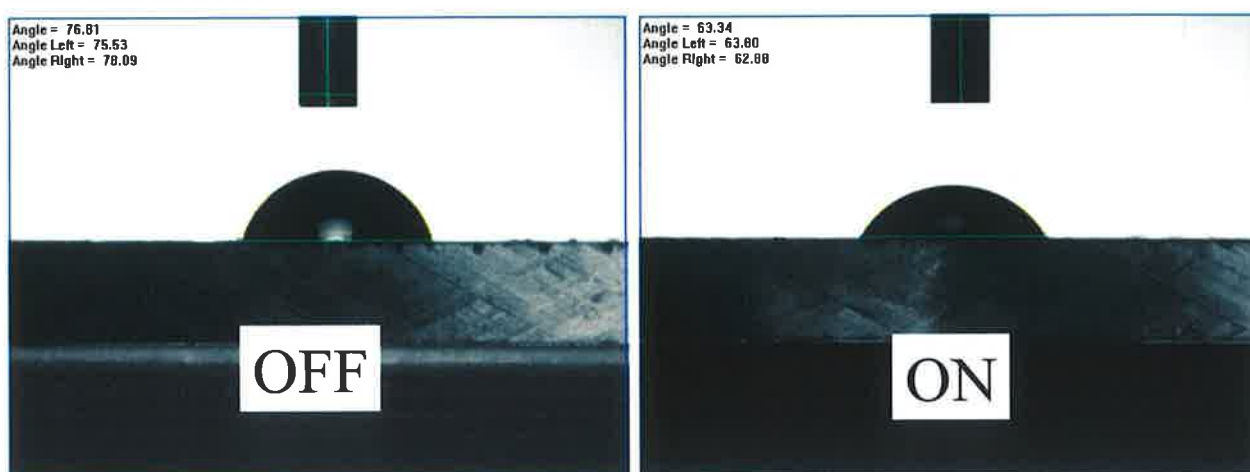
Figure 3.14. Contact angle measurement images of SP-8 film (left) and after 1 minute irradiation of UV light (right).

3.3 Experimental

3.3.1 Materials and Instrumentation

Polymethylmethacrylate (PMMA) sheets (0.5 mm thick) were cut to size and washed with Ethanol before use (Goodfellows). Styrene, Methacrylic acid, acetophenone, 6-Nitro-1´,3´,3´-trimethylspiro[2H-1]-benzopyran-2,2´-indoline, 98% (BSP), ethylenediamine 99% (redistilled), 1,4-diaminobutane 99%, 1,8-diaminooctane 99%, acetonitrile 99.8%, methacrylic acid 99% (redistilled) and ω, ω-dimethoxy-ω-phenylacetophenone (DMPA) were purchased from Aldrich. Polymethyl methacrylate (PMMA, 0.5 mm) was purchased from Goodfellow. Cobalt(II) chloride 99% and 1-ethyl-3-(3-dimethylaminopropyl) carbodiimide hydrochloride (EDC) were purchased from Fluka Scientific. The requisite spiropyran handle, 1´-(3-carboxypropyl)-3´,3´-dimethyl-6-nitrospiro[2H-1]-benzopyran-2,2´-indoline (SPCOOH) **Figure 3.15**, was produced in a three-step sequence as described elsewhere[31]. All spectra were recorded on a UV-Vis-NIR Perkin-Elmer Lambda 900 spectrophotometer. The ultraviolet irradiation source was a BONDwand UV-365 nm obtained from Electrolite Corporation. Samples were irradiated at a distance of 5 cm. The white light source was a Lumina obtained from Chiu Technical Corporation. In this case, samples were irradiated at a distance of 7 cm.

131
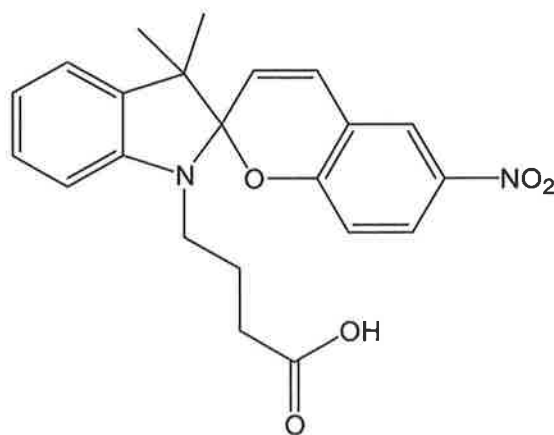
Figure 3.15. Molecular structure of SPCOOH.

3.3.2 UV-Vis absorption measurements in solution

Note that for all UV-Vis studies, the spiropyran samples (both solution and polymer bound) should be protected from ambient light.

For the Job's plot experiment, the absorption spectra measurements of the merocyanine–cobalt complex were carried out after 1 minute UV photo-irradiation of the various aliquots of spiropyran in acetonitrile (1×10^{-3} M), followed by immediate addition of cobalt(II) chloride in acetonitrile (1×10^{-3} M) and waiting for 10 minutes before measurement. The sum of concentrations for the spiropyran and cobalt(II) chloride was 1×10^{-3} M in each case.

3.3.3 Preparation of benzospiropyran entrapped polymer films

A 0.5mm thick PMMA slide (32mm x 22mm) was washed with ethanol to clean the surface and dried under a nitrogen stream. The slide was then placed in the spin coating chamber (Laurell Technology Corporation model NS-200-472) using a tweezers, exposed

side facing up, and 0.5ml of the BSP/ monomer solution was placed on the slide and left for 10 minutes. The spin coater was turned on for 30 seconds at 2000 rpm. The slide was then placed under a UV lamp (@ 254 nm) for 90 minutes to polymerize the film. Acetophenone was used as the free-radical initiator. The composition of the monomer solutions is listed in **Table 3.2**.

Solutions	Acetophenone	Methacrylic Acid (MA)	Styrene (Sty)	BSP
100% MA	25.0 mmol	25.0 mmol	0.0 mmol	0.025 mmol
50(MA):50(Sty)	25.0 mmol	12.5 mmol	12.5 mmol	0.025 mmol
100% Sty	25.0 mmol	0.0 mmol	25.0 mmol	0.025 mmol

Table 3.2. Monomer solutions for preparation of SP containing polymer films.

3.3.4 Kinetics of photochromic switching of polymer films using LED's

For the kinetic studies, samples were irradiated with a 380nm UV LED (Digi-key) and a 525nm LED (Stanley). Both the colouring and bleaching processes were monitored in real time using a Perkin-Elmer Photodiode array UV-Vis spectrometer. A schematic of the LED setup inside the UV-Vis spectrometer chamber is shown in **Scheme 3.2**. We followed the kinetics of the colouring and bleaching of the dye at 540 nm, which corresponded to the absorption maximum of the dye in the polymer films.
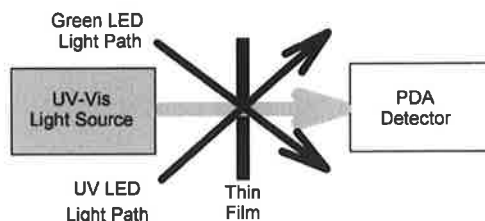
Scheme 3.2. Schematic of LED light source apparatus inside UV-Vis spectrometer chamber.

3.3.5 UV photo-polymerization of methacrylic acid onto a PMMA substrate

The PMMA substrate was thoroughly cleaned by immersing in a 50 :50 ethanol–water solution for 30 minutes, followed by rinsing with a large excess of deionised water. Methacrylic acid was distilled at 50 °C under reduced pressure to remove inhibitors. The PMMA substrate was placed in a spin coating chamber (Laurell Technology Corporation model NS-200-472) and the surface covered with a monomer solution (40 µl cm^{-2}) containing methacrylic acid and 3% (w/w) of the photo-initiator DMPA. This solution was allowed to absorb onto the PMMA substrate for 5 minutes and then excess monomer was removed by spinning at 1000 rpm for 5 seconds. The PMMA substrate was subsequently removed from the spin coater chamber and photo-polymerization was carried out in a UV curing chamber at a distance of 10 cm from a 254 nm UV light source (Mineral-Light® model UVG-54) for five hours at room temperature and left to dry for 24 hours. A polymethacrylic acid (PMAA) thin film is generated during this polymerization, yielding a carboxylic acid functionalized polymer. The PMAA

functionalized substrate (PMMA–PMAA) was then washed in deionised water for two hours and dried under a nitrogen stream.

3.3.6 Immobilization of spiropyran to PMAA *via* the requisite diamino tether

The PMMA–PMAA was further modified by immersing in a 2.5 mg ml^{-1} solution of EDC in deionised water for 10 minutes, followed by the addition of the requisite diamino tether (5.5 mg ml^{-1}). The mixture was stirred for 24 hours at room temperature to yield an amine-terminated polymer surface (PMMA–PMAA–NH$_2$). The amine-coated substrate was washed in a 50:50 ethanol–water solution for 30 minutes to remove unbound di-amino groups, and then rinsed with deionised water and dried under a nitrogen stream. A 3:1 solution of deionised water and ethanol containing EDC (2.5 mg ml^{-1}) and SPCOOH (2.5 mg ml^{-1}) was stirred at room temperature for 20 minutes. The PMMA–PMAA–NH$_2$ substrate was then added to this solution and stirred for 36 hours at room temperature. During this thirty-six hour period it was important to protect the polymer from light in order to minimize photo-degradation of the dye. The reaction yielded a polymer substrate with the BSP covalently immobilized to the polymer backbone (PMMA–PMAA–NH–BSP). The BSP-coated substrate was removed and washed in a 50:50 ethanol–water solution for 30 minutes to remove unbound SPCOOH. The film was then washed with copious amounts of deionised water and dried under a nitrogen stream. The PMMA–PMAA–NH–BSP substrate was stored in the dark for characterization.

135

3.3.7 Contact Angle Measurement

Contact angle measurements were recorded on the FTÅ-200 dynamic contact angle analyser. The 0.5mm PMMA substrates were subject to curving during immobilisation and it was necessary to eradicate this, as accurate contact angle measurements require extremely flat surfaces The BSP-8C polymer substrates were re-shaped to create a level surface using weighted pressure at 80°C for 5 hours. The polymer substrate was allowed to cool gradually to room temperature over 60 minutes to avoid cracking. After this process, the BSP-8C polymer was exposed to white light for 30 seconds before being used, to ensure the predominant form is BSP. 5µl of deionised water was placed on the polymer surface via an automated syringe under software control. BSP contact angle measurements were taken 1 minute after the initial addition of the water droplet. The polymer substrate was then exposed to 1 minute of vertical UV irradiation and the contact angle measurement taken after 1 minute.

3.3.8 Thickness of SP-polymer film

The thickness of the SP-polymer film measured using Prism and Reflector Imaging Spectroscopic System (PARISS) microscope - Nikon eclipse E800. Under imaging microscopy a cross section of the polymer substrate was analysed.

3.3.9 Photochromic switching and metal ion complexation of BSP modified polymer films

The photochromic switching experimental procedure that follows was carried out on the various carbon tethered polymer substrates. Absorbance spectra were obtained after each step.

1. Polymer irradiated with white light for 30 seconds to ensure the spiropyran (BSP) form is predominant

2. Polymer irradiated with the UV source for 1 minute

3. Polymer irradiated with white light for 30 seconds to regenerate the BSP form

The metal ion complexation experimental procedure that follows was carried out on the various carbon tethered polymer substrates. Absorbance spectra were obtained after each step.

1. Polymer irradiated with white light for 30 seconds to ensure the spiropyran (BSP) form is predominant

2. Polymer irradiated with the UV source for 1 minute and placed in vial of ethanol for 3 minutes to generate the merocyanine (MC) form (control)

3. Polymer irradiated with white light for 30 seconds to regenerate the SP form

4. Polymer irradiated with the UV source for 1 minute (to generate the MC form), and then placed in vial of 1×10^{-3} mol cobalt(II) chloride solution in ethanol for 3 minutes.

5. The polymer is removed from the solution, washed with ethanol, dried with a tissue, and the spectrum taken to test for complex formation.

In addition to the above, the following experimental procedure was carried out on the 8-carbon tether polymer substrate only:

1. Coated polymer substrate irradiated with white light for 60 seconds to generate the BSP form

2. Coated polymer substrate irradiated with UV light for 1 minute, to generate the MC form.

3. Substrate placed in vial of 1×10^{-3} mol cobalt (II) chloride in ethanol for 1 minute to test for complex formation.

4. Substrate exposed to white light for 1 minute while washing with water to test for regeneration the spiropyran from the merocyanine–metal ion complex.

This process was repeated on the same spiropyran coated polymer substrate a total of three times.

3.4 Conclusion

To our knowledge, this is the first demonstration of the cycling of covalently immobilised spiropyran on a solid support to merocyanine for repeated detection of metal ions. These results demonstrate a polymer-modified surface that can adapt its functionality through reversible molecular rearrangements triggered by external stimuli (photons). In principle, this means that the immobilised chemo-recognition sites can be maintained in an inactive or passive form until a measurement is required.

At this point, the surface is illuminated with UV-photons, which triggers the molecular rearrangement to the active form. The surface is self- indicating, as the presence of the active form is easily identified via the intense purple colour, and therefore some degree of self-diagnostics can be easily incorporated into measurements. Once in the active form, binding with metal ions such as Co^{2+} can occur, and once again it is self- indicating, as complexation shifts the absorbance of the active site and the colour changes to pink from purple. Once the measurement has been completed, illumination with white light expels the guest ion and returns the surface to the inactive form.

The implications of this research are that it may be possible, using this approach, to maintain a sensing surface in a passive mode that does not interact significantly with the external environment. When a measurement is required, the active form can be created and the population of active sites monitored via the density of the purple colour. The presence of the target species (e.g. Co^{2+}) can then be measured by ratioing the absorbance at, for example, 430 nm and 570 nm. A decrease 570 nm with an accompanying increase

at 430 nm is indicative of the presence of Co^{2+}. This raises the prospect of having sensing surfaces that do not change characteristics in a significant manner over time, which opens the possibility of calibration-free chemical sensors. The self- indicating nature of spiropyran is another powerful feature, which provides a degree of self-diagnostics and internal referencing of analytical measurements. In addition, covalent attachment to the polymer substrate prevents leaching of active sites into the sample. While the current investigation has focused on the detection of Co^{2+} ions, it is evident that modification of the binding site molecular architecture or analytical conditions could allow other ions to be targeted. In particular, amino acids are potential guests due to their ability to form complementary zwitterionic forms, and several amino acids, such as L-tryptophan, L-tyrosine and L-DOPA have already demonstrated interesting host–guest behaviour with the merocyanine form[97], **Figure 3.16**.
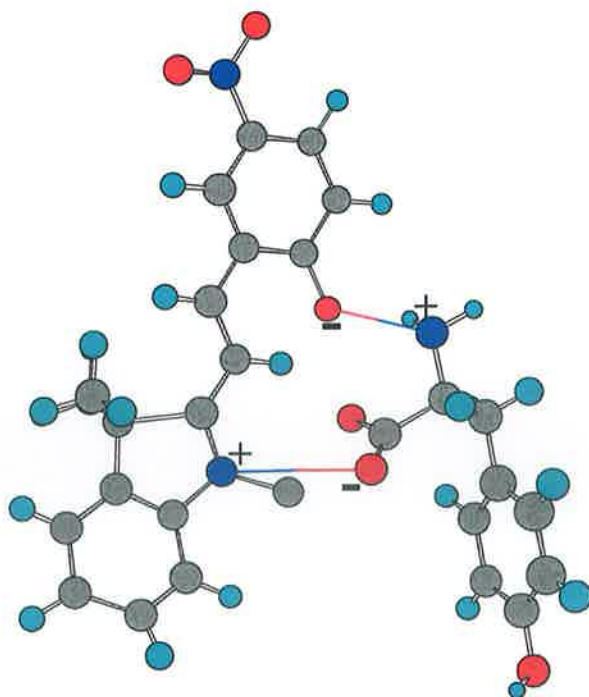
Figure 3.16. Complimentary zwitterionic complex of merocyanine and L-tyrosine.

In solution phase experiments, we have found that L-tryptophan will stabilise the merocyanine isomer for many weeks, preventing the natural slow rearrangement to the thermodynamically favoured spiropyran isomer, which typically occurs over a period of several hours, even when stored in the dark.

Combining the spiropyran film and novel LED-based sensor technology[98] developed in our laboratory, we ultimately hope to develop an economically viable colorimetric sensing system for metal ion detection, using this approach it may be possible to realise very low cost but reliable chemical sensors that could be scaled up for wide area deployment in chemosensor nets.

4.0 Photochromism of Benzospiropyran in Ionic Liquids

4.1 Introduction

Most chemical reactions carried out in the laboratory or in industry take place in solution. That means, the selection of a solvent, appropriate for the reaction under study, is, amongst other reaction parameters, of paramount importance for the success of a chemical process carried out in solution. It is well known, that solvents have a strong influence on the equilibria, on reaction rates, as well as the position and intensity of spectral absorption bands (e.g. UV-vis, IR, and NMR).

Solvents used typically, belong to the group of volatile organic compounds (VOC's), and these account for a significant amount of waste material; furthermore their use is often problematic owing to their toxicity, volatility, flammability, and environmental effects. Therefore the adoption of more environmentally friendly solvents or even solvent-free reactions continues to be of great interest as an important step in the direction of "Green Chemistry".

Among the alternative reaction media studied as substitutes for classical organic solvents are plain water, fluorous media (e.g. highly fluorinated alkanes, ethers, and tertiary amines), supercritical fluids (e.g. supercritical fluid CO_2), and particularly ionic liquids (ILs). Water, fluorous media and supercritical fluids belong to the well-known class of molecular liquids. In addition to molecular liquids, ILs represent a quite different group of solvents, consisting in the crystalline state entirely of ions and as molten salts at room temperature, **Figure 4.1**. An example of a room temperature IL is 1-(1-butyl)-3-methylimidazolium hexafluorophosphate (mp 12 °C), commonly abbreviated as

142

[bmim][PF$_6$]. Atomic liquids[1] are liquid sodium or mercury. Binary mixtures at the borderline between molecular and ionic liquids are also interesting media, such as, 5 M solution of lithium perchlorate in diethyl ether (LPDE).

Molecular Liquids
(e.g. organic solvents)

Na in
liquid NH$_3$

LiClO$_4$
in Et$_2$O

Atomic Liquids
(e.g liquid metals)

Ionic Liquids
(e.g. molten salts)
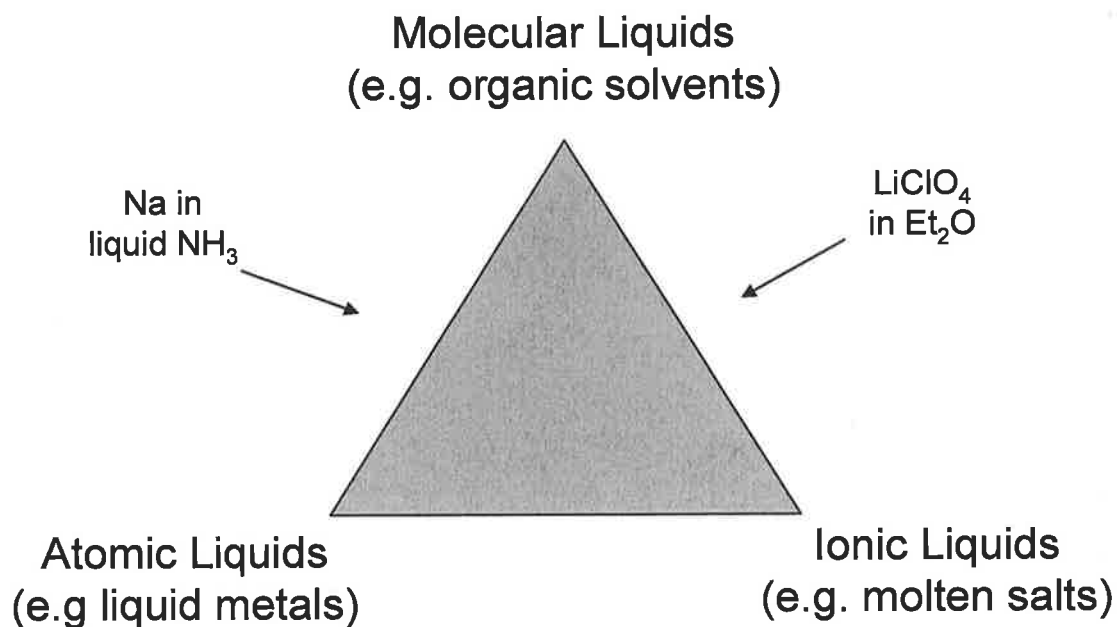
Figure 4.1. Classification of solvents according to their characteristic chemical bonds.

Such concentrated LiClO$_4$ solutions can be considered as diluted ILs because they contain only about one to two ether molecules per lithium cation, which is therefore not fully coordinated. Molecular solvents such as water can undergo autoprotolysis according to **Equation 4.1**, with $c(H_3O^+) = c(HO^-) = 10^{-7}$ mol L^{-1} at 25 °C, i.e. a very low but nevertheless non-negligible ion concentration.

---

[1] In must be noted that the term 'atomic liquid' is used in this context to define liquids consisting entirely of specific non-bonded atoms.

$$2\ H_2O_{(l)} \xrightleftharpoons{25\ ^\circ C} H_3O^+_{(aq)} + HO^-_{(aq)}$$
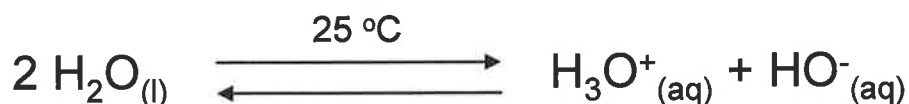
Equation 4.1.

In contrast, in ionic liquids such as [bmim][PF$_6$] the ion concentration is with c(bmim$^+$) =

c(PF$_6^-$) = 4.8 mol, i.e. more than 10^7 times larger than H$_2$O according to **Equation 4.2**:

$$[bmim^+PF_6^-]_{(s)} \xrightleftharpoons{>12\ ^\circ C} [bmim^+]_{(l)} + [PF_6^-]_{(l)}$$
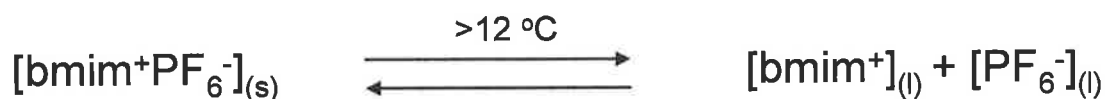
Equation 4.2.

Compounds which are already fully ionic in the crystalline state are called ionic, whereas

compounds with molecular crystal lattices which form ions only in solution by reaction

with solvent or with itself (autoprotolysis) are described as ionogens[99]. Therefore the

group of solvents located at the corner bottom-right of the solvent triangle of **Figure 4.1**

should be called non-aqueous, at room temperature liquid, (fully) ionic solvents

(NARTLIS)[100, 101]. ILs are defined as materials that are composed entirely of cations and

anion's and that melt at or below 100 °C. Ionic liquids are not a recent discovery, they

have been known since 1914 when ethylammonium nitrate (EtNH$_3^+$NO$_3^-$, mp 13-14 °C)

was purposely prepared for electric conductivity measurements.

Recently, the area of ionic liquids (ILs) has experienced a renaissance with the

introduction of highly asymmetric, diffusely charged organic cations and water-stable,

non-coordinating, bulky inorganic anion's, leading to frustrated molecular packing in the

crystal lattice. Amongst them are mono-, di-, tri-, and tetraalkylammonium salts,

tetraalkylphosphonium salts, 1-alkyl- as well as 1, 3- and 1, 4-dialkyl-pyridinium salts, and 1, 1-dialkylpyrrolidium salts. The current interest in ILs arises for three reasons:

(i)   they are considered as environmentally benign solvents, mainly because of their very low vapor pressure under ambient condition;

(ii)   the wide range of 'designer' solvents with tunable properties (polarity, acidity, functionality etc.) that can be generated form the large number of cations and anion's leading to new ionic solvents with specific properties; and

(iii) they can improve the reactivities of dissolved reactants in a variety of chemical processes.

These novel solvents with very interesting properties are attracting the attention of a growing number of scientists and engineers, as shown by the increasing number of publications in recent years[102], e.g. a quick search of the term 'ionic liquid' in SciFinder Scholar results in over 15,000 hits in the last 5 years. ILs are organic salts in the liquid state at ambient conditions and many show negligible volatility and non-flammability[103]. Hence, they are being actively investigated as alternative solvent media in synthesis[100], catalysis[104], polymerization[105-107], separations[108], electrochemistry[109, 110] and electrochemical devices[111, 112]. However, the basic science involved with fully characterizing these ILs is still in its infancy, and this may be inhibiting more effective utilization of these interesting solvents. Before the full potential of ILs as solvent systems can be explored, more information about their physicochemical properties needs to be gathered, as not all are suitable for "green" chemistry applications[113]. For example, the low melting points of ILs are often ascribed to both the bulky and asymmetrical structure of cation/anion and the charge delocalization over the cation and/or anion. The charge

delocalization over the N-C-N portion of the ring in the 1,3-dialkylimidazolium cation weakens the electrostatic interaction with the counter anion, and the asymmetrical structure caused by the alkyl chains of different length makes for poor packing of the crystal[101]. ILs can replace molecular solvents only if the chemist is able to compare ILs with generally used reaction media in a rational way; however, more extensive information is needed to allow the categorization of new and existing ILs more precisely in terms of solvent properties.

Chemists often attempt to understand solvent effects on chemical process in terms of the solvent polarity. The expression solvent polarity can be found in every chemistry textbook, however, mostly with a rather vague definition. What does solvent polarity really mean? Physical chemists have often used dielectric constants, dipole moments, and refractive indices as macroscopic physical solvent polarity parameters. However, solute-solvent interactions take place on a molecular scale, with individual, mutually interacting solvent molecules surrounding the ions or molecules of the solute, leading to loose or tight solvation shells, as shown in **Figure 4.2**. The solute species in **Figure 4.2** can have a polarizability α, a dipole moment μ, or a charge ze, responsible for nonspecific interaction forces, but it can also act as a hydrogen-bond donor (HBD; right hand side) and/or hydrogen-bond acceptor (HBA; left hand side) and as electron-pair donor (EPD; Lewis base) and electron-pair acceptor (HBA; Lewis acid) responsible for specific interaction forces. In highly structured solvents such as water, hydrophobic interactions are additionally possible. Because of this multitude of solute-solvent interactions, macroscopic physical solvent parameters have often failed to correlate solvents effects qualitatively and quantitatively.
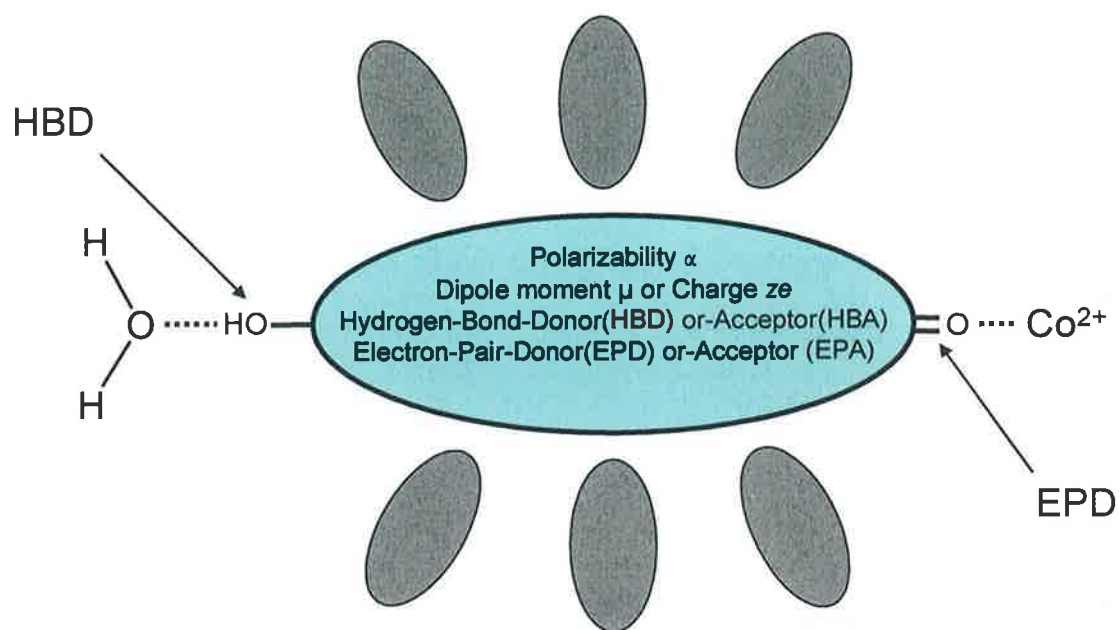
Figure 4.2. Schematic illustration of non-specific (grey objects) and specific (HBD--H$_2$O and EPD--Co^{2+}) intermolecular interaction forces between a solute species (neutral molecule) in the first solvation shell.

Therefore, solvent polarity should be defined in another way. The IUPAC definition for solvent polarity is defined as the "overall solvation capability (or solvation power) for (i) educts and products, which influences chemical equilibria; (ii) reactants and activated complexes (transition states), which determines reaction rates; and (iii) ions or molecules in their ground and first excited state, which are responsible for spectral absorbance bands in various wavelength regions. This overall solvation capability depends on the action of all, non specific and specific, intermolecular solute-solvent interactions, excluding such interactions leading to definite chemical alterations of the ions or molecules of the solute". Obviously, solvent polarity defined in this way cannot be

147

measured by single macroscopic physical solvent parameters. Instead, solvent polarity is much better described empirically by processes happening at the molecular scale. Carefully selected, well-understood, solvent-dependent behaviour, and the related empirical parameters better predict a multitude of possible solute-solvent interactions much better than attempting to quantify effects and explain behavioural trends using single physical constants. In this approach, solvents are considered as a discontinuous, more or less structured medium, consisting of individual, mutually interacting solvent molecules. The use of model processes to describe quantitatively the influence of internal parameters on chemical processes is not new: the correlation of substituents effects on chemical processes by means of the famous Hammett equation, derived empirically from the ionization of substituted benzoic acids in water at 25 °C as a reference reaction, is well know to all chemists[114].

It has been argued that the solvent properties of ILs may not be well accounted for by conventional macroscopic parameters like polarity and viscosity, which have been extensively used for molecular solvents. It seems ILs have specific local structures that underpin many of their intriguing properties. ILs appear to be homogeneous macroscopically, but they are likely to be heterogeneous at the nanometer scale. Recent molecular dynamics simulation results have supported this view, that ionic liquids are nanostructured fluids[115].

A number of fundamental photophysical studies in ILs ranging from the empirical determination of polarity utilizing the solvatochromic pyridinium N-phenolate betaine

dye, picosecond time-resolved fluorescence of 2-aminoquinoline to the photoisomerization of trans-stilbene have been used to understand the many specific (e.g. hydrogen bond donor and/or acceptor interactions) and non-specific interactions (e.g. Coulomb and Debye forces) within the ionic liquid.

$$\text{BSP} \rightleftharpoons {}^{+}\text{MC}^{-} \qquad K_e = \frac{[{}^{+}\text{MC}^{-}]}{[\text{BSP}]}$$

Equation 4.3. BSP-MC equilibrium.

The BSP$\leftrightarrow$MC equilibrium and its photoisomerization can reveal a significant amount of information about its surrounding molecular environment. For example,

(i)   at equilibrium an estimate of polarity can be calculated from the value K_e, **Equation 4.3**, the population of non-polar BSP versus the zwitterionic MC,

(ii)   MC isomer exhibits a large negative solvatochromic shift with increasing solvent polarity,

(iii)   the MC isomer possesses a large polarizable π-electron system, typical of systems that exhibit dispersion interactions,

(iv)   phenolate oxygen on the MC exhibits a highly basic electron pair donor (EPD) centre, suitable for interaction with hydrogen bond donors and Lewis acids, (e.g. the coordination with the metal ion Co^{2+}), and

(v)   thermal isomerization of MC to BSP is dependent on all of the above, (e.g. is the interaction of zwitterionic amino acids at the complimentary binding sites on the MC inhibiting the thermal back reaction).

149

In this chapter, the photo- and solvatochromic properties of BSP were investigated by UV-vis absorption spectroscopy in nine separate ionic liquids, **Figure 4.3**. A more detailed photo- and thermochromic study was undertaken with ILs containing the anion $[NTf_2]^-$ by UV-vis absorption spectroscopy *ab initio* molecular orbital theory and density functional theory (DFT) calculations.
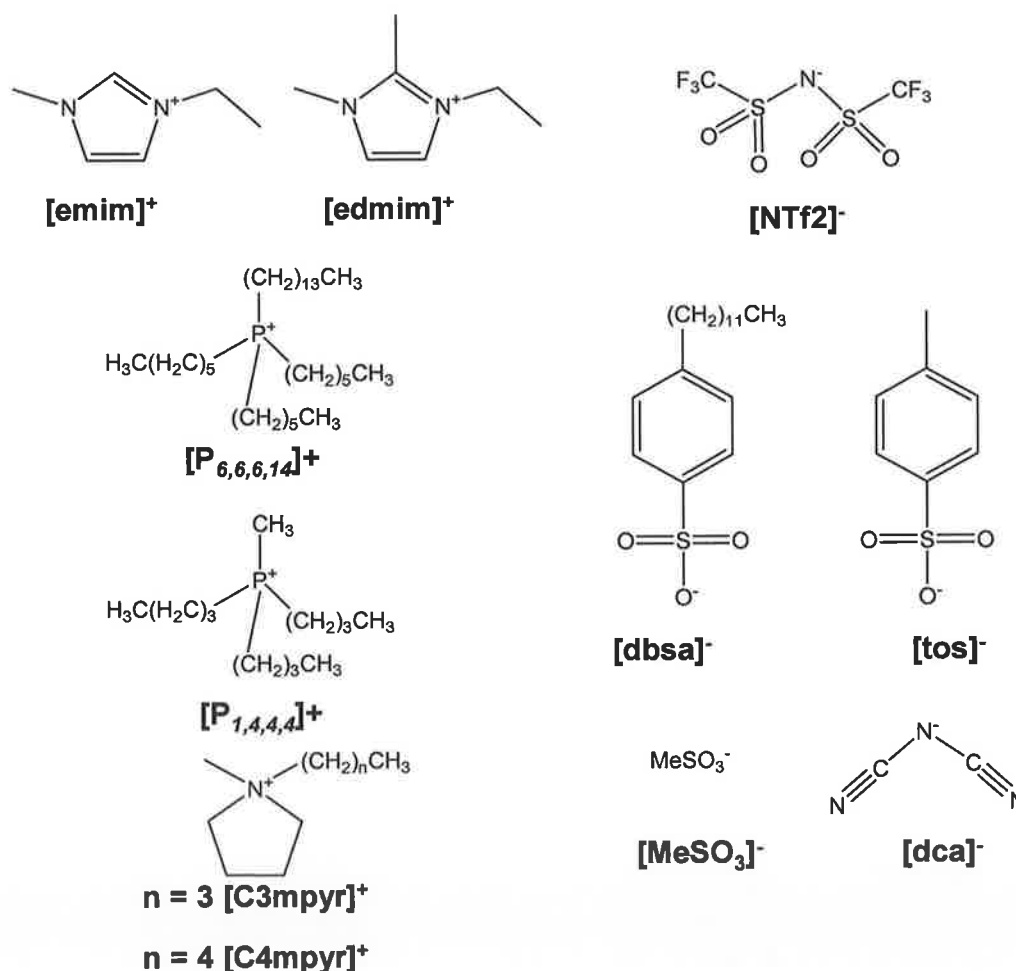
Figure 4.3. Cations and anion used in this study: N-propyl N-methyl-pyrrolidium $[C_3mpyr]^+$, N-butyl N-methyl-pyrrolidium $[C_4mpyr]^+$, ethyl methyl imidizolium $[emim]^+$, ethyl dimethyl imidazolium $[emim]^+$, trihexyltetradecyl phosphonium $[P_{6,6,6,14}]^+$, tributyl methyl phosohonium $[P_{1,4,4,4}]^+$, bis(trifluoromethanesulfonyl) amide $[NTf_2]^-$,

dicyanimide [dca]⁻, tosylate [tos]⁻, methylsulfate [MeSO₃]⁻ and dodecylbenzenesulfate [dbsa]⁻.

It was observed that in ILs containing the cations [C₃mpyr]⁺ and [C₄mpyr]⁺ that BSP's photo- and thermo- chromic behavior is similar to that of the molecular solvent acetonitrile. When BSP is irradiated with UV light in ILs containing the cations [emim]⁺ and [P₆,₆,₆,₁₄]⁺, a new band in the visible region (430 nm) appears; it appears that these particular cations are interacting with the phenolate group of the MC, forming a complex. Similar effects are also observed when BSP is heated with [emim]⁺. Unlike [emim]⁺, [P₆,₆,₆,₁₄]⁺ does not generate this band at 430 nm when heated BSP. This shows that complex generation in the case of [P₆,₆,₆,₁₄]⁺ is selective to only photo-irradiation. BSP thus serves as a model system for studying modes of interaction of the cations in ILs.

4.2 Results

4.2.1 UV-vis spectroscopic results

The polarity of ILs has been empirically determined by means of the ground state equilibrium between BSP and MC, specifically using the MC long-wavelength solvent dependent absorption band. **Scheme 4.1** illustrates the difference between BSP (uncharged) and MC (zwitterionic) when charged molecules solvate its first outer shell calculated by MOPAC-AM1 calculations. It can be seen for **Scheme 4.1(a)** that water molecules have no specific interactions with the BSP isomer, whereas the water molecules align themselves to the charges within MC appropriately and therefore promote the population of MC due to increased stabilization. As ILs consist entirely of charged ions, they should promote the population of the MC isomer over the BSP isomer as the model in **Scheme 4.1(b)** would suggest and therefore the value of K_e should

increase. It has been reported that a similar zwitterionic solute (betaine dye) in an IL, seems to be solvated by the molecular environment of the bulk molten salt and experience normal non-specific intermolecular electrostatic interactions[116, 117]. The solvatochromic shift of the MC band can also inform us if the solvating properties of the solvent as explained in **Figure 4.4,** for more in formation see chapter 2.
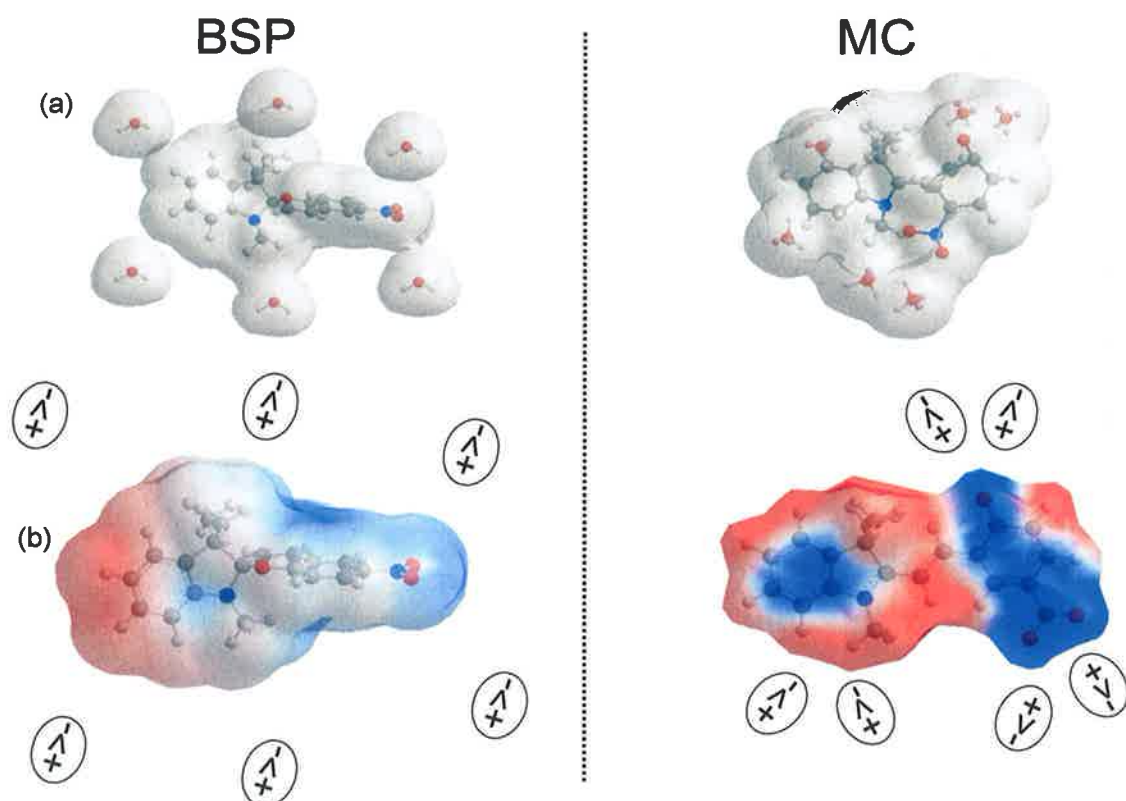
Scheme 4.1. Schematic three-dimensional representation of (a) energy minimized (MOPAC) interactions of BSP and MC with six H_2O molecules and (b) energy minimized (MOPAC-AM1) of the partial charges within BSP and MC, (blue colour represents the partial charges within the molecule).

152

The ground state physical properties of BSP in a selection of ILs have been summarized in **Table 4.1**. For the dialkylpyrrolidinium $[C_3mpyr]^+$ and $[C_4mpyr]^+$ salts containing the anion bis(trifluoromethanesulfonyl)imide $[NTf_2]^-$, λ_{max} values of 546 and 549 nm were observed for the MC band, respectively. Their K_e values, were quite similar also and were in a range expected for polar protic molecular solvents such as ethanol, see **Table 2.1**.

ILs of the imidazolium type can be divided into two classes, those with a 1-methyl-3-alkyl-substitution pattern, such as $[emim][NTf_2]$ and $[emim][MeSO_3]$, and those with an additional methyl substituent in the C(2) position, such as $[edmim][NTf_2]$. It is known that the 1-methyl-3-alkylimidazolium cations can act as weak hydrogen-bond donors because of the weakly acidic C(2)-H hydrogen atom at the heterocyclic ring. Therefore, it would be expected that these type of ILs should behave similarly to HBD solvents such as ethanol. The λ_{max} values of $[emim][NTf_2]$ and $[emim][MeSO_3]$ were 543 and 551 nm, values expected of HBD solvents. However, so does the C(2)-methyl imidazolium IL, $[edmim][NTf_2]$, with a $\lambda_{max} = 550$ nm. The C(2)-methyl imidazolium IL would be expected to red shift, similar to a less polar class of non-HBD solvents, with respect to the C(2)-H imidazolium ILs. The K_e values of the imidazolium ILs are also similar to that of HBD solvents, see **Table 2.1**.

Even under mildly basic conditions, the C(2)-H atom of the imidazolium ions can be removed to yield resonance-stabilized, nucleophilic singlet-diaminocarbenes[118]; these imidazolium based ILs are therefore chemically not inert[119], and will be studied in more detail later on in this chapter.
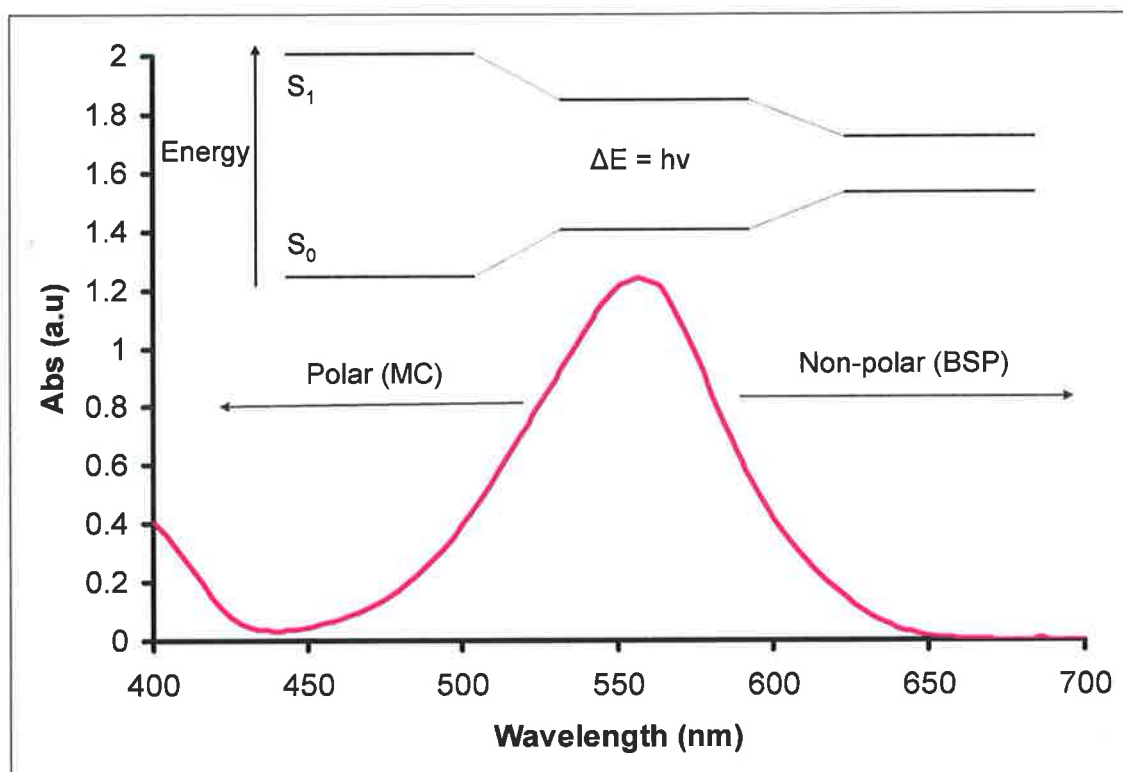
Figure 4.4. Solvatochromic affect on BSP-MC equilibrium. Intermolecular interactions between the solute and solvent modify the energy gap between the ground and excited states of the absorbing species, thus altering its absorption wavelength.

IL	λ_{max} (nm)	A_e	K_e
[C$_3$mpyr][NTf$_2$]	546	0.17	0.051
[C$_4$mpyr][NTf$_2$]	549	0.16	0.047
[emim][NTf$_2$]	543	0.15	0.044
[edmim][NTf$_2$]	550	0.12	0.035
[emim][MeSO$_3$]	551	0.29	0.09
[P$_{6,6,6,14}$][NTf$_2$]	574	0.02	0.005
[P$_{6,6,6,14}$][dbsa]	425*		
[P$_{6,6,6,14}$][dca]	566	0.09	0.026
[P$_{1,4,4,4}$][tos]	476*		
Acetonitrile	554	0.13	0.038

Table 4.1. Ground state physical properties of 10^{-4}M BSP in selected ILs.
* MC absorption band not observed within expected region, therefore K_e value could not be calculated.
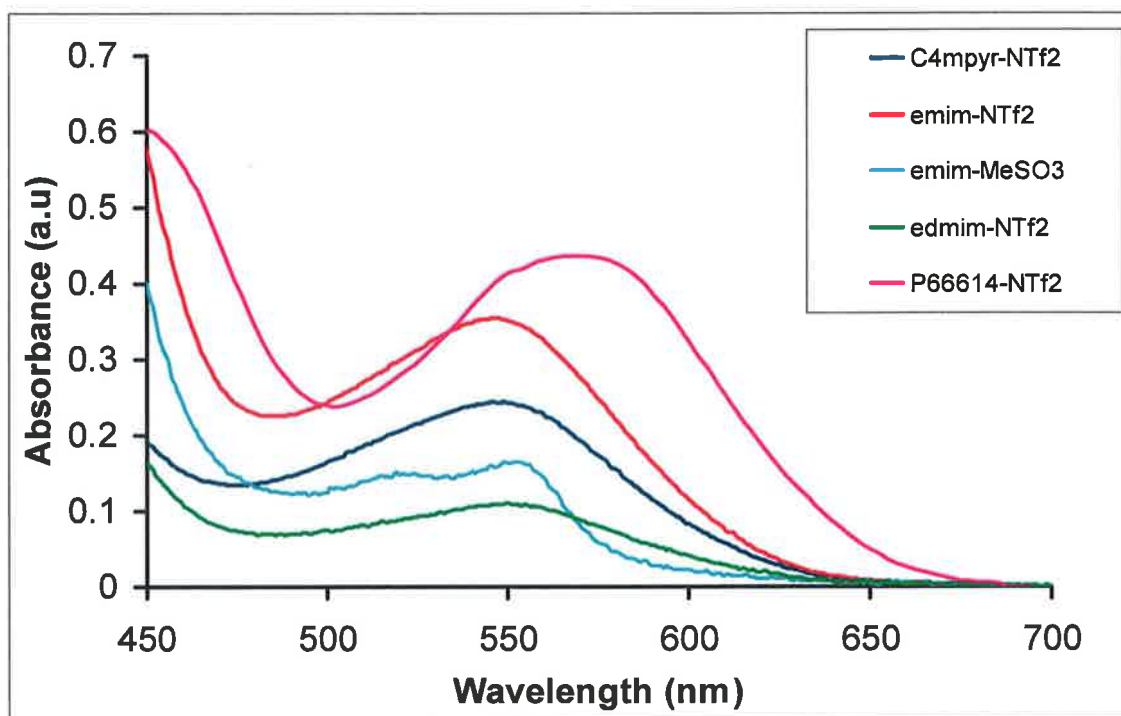
Figure 4.5. UV-vis spectrum of 10^{-4}M BSP in selected ILs after 60 seconds of 365 nm UV light, normalized at 700 nm.

Tetralkylphosphonium salts are reported in the literature to exhibit similar solvation properties to that of dipolar non-HBD molecular solvents. $[P_{6,6,6,14}][NTf_2]$ and $[P_{6,6,6,14}][dca]$ ILs exhibit λ_{max} values of 574 nm, 566 nm and K_e values of 0.02 and 0.09 respectively, these values correspond to non-HBD solvents such as DMF.

Figure 4.5 illustrates the UV-vis spectra of the MC isomer after 60 seconds of UV light in selected ILs. For all ILs except [emim][MeSO₃], the MC band characteristic is similar to that in molecular solvents, albeit with relatively high absorbances at 450 nm for [emim][NTf₂] and $[P_{6,6,6,14}][NTf_2]$. The spectrum from [emim][MeSO₃] exhibits two absorption bands at 520 and 551 nm, which is not dissimilar to the spectrum observed for

MC in DMSO, although negative-photochromism is not observed for BSP in the [emim][MeSO$_3$] IL.

In contrast, [P$_{6,6,6,14}$][dbsa] and [P$_{1,4,4,4}$][tos] ILs do not exhibit any absorption band within the reported MC region of the spectrum. Instead absorption bands at 425 nm and 476 nm respectively, are observed. The K_e value could not be calculated as no presence of the MC absorption band was found. **Figure 4.6** illustrates the UV-vis spectra of BSP in [P$_{6,6,6,14}$][dbsa] and [P$_{1,4,4,4}$][tos] after 60 seconds UV light. It can be seen that normal MC band is absent. The shoulder observed for [P$_{6,6,6,14}$][dbsa] at 425 nm represents a definite change in the spectroscopy of BSP relative to molecular solvents in general, although this shoulder band has been observed in the case of BSP in DMSO, albeit without the broad band at 476 nm in [P$_{1,4,4,4}$][tos]. These dramatic changes in the visible spectrum do occur, however when MC solutions or polymers are exposed to metal ions, see chapter 2 and 3. In these cases, the interpretation is that the metal ion is interacting with the MC phenolate group. Therefore a possible explanation is that in certain ILs, the cation is interacting in a similar way with the MC phenolate, i.e. this not a simple solvation/polarity effect.

In order to investigate the importance of the cation a more detailed study was undertaken studying the BSP in ILs containing the anion [NTf$_2$]-, and varying the cation. This allowed the effect of the cation to be examined on polarity, thermal ring closing kinetics and possible interactions with the phenolate of the MC.
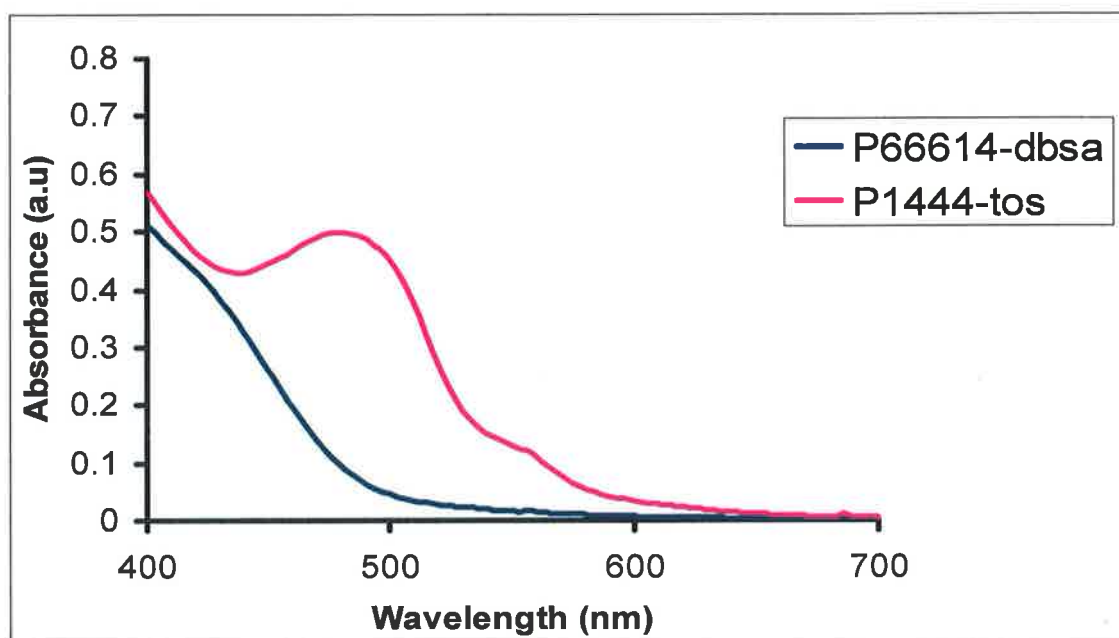
Figure 4.6. UV-vis spectra of 10^{-4}M BSP in $[P_{6,6,6,14}]$[dbsa] and $[P_{1,4,4,4}]$[tos] after 60 seconds of 365 nm UV light, normalized at 700 nm.

Usually, the equilibrium between BSP and MC is strongly displaced upon irradiation with visible ($\geq$450 nm) light towards the BSP isomer and when irradiated with UV light (360nm) towards the MC isomer. **Figure 4.7** displays the resulting spectra of all IL solutions after 2 minutes of UV irradiation. The effect of visible irradiation is shown for comparison (spectrum [emim]+-BSP). It is also noted that upon exposure to UV light a new band appears at 430nm for the $[P_{6,6,6,14}]^+$ and [emim]+ ILs, but not for [C3mpyr]+ and [C4mpyr]+.
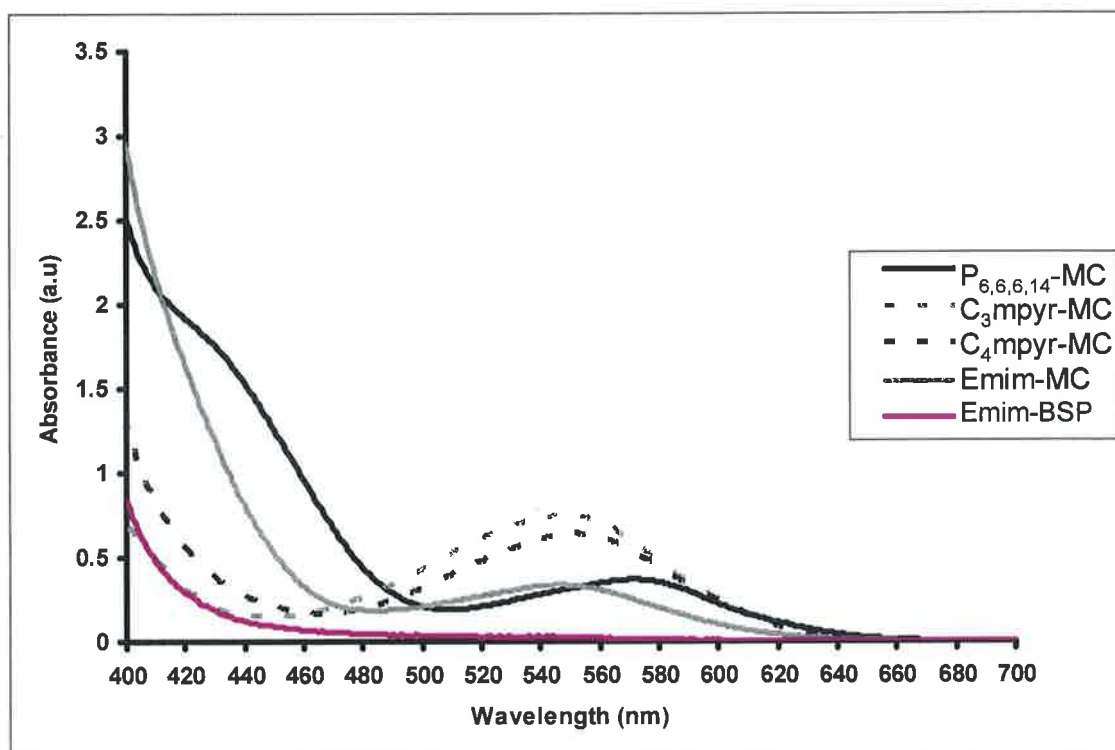
Figure 4.7. [$P_{6,6,6,14}$], [C_3mpyr]$^+$, [C_4mpyr]$^+$, and [emim]$^+$ [NTf$_2$]$^-$ IL solutions of BSP exposed to 2 minutes UV irradiation (365 nm). [emim]$^+$ IL solution of BSP exposed to 1 min irradiation of visible light ($\geq$450nm).

An increase of absorbance in this particular region is very similar to the acidichromic properties of the MC isomer reported by Sun,[72] but that effect involves irreversible ring closure to the BSP induced by visible light. Protonation as a reason for the spectral changes seen here can be excluded for a number of reasons. Firstly, the ILs do not contain any labile protons and cannot therefore protonate the MC. Secondly, acidic impurities within the IL were ruled out through control experiments using the structurally similar solvatochromic probe betaine-30 dye (Reichardt's dye), which showed no spectroscopic evidence of protonation of the phenolate group; see **Figure A1** in appendix. Finally, in contrast to Sun, we observe a *reversible* process. Considering that

the anion $[NTf_2]^-$ is constant in all the ILs, and no significant increase in absorbance at 430nm is seen for $[C_3mpyr]^+$ and $[C_4mpyr]^+$, it appears that the $[P_{6,6,6,14}]^+$ and $[emim]^+$ cations interact with the phenolate group of the MC causing this new band. This interpretation is supported by recent results reported by Iwata, which suggested that imidazolium cations, such as $[emim]^+$, selectively form π-π aromatic complexes with the fluorescent probe 2-aminoquinoline in preference to non-aromatic cations.[120]
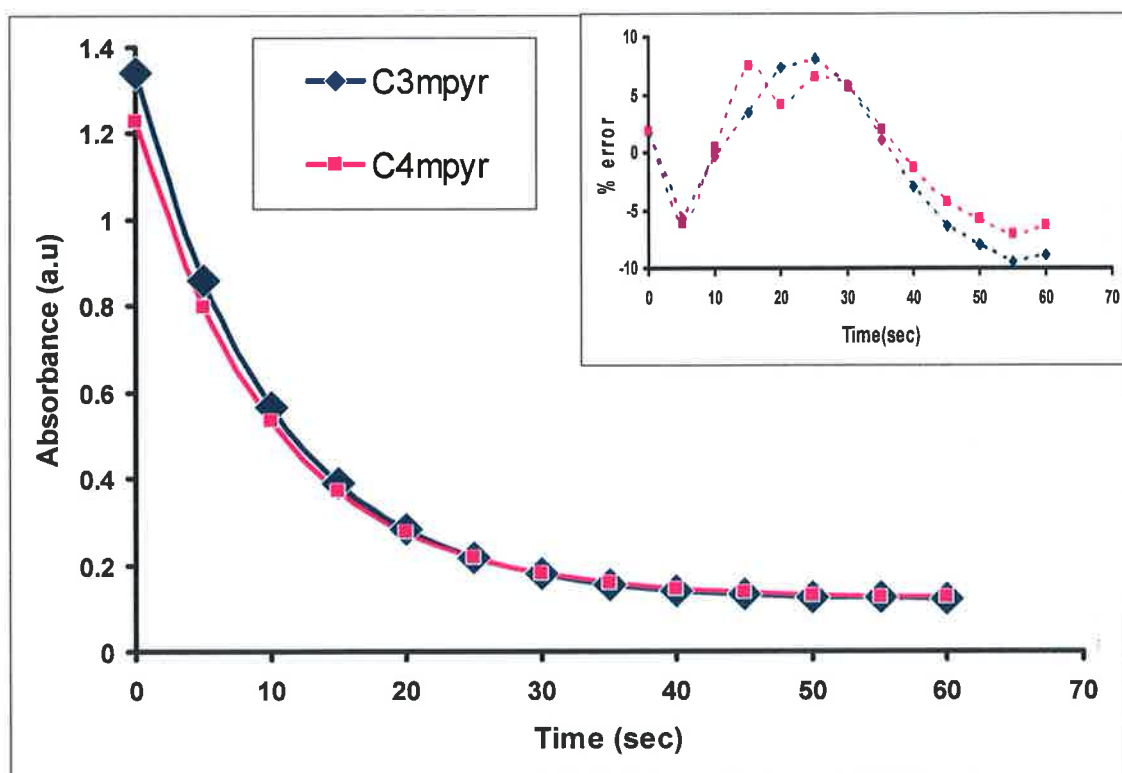
Figure 4.8. Thermal relaxation of MC isomer in $[C_3mpyr][NTf_2]$ and $[C_4mpyr][NTf_2]$ after two minutes UV irradiation, data fitted to a non-linear single exponential (first order) model. Inset: Residual plot of percentage error for the single exponential model.

In most cases, after removal of UV light, the predominant MC form generated will thermally isomerize back to an equilibrium state (A_e), The associated decay in

159

absorbance typically follows first order kinetics[41] in molecular solvents. In the case of ILs containing the cations $[C_3mpyr]^+$ and $[C_4mpyr]^+$, it was found that the MC thermal relaxation followed first order kinetics according to the data fitted to a non-linear single exponential (first order) model (**Equation 2.2**), as seen from **Figure 4.8**. Rate constants were calculated for $[C_3mpyr]^+$ (0.10 s^{-1}) and $[C_4mpyr]^+$ (0.09 s^{-1}) from the single exponential model, these are very similar to that of the molecular solvent acetonitrile (0.08 s^{-1}). The inset illustrates the residual plot of percentage error for the single exponential model and the experimental absorbance, this percentage error is deemed to be acceptable. Similarly with ILs containing the cations $[P_{6,6,6,14}]^+$ and $[emim]^+$, it was found that the MC thermal relaxation did follow first order kinetics according to the single exponential (first order) model. Therefore, rate constants were obtained from the slope of the line from the plots of time (in seconds) versus $\ln(A_t/A_0)$, where A_t and A_0 denote the absorbance at a particular time and the initial absorbance values, respectively.

Figure 4.9 and **Figure 4.10** illustrate the first order kinetic plots for the thermal relaxation of MC at its particular maxima and at 430nm (the observed "interaction band" λ_{max} for $[P_{6,6,6,14}]^+$ and $[emim]^+$) respectively. Monitoring the relaxation of the "interaction band" at 430nm for $[P_{6,6,6,14}]^+$ and $[emim]^+$ cations should also give us an indication of the type of interaction or process taking place.

Solvent	k (s^{-1}) λ_{max}	k (s^{-1}) 430 nm
Acetonitrile	$9.7 \times 10^{-4} \pm 2.5 \times 10^{-5}$	N/A
[C$_3$mpyr][NTf$_2$]	$1.2 \times 10^{-3} \pm 3.0 \times 10^{-5}$	N/A
[C$_4$mpyr][NTf$_2$]	$1.1 \times 10^{-3} \pm 2.1 \times 10^{-5}$	N/A
[P$_{6,6,6,14}$][NTf$_2$]	$3.4 \times 10^{-5} \pm 3.2 \times 10^{-6}$	$2.8 \times 10^{-5} \pm 1.6 \times 10^{-6}$
[emim][NTf$_2$]	$6.9 \times 10^{-5} \pm 3.8 \times 10^{-6}$	$8.0 \times 10^{-5} \pm 4.9 \times 10^{-6}$

Table 4.2. Thermal relaxation kinetics at the MC λ_{max} and at 430 nm (average of 3 kinetic runs).

Table 4.2 includes the calculated first order rate constants. As expected, [C$_3$mpyr]$^+$ and [C$_4$mpyr]$^+$ exhibit similar rate constants to acetonitrile at their respective MC maxima. On the other hand, [P$_{6,6,6,14}$]$^+$ and [emim]$^+$ exhibit much slower thermal reversion to BSP than [C$_3$mpyr]$^+$ and [C$_4$mpyr]$^+$, with rate constants that are broadly similar to those exhibited by protic molecular solvents, such as ethanol under similar conditions[41, 121].
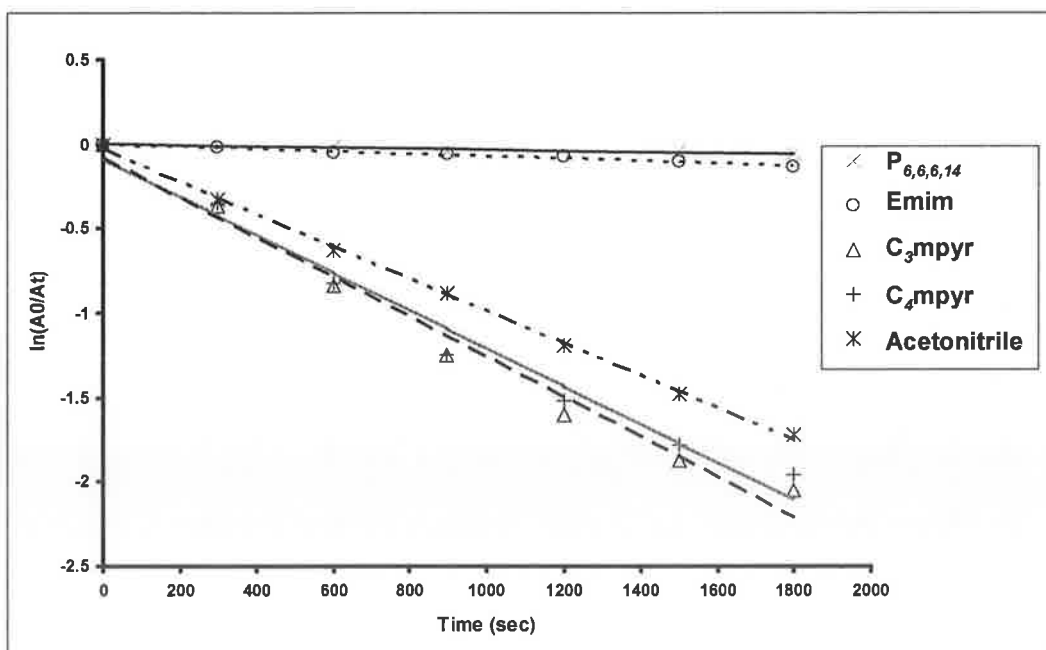
Figure 4.9. First order kinetic plot of the photo-relaxation at the MC maxima in acetonitrile, and the various ILs.

In the case of $[P_{6,6,6,14}]^+$ a difference of two orders of magnitude is observed; this is interesting as the $[P_{6,6,6,14}]^+$ IL exhibits a solvatochromic shift similar to non-polar molecular solvents. Normally this would produce a decay at the MC maxima faster than $[C_3mpyr]^+$ and $[C_4mpyr]^+$ as the equilibrium strongly resides in the BSP state in a non-polar environment, see **Table 2.1**. Therefore, a process is inhibiting the thermal reversion back to BSP in $[P_{6,6,6,14}]^+$ and $[emim]^+$ ILs. In the case of the $[emim]^+$ IL, the process inhibiting the thermal reversion could be explained by the acidic proton at the C-2 position but initial results obtained from the $[edmim]^+$ cation show similar spectroscopic characteristics, which could suggest that it arises from the imidazolium cation interacting with the phenolate and not the proton at the C-2 position of the $[emim]^+$ IL.
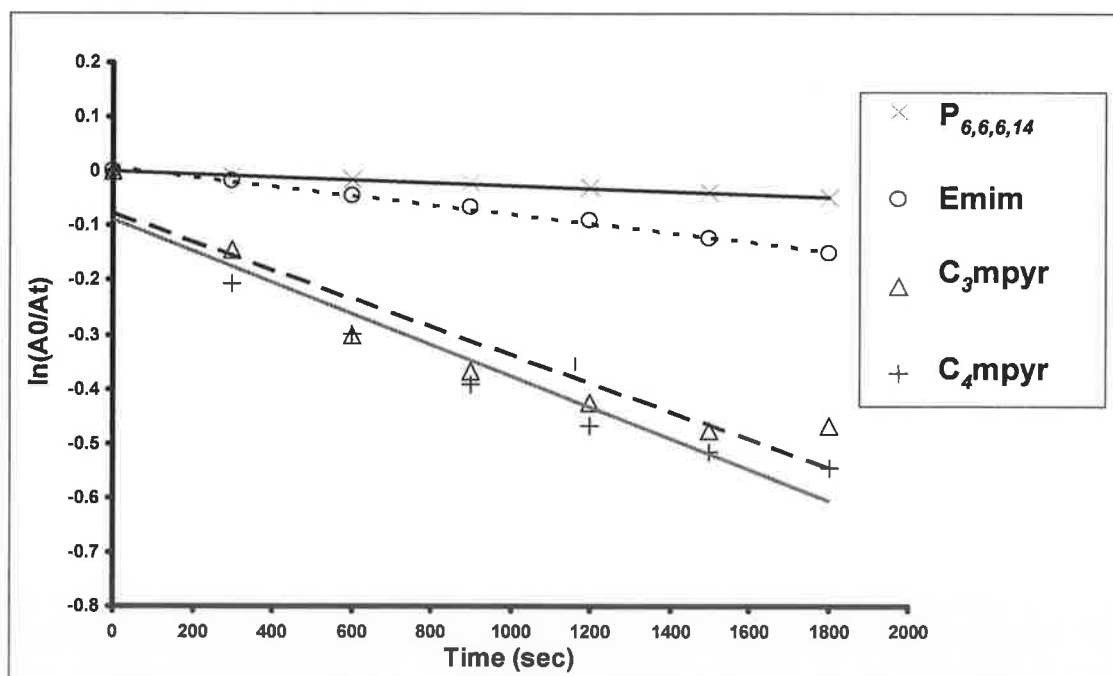
Figure 4.10. First order kinetic plot of the photo-relaxation at 430nm in the various ILs.

From this evidence (and **Figure 4.7**) we can hypothesise that a solute-solvent interaction has indeed formed in these ILs, disturbing the equilibrium between the BSP and MC isomers, as illustrated by **Scheme 4.2** . As the MC reverts back to equilibrium, the rate of decay of MC absorbance appears to be similar to the rate of decay of the complex absorbance as can be seen from the data in **Table 4.2** for the cases of the $[P_{6,6,6,14}]^+$ and $[emim]^+$ ILs. This indicates a relatively stable complex is formed that is in equilibrium with the MC form.

$$BSP \leftrightarrow MC \leftrightarrow MC\text{--}[P_{6,6,6,14}]^+$$

◄ ••
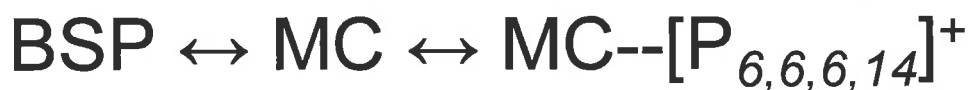
Scheme 4.2. MC--$[P_{6,6,6,14}]^+$ complex is the rate determining step in the overall equilibrium.

Table 4.3 shows the effect of temperature on the BSP↔MC equilibrium and the MC-IL "pseudo complex" interaction. The absorbance values of the MC and 430 nm were recorded at the following conditions at equilibrium (A_e), at 100 °C (taken after 10 minutes at 100 °C, $A_{100°C}$), and after 15 hours cooling (A_t). The increase in temperature from room temperature to 100 °C causes a substantial (and immediate) increase in absorbance due to MC in all cases, indicating a shift in the equilibrium towards the MC state at higher temperatures. Samples were only held at 100 °C for 10 minutes to minimize possible degradation of BSP. **Figure 4.11** shows the spectra of BSP in the ILs at 100 °C.

163

	Absorbance at λ_{max}			430 nm		
Solvent	A_e	$A_{100\,oC}{}^a$	$A_t{}^b$	A_e	$A_{100\,oC}{}^a$	$A_t{}^b$
[C$_3$mpyr][NTf$_2$]	0.23	0.52	0.23	0.10	0.45	0.11
[C$_4$mpyr][NTf$_2$]	0.22	0.56	0.22	0.11	0.51	0.11
[P$_{6,6,6,14}$][NTf$_2$]	0.02	0.11	0.04	0.42	0.56	0.51
[emim][NTf$_2$]	0.15	0.67	0.58	0.73	1.85	1.42

[a] Absorbance measured after 10 minutes at 100 °C.
[b] Absorbance measured after allowing a cooling period of 15 hours after thermal irradiation to 100 °C.

Table 4.3. Thermochromic behaviour of BSP in selected ILs at MC λ_{max} and 430 nm.
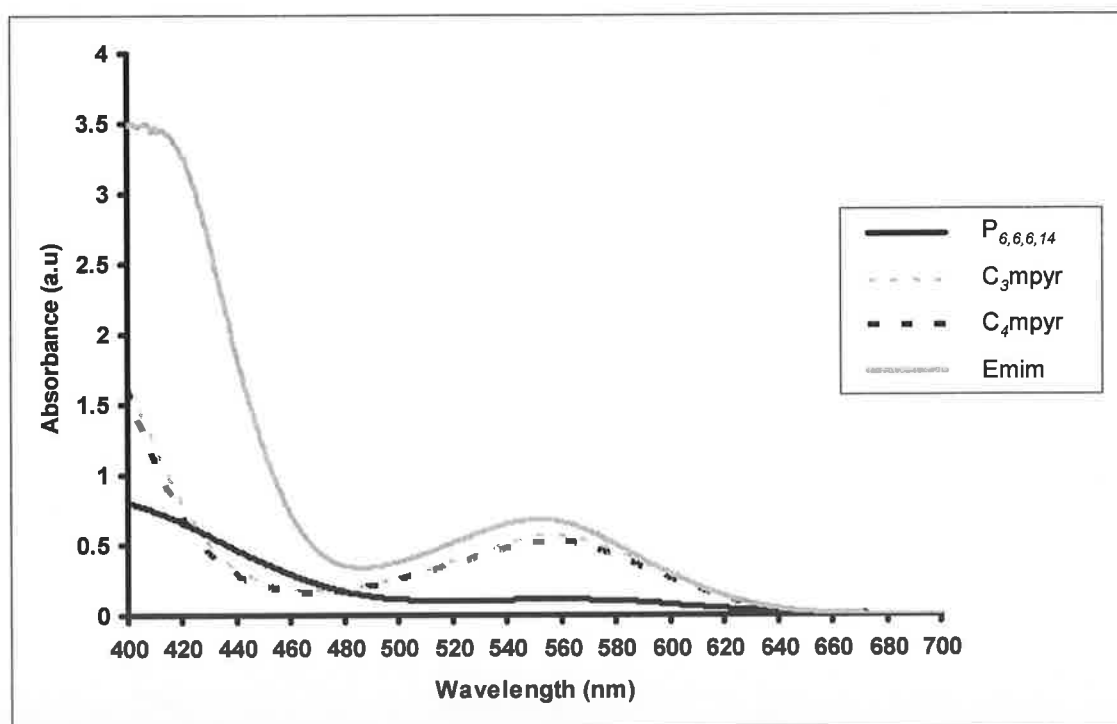
Figure 4.11. UV-vis spectra of BSP in [P$_{6,6,6,14}$]$^+$, [C$_3$mpyr]$^+$, [C$_4$mpyr]$^+$, and [emim]$^+$ [NTf$_2$]$^-$ IL solutions at 100 °C.

As before, [C$_3$mpyr]$^+$ and [C$_4$mpyr]$^+$ behave very similarly to standard polar solvents. The [P$_{6,6,6,14}$]$^+$-MC band intensity increased when heat was applied but not to the extent

164

caused by irradiation with UV light. The [emim]$^+$-MC band increased quite significantly in intensity when heated to 100 °C, in comparison to UV irradiation. It can also be seen from the A_t values that unlike the other ILs, [emim]$^+$-MC did not relax back to its original A_e value after thermal treatment, even after 15 hours in the dark at 25 °C. This pattern is also observed at 430 nm, for the [emim]$^+$-MC complex. It seems that during the 15hrs relaxation period the absorbance comes to a steady state value above that of A_e. It must be noted that thermal decomposition of BSP could be strongly enhanced in the presence of the chemically reactive imidazolium IL[118, 119].
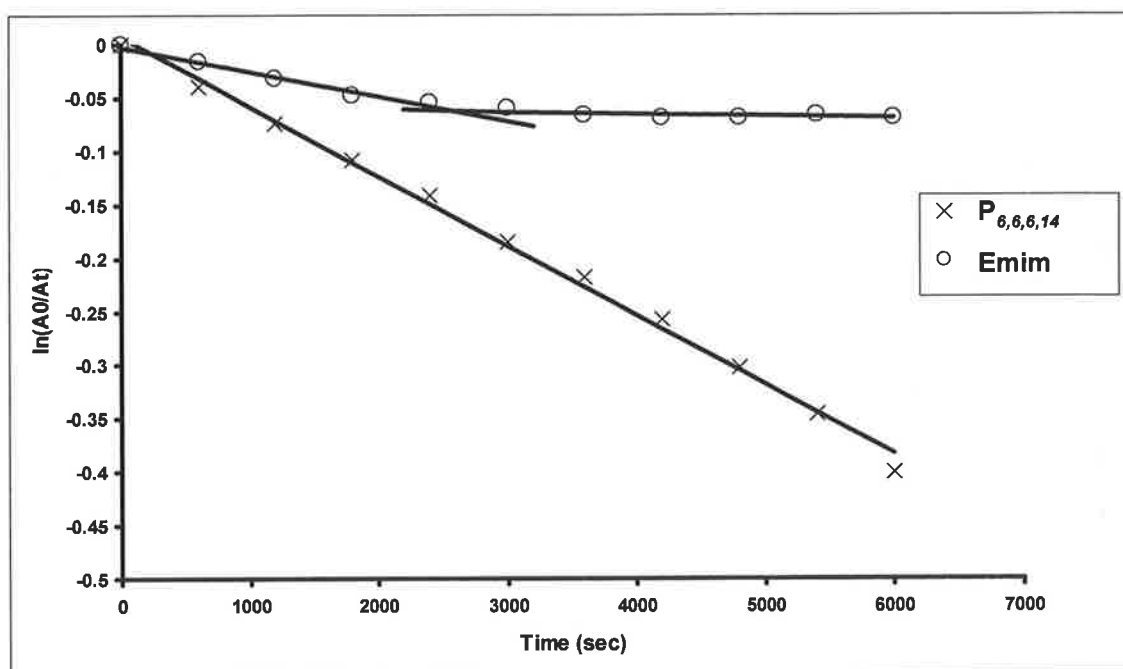
Figure 4.12. Relaxation of absorption value at 430 nm after thermal irradiation to 100 °C.

The MC-complex band (430nm) relaxation from 100 °C was plotted using first order kinetic model for [P$_{6,6,6,14}$]$^+$ and [emim]$^+$. [P$_{6,6,6,14}$]$^+$ and [emim]$^+$ exhibit rate constants for the first 2400 seconds of 7 x 10^{-5} s^{-1} and 2 x 10^{-5} s^{-1}, respectively. It can be seen from

Figure 4.12 that [emim]$^+$-MC, after this initial decay, has reached an equilibrium at 2400 seconds, whereas [P$_{6,6,6,14}$]$^+$ seems to decay in a first order fashion for up to 6000 seconds. It thus appears that the [P$_{6,6,6,14}$]$^+$-MC complex appears to be labile and follows a first order equilibration process back to its original state on returning to room temperature. On the other hand the [emim]$^+$-MC complex relaxes slightly, but clearly the mixture does not return to its original room temperature state. Thus it appears that the complex in this case is either the thermodynamically stable state (because of the strength of the interaction involved) which needs elevated temperatures to be formed, or that the barrier to dissociation of the complex is sufficiently high that it becomes inert once formed. These observations raise some interesting issues about the strength of the interaction in the complexes and the activation processes required to form and disrupt them. These questions are investigated further below by means of *ab initio* theoretical calculations.

4.2.2 Ab-initio Calculations

Standard *ab initio* molecular orbital theory and density functional theory (DFT) calculations were carried out using GAUSSIAN 03.[122] The open form of BSP (the MC isomer) together with the complexes that can be formed with [emim]$^+$, [C$_3$mpyr]$^+$, [P$_{6,6,6,14}$]$^+$ and [NTf$_2$]$^-$ were optimised at B3LYP/6-31+G(d) level of theory. As the optimization for the [P$_{6,6,6,14}$]$^+$ cation was not feasible, a model cation, [P$_{2,2,2,2}$]$^+$, was used instead. It is important to note that these calculations represent descriptions of the gas phase molecules and complexes only. However, the ability of gas phase calculations to estimate the real $n - \pi^*$ and $\pi - \pi^*$ electronic transition energies in organic molecules has been demonstrated previously.[123] The optimized geometries are shown in **Figure 4.13**.

166

The excitation energies of the MC isomer were computed at CIS(D)/6-31+G(d,p) level.

All molecular orbitals were plotted using the HF/6-31+G(d,p) electron density.
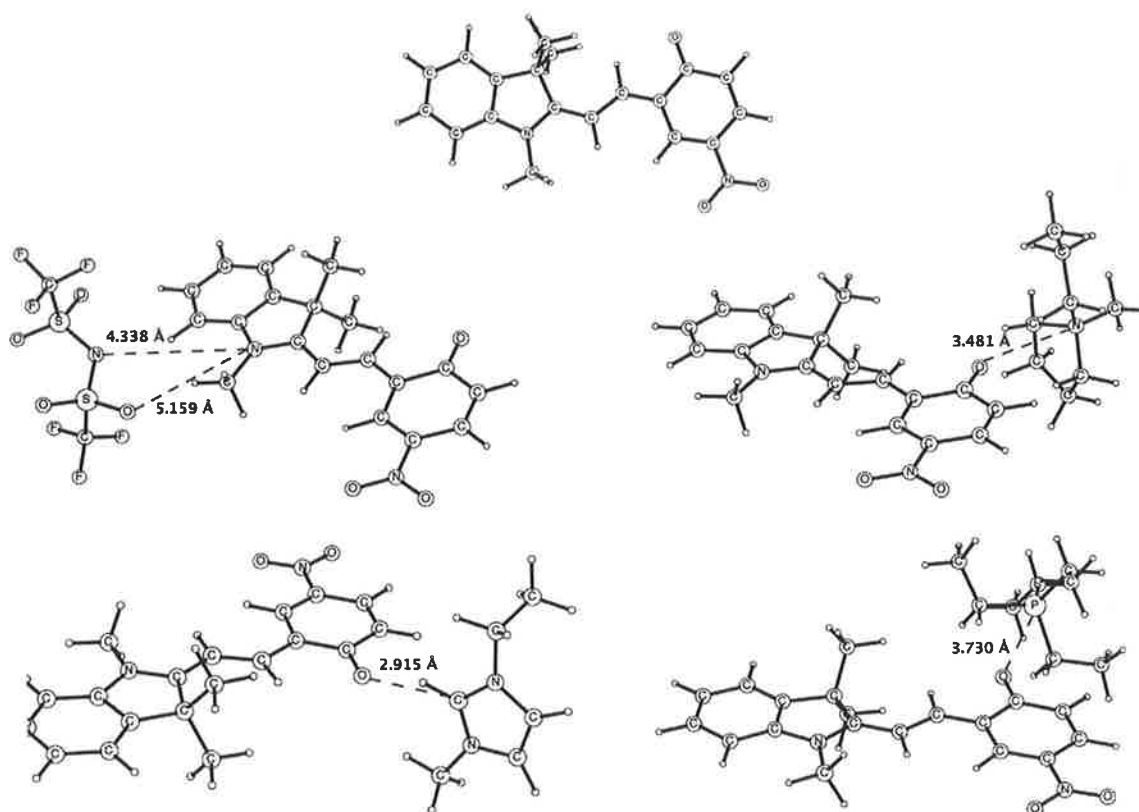
Figure 4.13. Optimized structures of (i) MC isomer together with the complexes that can be formed with (ii) [NTf$_2$]$^-$, (iii) [C$_3$mpyr]$^+$, (iv) [emim]$^+$, (v) [P$_{2,2,2,2}$]$^+$ at B3LYP/6-31+G(d).

4.3 Discussion

From the spectroscopic results obtained, we see that the ILs containing the ions [C$_3$mpyr]$^+$ and [C$_4$mpyr]$^+$ together with [NTf$_2$]$^-$ seem to have no profound effect on the BSP spectroscopy, only a solvatochromic effect similar to that of the molecular solvent acetonitrile. The IL containing the ions [emim]$^+$ and [NTf$_2$]$^-$ does have an effect on the BSP spectroscopy, as seen in **Figure 4.7**, a new band being formed at 430 nm. The photo-kinetic measurements obtained for [emim][NTf$_2$], reveal that this interaction is thermodynamically stable after 3000 seconds, inhibiting the isomerization of the MC back to BSP, unlike that of [C$_3$mpyr][NTf$_2$] and [C$_4$mpyr][NTf$_2$], where the MC isomerizes back to the BSP thermally, **Figure 4.8**. This interaction, associated with the band at 430 nm, is also seen when the solution is heated to 100°C. The IL containing the ions [P$_{6,6,6,14}$]$^+$ and [NTf$_2$]$^-$ also forms a new band at 430nm, as seen in **Figure 4.11**. The photo-kinetic measurements are similar to that of [emim]$^+$ but differ in their thermo-kinetics, **Figure 4.12**. It seems that the complex between [P$_{6,6,6,14}$]$^+$ cation and the MC is quite labile and the MC isomerizes back to the BSP on cooling.

The appearance of a new band at 430 nm in the case of [P$_{6,6,6,14}$]$^+$ and [emim]$^+$ may be a result of a cation interactions with the phenolate oxygen. This hypothesis is reinforced by molecular orbital calculations of the effect of charge delocalization in the ions. Since we are observing changes in spectroscopy of the planar MC isomer, it is important to investigate the excitation energies. The molecular orbitals on the MC isomer are shown in **Figure 4.14**. The first excitation arising from the HOMO has a predicted λ_{max} of 569 nm;

this excitation is allowed by symmetry and is seen in the visible spectrum. An excitation arising from HOMO-4 (the π orbital on the phenolate oxygen) has a predicted λ_{max} of 418 nm; this is not seen in experiments due to the fact that the transition is forbidden due to the symmetry of this orbital, the oscillator strength being zero. However, should the symmetry of this transition be altered through interactions with cations and/or polarization by cations, the transition may be seen in the absorption spectrum. Thus this transition may be responsible for the 430 nm band if the interaction between the phenolate oxygen and the cation is sufficiently strong.
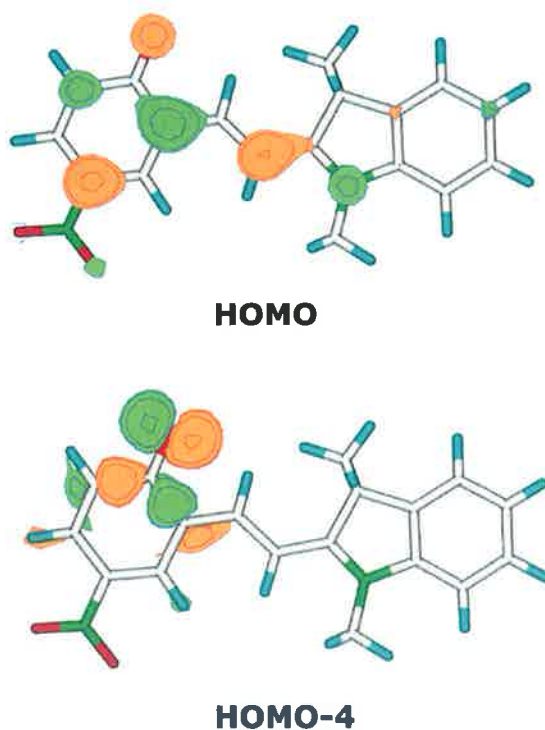
HOMO

HOMO-4

Figure 4.14. HOMO and HOMO-4 molecular orbitals of the MC isomer.

Molecular orbital calculations for the gas phase complexes show that the anion resides approximately 4.3 Å from the positively charged MC nitrogen. Hence the anion may only weakly polarize the molecular system. This distance is comparable with that found in the

169

pure [C₁mpyr][NTf₂] plastic crystal, in which the N···N separation lies in the range of 4.5 and 6.3 Å.[124] Thus the anion [NTf₂]⁻ does not appreciably interact with the positively charged nitrogen on the MC and is not expected to influence the spectroscopy beyond a possible solvatochromic effect. As [NTf₂]⁻ is the anion in all of the ILs studied, the difference in spectroscopy observed therefore is determined by the different cations. [C₃mpyr]⁺ and [C₄mpyr]⁺ behave very similarly in the spectroscopic experiments. The *ab initio* calculations of the gas phase complexes suggest that, in the case of [C₃mpyr]⁺, the pyrrolidinium nitrogen of the cation is positioned approximately 3.5 Å away from the phenolate oxygen. The sum of the van der Waals radii of N and O is 3.07 Å, i.e. this is not a close contact. Hence the solvatochromic shift of the MC maxima observed could be considered to be a simple reflection of the electrostatic interaction. Moreover, the kinetic data show a rapid conversion of MC to the aplanar BSP on irradiation, suggesting no barrier to ring closure that might indicate complex formation.

According to the spectral analysis, [emim]⁺ was found to behave differently than the pyrrolidinium cations. The [emim]⁺ cation appears to interact predominantly via the C2 carbon which resides only 2.915 Å (the C···O distance on **Figure 4.13**) away from the phenolate oxygen. The sum of the van der Waals radii of the carbon and oxygen atoms is 3.22 Å and hence, the C···O separation appears to be considerably shorter than a normal close contact. This C2 hydrogen is in fact known to be quite acidic.[125] The C2 hydrogen atom sits in between the carbon and oxygen atoms (CHO bond angle close to linear) introducing a very short/strong hydrogen bond of just 1.865 Å (H---O distance). As a comparison, a strong hydrogen bond, e.g. O—H···O, is slightly longer in length, around

1.9 Å.[126] Moreover, such a close proximity of the two ions results in a through-space orbital interaction, with molecular orbitals on both oxygen and carbon atoms overlapping, **Figure 4.15**, thus forming a relatively strong bond. The possibility of complete proton transfer was ruled out by comparing the pKa values of phenol (pKa = 10) and the unsubstituted imidazolium cation (pKa = 23).[127] Due to the through space interaction, the complex formed is likely to be quite stable and will thus hinder conversion of the MC form back to the aplanar isomer. The complex formation will have a polarizing effect on the MC moeity, disrupting the symmetry of the π orbital on the phenolate and allowing the π-π^* transition of the MC at calculated excitation energy of 418 nm. This is in accordance with the spectroscopic results, accounting for the band at 430 nm and the hypothesis that [emim]$^+$ forms a stable complex with MC.
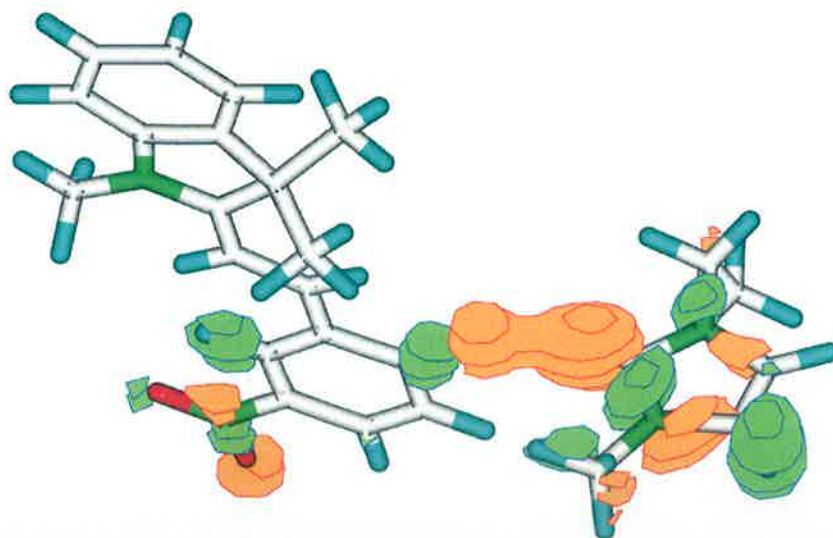
Figure 4.15. Molecular orbital of the [emim]$^+$[MC] complex showing a through space interaction between the phenolate oxygen and the carbon atom (the C$_2$ position) on [emim]$^+$.

$[P_{6,6,6,14}]^+$ was also found to behave differently to $[C_3mpyr]^+$; from the spectroscopy it is evident that some interaction is occurring with the phenolate, similar to that of $[emim]^+$. The geometry optimization on the model phsophonium cation, $[P_{2,2,2,2}]^+$, shows that the cation resides 3.730 Å from the phenolate, this interaction distance being larger by 0.25 Å than that for $[C_3mpyr]^+$. The van der Waals radius of phosphorus is 0.35 Å larger than that of nitrogen and is also more polarisable, therefore the phosphonium cation orbitals can overlap more strongly with the phenolate orbitals than the pyrrolidinium cation. Thus we believe that the $[P_{6,6,6,14}]^+$ cation is capable of disrupting the symmetry of the π orbital on the phenolate, allowing the band at 418 nm to appear.

4.4 Conclusion

To our knowledge this is the first demonstration of photochromic and thermochromic behavior of spiropyran in a selection of ionic liquids. Our results clearly show that the kinetics and thermodynamics of the process are sensitive to the nature of the ionic liquids cation. It was found that the polarity of ILs ranged from polar aprotic to polar protic solvents.

It was also observed that the imidazolium and phosphonium cations formed complexes with the MC isomer; this is due to strong interactions with these cations. This affects the polarization of the phenolate oxygen and thus the normal symmetry forbidden band at 430 nm is allowed, and the band appears. Relatively diffuse cations like imidazolium can form a through space orbital interaction rather than just electrostatic interactions, thus inhibiting the MC conversion back to the aplanar isomer.

One of the important practical outcomes of this work is that the phosphonium based system selectively exhibits photochromism only (i.e. no thermal relaxation), thus producing a potentially permanent effect or certainly a sufficiently long term effect for many applications. This observation may contribute to the development of novel molecular materials and photonic devices.

In conclusion, it has been demonstrated that, in principle, we can optically switch on/off cation binding to the merocyanine, and this process can be recycled. We regard these preliminary results as pointing the way towards more sophisticated materials capable of switching reversibly between two distinct forms, and simultaneously providing a number of transduction modes for gathering information about the molecular environment in the immediate vicinity of the binding site and its surrounding environment.

4.5 Experimental

2,3-dihydro-1',3',3'-trimethyl-6-nitrospiro[1-benzopyran-2,2'-1H-indole] (BSP) was purchased from Aldrich and used as received. Acetonitrile was HPLC grade and used without further purification. The phosphonium ILs [P$_{6,6,6,14}$][NTf$_2$], [P$_{6,6,6,14}$][dbsa], [P$_{6,6,6,14}$][dca] and [P$_{1,4,4,4}$][tos] were supplied by Cytec industries. [C$_3$mpyr][NTf$_2$], [C$_4$mpyr][NTf$_2$], and [emim][NTf$_2$] were synthesized as described previously[128, 129]. [emim][MeSO$_3$] and [edmim][NTf$_2$] were kindly supplied by Prof. MacFarlane's group. ILs were purified to spectroscopic grade as described by Earle et al. before spectroscopic analysis[130].

Absorption spectra were recorded on a Varian Cary 100 Bio UV-Visible Spectrophotometer, this instrument is also equipped with a temperature controlled 6 x 6 multicell holder, allowing precise thermal control from -10 to 100 °C. The ultraviolet irradiation source was a Spectroline ENF-24OC/FE UV-365 nm obtained from Spectronics Corporation. The white light source was a Leica CLS 150x, 150W obtained from Leica Microsystems. Samples were irradiated at a distance of 7 cm in a quartz cuvette. To determine the equilibrium constant K_e between BSP and MC in the various solvents, standard solutions of BSP were made up to 10^{-3}M in acetonitrile. 1 ml of this solution was placed in a vial and the solvent removed by N_2 stream. To this 10ml of the selected IL was added to the vial and sealed under nitrogen. Vials were then placed in sonicator for 20 minutes at 25 °C. Samples were stored in the dark at 25 °C for 15 hours before absorbance measurement was taken.

Thermal treatment experiments were conducted as follows, after 15 hrs equilibration at room temperature samples were brought to 100 °C and maintained at this temperature for 10 minutes before allowing to cool back to room temperature. Absorbance measurements, $A_{100°C}$, were taken after 10 minutes at 100 °C, A_t was measured after the sample was then allowed to cool naturally to 25 °C over a period of 15hrs.

Standard *ab initio* molecular orbital theory and density functional theory (DFT) calculations were carried out using GAUSSIAN 03.[122] The open form of BSP (the MC isomer) together with the complexes that can be formed with [emim]$^+$, [C$_3$mpyr]$^+$,

174

$[P_{6,6,6,14}]^+$ and $[NTf_2]^-$ were optimised at B3LYP/6-31+G(d) level of theory. Standard semi-empirical computations were carried out using CS MOPAC® Pro.

5. Adaptive Materials

5.1 Introduction

Intelligent materials can adaptively change or respond to an external environmental stimulus in a timely manner, producing a useful effect. The stimuli may include mechanical stress, temperature, an electric or magnetic field, photon irradiation, or chemicals (pH, ionic strength). The effect is reversible and often arises from an abrupt change in physical characteristics that can be used to generate a special function. One example is the control of rheological properties in fluids by external stimuli[131-133]. This area of research is of longstanding fundamental and practical interest, with possible applications in clutches, brakes, hydraulic pumps, vibration damping, seismic protection of structures, and other fields[131, 134-136]. In order to achieve reversible switching of the viscosity of fluids, macroscopic physical phenomena as well as effects at the molecular level may be utilized.

5.1.1 Electrorheological switching

Electrorheological (ER) fluids are such smart materials whose rheological properties (viscosity, yield stress, shear modulus, etc.) can be readily controlled using an external electric field. They can switch from a liquid-like material to a solid-like material within a millisecond with the aid of an electric field, by means of the so-called the ER effect.[137, 138] The unique feature of the ER effect is that ER fluids can reversibly and continuously change from a liquid state to a solid state. ER fluids can therefore be used as electrical and mechanical interfaces in various industries, including the automotive and robotics industry.

Three types of ER effects have been observed so far;

- The positive ER effect: occurs when the rheological properties of a fluid increase with applied electric field,

- The negative ER effect; occurs when the rheological properties decrease with applied electric field,

- The photo-electrorheological (PER) effect; both the positive and negative ER effect can be enhanced by UV illumination in some ER systems.

Much effort has been focused on developing high-performance positive ER materials. A good positive ER fluid should have the following features; (i) a high yield stress preferably equal to or larger than 5 k.Pa under an electric field of 2 kV/mm; (ii) a low current density passing through the ER fluid; preferably less than 20 $\mu A/cm^2$; (iii) a strong ER effect within a wide temperature range from -30 to 120 °C; (iv) a short response time, usually less than 10^{-3} s; (v) a high stability and no particle sedimentation or material degradation problems[131, 138].

Amorphous silicate ceramics are very important ER materials and constitute a large number of ER fluids[139, 140]. Aluminosilicates are popularly used to make hydrous and anhydrous ER fluids with a strong ER effect, the yield stress of such an ER material can easily reach 10 k.Pa at 2.5 kV/mm and a particle loading of 45 wt.%. Organic and polymeric semiconductive materials also show a strong ER effect. They are generally electronic conductive materials with a π-conjugated bond structure. It is believed that

they have better dispersing ability compared to inorganic materials. However, the ER effect of organic and polymeric ER fluids is relatively weak compared to that of aluminosilicate materials.

Polyanalines and polypyrroles, **Figure 5.1**, including their derivatives, are popularly used positive ER materials, as they can be easily prepared. These organic polymers are soft and non-abrasive to ER devices, and have attracted a great deal of attention over the past few years, resulting in a large number of publications[141, 142]. However, several problems are associated with these systems, such as poor dispersion stability due to strong particle aggregation and high current density. Various approaches have thus been proposed to improve the performance; for example, coating polyanaline surfaces with non-conductive polymer, synthesizing N-substituted copolyanaline or polypyyrole.
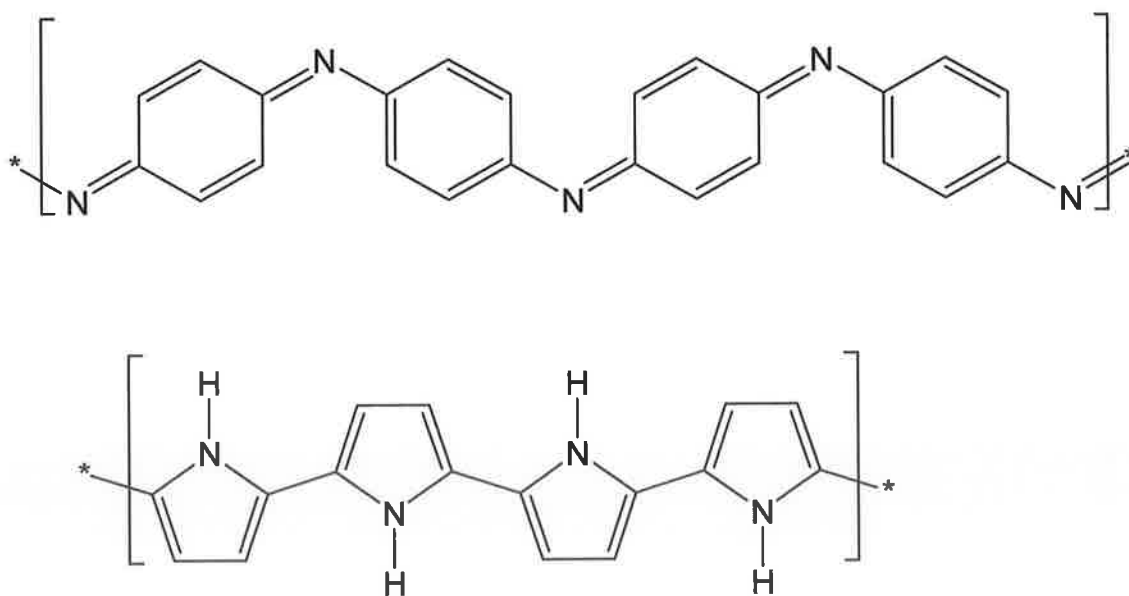
Figure 5.1. Molecular structure of polyaniline (above) and polypyrrole (below).

Electric fields have been used for over 50 years to switch the viscosity of solvents in electrorheological systems[143], as discussed above, but the use of electrochemistry based on molecular redox chemistry is more recent. Abe and co-workers[144] recently reported an iron-containing cationic surfactant, **Scheme 5.1**, which forms wormlike micelles in water in the presence of sodium salicylate. Freeze fracture TEM studies showed that these micelles are up to several micrometers long and form an entangled network displaying remarkable viscoelasticity. Upon electrolytic oxidation of the system at a very low voltage, the ferrocenyl group was oxidized to a ferricinium cation. In this way, the ferrocene head group was switched from hydrophobic to hydrophilic (**Scheme 5.1**). This oxidation breaks down the long wormlike micelles to elliptic micelles and single surfactant molecules. Whereas the mixture of ferrocenyl compound in water had a zero shear viscosity of 15 Pa.s, the viscosity dropped to 2.5×10^{-3} Pa.s upon oxidation. Although the reduction process takes a significant amount of time, the 6000-fold decrease in viscosity is nonetheless dramatic.
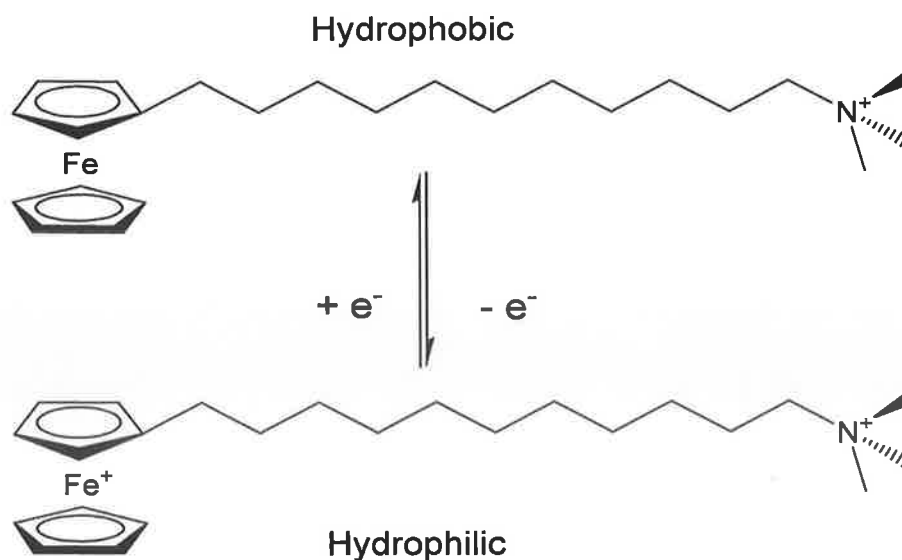
Scheme 5.1. Redox switching of head group affinity in (11-ferrocenylundecyl)trimethyl-ammonium bromide.

5.1.2 Photo-rheological switching

While applications of electrorheology show the strength of macroscopic approaches, recent developments point out promising perspectives in molecule-based switching of rheological behaviour. Chemists can contribute to this area by the design and development of molecules that are better able to transduce external stimuli into a reversible change in viscosity or even induce gelation. Some of the most successful molecular approaches in this field are the use of photochemistry.

Wolff et al.[145] were among the first to report the ability to switch between sol and gel states by the conformational changes that can be brought about by irradiation with light. Their studies concerned the selective production of the unstable 9-methylanthracene by pre-organization in micellar solutions of cetyltrimethylammonium bromide and subsequent irradiation with light, **Scheme 5.2**.
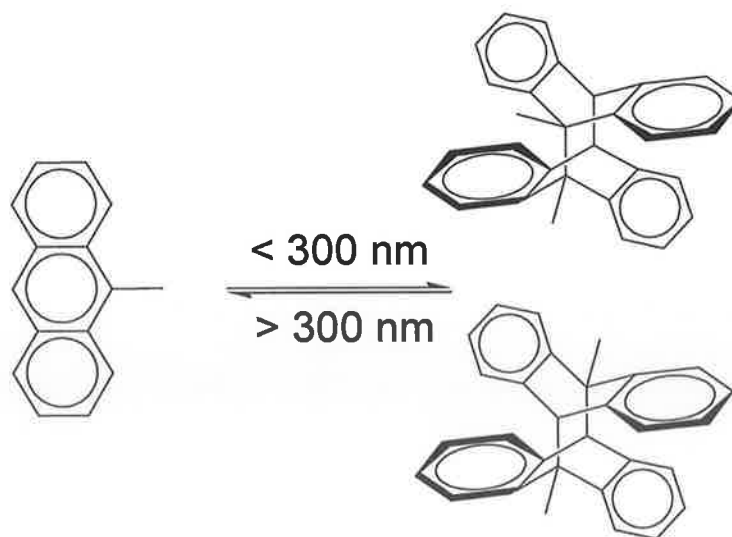
Scheme 5.2. Photodimerization of 9-methyl-anthracene leading to head-to-head (top) and head-to-tail (bottom) dimers.

As a side effect the rheological properties of the solutions also changed when irradiated, which led the authors to investigate further. The addition of 9-methylanthracene led to a strong enhancement of viscosity, upon photodimerization (λ > 300 nm), viscosity was reduced to approximately half the value. Subsequent irradiation with light of shorter wavelength (λ < 300 nm) led to an increase in the viscosity.

The *cis-trans* isomerization in azo compounds and stilbene has been used for switching viscosity[130, 146]. Shinkai et al.[147] developed a cholesterol-based gelator containing azobenzene, irradiation of the system at 330-380 nm led to isomerization of the *trans* azo linkage to its *cis* conformation and thereby disrupted gelation. Irradiation of the sol at wavelengths longer than 460 nm resulted in reversal of the isomerization and re-formation of the gel. Pozzo and co-workers[148] employed the photochromic equilibrium of 3,3-diphenyl-*3H*-naphthopyran, which brings about a large conformational change, **Scheme 5.3**. Two forms of the naphthopyran can be distinguished: a coloured open form and a colourless closed form. When the naphthopyran unit is in its closed form, it does not influence the stacking process and the molecule acts an efficient gelator. Irradiation with UV light converts the naphthopyran unit into the open form and prevented the carbamate group from stacking. The isomerization is accompanied by a colour change, and while the gel liquefied it became yellow. Heating converted the pyran unit back into the closed form, and upon cooling a colourless gel was again obtained.
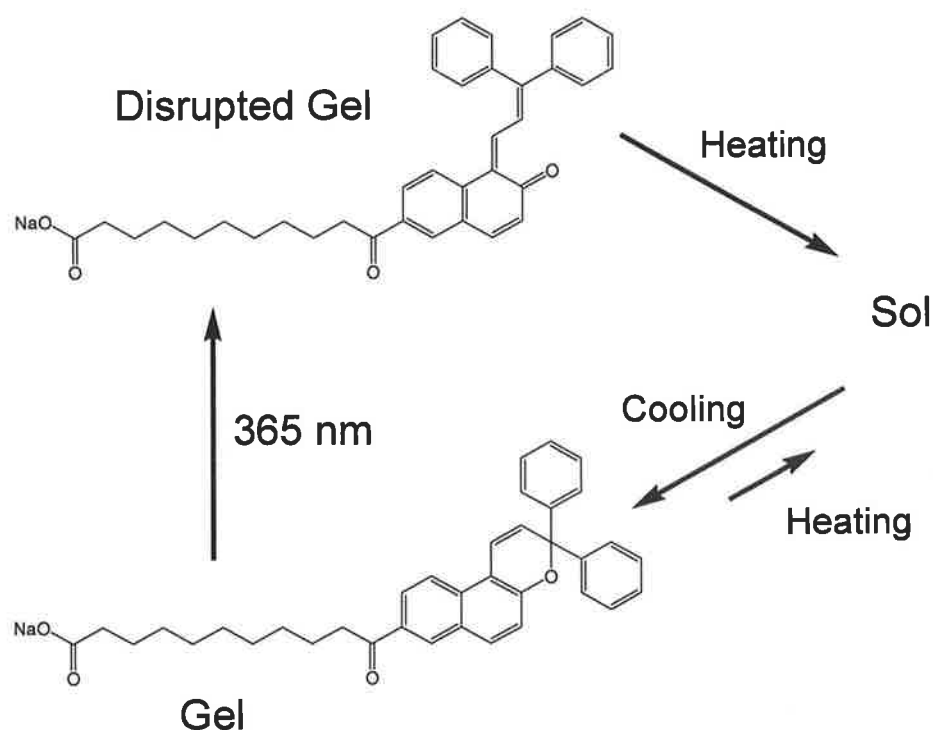
Scheme 5.3. Light-induced switching between open and closed isomers of naphthopyrans.

5.1.3 Ionic liquids as adaptive materials

Room-temperature ionic liquids (ILs) are composed solely of ions and show melting points below 100 °C. The positive and negative charges carried by these ions produce a variety of electrostatic environments that should affect the behaviour of electrons in ionic liquid systems. Because chemical reactions are, in a sense, relocation processes of valence electrons, the charge distribution in the ionic liquids should profoundly affect the chemical reactions proceeding within them. Due to these unique properties, and others described in chapter 4, ILs have been investigated for many applications such as synthesis[100], catalysis[104], polymerization[105-107], separation[108], electrochemistry[109, 110] and electrochemical devices[111, 112]. ILs are expected to substitute existing electrolyte solutions

as they are considered a safer and 'greener' alternative, however electrolyte solutions, including ILs always need to be contained and there is the possibility of leakage due to physical stress. Therefore it is inevitable that solid-state ion conductors will be developed, recent work in this field includes polymerization of ILs and simple mixing of polymers and ILs. On the other hand, Tamada and Horie[149] have investigated "stimulus-responsive gels" utilizing the photochemical reaction of a polymeric azobenzene unit doped with IL, **Figure 5.2**. Photoisomerization of the azobenzene group resulted in shrinkage of the irradiated site, it was also reported that ionic conductivity of the gel could be controlled by photoirradiation. The ionic conductivity of the gel decreased after UV light irradiation, this effect was coupled with an increase in viscosity, in turn suppressing diffusion of the component ions within the gel.
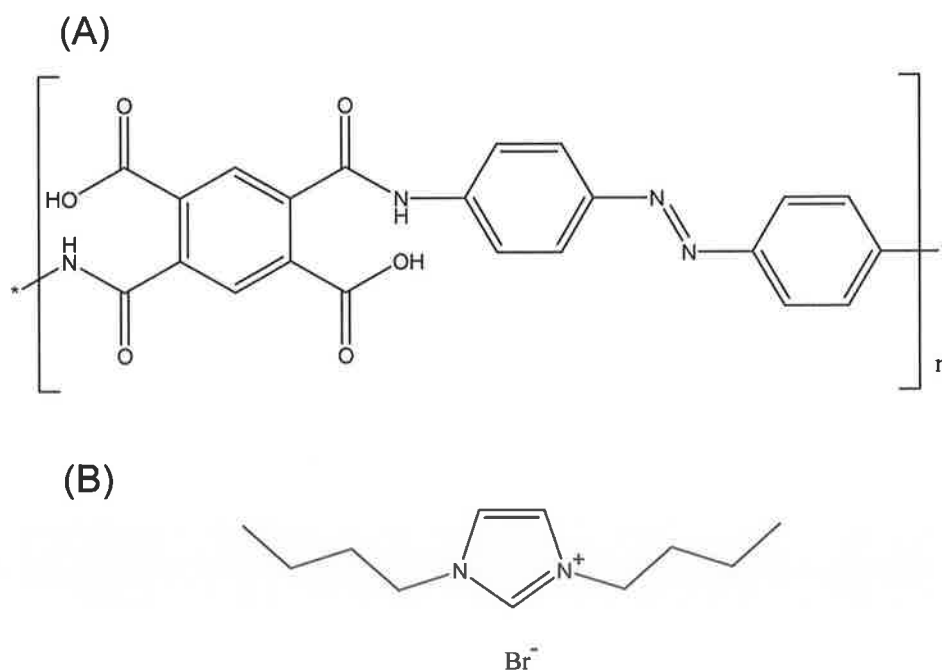
Figure 5.2 Structure of gel components (A) poly(amideacid) azobenzene, (B) 1,3 dibutylimidazolium bromide [bbim][Br].

In the framework of supramolecular chemistry, benzospiropyran (BSP) can be envisaged as a molecular system that exists in different forms (multi-state), which exhibit different chemical and physical properties. These different states can also be interconverted by different external stimuli (multifunctional), similar to azobenzene. From chapter 4, it appears that the photo- and thermochromic behavior of BSP in ILs are sensitive to the nature of the ions, it was also observed that the imidazolium and phosphonium cations formed complexes with the MC isomer. The phosphonium based IL was found to selectively exhibit photochromism only (i.e. no thermal relaxation), this particular result prompted a further study into the photo- and thermochromic properties of BSP in phosphonium based ILs. Control of interactions at the molecular scale is the ultimate goal, as this in turn determines all macroscale behaviour.

5.2 Results

In chapter 4, the BSP↔MC equilibrium was studied in various ILs. It was found that for ILs containing the cation phosphorus some interesting solute-solvent interactions were observed. The photoisomerisation of BSP was investigated in $[P_{6,6,6,14}][NTf_2]$, $[P_{6,6,6,14}][dca]$, $[P_{6,6,6,14}][dbsa]$ and $[P_{1,4,4,4}][tos]$, **Figure 5.3**, by spectroscopic and bulk analysis.
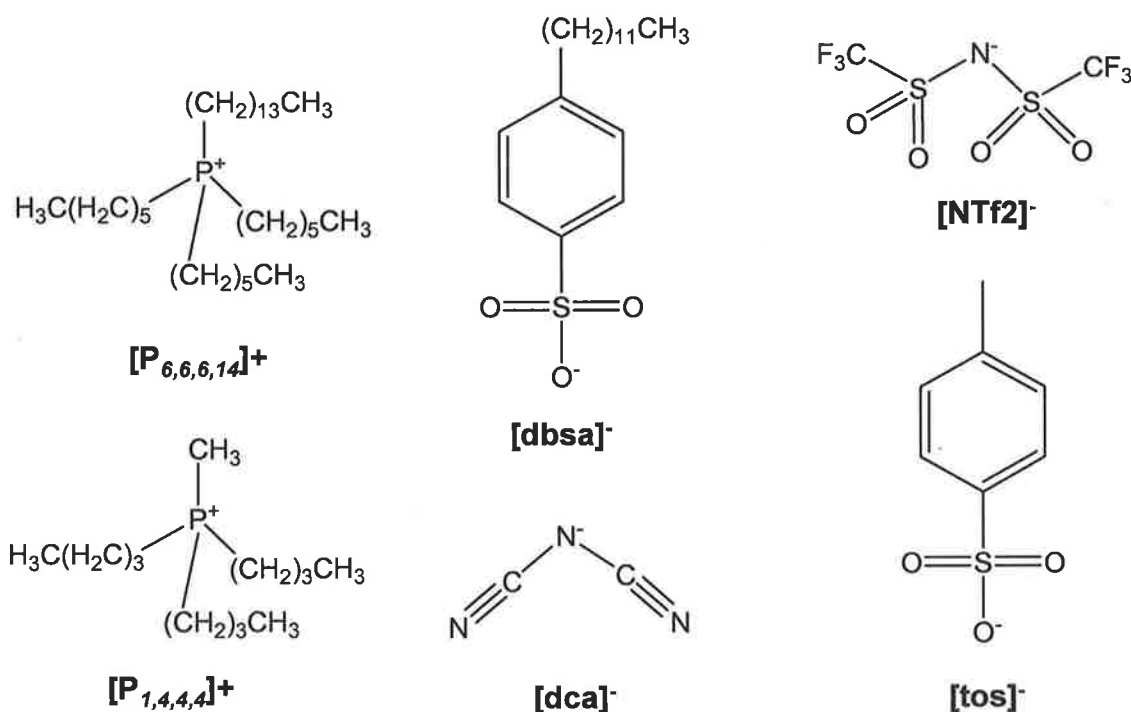
Figure 5.3. Cations and anion's analyzed in this study, trihexyl tetradecyl phosphonium $[P_{6,6,6,14}]^+$, tributyl methyl phosohonium $[P_{1,4,4,4}]^+$, bis(trifluoromethanesulfonyl) amide $[NTf_2]^-$, dicyanimide $[dca]^-$, tosylate $[tos]^-$, dodecylbenzene sulfate $[dbsa]^-$.

5.2.1 UV-vis spectroscopy of solute-solvent complex

Figure 5.4 depicts the absorption spectra of the ILs used in this study, in neat form. In all cases, the absorbance is significant (around 0.02-0.16) even at 350 nm. The other notable

185

feature of the spectra is that the absorption tail is fairly long and it extends even beyond

450 nm.
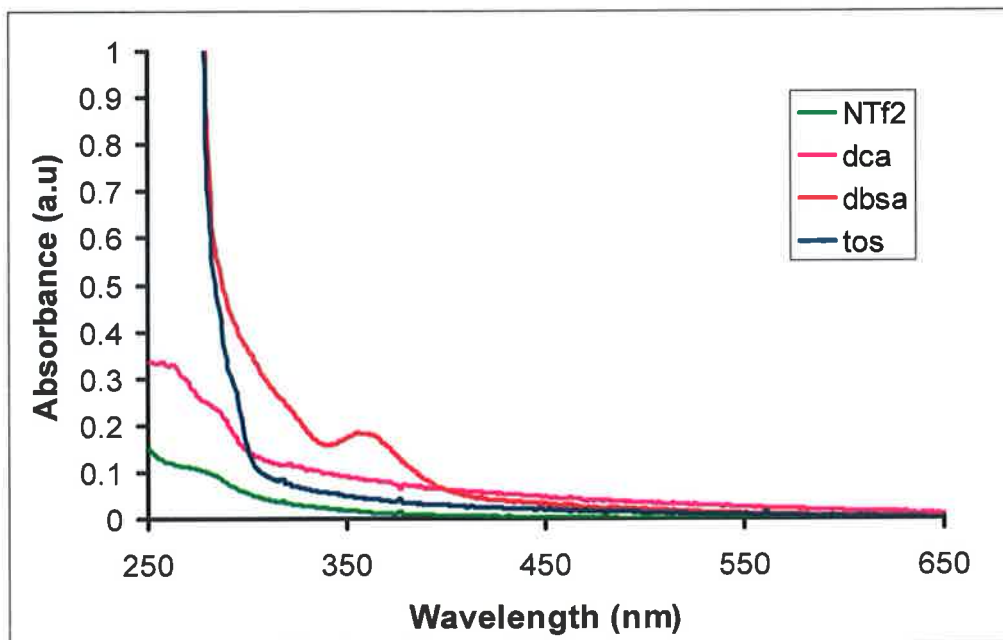
Figure 5.4. UV-vis absorption spectra of neat $[P_{6,6,6,14}][NTf_2]$, $[P_{1,4,4,4}][tos]$, $[P_{6,6,6,14}][dca]$, and $[P_{6,6,6,14}][dbsa]$. ILs were dissolved by 50v/v % in acetonitrile.

Photochromism was observed in all phosphonium based ILs containing 10^{-4}M BSP, albeit

an unusual photochromic shift with respect to the well studied photochromic properties of

BSP in molecular solvents. Upon UV irradiation to $[P_{6,6,6,14}][NTf_2]$ containing 10^{-4}M

BSP, it was observed that two absorption bands appeared at 572 and 440 nm. When this

sample was exposed to visible light, these bands disappeared, see **Figure 5.5(a)**. When

$[P_{1,4,4,4}][tos]$ containing 10^{-4}M BSP is exposed to UV irradiation an absorption band at

482 nm appears with a small shoulder at 560 nm, on exposure to visible light this band

disappears, as seen in **Figure 5.5(b)**. Absorption spectrum for 10^{-4}M BSP in

$[P_{6,6,6,14}][dca]$ when exposed to UV light results in a sharp absorption band at 440 nm,

when irradiated with visible light this band does not completely disappear but decreases in intensity, as seen from **Figure 5.5(c)**. Photochromism of 10^{-4}M BSP in [P$_{6,6,6,14}$][dbsa] results in an increase in intensity at 440 nm when irradiated with UV light, this shoulder disappears with exposure to visible light, see **Figure 5.5(b)**.
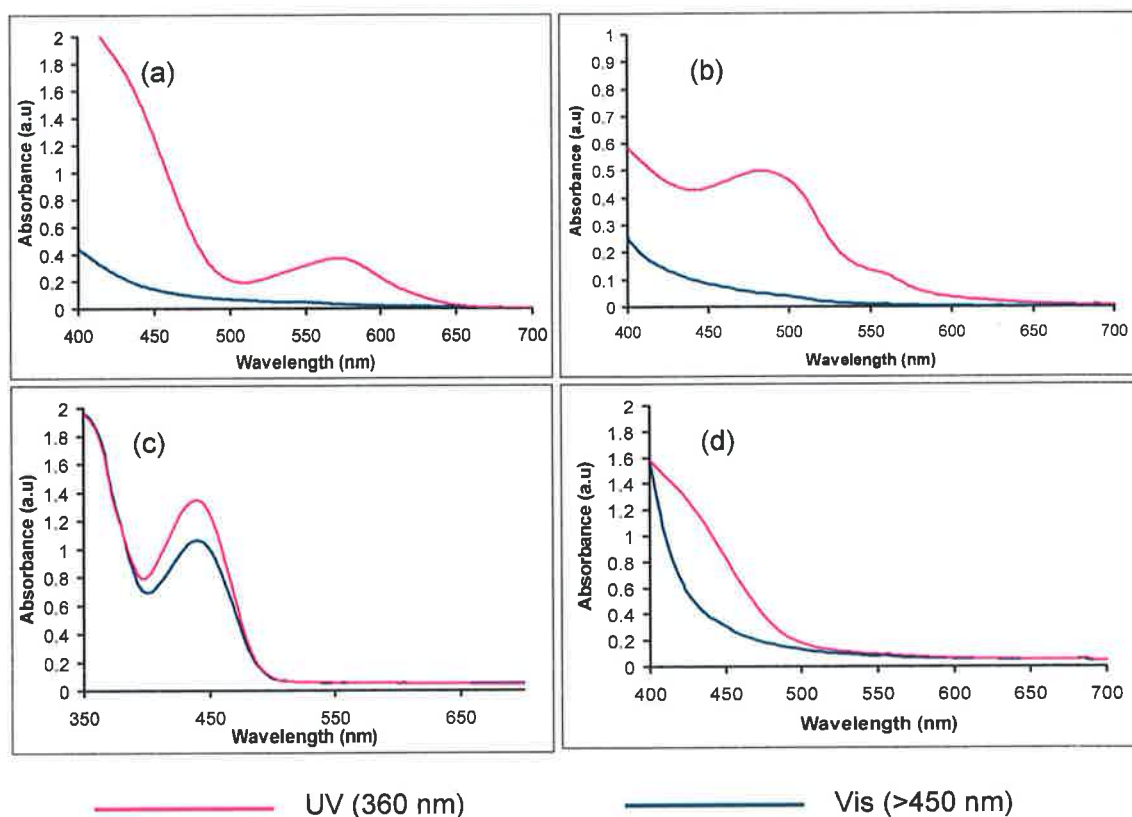
Figure 5.5. Absorption spectroscopy of the photochromic properties of 10^{-4}M BSP in (a) [P$_{6,6,6,14}$][NTf$_2$], (b) [P$_{1,4,4,4}$][tos], (c) [P$_{6,6,6,14}$][dca], and (d) [P$_{6,6,6,14}$][dbsa]. Samples irradiated with UV (360 nm) and Vis (>450 nm) light for 60 seconds to generate spectra.

Due to sensitivity issues of spectroscopic methods such as IR, Raman, and NMR, the BSP concentration needed to be increased. Therefore, it was decided to add 5 mol% of BSP to the selected IL. Due to the high extinction coefficient of BSP at 5 mol%, absorbance measurement below 550 nm could not be attained due to complete absorption

187

of light. Although, upon UV irradiation of 5 mol% BSP in the ILs, a new absorbance band was observed at 636, 633 and 646 nm for $[P_{6,6,6,14}][dbsa]$, $[P_{6,6,6,14}][NTf_2]$, and $[P_{1,4,4,4}][tos]$ respectively, see **Figure 5.6**. Absorption in this region is usually coupled with *J*-aggregation. There was no absorption band located in this region for $[P_{6,6,6,14}][dca]$.
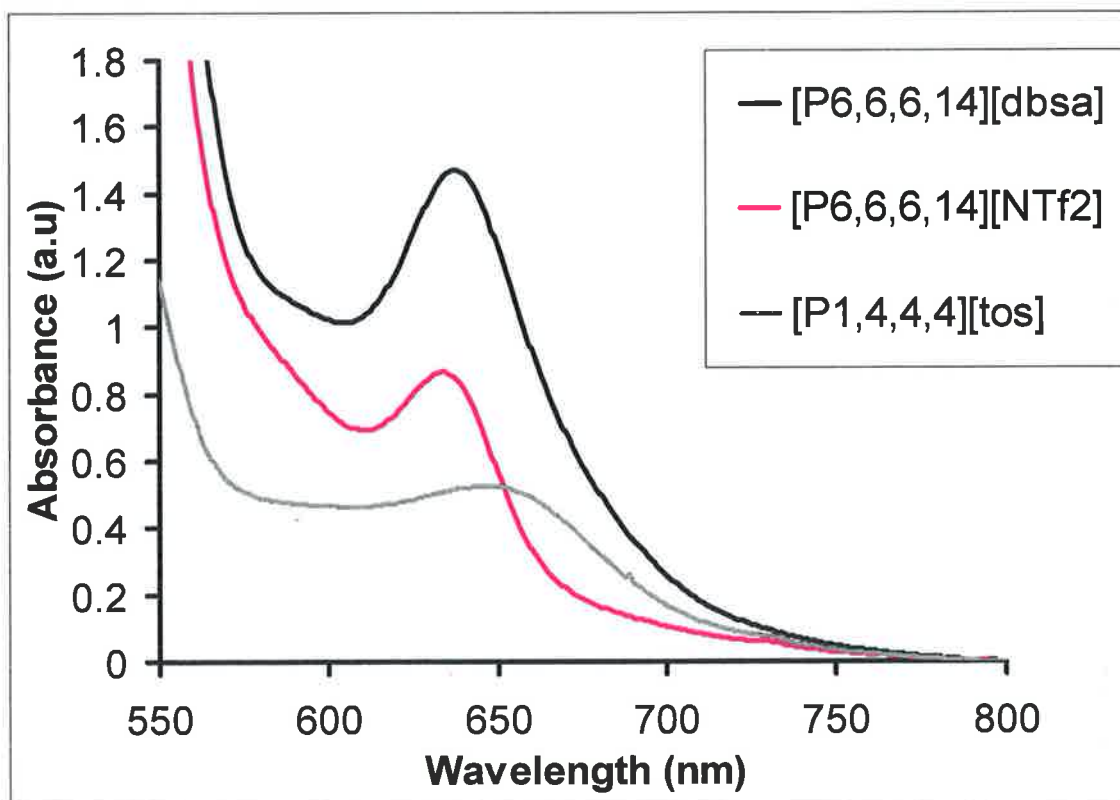
Figure 5.6. Absorbance spectra of 5 mol% BSP in $[P_{6,6,6,14}][dbsa]$, $[P_{6,6,6,14}][NTf_2]$, and $[P_{1,4,4,4}][tos]$ after 60 seconds UV (365 nm) light.

5.2.2 Fluorescence of solute-solvent complex

Luminescence spectral studies involving several dye molecules have been carried out to measure the polarity or solvent strength of many ILs[116, 120]. On the other hand, several

optical studies have noted peculiar fluorescent behaviour of the ILs themselves, but have never focused on the origins of this behaviour[150]. It was also reported that for the case of imidazolium based ILs, there were clearly several structures with both short and long-range spatial correlations of the cation-anion and cation-cation pairs, termed 'associated species'. The existence of multiple structures, and the large region of probability of finding an anion in the vicinity of a cation and vice-versa, is expected to broaden the energy states of the absorbing species, leading to long emission tails[151]. The liquid states of ILs are still not fully understood and the presence of various associated species that are energetically different could not be ruled out. Therefore, the fact that ILs exhibit this type of fluorescent behaviour, one needs to be extremely careful in fluorescence measurements.

The fluorescence behaviour of neat $[P_{6,6,6,14}][NTf_2]$, $[P_{6,6,6,14}][dca]$, $[P_{1,4,4,4}][tos]$, and $[P_{6,6,6,14}][dbsa]$ is illustrated in **Figure 5.7** (a), (b), (c), and (d), respectively. As can be seen, the spectral behaviour is strongly dependent on the excitation wavelength. When excited at wavelengths below 300 nm, $[P_{6,6,6,14}][NTf_2]$ exhibits an emission band centered around 315 nm and the band profile extending beyond 450 nm. However, as the excitation wavelength is shifted to longer wavelengths, which correspond to the tail portion of the absorption band, the fluorescence maxima starts to shift toward longer wavelength with progressive decrease of the overall intensity; excitation at 400 nm exhibits an emission band centered around 450 nm. This fluorescence behaviour is seen in all of the ILs studied as can be seen in **Figure 5.7**, particularly in the case of $[P_{6,6,6,14}][dbsa]$. When excited at 293 nm, $[P_{6,6,6,14}][dbsa]$ exhibits an emission band

189

centered around 315 nm, similar to [P$_{6,6,6,14}$][NTf$_2$], although the emission intensity being 4-fold larger. As with [P$_{1,4,4,4}$][tos], an increase in emission intensity is observed with respect to [P$_{6,6,6,14}$][NTf$_2$] and [P$_{6,6,6,14}$][dca]. This increase in fluorescence can be explained due to the anion's unsaturated ring system, see **Figure 5.3**.
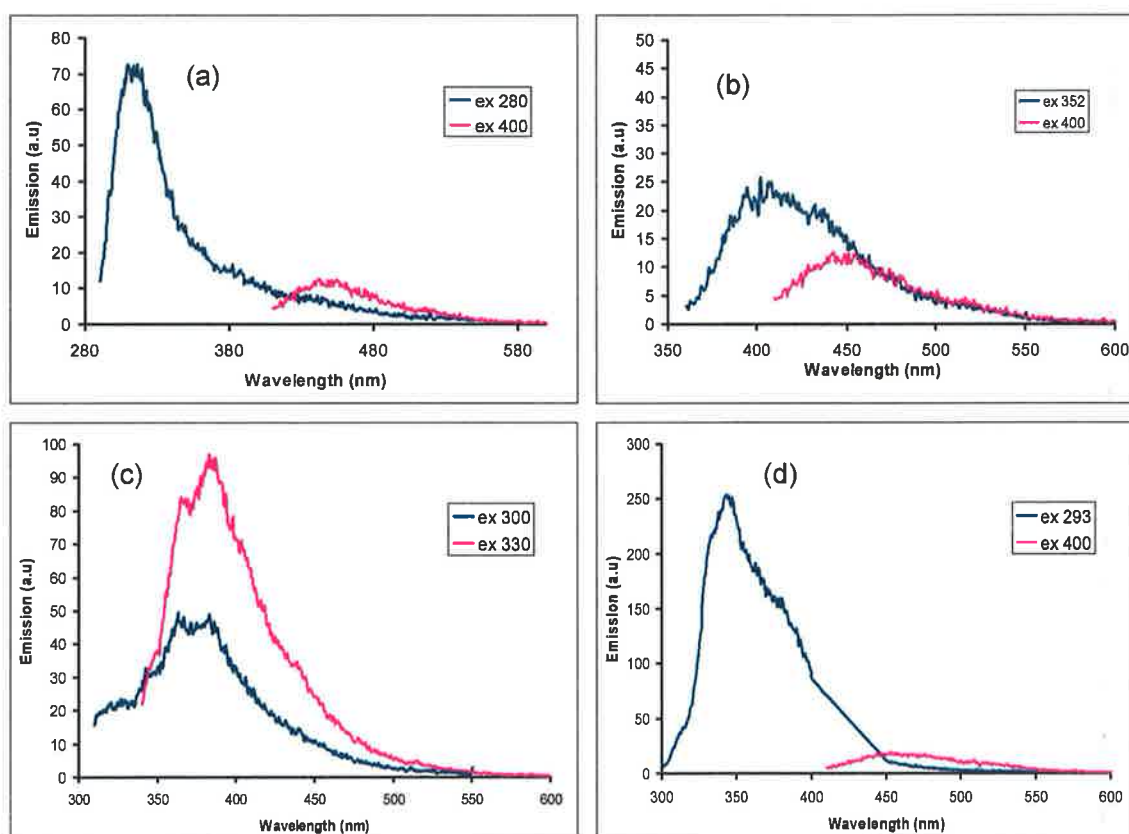
Figure 5.7. Emission spectra of neat (a) [P$_{6,6,6,14}$][NTf$_2$], (b) [P$_{6,6,6,14}$][dca], (c) [P$_{1,4,4,4}$][tos], and (d) [P$_{6,6,6,14}$][dbsa].

The absorbance above 400 nm of the phosphonium based ILs is rather small and as such, should not constitute any serious interference to fluorescence measurements of BSP. The MC isomer has an emission band located at 616 nm in acetonitrile when excited between 400 and 600 nm. The fluorescence behaviour of BSP in [P$_{6,6,6,14}$][NTf$_2$] was first examined. The emission spectra for UV irradiated [P$_{6,6,6,14}$][NTf$_2$]-BSP, when excited at

505 and 630 nm is shown in **Figure 5.8**. The emission band observed when excited at

505 nm is centered at 565 nm. Surprisingly, when excited at 630 nm, an emission band

centered at 665 nm is observed, this band is quite sharp and twice the intensity of the

emission band at 565 nm. Also, Stokes shift of 35 nm is quite small and fits well to the

profile that J-aggregates are present within the IL matrix. Emission bands at this

wavelength correspond to MC J-aggregate emission[62].
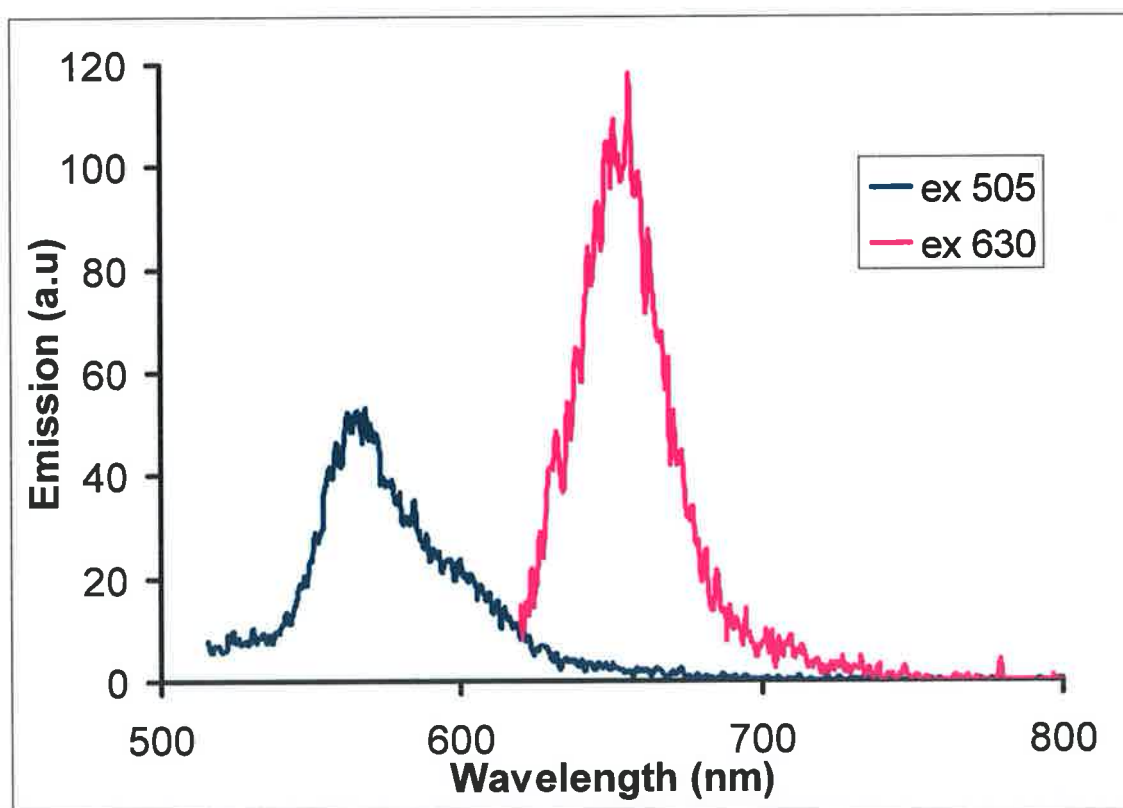
Figure 5.8. Emission spectra of [P$_{6,6,6,14}$][NTf$_2$]-BSP. Irradiated with UV light for 60

seconds.

The fluorescence behaviour of 5 mol% BSP in [P$_{6,6,6,14}$][dca] was examined as its

absorption spectroscopy differed to that of the other three ILs examined. The emission

191

spectra for UV irradiated [P$_{6,6,6,14}$][dca]-BSP, when excited at 370 and 490 nm is shown in **Figure 5.9**. The emission observed when excited at 370 nm results in two emission bands at 403 and 480 nm, the latter having greater intensity. When this sample is excited at 490 nm, an emission band centered at 530 nm appears. No emission bands were found above 600 nm.
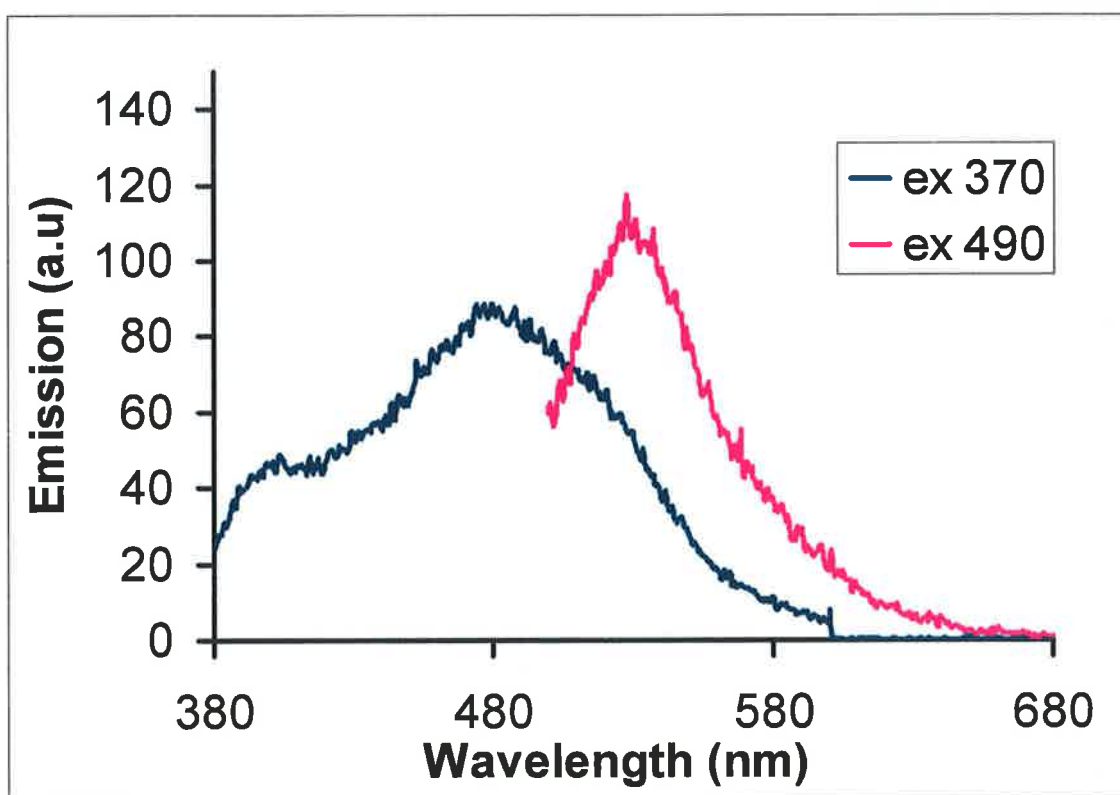
Figure 5.9. Emission spectra of [P$_{6,6,6,14}$][dca]-BSP. Irradiated with UV light for 60 seconds.

5.2.3 FT-IR of solute-solvent complex

The characterization of tetralkylphosphonium salts has been carried out by FT-IR. **Figure 5.10** shows the overlaid FT-IR spectra of [$P_{6,6,6,14}$][dca], [$P_{6,6,6,14}$][dbsa], [$P_{1,4,4,4}$][tos], and [$P_{6,6,6,14}$][NTf$_2$]. The common vibrational bands seen in the tetralkylphosphonium ILs are the P-CH$_2$ bending located approximately at 1460 cm^{-1}, and the sp^2 and sp^3 C-H stretching of the tetralkyl groups located at 2850 and 2920 cm^{-1}, respectively. The spectra of [$P_{6,6,6,14}$][dbsa] (**Figure 5.10b**) and [$P_{1,4,4,4}$][tos] (**Figure 5.10c**) are also very alike due to their similar anion's, which contain *para*-substituted benzenesulfonates. These anion's have several common vibrational bands including the sulfonate asymmetric and symmetric stretching located at 1200 and 1115 cm^{-1}, respectively. Also, the S-O$^-$ stretch has two sharp bands at 1010 and 1033 cm^{-1}. For [$P_{6,6,6,14}$][dca] (**Figure 5.10a**), the nitrile band is quite specific, located at 2123 and 2221 cm^{-1} with the C-N$^-$ stretch located at 1297 cm^{-1}. Due to the structural features of the anion in [$P_{6,6,6,14}$][NTf$_2$], there are many functionalities with specific vibrational bands (**Figure 5.10d**) . The asymmetric and symmetric stretching of the sulfonate are located at 1346 and 1133 cm^{-1}, respectively. The CF$_3$ groups exhibit an asymmetric stretch at 1175 cm^{-1}, with symmetric and asymmetric bending at 738 and 514 cm^{-1}, respectively. The S-N-S section of the anion exhibit asymmetric and symmetric stretching at 1049 and 784 cm^{-1}, respectively. It is important to characterize the bands that are specific to each IL, so it will be possible to distinguish the bands corresponding to the MC isomer, or even new bands arising from solute-solvent interaction.
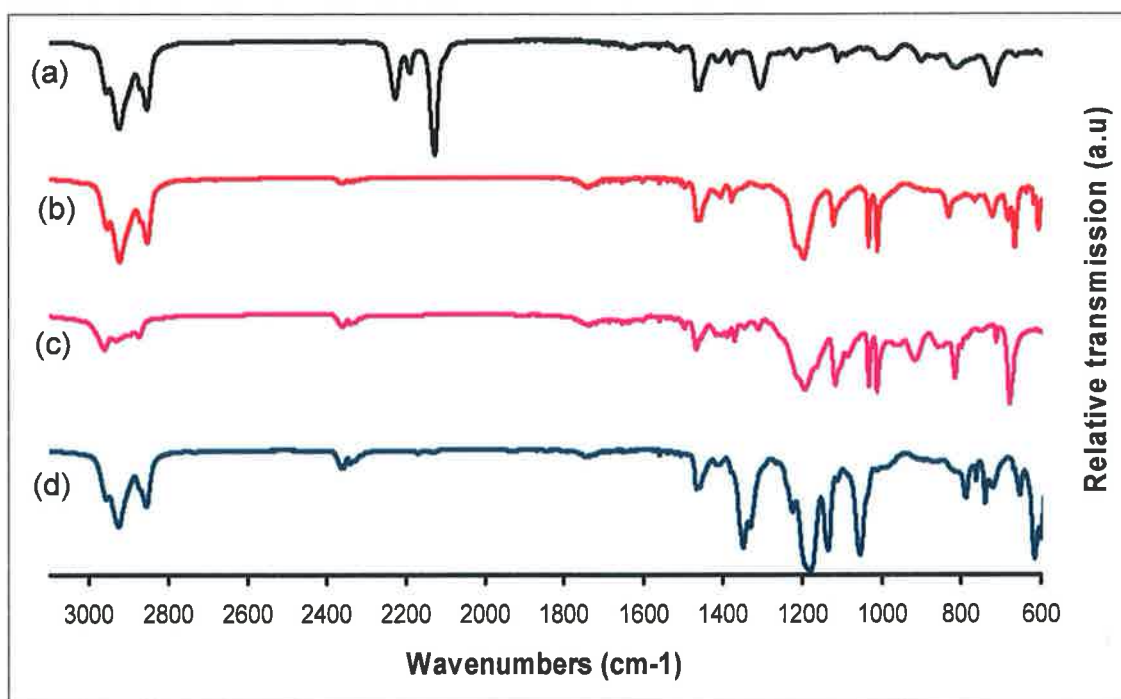
Figure 5.10. Overlaid FT-IR spectra of neat (a) [$P_{6,6,6,14}$][dca], (b) [$P_{6,6,6,14}$][dbsa], (c) [$P_{1,4,4,4}$][tos], and (d) [$P_{6,6,6,14}$][NTf$_2$].

Infrared spectroscopy gives a more detailed information with respect to specific molecular interactions than UV-vis and fluorescence. We have observed through UV-vis spectroscopy that each IL affects BSP differently, therefore it is important that we analyze each spectrum separately. Due to the limited concentration capacity of the tetralkylphosphonium salts for BSP, 5 mol% of BSP was the loading concentration that was used in each IL. The concentration of BSP, while low in comparison with the solvent, should still be detectable by the FT-IR instrument. **Figure 5.11** represents overlaid spectra of BSP, [$P_{6,6,6,14}$][NTf$_2$], and [$P_{6,6,6,14}$][NTf$_2$] containing 5 mol% BSP. It is quite evident from **Figure 5.11** that a new vibrational band located at 1735 cm^{-1} indicative of a carbonyl group is only present in the [$P_{6,6,6,14}$][NTf$_2$]-BSP spectrum. It should also be noted that the nitro group features in the BSP spectrum, with its strong

194

vibrational bands that include asymmetric at 1511 cm^{-1} and symmetric at 1341 cm^{-1} stretching modes are not present in the [P$_{6,6,6,14}$][NTf$_2$]-BSP spectrum. Due to the many vibrational bands from the [NTf$_2$]$^-$ ion, it was not possible to decipher many other changes in the IL-BSP mixture. Although the emergence of a shoulder at 1380 cm^{-1} in the [P$_{6,6,6,14}$][NTf$_2$]-BSP spectrum, represents the N$^+$-O$^-$ vibration.
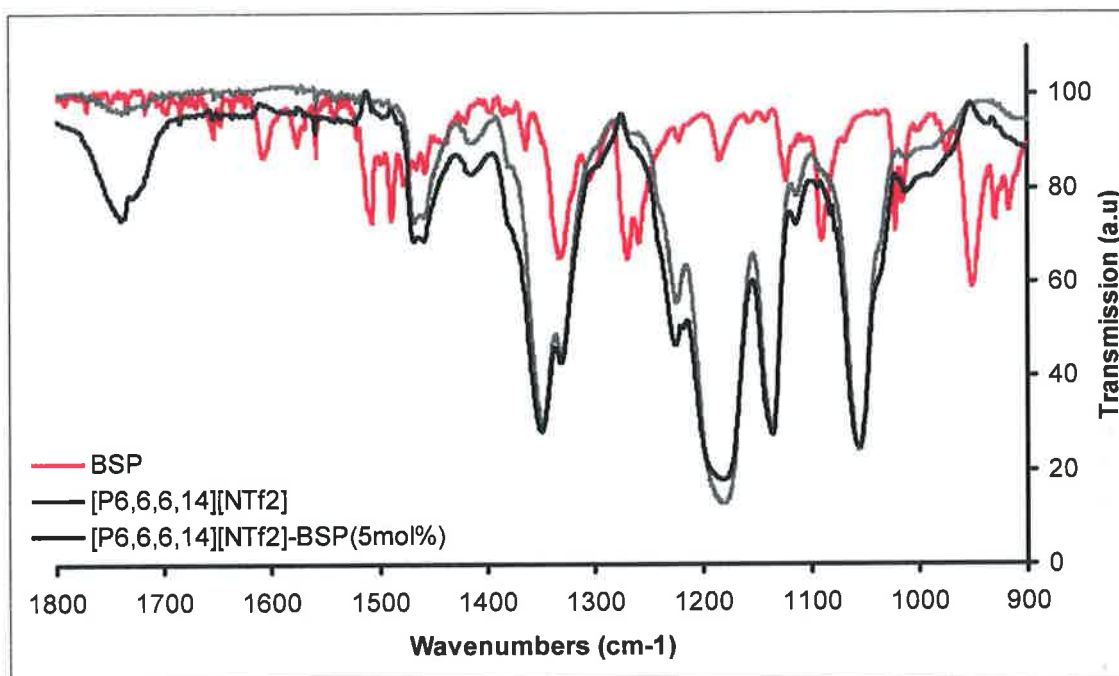
Figure 5.11. Overlaid FT-IR spectra of BSP, [P$_{6,6,6,14}$][NTf$_2$], and [P$_{6,6,6,14}$][NTf$_2$] containing 5 mol% BSP, irradiated with UV light for 60 seconds.

The IL [P$_{6,6,6,14}$][dca] has significantly fewer vibrational bands than any other of the ILs studied, which makes it ideal for studying solute-solvent interactions. As can be seen in **Figure 5.12**, there is quite a difference between the [P$_{6,6,6,14}$][dca] spectrum and the [P$_{6,6,6,14}$][dca]-BSP spectrum. Firstly, as seen in the [P$_{6,6,6,14}$][NTf$_2$]-BSP spectrum in **Figure 5.11**, the band located at 1735 cm^{-1} is present within the [P$_{6,6,6,14}$][dca]-BSP

spectrum, indicative of a compound containing a carbonyl group. This band is present in both IL samples containing BSP. Another very interesting observation is found in the $[P_{6,6,6,14}][dca]$-BSP spectrum at 1590 cm^{-1}. This band is not found in the pure $[P_{6,6,6,14}][dca]$ or BSP spectra. The band located at 1608 cm^{-1} in the BSP spectrum corresponds to the C=C bond in the methylene bridge of the BSP structure, which upon photo-isomerization of the BSP to MC, becomes incorporated within a conjugated system, lowering the absorbance band to 1590 cm^{-1}. Conjugation of a C=C double bond with another double bond provides the multiple bond with more single-bond character (through resonance effects), and thus a lower frequency of vibration. It is also important to note that the nitro vibrations seen in the BSP spectrum are still present within the $[P_{6,6,6,14}][dca]$-BSP spectrum. For example, the asymmetric NO_2 stretching band is located at 1516 cm^{-1}, the NO_2 symmetric stretch is masked by the $[dca]^-$ anion C-N$^-$ stretch at 1297 cm^{-1}. The NO_2-phenyl stretch in BSP is also seen in the $[P_{6,6,6,14}][dca]$-BSP spectrum, located at 1265 cm^{-1}. This data correlates well with UV-vis and fluorescence spectroscopic results for $[P_{6,6,6,14}][dca]$-BSP as no observation of *J*-aggregates were seen. It can also be seen that the zwitterionic character of the MC isomer is present within the $[P_{6,6,6,14}][dca]$-BSP spectrum due to the observation of the $C_{aryl}=N^+$ bond vibration at 1143 cm^{-1} and the presence of the C-O$^-$ phenolate vibration at 1230 cm^{-1}.
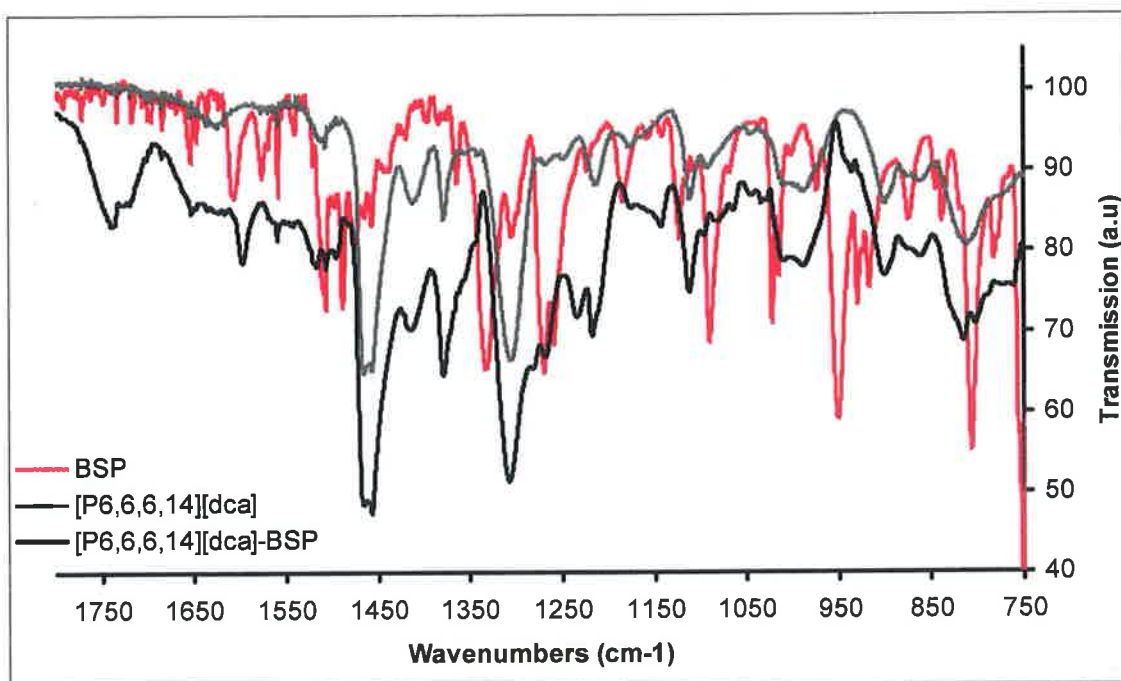
Figure 5.12. Overlaid FT-IR spectra of BSP, [P$_{6,6,6,14}$][dca], and [P$_{6,6,6,14}$][dca] containing 5 mol% BSP, irradiated with 60 seconds UV light.

Unfortunately, the FT-IR analysis of [P$_{6,6,6,14}$][dbsa] (**Figure 5.13**) and [P$_{1,4,4,4}$][tos] (**Figure 5.14**) ILs containing 5 mol% was less than informative than the two previous samples. Although it can be seen that the C=C bond in the methylene bridge of the BSP isomer (1608 cm^{-1} in the BSP spectrum) has shifted to a lower frequency due to the formation of the conjugated MC system. The absence of the asymmetric stretching of the nitro group, in both samples, leads to the conclusion that the nitro group has been altered.
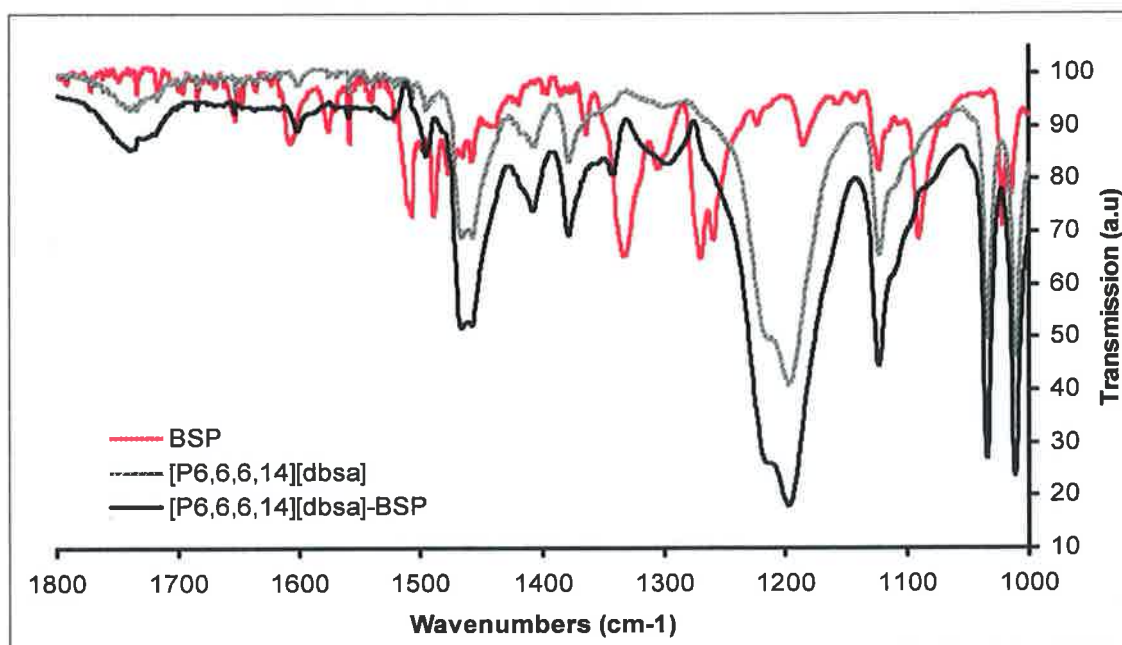
Figure 5.13. Overlaid FT-IR spectra of BSP, [P$_{6,6,6,14}$][dbsa], and [P$_{6,6,6,14}$][dbsa] containing 5 mol% BSP, irradiated with 60 seconds UV light.
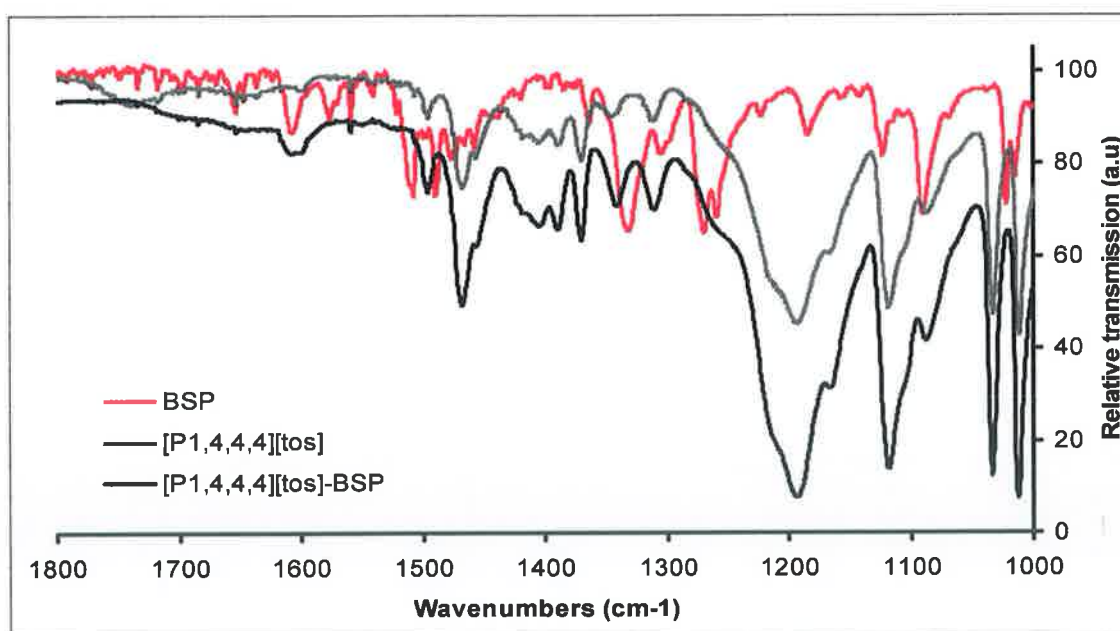
Figure 5.14. Overlaid FT-IR spectra of BSP, [P$_{1,4,4,4}$][tos], and [P$_{1,4,4,4}$][tos] containing 5 mol% BSP, irradiated with 60 seconds UV light.

As a complimentary technique to infrared spectroscopy, the ionic liquids containing BSP were analyzed by Raman spectroscopy (excitation laser source 680 nm). Excellent spectra were obtained for all neat ILs and BSP separately, unfortunately, for ILs containing BSP no spectra were obtained due to the interference from fluorescence, see **Figures A2-6** in appendix.

5.2.4 NMR of solute-solvent complex

NMR is a spectroscopic method which provides detailed structural information about the number of magnetically distinct atoms and the nature of their immediate environment. From the optical and vibrational spectroscopic results of BSP in the ILs studied, it appears there are significant solute-solvent interactions, such as electrostatic interactions and the polarization of the phenolate by the phosphonium cation. Due to the zwitterionic character of the MC isomer and the ions within the IL solvent, it can be presumed that a multitude of interactions are the cause of the observed shifts and new bands in the IR and UV-vis spectroscopy. Therefore, the signals of the ^{1}H- and ^{31}P- NMR should also be affected at specific locations on the molecule and ion. Due to the low concentration of BSP in the IL solvent along with addition of deuterated solvent, the NMR signals are weak. Therefore, minimal deuterated solvent was added to obtain decent spectrum. ^{1}H-NMR was carried out for all the ILs containing 5 mol% BSP. For the ILs containing the anion's [tos]⁻ and [dbsa]⁻, the protons located on their phenyl ring occupy the region of interest for the BSP. Fortunately, for [P$_{6,6,6,14}$][NTf$_2$] and [P$_{6,6,6,14}$][dca], none of their protons are located within this region of interest. From the results in chapter 4, it can be concluded that in the IL [P$_{6,6,6,14}$][NTf$_2$], the anion [NTf$_2$]⁻ has no specific interaction with

the BSP or MC isomer. The UV-vis and IR spectroscopy discussed earlier suggests that [P$_{6,6,6,14}$][dca] has a different effect on the BSP spectroscopy compared to [P$_{6,6,6,14}$][NTf$_2$]. Due to the presence of a common cation this is likely to be due to the anion [dca]⁻.
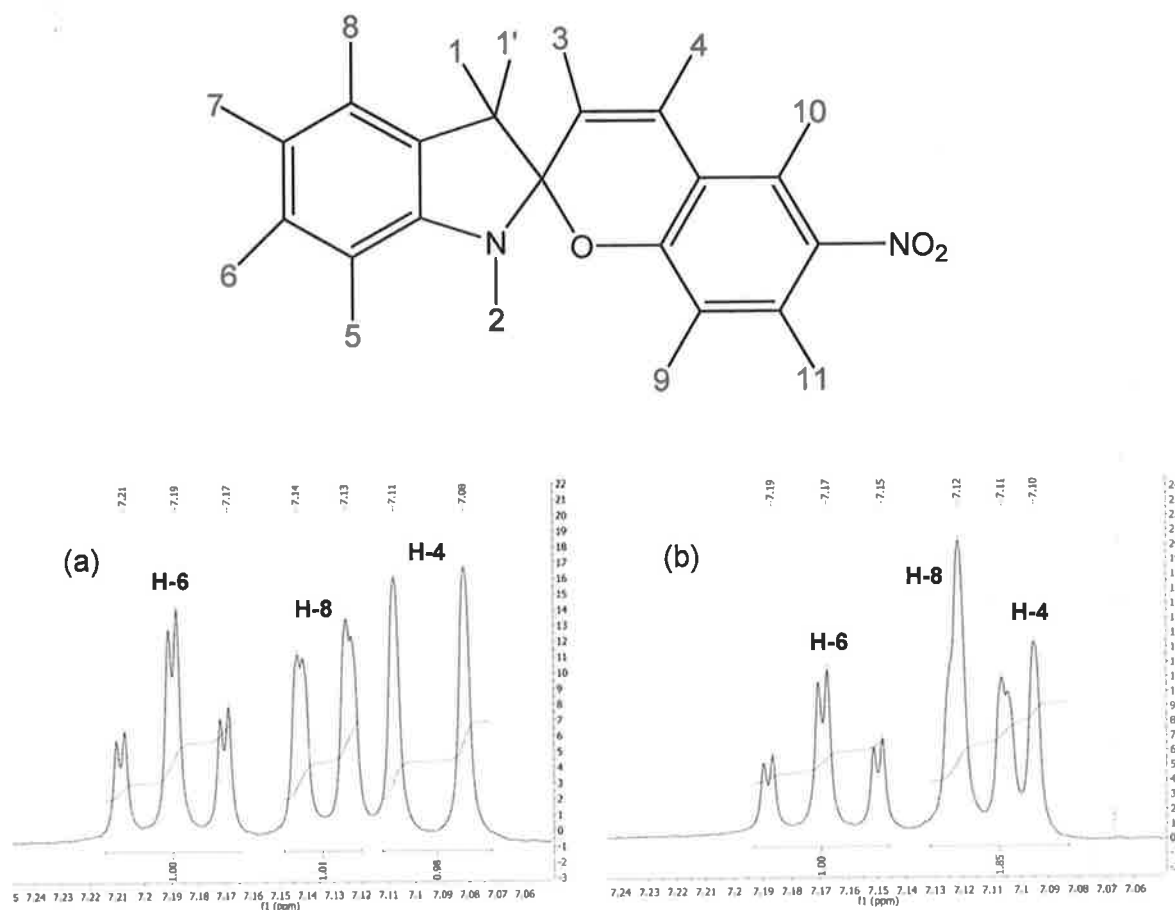
Figure 5.15. ^{1}H-NMR spectra for (a) [P$_{6,6,6,14}$][NTf$_2$] and (b) [P$_{6,6,6,14}$][dca] both containing 5 mol% BSP.

The ^{1}H-NMR spectrum of [P$_{6,6,6,14}$][NTf$_2$] containing 5 mol% BSP is represented in **Figure 5.15(a)**. H-6, H-8 and H-4 are located at 7.19 (t), 7.13 (dd) and 7.08 (d) ppm, respectively. H-4 represents the vinylic proton in the methylene bridge, with a coupling

200

constant of 10.35 Hz (H3-H4), corresponding to that of a *cis*-conformation. These values are very similar to that of BSP in acetonitrile, **see Table 2.2**. The ^{1}H-NMR spectrum of [P$_{6,6,6,14}$][dca] containing 5 mol% BSP is represented in **Figure 5.15(b)**. H-6, H-8 and H-4 are located at 7.17 (t), 7.12 (d) and 7.1 (d) ppm, respectively. These shifts and splitting patterns differ to that of BSP in [P$_{6,6,6,14}$][NTf$_2$] as H-8 has shifted up-field by 0.7 ppm and its splitting pattern has changed. Also, H-6 has shifted up-field by 0.02 ppm, whereas H-4 has shifted down-field by 0.02 ppm, the coupling constant could not be calculated due to the amalgamation of the H-4 and H-5 signals. H-8 and H-6 are located on the indoline section of BSP, this section contains the positively charged nitrogen which should attract anion's by electrostatic interactions.

If the phenolate on the MC isomer is interacting with the phosphonium cation, a chemical shift would be expected as interactions induce a deformation of the atomic orbitals (e.g. ^{31}P nucleus) and thereby change the 'effective magnetic field' at the nucleus which is addressed as the NMR chemical shift. ^{31}P-NMR was carried out on all IL samples containing 5mol % BSP. **Figure 5.16** presents the ^{31}P-NMR of [P$_{6,6,6,14}$][NTf$_2$] containing 5 mol% BSP, it can be seen that a new signal (67.83 ppm) appears along with the parent cation [P$_{6,6,6,14}$]$^{+}$ signal (28.86 ppm). **Figure 5.17** presents the ^{31}P-NMR of [P$_{6,6,6,14}$][dca] containing 5 mol% BSP, a new peak is also observed at 46.88 ppm along with the parent cation [P$_{6,6,6,14}$]$^{+}$ signal (33.45 ppm). These NMR results along with the vibrational and optical spectroscopic results indicate confirm that solute-solvent interactions within these IL-BSP samples are happening.
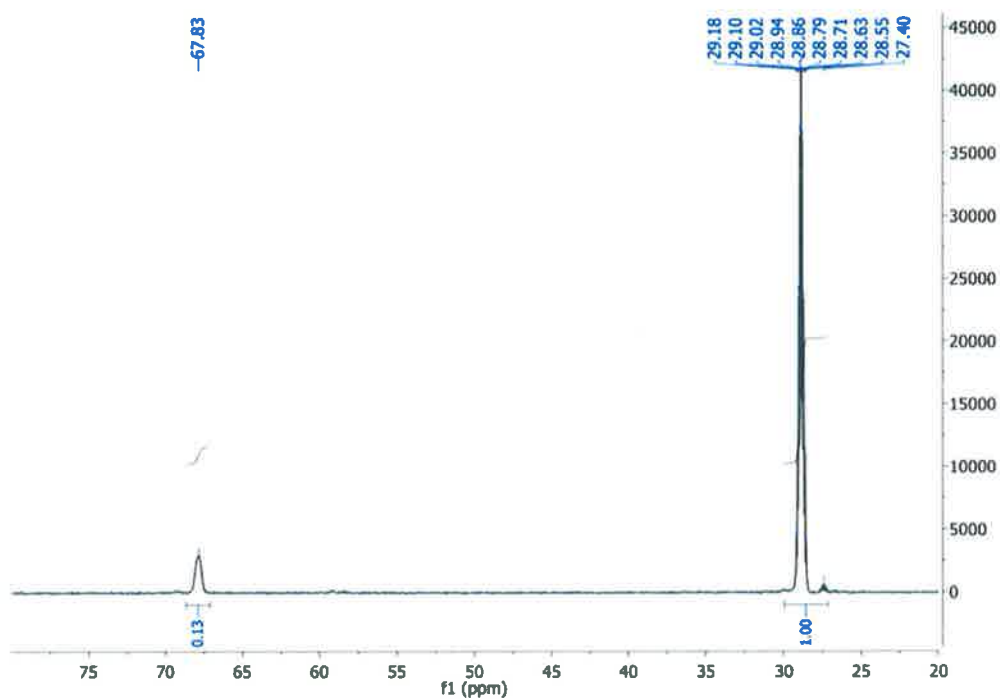
Figure 5.16. ^{31}P-NMR spectrum of [P$_{6,6,6,14}$][NTf$_2$] containing 5 mol% BSP.
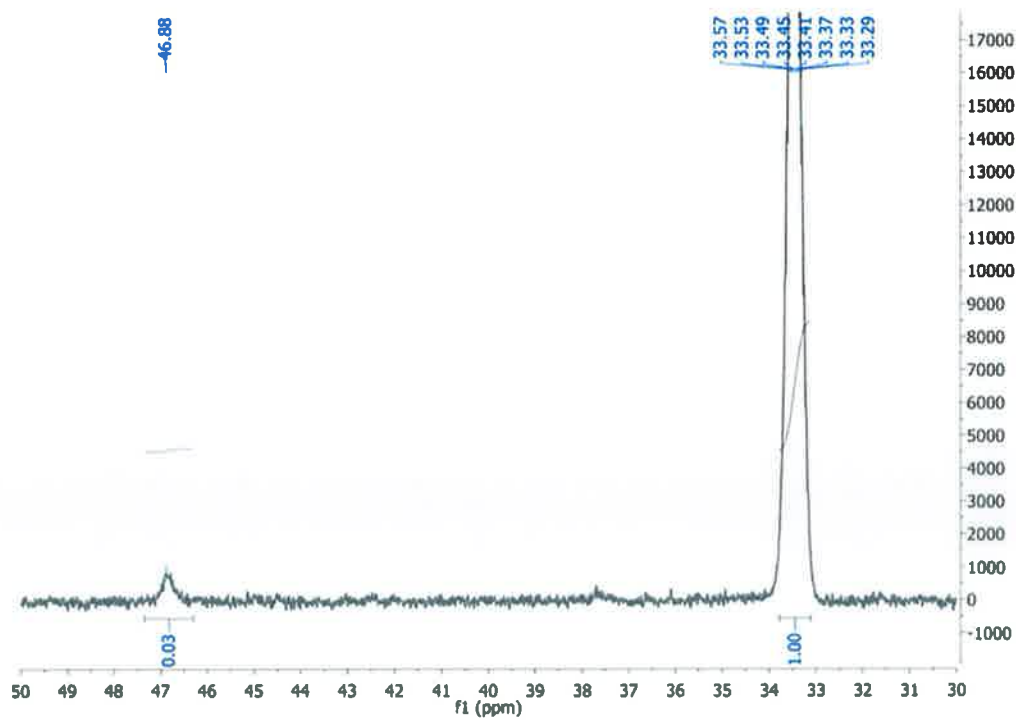
Figure 5.17. ^{31}P-NMR spectrum of [P$_{6,6,6,14}$][dca] containing 5 mol% BSP.

5.2.5 Physical properties of solute-solvent complex

TGA (thermogravimetric analysis) and DSC (differential scanning calorimetry) measurements were carried out on $[P_{6,6,6,14}][NTf_2]$ and $[P_{6,6,6,14}][dca]$ ILs containing 5 mol% BSP. TGA and DSC measurements combined together should give an insight to the thermal stability of the samples and indicate whether the IL structure has been modified by the introduction of BSP. The TGA and DSC scans can be found in appendix, **Figure A7-10**, results of the samples are summarized in **Table 5.1**. The melt point in the DSC scan is lowered by nearly 1 °C upon the addition of BSP to $[P_{6,6,6,14}][NTf_2]$, whereas, there is a negligible difference upon the addition of BSP to $[P_{6,6,6,14}][dca]$. This pattern is also seen in the TGA scans, in which the onset decomposition temperature has increased by 47 °C upon addition of BSP to $[P_{6,6,6,14}][NTf_2]$, with a decrease of only 4 % upon addition of BSP to $[P_{6,6,6,14}][dca]$.

Sample	DSC (°C)	TGA (onset °C)
$[P_{6,6,6,14}][NTf_2]$	-69.07	386
$[P_{6,6,6,14}][NTf_2]$-BSP	-69.98	433
$[P_{6,6,6,14}][dca]$	-64.19	393
$[P_{6,6,6,14}][dca]$-BSP	-64.13	389

Table 5.1. Thermal analysis of $[P_{6,6,6,14}][NTf_2]$ and $[P_{6,6,6,14}][dca]$ ILs containing 5 mol% BSP.

Ionic conductivity and viscosity are also important characterization techniques in the bulk physical properties of our samples; ionic conductivity tells us the relative diffusion of the component ions in the sample whereas viscosity is a measure of the resistance of a fluid to deform under stress, commonly perceived as resistance to flow. More importantly,

these techniques allow us to monitor dynamic effects arising from external stimuli, such as light. The results of these experiments are summarized in **Table 5.2**. The ionic conductivity of $[P_{6,6,6,14}][NTf_2]$-BSP when exposed to UV light decreases by 12 %, whereas the viscosity increases by 6 %. This photo-effect is also manifested in $[P_{6,6,6,14}][dca]$-BSP. In this case, ionic conductivity of $[P_{6,6,6,14}][dca]$-BSP decreases by only 6 % but the viscosity increases by nearly 25 %. Upon exposure to 5 minutes of visible light, these values reverted back to there original values.

Sample	Ionic conductivity log(S cm^{-1})	Viscosity (mPa.S)
$[P_{6,6,6,14}][NTf_2]$-BSP[a]	-4.1481	312
$[P_{6,6,6,14}][NTf_2]$-MC[b]	-4.7132	332
$[P_{6,6,6,14}][dca]$-BSP[a]	-4.0574	256
$[P_{6,6,6,14}][dca]$-MC[b]	-4.341	319

[a] Measurement taken after 15hrs in dark.
[b] Measurement taken 5 minutes after irradiation of UV light for 60 seconds.

Table 5.2. Ionic conductivity and viscosity measurements of $[P_{6,6,6,14}][NTf_2]$ and $[P_{6,6,6,14}][dca]$ ILs containing 5 mol% BSP, before and after irradiation of UV light.

5.2.6 Ab-initio Calculations

Standard *ab initio* molecular orbital theory and density functional theory (DFT) calculations were carried out using GAUSSIAN 03.[122] The open form of BSP (the MC isomer) together with the complexes that can be formed with [dca]$^-$ and $[P_{6,6,6,14}]^+$ were optimised at B3LYP/6-31+G(d) level of theory. As the optimization for the $[P_{6,6,6,14}]^+$ cation was not feasible, a model cation, $[P_{2,2,2,2}]^+$, was used instead. It is important to note that these calculations represent descriptions of the gas phase molecules and

204

complexes only. However, the ability of gas phase calculations to estimate the real n −

π* and π − π* electronic transition energies in organic molecules has been demonstrated

previously.[123] The optimized geometries are shown in **Figure 5.18**. The excitation

energies of the MC isomer were computed at CIS(D)/6-31+G(d,p) level.
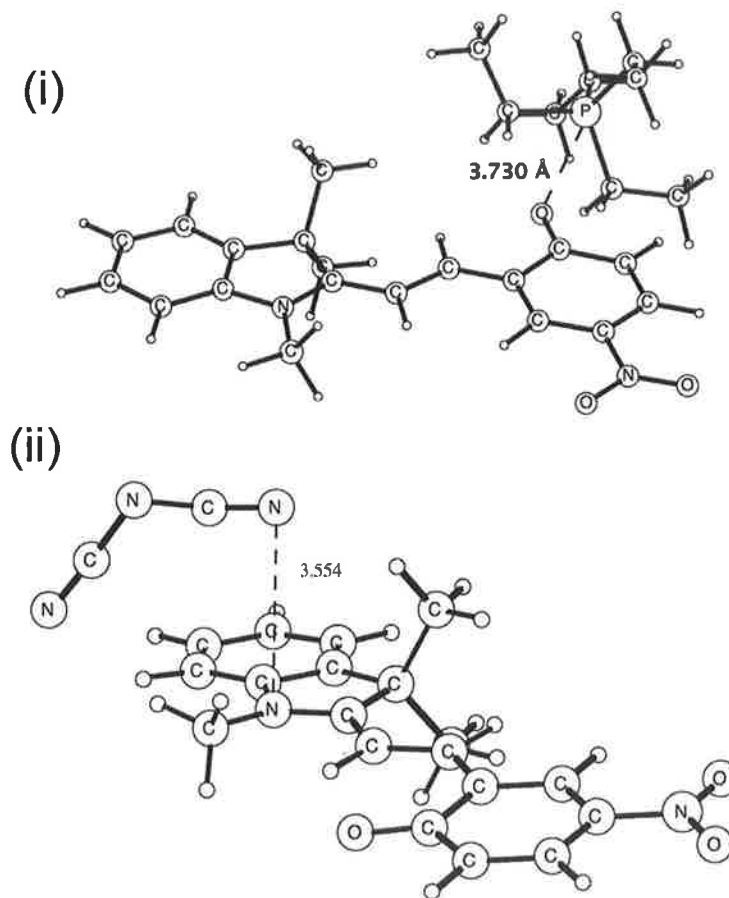
Figure 5.18. Optimized structures of (i) MC isomer together with the complexes that can be formed with (i) [dca]⁻ and (ii) $[P_{2,2,2,2}]^+$ at B3LYP/6-31+G(d).

5.3 Discussion

From the UV-vis spectroscopic results obtained, it is clear that the ILs containing BSP exhibit photoswitchable behaviour, albeit, not the behaviour that BSP exhibits in molecular solvents. UV irradiation to [$P_{6,6,6,14}$][NTf$_2$] containing 10^{-4}M BSP, leads to two absorption bands at 572 nm and 440 nm. These bands disappear upon exposure to 60 seconds of visible light, **Figure 5.5(a)**. The band at 572 nm is constant with absorbance behaviour of the MC isomer while the band located at 440 nm relates to the phenolate interaction with a phosphonium cation, as discussed in Chapter 4. Similar photochromic properties were observed within [$P_{1,4,4,4}$][tos] containing 10^{-4}M BSP, **Figure 5.5(b)**. In this case, a band at 482 nm appeared upon exposure to UV light along with a small shoulder resembling the MC isomer at 560 nm. These bands disappeared upon exposure to 60 seconds of visible light. [$P_{1,4,4,4}$][tos] contains a smaller phosphonium cation compared to the other ILs and in theory should interact with the phenolate with less steric hindrance. Photoswitchable behaviour was also observed in [$P_{6,6,6,14}$][dbsa] containing 10^{-4}M BSP, **Figure 5.5(d)**. No actual band was observed, rather a shoulder increase at 440 nm upon UV irradiation. For the IL-BSP systems studied above, the effect was reversible, indicating that the molecular interaction can be controlled by light. The IL [$P_{6,6,6,14}$][dca] containing 10^{-4}M BSP exhibited a distinct spectral band at 440 nm upon exposure to UV light but interestingly enough upon exposure to 60 seconds of visible light this band only decreased in intensity by 25 %. This implies that there is another process inhibiting the ring-closure of MC to BSP other than the interaction with the phosphonium cation. It was found in molecular orbital calculations that the anion [dca]$^-$ resides above/below the plane of the indoline section of the MC isomer due to electrostatic interaction with the

206

positively charged nitrogen on the MC. Charge delocalization throughout the [dca]⁻ ion and extensive π-conjugation in the indoline section results in the [dca]⁻ anion residing approximately 3.5 Å from the positively charged MC nitrogen. This interaction results in a physical change of the MC structure, the indoline and benzene section of the MC molecule bend out of plane. This is clearly seen in **Figure 5.19,** the two conjugated systems (indoline and benzene section) are tilted away from each other, and this tilt is enough to the change the excitation spectrum of the MC isomer as the indoline and benzene section of the molecule interact less. These results explain why *J*-aggreagtion is not observed in phosphonium based ILs containing the anion [dca]⁻.
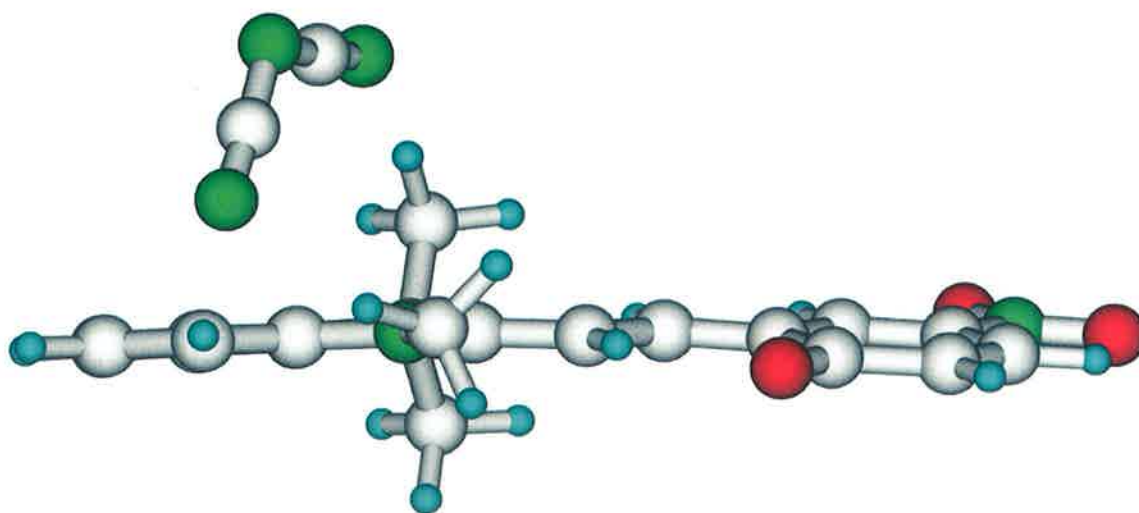
Figure 5.19. Optimized structures of MC and [dca]⁻ anion at B3LYP/6-31+G(d).

When 5 mol% of BSP is dissolved in [P$_{6,6,6,14}$][NTf₂], [P$_{6,6,6,14}$][dbsa] and [P$_{1,4,4,4}$][tos] and irradiated with UV light, a new band is observed at approximately 640 nm. Absorption in this region is usually associated with *J*-aggregation; this would be expected due to the high concentration of BSP within the IL system. *J*-aggregation of MC isomers

is attributed to the coordination of separate MC isomers through the nitro group of one

and the positively charged indoline nitrogen of another[77], **Scheme 5.4.**
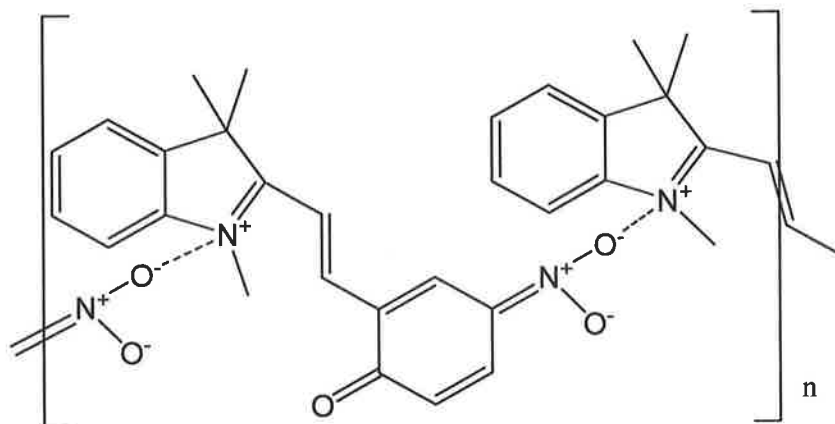
Scheme 5.4. Unit structure proposed for the J-aggregate of MC. [77]

This *J*-aggregate band is not observed in $[P_{6,6,6,14}][dca]$ containing 5 mol% BSP. MC

isomer *J*-aggregation requires that corresponding dipoles interact by electrostatics,

Scheme 5.4. The [dca]⁻ anion is found to interact with the positively charged nitrogen on

the indoline therefore inhibiting the nitro group coordination and thus no aggregation is

observed.

Before fluorescence measurements were carried out on ILs containing BSP, neat ILs

were analyzed for fluorescence. It was found that the neat ILs exhibited excitation

wavelength dependence, **Figure 5.7**, this behaviour has been seen in other ILs[151]. The ILs

studied appear to contain many energetically different species that, when excited, result

in the long-wavelength emission observed. It has been proposed that while ILs would

appear to be homogeneous macroscopically, they are likely to be composed of multiple

loacally-structured regions existing in the nanometer range[120]. Therefore one needs to be

careful when studying fluorescence in ILs. Fortunately, it was possible to observe fluorescence of the *J*-aggregates within [P$_{6,6,6,14}$][NTf$_2$]-BSP as seen in **Figure 5.8**. When [P$_{6,6,6,14}$][dca]-BSP was analyzed no emission was observed above 600 nm, **Figure 5.9**, as formation of *J*-aggregates in [P$_{6,6,6,14}$][dca] is inhibited due to the interaction of the [dca]$^-$ anion with the MC isomer. For the remainder of this discussion, the behaviour of BSP in [P$_{6,6,6,14}$][NTf$_2$] and [P$_{6,6,6,14}$][dca] will only be discussed, due to the similarity of results obtained in [P$_{6,6,6,14}$][NTf$_2$], [P$_{1,4,4,4}$][tos], and [P$_{6,6,6,14}$][dbsa].

FT-IR analysis of [P$_{6,6,6,14}$][NTf$_2$]-BSP indicates the loss of vibrational bands associated with BSP and the emergence of new bands, **Figure 5.11**. In particular, the nitro group has distinct stretching patterns in the BSP spectrum, and these vibrations are lost in the [P$_{6,6,6,14}$][NTf$_2$]-BSP spectrum, but replaced by aci-nitro stretching, in which the two N-O bonds are non-equivalent. It has been reported that when positions and intensities of the nitro group are effected in this manner within [P$_{6,6,6,14}$][NTf$_2$], it corresponds to Fermi resonance, meaning the nitro group couples with other vibrational modes in the molecule altering the chemical nature of the group, see **Scheme 5.4**. This effect has been related to the formation of aggregates[62, 77]. The hypothesis that MC aggregates cannot form within [P$_{6,6,6,14}$][dca] has been shown by MO calculations and experimentally by UV-vis absorption results. If this hypothesis is correct, then the nitro group vibrational pattern should remain unchanged within [P$_{6,6,6,14}$][dca]. As seen in **Figure 5.12**, the nitro stretching remains unchanged in [P$_{6,6,6,14}$][dca] and hence no MC J-aggregates are present. It must be noted that there are similar vibrations in both samples; e.g. a band arises from a carbonyl stretch located at 1735 cm^{-1} in both spectra. This arises from the

polarization of the phenolate group by the phosphonium cation. Consequently, the bond length between the phenolic oxygen and the aromatic carbon becomes shorter, resulting in a carbonyl vibration. The presence of the vibration at 1230 cm^{-1} also represents the single bond character of the C-O⁻ phenolate.

The ^{1}H-NMR spectrum of [P$_{6,6,6,14}$][dca]-BSP was found to be different to that of [P$_{6,6,6,14}$][NTf$_2$]-BSP. The protons on the indoline section of BSP in [P$_{6,6,6,14}$][dca] were found to be shifted up-field and in the case of H-8, the splitting pattern completely changed relative to what is observed in [P$_{6,6,6,14}$][NTf$_2$], see **Figure 5.15**. This observation reinforces the hypothesis that the [dca]⁻ anion is specifically interacting with the indoline section of the molecule, as seen in **Figure 5.19**. ^{31}P-NMR experiments were carried out on the samples to see if the phosphonium cation was causing the change in absorption spectroscopy. **Figure 5.16** and **Figure 5.17** shown the ^{31}P-NMR signals, it can be clearly seen that a new signal accompanies the [P$_{6,6,6,14}$] parent signal. These results clearly indicate that the phosphonium cation is affected by the presence of the MC isomer.

The spectroscopic results show that interactions between the IL and MC isomer are occurring. Furthermore, as it is possible to switch between the BSP and MC isomer through the use of light, this interaction between the IL and MC isomer can be controlled. This ability to control the interaction of ions at the molecular level should also affect the bulk properties of the system. Thermal analysis of [P$_{6,6,6,14}$][NTf$_2$] containing BSP suggests an alteration of the structure, due to the increase of energy required to melt the

crystal (DSC analysis) and for decomposition (TGA). As for $[P_{6,6,6,14}][dca]$, no real effect was observed when BSP was added.

As mentioned in the introduction, adaptive materials are one with a 'useful effect'. Controlling properties such as ionic conductivity and viscosity by external stimuli such as light is one such 'useful effect'. The conductivity and viscosity of $[P_{6,6,6,14}][NTf_2]$-BSP was recorded at equilibrium and after irradiation of UV light for 60 seconds, it was observed that the ionic conductivity decreased by 12 % and the viscosity increased by 6 %. The same experiment was set up for $[P_{6,6,6,14}][dca]$-BSP and found that the ionic conductivity decreases by only 6 % but the viscosity increases by nearly 25 %. It is clear from these results that the photo-isomerization of BSP to MC results in a bulk effect, due to the molecular interactions between the MC and the ions within the IL, this process was shown to be reversible. As the ionic conductivity decreases, due to increased electrostatic interactions of the ions with the MC zwitterion, the local structures become larger and less mobile hence increasing viscosity. Although, from the ionic conductivity results of $[P_{6,6,6,14}][NTf_2]$-MC (12 % decrease), one would expect a larger increase in viscosity than 6 %. In contrast, $[P_{6,6,6,14}][dca]$-MC shows a decrease of only 6 % ionic conductivity whereas an increase of nearly 25 % in viscosity. The spectroscopic data for $[P_{6,6,6,14}][NTf_2]$-BSP suggests that J-aggregates are formed upon exposure to UV light; it is possible that aggregates suppress ion diffusion within the IL, while the MC interaction with the phosphonium cation increases the local size of the structure and in turn increases viscosity. The spectroscopic data for $[P_{6,6,6,14}][dca]$-BSP suggests that both the cation and anion interact with the MC isomer, this would suggest a greater conformational change

211

upon irradiation of UV light than that of $[P_{6,6,6,14}][NTf_2]$-MC. It must be noted that these explanations are ambiguous, the liquid state structure of ILs are still not fully understood and the possible interactions of the MC isomer with itself and its molecular environment within an IL could be vast.

5.4   Conclusion

The results presented here demonstrate that, for phosphonium based ILs containing BSP, a specific molecular interaction between solute and solvent can be controlled by photons. The photo-isomerization of BSP results in a zwitterionic isomer (MC), the MC isomer contains a phenolate that interacts through electrostatics with the phosphonium cation of the IL. This electrostatic interaction induces a polarization effect on the MC isomer, thus altering its UV-vis, fluorescence, infrared and NMR spectroscopic properties. It was also found that upon UV irradiation to $[P_{6,6,6,14}][dca]$-BSP, both the cation and anion coordinated with the MC isomer. In fact, the [dca]⁻ anion interaction results in a bend of the MC geometry.

The control of this solute-solvent interaction by photons was coupled with an increase in viscosity and decreases in ionic conductivity. The demonstration of this reversible photo-viscosity effect has quite important practical outcomes as the rheological properties of the IL can be altered by photons. This "photo-rheological" material has the possibility to transduce photonic energy into mechanical energy, thus the potential applications area includes the robotics and automotive industries, but a more realistic application would

involve this material incorporated into a micro-fluidics system acting as a fluid pump or valve controlled by small low powered light sources such as LED's.

Although, the viscosity effects are not dramatic, it must be noted that this effect is the result of reversible molecular interactions, it may well be conceived that this "photo-rheological" effect could be enhanced by the incorporation of BSP molecules into a polymer backbone. This method of approach has had success with other photo-rheological materials and seems the most appropriate way forward.[149] Hopefully, this observation may contribute to the development of 'adaptive' molecular materials based on benzospiropyran.

5.5 Experimental

2,3-dihydro-1',3',3'-trimethyl-6-nitrospiro[1-benzopyran-2,2'-1H-indole] (BSP) was purchased from Aldrich and used as received. The phosphonium ILs [P$_{6,6,6,14}$][NTf$_2$], [P$_{6,6,6,14}$][dbsa], [P$_{6,6,6,14}$][dca] and [P$_{1,4,4,4}$][tos], **Figure 5.3**, were supplied by Cytec industries. ILs were purified to spectroscopic grade as described by Earle et al before spectroscopic analysis[130]. Acetonitrile was HPLC grade and used without further purification. UV-vis measurements were recorded on UV-Vis-NIR Perkin-Elmer Lambda 900 spectrometer. Fluorescence spectra were recorded on a Perkin Elmer luminescence spectrometer model LS50B, excitation wavelengths were selected from emission and excitation pre-scan experiments. In all cases, 1 cm quartz cuvettes were used. FT-IR analysis was measured on a Perkin-Elmer Spectrum GX FT-IR system using an ATR

sample holder. Raman spectroscopy was measured on an Avalon Raman*Station*-FS, using a 680 nm excitation laser. NMR spectroscopy was carried out using a Bruker UXNMR-XWIN-NMR 400 MHz. The Ultraviolet irradiation source was a BONDwand UV-365 nm obtained from Electrolite Corporation. Samples were irradiated at a distance of 5 cm. The white light source was a Lumina obtained from Chiu Technical Corporation. In this case, samples irradiated at a distance of 7 cm.

Thermal analysis and temperature dependent phase behavior was studied in the range of − 150 °C to 200 °C by differential scanning calorimetry (DSC T.A Q100 series). Thermal scans above room temperature were calibrated using the indium melting point of 156.6 °C. Transition temperatures were recorded as the peak maximum of the thermal transition. Thermogravimetric analysis was conducted using a Perkin-Elmer Pyris TGA 1 in a flowing dry nitrogen atmosphere (50 mL/min.) between 25 and 500 °C with a heating rate of 10 °C/min. Sample sizes ranged between 10 - 20mg. The instrument was calibrated using the curie points of four reference materials, Alumel, perkin-alloy, iron and nickel. Platinum pans were used in all experiments. Density measurements were carried out using an Anton Paar DMA 5000 density meter. Viscosity measurements were carried out using an Anton Paar AMVn viscosity meter. Conductivities were obtained by measurement of the complex impedance spectra between 10 MHz and 0.01 Hz on a Solartron SI 1296 Dielectric interface. The conductance was determined from the first real axis touchdown point in the Nyquist plot of the impedance data. The cell constant was determined with a solution of 0.01 M KCl at 25 °C.

6. Conclusions and Future Work

Conclusions

The photo-, thermo- and solvatochromic behavior of spiropyran derivatives in various media were investigated by spectroscopic methods in this thesis. It was found that the molecular environment controlled the BSP-MC equilibrium, solvatochromic shift and specific interactions with itself (aggregation) and with guest ions (metal ions). It must be noted that as analytical results are generated with relative ease, the understanding of a dynamic equilibrium and its specific and non-specific interactions with its surroundings must not be underestimated.

In Chapter 2, the photo-, thermo-, and solvatochromic compound BSP was investigated using UV-vis, fluorescence, FT-IR, and NMR spectroscopy. It was found that the BSP↔MC system, its molecular interactions, such as metal ion binding, and the formation of aggregates can be controlled by light. These molecular interactions which can be formed upon exposure to UV light holds promise for the possibility of altering a systems macro-environment. Although, from the results reported, more research must be carried out on the BSP↔MC system and its specific molecular interactions, as it would appear that deeper interactions are present within this system that account for unexpected behaviour we have seen. Classification of this system by solvation interactions and thermal ring closing kinetics would seem to simplistic for this unique molecule.

In Chapter 3, a benzospiropyran derivative was immobilized via a diamino linker to a polymer support for chemical sensing applications. To our knowledge, this is the first

216

demonstration of the cycling of covalently immobilised spiropyran on a solid support to merocyanine for repeat detection of metal ions. These results demonstrate a polymer-modified surface that can adapt its functionality through reversible molecular rearrangements triggered by external stimuli (photons). While the current investigation has focused on the detection of Co^{2+} ions, it is evident that modification of the binding site molecular architecture or analytical conditions could allow other ions to be targeted. Combining the spiropyran film and novel LED-based sensor technology[98] developed in our laboratory, we ultimately hope to develop an economically viable colorimetric sensing system for metal ion detection, using this approach it may be possible to realise very low cost but reliable chemical sensors that could be scaled up for wide area deployment in chemosensor nets[59].

The photo- thermo and solvatochromic behavior of benzospiropyran was studied in a selection of ionic liquids, in Chapter 4. Our results clearly show that the kinetics and thermodynamics of the process are sensitive to the nature of the ionic liquids cation. It was found that the polarity of ILs ranged from polar aprotic to polar protic solvents. It was also observed that the imidazolium and phosphonium cations formed complexes with the MC isomer; this is due to strong interactions with these cations. Relatively diffuse cations like imidazolium can form a through space orbital interaction rather than just electrostatic interactions, thus inhibiting the MC conversion back to the aplanar isomer. One of the important practical outcomes of this work is that the phosphonium based system selectively exhibits photochromism only (i.e. no thermal relaxation), thus producing a potentially permanent effect or certainly a sufficiently long term effect for

many applications. This observation may point the way towards more sophisticated materials capable of switching reversibly between two distinct forms, and simultaneously providing a number of transduction modes for gathering information about the molecular environment in the immediate vicinity of the binding site and its surrounding environment.

From the results in Chapter 4, a more thorough spectroscopic investigation was undertaken in Chapter 5 into photochromic reactions of BSP in phosphonium based ILs. The spectroscopic results confirmed that, for phosphonium based ILs containing BSP, a specific molecular interaction occurs between the solute and solvent when irradiated with UV light. The control of this solute-solvent interaction by photons was coupled with an increase in viscosity and decreases in ionic conductivity. The demonstration of this reversible photo-viscosity effect has quite important practical outcomes as the rheological properties of the IL can be altered by photons. This "photo-rheological" material has the possibility to transduce photonic energy into mechanical energy, thus the potential applications area includes the robotics and automotive industries, but a more realistic application would involve this material incorporated into a micro-fluidics system acting as an actuator or valve controlled by small low powered light sources such as LED's.

Future work

Of particular interest at the moment is the development of micro-fluidics systems for drug delivery and environmental monitoring; however micro-fluidics devices have found limited use in these areas. The reason for the lack of suitable devices stems primarily from the fabrication schemes used to make micro-fluidic systems. Traditional micro-

fluidic systems use silicon and Pyrex as structural materials, which require long and costly processing procedures such as wet and dry etching, metal evaporation and anodic bonding. Silicon-based microelectromechanical systems (MEMS) have proven well suited to optical and physical sensing applications but the incorporation of electronic control tends to increase system complexity.

In nature, biological control is achieved at all scales, from the human body (e.g. temperature) down to the single cell (e.g. membrane potential) by organic materials and efficient chemical mechanisms. For example, a complex (but all-organic) homeostatic control system functions to maintain the body's temperature. The system continually monitors the temperature of the body and triggers a variety of responses based on the sensing inputs. A decrease in body temperature can trigger a variety of responses ranging from blood vessel constriction to shivering. Using biological control systems as an inspiration leads one to explore different types of fabrication, materials and system designs than those typical in the traditional engineering sense[152].

The use of our "photo-rheological" materials as actuators or valves in flow control systems could greatly reduce system complexity. This photo-actuating material could control volumetric changes in response to photons from simple LEDs, as **Scheme 6.33** suggests. Achieving fluid control with these materials without the use of major electronic components enables more freedom for micro-fluidic systems, as these actuators could be made at a fraction of the cost of the more complex electronic control systems.

219
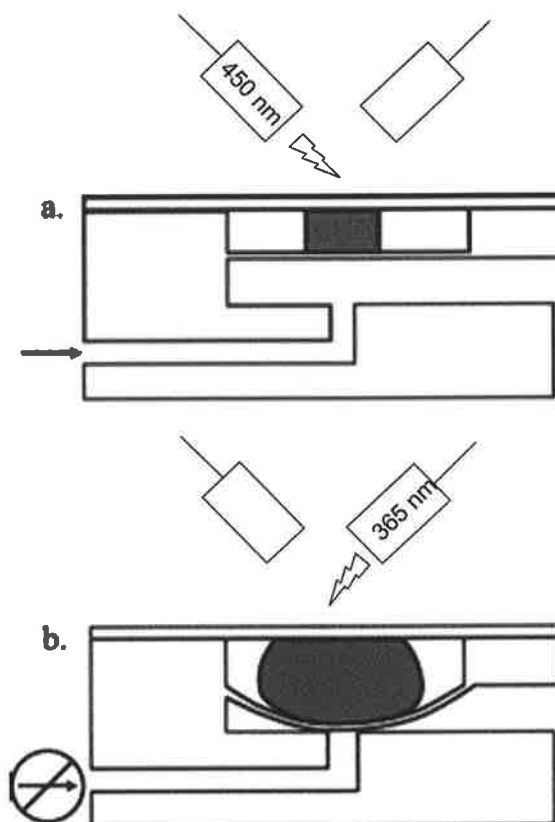
Scheme 6.33. Schematic cross section of a microfludic system containing our photo-rheological material. The valve is open in panel (a) and when irradiated with UV light swells to close in panel (b).

More than 50 years after their discovery, spiropyrans continue to bemuse, challenge and entertain chemists. Due to their unique properties, this compound still captivates the imagination to the possible applications that lie ahead for it. The continuing research ranges from the fundamental photo-physical processes within the molecule to drug delivery systems and from 3-D memory devices to smart paints. Spiropyrans are still at the forefront of scientific journals and it seems they will be for a long time.

A. Appendix
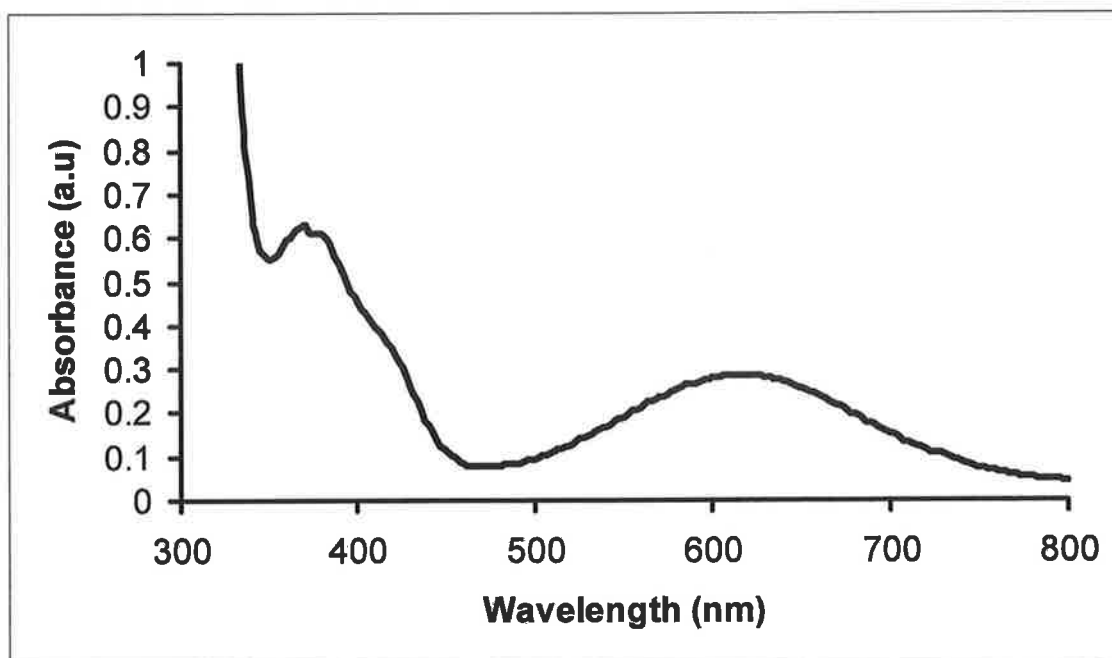
Figure A88. UV-vis spectrum of Reichardt's dye 10^{-4}M in [$P_{6,6,6,14}$] [NTf$_2$].
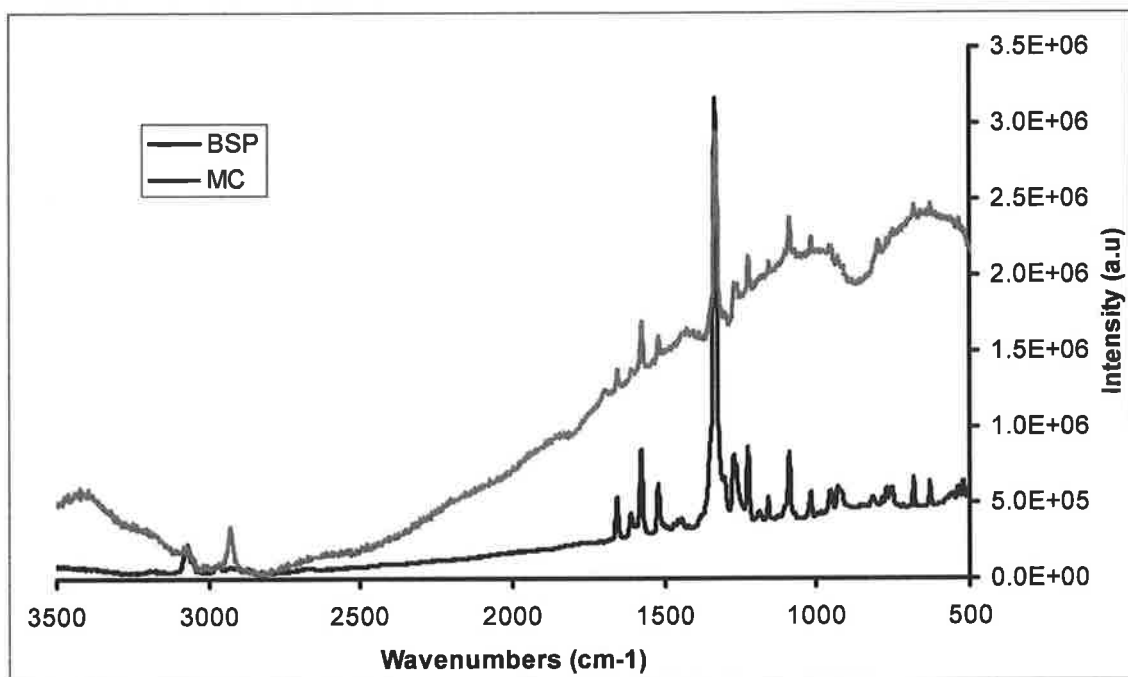
Figure A89. Overlaid Raman spectra of BSP and MC (BSP irradiated with UV light for
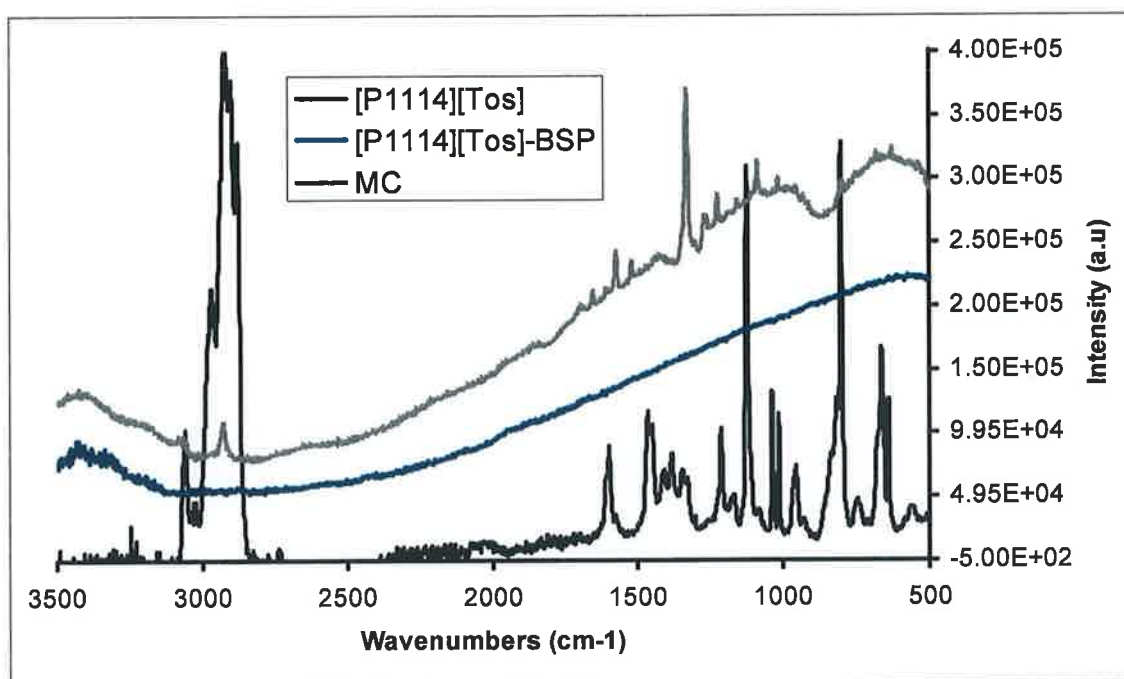
60 seconds)

Figure A90. Overlaid Raman spectra of [P$_{1,4,4,4}$][tos], [P$_{1,4,4,4}$][tos] containing 5 mol% BSP, irradiated with 60 seconds UV light and MC.
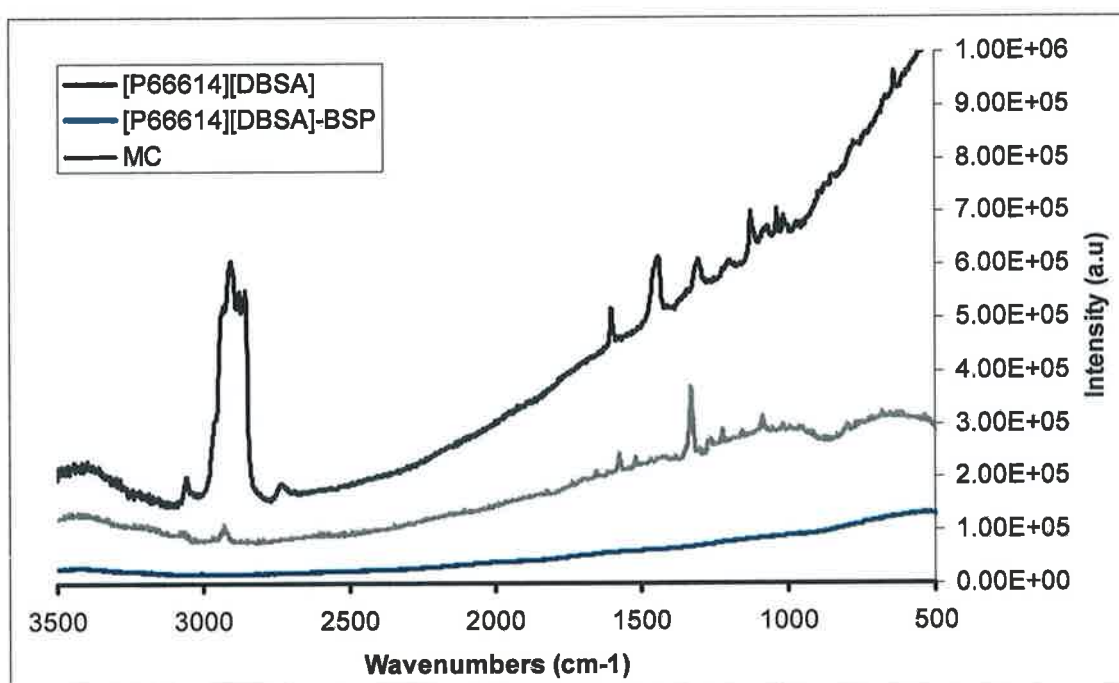
Figure A91. Overlaid Raman spectra of [P$_{6,6,6,14}$][dbsa], [P$_{6,6,6,14}$][dbsa] containing 5 mol% BSP (irradiated with 60 seconds UV light) and MC.
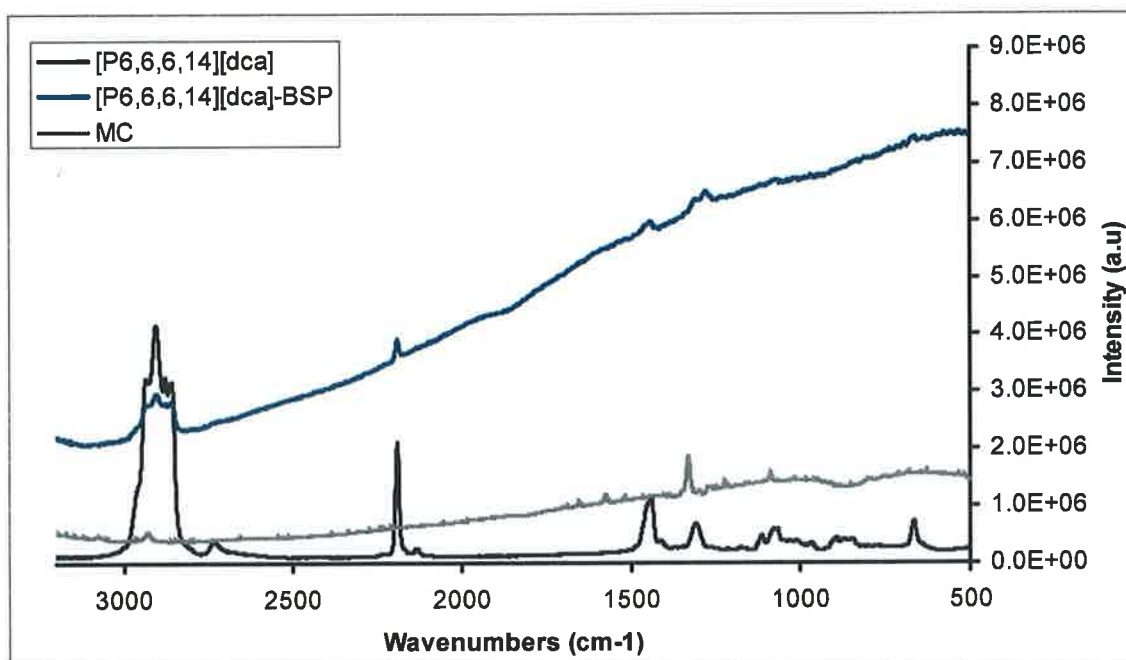
Figure A92. Overlaid Raman spectra of [P$_{6,6,6,14}$][dca], [P$_{6,6,6,14}$][dca] containing 5 mol% BSP (irradiated with 60 seconds UV light) and MC.
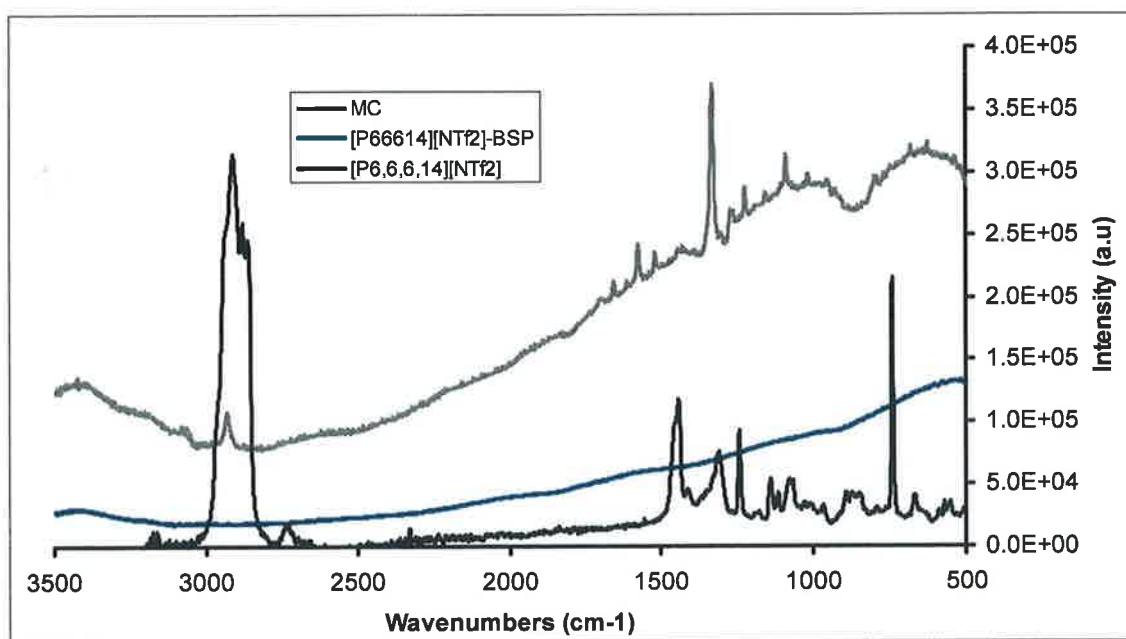
Figure A93. Overlaid Raman spectra of $[P_{6,6,6,14}][NTf_2]$, $[P_{6,6,6,14}][NTf_2]$ containing 5 mol% BSP (irradiated with UV light for 60 seconds) and MC.
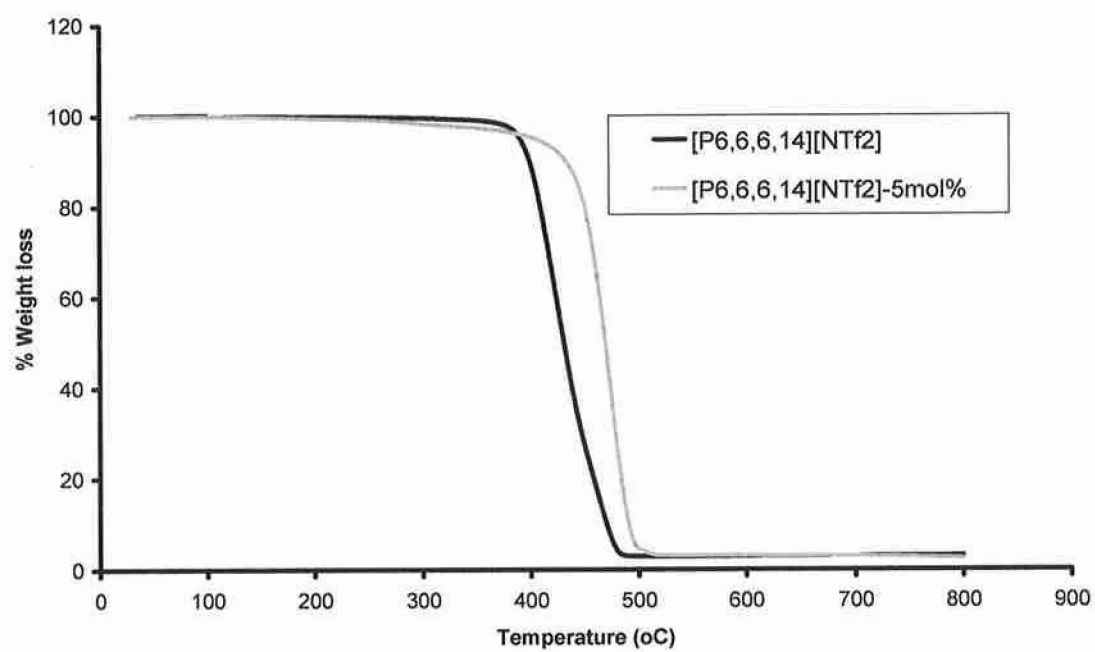
Figure A94. TGA scan of $[P_{6,6,6,14}][NTf_2]$, $[P_{6,6,6,14}][NTf_2]$ containing 5 mol% BSP (irradiated with UV light for 60 seconds).
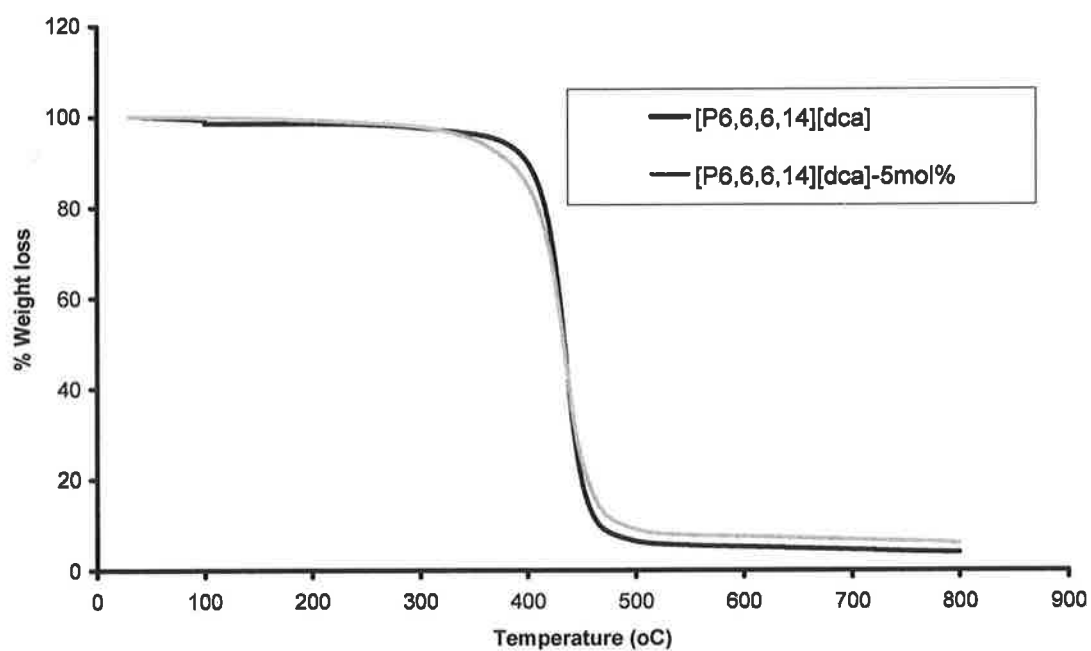
Figure A95. TGA scan of $[P_{6,6,6,14}][dca]$, $[P_{6,6,6,14}][dca]$ containing 5 mol% BSP (irradiated with UV light for 60 seconds).
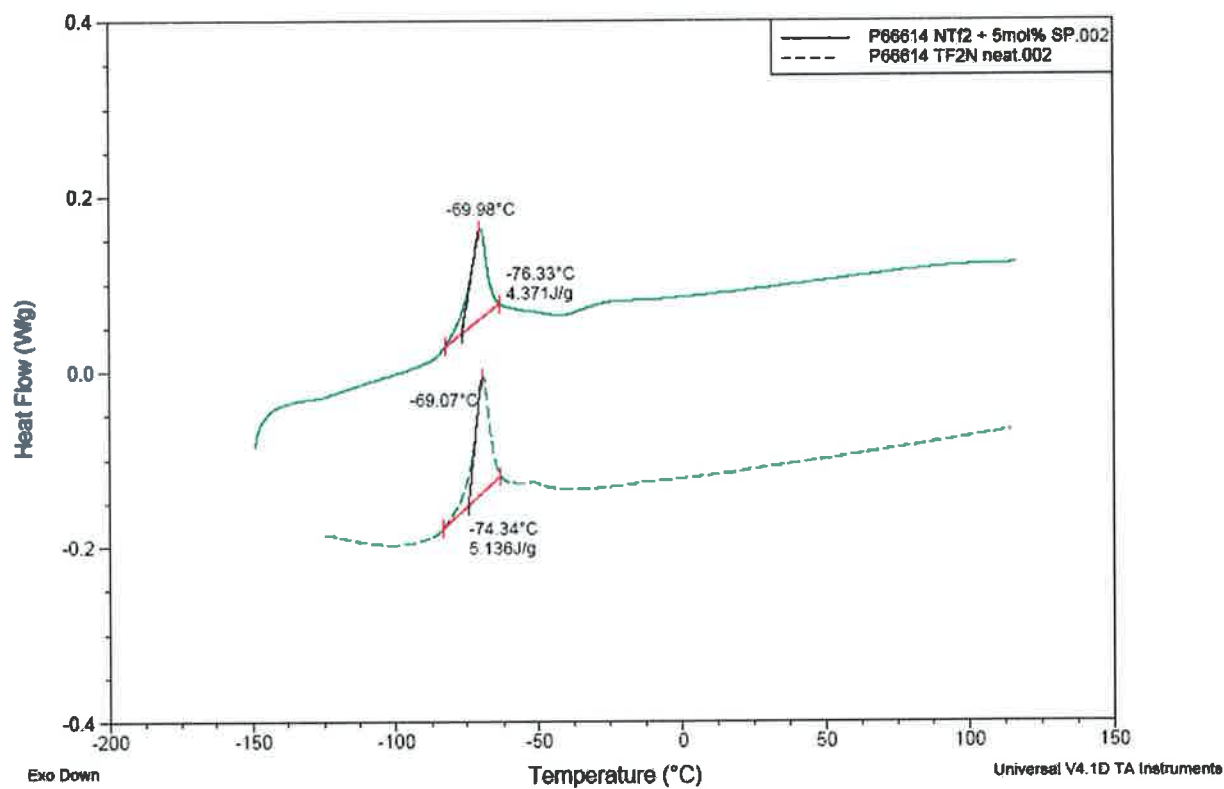
Figure A96. DSC scan of of [P$_{6,6,6,14}$][NTf$_2$], [P$_{6,6,6,14}$][NTf$_2$] containing 5 mol% BSP (irradiated with UV light for 60 seconds).
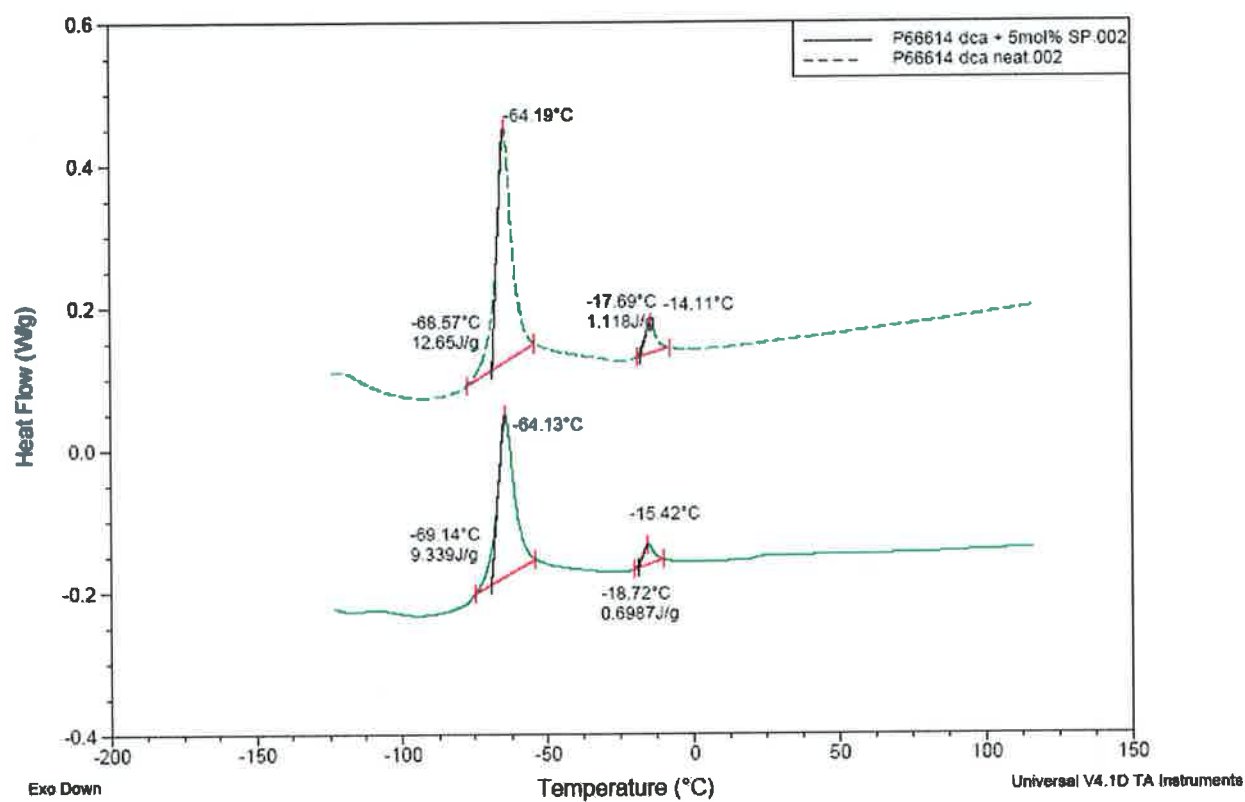
Figure A97. DSC scan of [P$_{6,6,6,14}$][dca], [P$_{6,6,6,14}$][dca] containing 5 mol% BSP (irradiated with UV light for 60 seconds).

List of figures

234

235

238

241

Figure of schematics

242

List of equations

List of tables

References

(1) Fritsche, M. *Comp. Rend* **1867**, *69*, 1035.

(2) Meer, E. t. *Ann. Chem* **1876**, *1*.

(3) Phipson, T. L. *Chem. News* **1881**, *43*, 283.

(4) Marckwald, W. *Z.phys.Chem* **1899**, *30*, 140.

(5) Neumuller.O.A *Franckhsche Verlagshandlung,Stuttgart* **1977**.

(6) Hirshberg, Y. J. *Compt.Rend* **1950**, *231*, 903.

(7) Fischer, E.; Hirshberg, Y. J. *Chem. Soc.* **1952**, 4522.

(8) Hirshberg, Y. J. *New Scientist* **1960**, 1243.

(9) Bertelson, R. C. *Organic Photochromic and Thermochromic Compounds* **1999**, 11-83.

(10) Crano, J. C.; Flood, T.; Knowles, D.; Kumar, A.; Van Gemert, B. *Pure and Applied Chemistry* **1996**, *68*, 1395-1398.

(11) Hoffmann, R. *Accounts of Chemical Research* **1971**, *4*, 1-9.

(12) Bertelson, R. C. *Techniques of Chemistry (New York)* **1971**, *3*, 45-431.

(13) Guglielmetti, R. *Studies in Organic Chemistry (Amsterdam)* **1990**, *40*, 855-878.

(14) Minkin, V. I. *Chemical Reviews (Washington, DC, United States)* **2004**, *104*, 2751-2776.

(15) Maslak, P.; Chopra, A. *Journal of the American Chemical Society* **1993**, *115*, 9331-9332.

(16) Pichko, V. A.; Simkin, B. Y.; Minkin, V. I. *Journal of Organic Chemistry* **1992**, *57*, 7087-7092.

(17) Kirby, A. J. *The Anomeric Effect and Stereoelectronic Effects at Oxygen*; Springer: New York.

(18) Minkin, V. I.; Minyaev, R. M. *Chemical reviews FIELD Publication Date:2001*, *101*, 1247-1265. FIELD Reference Number: FIELD Journal Code:2985134R FIELD Call Number:.

(19) Berkovic, G.; Krongauz, V.; Weiss, V. *Chemical Reviews (Washington, D. C.)* **2000**, *100*, 1741-1753.

(20) Kimura, K.; Sakamoto, H.; Nakamura, M. *Bulletin of the Chemical Society of Japan* **2003**, *76*, 225-245.

(21) Kobatake, S.; Irie, M. *Annual Reports on the Progress of Chemistry, Section C: Physical Chemistry* **2003**, *99*, 277-313.

(22) Shao, N.; Zhang, Y.; Cheung, S.; Yang, R.; Chan, W.; Mo, T.; Li, K.; Liu, F. *Analytical Chemistry* **2005**, *77*, 7294-7303.

(23) Nakamura, M.; Sakamoto, H.; Kimura, K. *Analytical Sciences* **2005**, *21*, 403-408.

(24) Minkin, V. I.; Metelitsa, A. V.; Dorogan, I. V.; Lukyanov, B. S.; Besugliy, S. O.; Micheau, J.-C. *Journal of Physical Chemistry A* **2005**, *109*, 9605-9616.

(25) Kado, S.; Yamada, K.; Murakami, T.; Kimura, K. *Journal of the American Chemical Society* **2005**, *127*, 3026-3030.

(26) Willner, I.; Willner, B. *Journal of Materials Chemistry* **1998**, *8*, 2543-2556.

(27) Amini, A.; Bates, K.; Benniston, A. C.; Lawrie, D. J.; Soubeyrand-Lenoir, E. *Tetrahedron Letters* **2003**, *44*, 8245-8247.

(28) Winkler, J. D.; Bowen, C. M.; Michelet, V. *Journal of the American Chemical Society* **1998**, *120*, 3237-3242.

(29)   Aviram, A. *Journal of the American Chemical Society* **1988**, *110*, 5687-5692.

(30)   Willner, I.; Rubin, S.; Shatzmiller, R.; Zor, T. *Journal of the American Chemical Society* **1993**, *115*, 8690-8694.

(31)   Garcia, A. A.; Cherian, S.; Park, J.; Gust, D.; Jahnke, F.; Rosario, R. *Journal of Physical Chemistry A* **2000**, *104*, 6103-6107.

(32)   Hobley, J.; Malatesta, V. *Physical Chemistry Chemical Physics* **2000**, *2*, 57-59.

(33)   Abe, Y.; Okada, S.; Horii, T.; Nakao, R.; Irie, M. *Molecular Crystals and Liquid Crystals Science and Technology, Section A: Molecular Crystals and Liquid Crystals* **2000**, *345*, 95-100.

(34)   Favaro, G.; Masetti, F.; Mazzucato, U.; Ottavi, G.; Allegrini, P.; Malatesta, V. *Journal of the Chemical Society, Faraday Transactions* **1994**, *90*, 333-338.

(35)   Chibisov, A. K.; Goerner, H. *Journal of Physical Chemistry A* **1997**, *101*, 4305-4312.

(36)   Chibisov, A. K.; Goerner, H. *Journal of Photochemistry and Photobiology, A: Chemistry* **1997**, *105*, 261-267.

(37)   Chibisov, A. K.; Gorner, H. *Physical Chemistry Chemical Physics* **2001**, *3*, 424-431.

(38)   Celani, P.; Bernardi, F.; Olivucci, M.; Robb, M. A. *Journal of the American Chemical Society* **1997**, *119*, 10815-10820.

(39)   Dvornikov, A. S.; Malkin, J.; Rentzepis, P. M. *Journal of Physical Chemistry* **1994**, *98*, 6746-6752.

(40)   Atabekyan, L. S.; Zakharova, G. V.; Chibisov, A. K. *High Energy Chemistry* **2001**, *35*, 349-354.

(41)   Gorner, H. *Physical Chemistry Chemical Physics* **2001**, *3*, 416-423.

(42)   Zhang, J. Z.; Schwartz, B. J.; King, J. C.; Harris, C. B. *Journal of the American Chemical Society* **1992**, *114*, 10921-10927.

(43)   Gorner, H.; Chibisov, A. K. *Journal of the Chemical Society-Faraday Transactions* **1998**, *94*, 2557-2564.

(44)   Chibisov, A. K.; Gorner, H. *Chemical Physics* **1998**, *237*, 425-442.

(45)   Mo, Y.-G.; Dillon, R. O.; Snyder, P. G. *Journal of Vacuum Science & Technology, A: Vacuum, Surfaces, and Films* **1999**, *17*, 170-175.

(46)   Levy, D. *Molecular Crystals and Liquid Crystals Science and Technology, Section A: Molecular Crystals and Liquid Crystals* **1997**, *297*, 31-39.

(47)   Zhou, J.; Sui, Q.; Huang, B. *Journal of Photochemistry and Photobiology, A: Chemistry* **1998**, *117*, 129-136.

(48)   De Leon, L.; Biewer, M. C. *Tetrahedron Letters* **2000**, *41*, 3527-3530.

(49)   Evans, L., III; Collins, G. E.; Shaffer, R. E.; Michelet, V.; Winkler, J. D. *Analytical Chemistry* **1999**, *71*, 5322-5327.

(50)   Phillips, J. P.; Mueller, A.; Przystal, F. *Journal of the American Chemical Society* **1965**, *87*, 4020-&.

(51)   Winkler, J. D.; Deshayes, K.; Shao, B. *Journal of the American Chemical Society* **1989**, *111*, 769-770.

(52)   Collins, G. E.; Choi, L.-S.; Ewing, K. J.; Michelet, V.; Bowen, C. M.; Winkler, J. D. *Chemical Communications (Cambridge)* **1999**, 321-322.

(53)   Bardez, E.; Devol, I.; Larry, B.; Valeur, B. *Journal of Physical Chemistry B* **1997**, *101*, 7786-7793.

(54) Suzuki, T.; Kawata, Y.; Kahata, S.; Kato, T. *Chemical Communications (Cambridge, United Kingdom)* **2003**, 2004-2005.

(55) Suzuki, T.; Kato, T.; Shinozaki, H. *Chemical Communications (Cambridge, United Kingdom)* **2004**, 2036-2037.

(56) Yoshida, T.; Morinaka, A. *Journal of Photochemistry and Photobiology, A: Chemistry* **1994**, *78*, 179-183.

(57) Byrne, R. J.; Stitzel, S. E.; Diamond, D. *Journal of Materials Chemistry* **2006**, *16*, 1332-1337.

(58) Stitzel, S.; Byrne, R.; Diamond, D. *Journal of Materials Science* **2006**, *41*, 5841-5844.

(59) Byrne, R.; Diamond, D. *Nature Materials* **2006**, *5*, 421-424.

(60) Gorner, H. *Chemical Physics Letters* **1998**, *282*, 381-390.

(61) Futami, Y.; Chin, M. L. S.; Kudoh, S.; Takayanagi, M.; Nakata, M. *Chemical Physics Letters* **2003**, *370*, 460-468.

(62) Uznanski, P. *Synthetic Metals* **2000**, *109*, 281-285.

(63) McCoy, C. P.; Donnelly, L.; Jones, D. S.; Gorman, S. P. *Tetrahedron Letters* **2007**, *48*, 657-661.

(64) Drummond, C. J.; Furlong, D. N. *Journal of the Chemical Society, Faraday Transactions* **1990**, *86*, 3613-3621.

(65) Kosower, E. M. *Journal of the American Chemical Society* **1958**, *80*, 3253-3260.

(66) Brooker, L. G. S.; Craig, A. C.; Heseltine, D. W.; Jenkins, P. W.; Lincoln, L. L. *Journal of the American Chemical Society* **1965**, *87*, 2443-2450.

(67) Brownstein, S. *Canadian Journal of Chemistry* **1960**, *38*, 1590-1596.

(68) Song, X.; Zhou, J.; Li, Y.; Tang, Y. *Journal of Photochemistry and Photobiology, A: Chemistry* **1995**, *92*, 99-103.

(69) Flannery, J. B., Jr. *Journal of the American Chemical Society* **1968**, *90*, 5660-5671.

(70) Uznanski, P. *Langmuir* **2003**, *19*, 1919-1922.

(71) Diamond, D.; Hanratty, V. C. A. *Spreadsheet Applications in Chemistry Using Microsoft Excel*; Wiley, 1997.

(72) Sun, X. D.; Fan, M. G.; Meng, X. J.; Knobbe, E. T. *Journal of Photochemistry and Photobiology, A: Chemistry* **1997**, *102*, 213-216.

(73) Zhou, J.; Li, Y.; Tang, Y.; Zhao, F.; Song, X.; Li, E. *Journal of Photochemistry and Photobiology, A: Chemistry* **1995**, *90*, 117-123.

(74) Krongauz, V. A. F., S. N.; Goldburt, E. S. *Journal of Physical Chemistry* **1978**, *82*, 2469-2474.

(75) Kimura, K.; Nakamura, M.; Sakamoto, H.; Uda, R. M.; Sumida, M.; Yokoyama, M. *Bulletin of the Chemical Society of Japan* **2003**, *76*, 209-215.

(76) Hashida, T. *Chemistry of Functional Dyes* **1993**, *2*, 345.

(77) Onai, Y., Michiko Mamiya, Toshio Kiyokawa, Ken-ichi Okuwa, Makoto Kobayashi,; Hisanori Shinohara, a. H. S. *Journal of Physical Chemistry* **1993**, *97*, 9499-9505.

(78) Bakker, E.; Diamond, D.; Lewenstam, A.; Pretsch, E. *Analytica Chimica Acta* **1999**, *393*, 11-18.

(79) Levy, D. *Chemistry of Materials* **1997**, *9*, 2666-2670.

(80) Willner, I. *Accounts of Chemical Research* **1997**, *30*, 347-356.

(81)   Rosario, R.; Gust, D.; Hayes, M.; Springer, J.; Garcia, A. A. *Langmuir* **2003**, *19*, 8801-8806.

(82)   Tsujioka, T.; Kume, M.; Irie, M. *Japanese Journal of Applied Physics, Part 2: Letters* **1996**, *35*, L 1532-L 1534.

(83)   Tork, A.; Boudreault, F.; Roberge, M.; Ritcey, A. M.; Lessard, R. A.; Galstian, T. V. *Applied Optics* **2001**, *40*, 1180-1186.

(84)   Julthongpiput, D.; Lin, Y.-H.; Teng, J.; Zubarev, E. R.; Tsukruk, V. V. *Langmuir* **2003**, *19*, 7832-7836.

(85)   Hagen, J. P.; Becerra, I.; Drakulich, D.; Dillon, R. O. *Thin Solid Films* **2001**, *398-399*, 104-109.

(86)   Lee, B. J.; Kim, J. H.; Cho, M. J.; Lee, S. H.; Choi, D. H. *Dyes and Pigments* **2004**, *61*, 235-242.

(87)   Ambrose, T. M.; Meyerhoff, M. E. *Electroanalysis* **1996**, *8*, 1095-1100.

(88)   Heng, L. Y.; Hall, E. A. *Analytical chemistry FIELD Publication Date:2000*, *72*, 42-51. FIELD Reference Number: FIELD Journal Code:0370536 FIELD Call Number:.

(89)   Hodge, P. *Chem. Soc. ReV* **1997**, *26*, 417-424.

(90)   Reverchon, E.; Cardea, S.; Rappo, E. S. *Journal of Membrane Science* **2006**, *273*, 97-105.

(91)   Bowden, M.; Diamond, D. *Sensors and Actuators, B: Chemical* **2003**, *B90*, 170-174.

(92)   Daridon, A.; Sequeira, M.; Pennarun-Thomas, G.; Dirac, H.; Krog, J. P.; Gravesen, P.; Lichtenberg, J.; Diamond, D.; Verpoorte, E.; de Rooij, N. F. *Sensors and Actuators, B: Chemical* **2001**, *B76*, 235-243.

(93)   Hayes, M. A.; Polson, N. A.; Phayre, A. N.; Garcia, A. A. *Analytical Chemistry* **2001**, *73*, 5896-5902.

(94)   Digilov, R. *Langmuir* **2000**, *16*, 6719-6723.

(95)   Liang, L.; Feng, X.; Peurrung, L.; Viswanathan, V. *Journal of Membrane Science* **1999**, *162*, 235-246.

(96)   Rosario, R.; Gust, D.; Hayes, M.; Jahnke, F.; Springer, J.; Garcia, A. A. *Langmuir* **2002**, *18*, 8062-8069.

(97)   Ipe, B. I.; Mahima, S.; Thomas, K. G. *Journal of the American Chemical Society* **2003**, *125*, 7174-7175.

(98)   Lau, K. T.; Baldwin, S.; Shepherd, R. L.; Dietz, P. H.; Yerzunis, W. S.; Diamond, D. *Talanta* **2004**, *63*, 167-173.

(99)   Fuoss, R. *Journal of Chemical Education* **1955**, 527.

(100)   Wasserscheid, P. *Organic Synthesis Highlights V* **2003**, 105-117.

(101)   Chiappe, C.; Pieraccini, D. *Journal of Physical Organic Chemistry* **2005**, *18*, 275-297.

(102)   Rogers, R. D.; Seddon, K. R.; Editors *Ionic Liquids: Industrial Applications for Green Chemistry. (Proceedings of a Symposium held 1-5 April 2001 in San Diego, California.) [In: ACS Symp. Ser., 2002; 818]*, 2002.

(103)   Forsyth, S. A.; Pringle, J. M.; MacFarlane, D. R. *Australian Journal of Chemistry* **2004**, *57*, 113-119.

(104) Olah, G. A.; Mathew, T.; Goeppert, A.; Toeroek, B.; Bucsi, I.; Li, X.-Y.; Wang, Q.; Marinez, E. R.; Batamack, P.; Aniszfeld, R.; Prakash, G. K. S. *Journal of the American Chemical Society* **2005**, *127*, 5964-5969.

(105) Hardacre, C.; Holbrey, J. D.; Katdare, S. P.; Seddon, K. R. *Green Chemistry* **2002**, *4*, 143-146.

(106) Vijayaraghavan, R.; MacFarlane, D. R. *Chemical Communications (Cambridge, United Kingdom)* **2004**, 700-701.

(107) Vijayaraghavan, R.; MacFarlane, D. R. *Australian Journal of Chemistry* **2004**, *57*, 129-133.

(108) Gutowski, K. E.; Broker, G. A.; Willauer, H. D.; Huddleston, J. G.; Swatloski, R. P.; Holbrey, J. D.; Rogers, R. D. *Journal of the American Chemical Society* **2003**, *125*, 6632-6633.

(109) Bhatt, A. I.; May, I.; Volkovich, V. A.; Hetherington, M. E.; Lewin, B.; Thied, R. C.; Ertok, N. *Journal of the Chemical Society, Dalton Transactions* **2002**, 4532-4534.

(110) Pringle, J. M.; Forsyth, M.; Wallace, G. G.; MacFarlane, D. R. *Macromolecules* **2006**, *39*, 7193-7195.

(111) Lu, W.; Fadeev, A. G.; Qi, B.; Smela, E.; Mattes, B. R.; Ding, J.; Spinks, G. M.; Mazurkiewicz, J.; Zhou, D.; Wallace, G. G.; MacFarlane, D. R.; Forsyth, S. A.; Forsyth, M. *Science (Washington, DC, United States)* **2002**, *297*, 983-987.

(112) Howlett, P. C.; MacFarlane, D. R.; Hollenkamp, A. F. *Electrochemical and Solid-State Letters* **2004**, *7*, A97-A101.

(113) MacFarlane, D. R.; Seddon, K. R. *Australian Journal of Chemistry* **2007**, *60*, 3-5.

(114) Hammett, L. P. *Physical Organic Chemsitry, 2nd Edition* **1970**, McGraw-Hill, New York.

(115) Canongia Lopes, J. N. A.; Padua, A. A. H. *Journal of Physical Chemistry B* **2006**, *110*, 3330-3335.

(116) Fletcher, K. A.; Storey, I. A.; Hendricks, A. E.; Pandey, S.; Pandey, S. *Green Chemistry* **2001**, *3*, 210-215.

(117) Reichardt, C. *Green Chemistry* **2005**, *7*, 339-351.

(118) Aggarwal, V. K.; Emme, I.; Mereu, A. *Chemical Communications (Cambridge, United Kingdom)* **2002**, 1612-1613.

(119) Hsu, J.-C.; Yen, Y.-H.; Chu, Y.-H. *Tetrahedron Letters* **2004**, *45*, 4673-4676.

(120) Iwata, K.; Kakita, M.; Hamaguchi, H.-O. *Journal of Physical Chemistry B* **2007**, *111*, 4914-4919.

(121) Sciaini, G.; Wetzler, D. E.; Alvarez, J.; Fernandez-Prini, R.; Laura Japas, M. *Journal of Photochemistry and Photobiology, A: Chemistry* **2002**, *153*, 25-31.

(122) Frisch, M. J. T., G. W.; Schlegel, H. B.; Scuseria, G. E.; Robb, M. A.; Cheeseman, J. R.; Montgomery, Jr., J. A.; Vreven, T.; Kudin, K. N.; Burant, J. C.; Millam, J. M.; Iyengar, S. S.; Tomasi, J.; Barone, V.; Mennucci, B.; Cossi, M.; Scalmani, G.; Rega, N.; Petersson, G. A.; Nakatsuji, H.; Hada, M.; Ehara, M.; Toyota, K.; Fukuda, R.; Hasegawa, J.; Ishida, M.; Nakajima, T.; Honda, Y.; Kitao, O.; Nakai, H.; Klene, M.; Li, X.; Knox, J. E.; Hratchian, H. P.; Cross, J. B.; Bakken, V.; Adamo, C.; Jaramillo, J.; Gomperts, R.; Stratmann, R. E.; Yazyev, O.; Austin, A. J.; Cammi, R.; Pomelli, C.; Ochterski, J. W.; Ayala, P. Y.; Morokuma, K.; Voth, G. A.; Salvador, P.; Dannenberg, J. J.; Zakrzewski, V. G.;

Dapprich, S.; Daniels, A. D.; Strain, M. C.; Farkas, O.; Malick, D. K.; Rabuck, A. D.; Raghavachari, K.; Foresman, J. B.; Ortiz, J. V.; Cui, Q.; Baboul, A. G.; Clifford, S.; Cioslowski, J.; Stefanov, B. B.; Liu, G.; Liashenko, A.; Piskorz, P.; Komaromi, I.; Martin, R. L.; Fox, D. J.; Keith, T.; Al-Laham, M. A.; Peng, C. Y.; Nanayakkara, A.; Challacombe, M.; Gill, P. M. W.; Johnson, B.; Chen, W.; Wong, M. W.; Gonzalez, C.; and Pople, J. A.; Gaussian Inc: Wallingford CT, 2004.

(123) Grimme, S.; Izgorodina, E. I. *Chemical Physics* **2004**, *305*, 223-230.

(124) Forsyth, C. M.; MacFarlane, D. R.; Golding, J. J.; Huang, J.; Sun, J.; Forsyth, M. *Chemistry of Materials* **2002**, *14*, 2103-2108.

(125) MacFarlane, D. R.; Pringle, J. M.; Johansson, K. M.; Forsyth, S. A.; Forsyth, M. *Chemical Communications (Cambridge, United Kingdom)* **2006**, 1905-1917.

(126) Modig, K.; Pfrommer, B. G.; Halle, B. *Physical Review Letters* **2003**, *90*, 075502/075501-075502/075504.

(127) Magill, A. M.; Yates, B. F. *Australian Journal of Chemistry* **2004**, *57*, 1205-1210.

(128) MacFarlane, D. R.; Meakin, P.; Sun, J.; Amini, N.; Forsyth, M. *Journal of Physical Chemistry B* **1999**, *103*, 4164-4170.

(129) De Diego, T.; Lozano, P.; Gmouh, S.; Vaultier, M.; Iborra, J. L. *Biotechnology and Bioengineering* **2004**, *88*, 916-924.

(130) Earle, M. J.; Gordon, C. M.; Plechkova, N. V.; Seddon, K. R.; Welton, T. *Analytical Chemistry* **2007**, *79*, 758-764.

(131) Hao, T. *Advanced Materials (Weinheim, Germany)* **2001**, *13*, 1847-1857.

(132) Koumura, N.; Kudo, M.; Tamaoki, N. *Langmuir* **2004**, *20*, 9897-9900.

(133) Lee, C. T., Jr.; Smith, K. A.; Hatton, T. A. *Macromolecules* **2004**, *37*, 5397-5405.

(134) Weiss, K. D.; Nixon, D. A.; Carlson, J. D.; Margida, A. J. *Polymer Preprints (American Chemical Society, Division of Polymer Chemistry)* **1994**, *35*, 325-326.

(135) Hao, T. *Adv Colloid Interface Sci FIELD Full Journal Title:Advances in colloid and interface science* **2002**, *97*, 1-35.

(136) Wen, W.; Huang, X.; Yang, S.; Lu, K.; Sheng, P. *Nature Materials* **2003**, *2*, 727-730.

(137) Halsey, T. C.; Martin, J. E.; Adolf, D. *Physical Review Letters* **1992**, *68*, 1519-1522.

(138) Weiss, K. D.; Carlson, J. D. *International Journal of Modern Physics B: Condensed Matter Physics, Statistical Physics, Applied Physics* **1992**, *6*, 2609-2623.

(139) Hao, T.; Kawai, A.; Ikazaki, F. *International Journal of Modern Physics B* **1999**, *13*, 1758-1766.

(140) Hao, T.; Kawai, A.; Ikazaki, F. *Langmuir* **1998**, *14*, 1256-1262.

(141) Gozdalik, A.; Wycislik, H.; Plocharski, J. *Synthetic Metals* **2000**, *109*, 147-150.

(142) Lim Yong, T.; Park Jong, H.; Park, O. O. *J Colloid Interface Sci FIELD Full Journal Title:Journal of colloid and interface science* **2002**, *245*, 198-203.

(143) Winslow, W. M. *Journal of Applied Physics* **1949**, *20*, 1137.

(144) Tsuchiya, K.; Orihara, Y.; Kondo, Y.; Yoshino, N.; Ohkubo, T.; Sakai, H.; Abe, M. *Journal of the American Chemical Society* **2004**, *126*, 12282-12283.

(145) Wolff, T., Muller, N. *Journal of Photochemistry* **1983**, *23*, 131.

(146) Miljanic, S.; Frkanec, L.; Meic, Z.; Zinic, M. *Langmuir* **2005**, *21*, 2754-2760.

(147) Murata, K.; Aoki, M.; Suzuki, T.; Harada, T.; Kawabata, H.; Komori, T.; Ohseto, F.; Ueda, K.; Shinkai, S. *Journal of the American Chemical Society* **1994**, *116*, 6664-6676.

(148) Ahmed, S. A.; Sallenave, X.; Fages, F.; Mieden-Gundert, G.; Mueller, W. M.; Mueller, U.; Voegtle, F.; Pozzo, J.-L. *Langmuir* **2002**, *18*, 7096-7101.

(149) Tamada, M.; Watanabe, T.; Horie, K.; Ohno, H. *Chemical Communications (Cambridge, United Kingdom)* **2007**, 4050-4052.

(150) Karmakar, R.; Samanta, A. *Chemical Physics Letters* **2003**, *376*, 638-645.

(151) Mandal, P. K.; Paul, A.; Samanta, A. *Journal of Photochemistry and Photobiology, A: Chemistry* **2006**, *182*, 113-120.

(152) Eddington David, T.; Beebe David, J. *Adv Drug Deliv Rev FIELD Full Journal Title:Advanced drug delivery reviews* **2004**, *56*, 199-210.